ALADIN Newsletter 24 - ALATNET Newsletter 7

ALADIN Newsletter 24

January - June 2003

ALATNET Newsletter 7

January - June 2003

ALADIN and ALATNET News
(postscript)

The operational ALADIN models
(postscript)

ALADIN PhD Studies

1. Radi AJJAJI : "Incrementality deficiency in ARPEGE 4d-var assimilation system"
2. Karim BERGAOUI : "Investigation of the potential of a convection scheme using prognostic mass fluxes for NWP in the African-Mediterranean domain"
3. Vincent GUIDARD : "Evaluation of assimilation cycles in a mesoscale limited area model" (ps file)
4. Jean-Marcel PIRIOU : "Correction of compensating errors in physical packages; validation with special emphasis on cloudiness representation"
5. Wafaa SADIKI : "A posteriori verification of analysis and assimilation algorithms and study of the statistical properties of the adjoint solutions"
6. Filip VANA : "The dynamical and physical control of kinetic energy spectra in a NWP spectral semi-lagrangian model" (ps file)

ALATNET PhD and Post-Doc Studies (postscripts)

1. Steluta ALEXANDRU : "Scientific strategy for the implementation of a 3D-VAR data assimilation scheme for a double nested limited area model" Part 1 Part 2 (ps file)
2. Margarida BELO PEREIRA : "Improving the assimilation of water in a NWP model" (ps file)
3. Martin GERA : "Improved representation of boundary layer" (ps file)
4. Raluca RADU : "Extensive study of the coupling problem for a high resolution limited area model""
5. André SIMON : "Study of the relationship between turbulent fluxes in deeply stable PBL situations and cyclogenetic activity" (ps file)
6. Cornel SOCI : "Sensitivity study at high resolution using a limited-area model and its adjoint for the mesoscale range"
7. Klaus STADLBACHER : "Systematic qualitative evaluation of high-resolution non-hydrostatic model" (ps file)
8. Malgorzata SZCZECH-GAJEWSKA : "Use of IASI / AIRS observations over land" (ps file)
9. Jozef VIVODA : "Application of the predictor-corrector method to non-hydrostatic dynamics" (ps file)

1. Report on the present parallelization level of ALADIN code and on the re-design of coupling data stream to make it conform with "B-level" parallelization (ps file)
2. New cycle CY26T1/AL26T1
3. Improvements of the compiling procedure "gmkpack"
4. Progress of the AROME project (ps file)

1. One month parallel run of the Seidl-Kann cloudiness scheme (ps file)
2. Some results of the sensitivity studies using the adjoint version of the ALADIN model (ps file)
3. False mesoscale cyclogenesis in the ALADIN model - Sensitivity study on initialconditions, physical parameterisations and horizontal diffusion (ps file)
4. Impact of the topography and LBC on the ALADIN precipitation forecast (ps file)
5. Forecasting stratus formation : some insights from 1d experiments (ps file)
6. Evapotranspiration effects on mountain convection in ALADIN (ps file)
7. Toward the assimilation of radar in AROME and ALADIN : a discussion paper (ps file)
8. Pre-Processing of the AMDAR data at HMS (ps file)
9. Impact of the ATOVS data on the mesoscale ALADIN/HU model (ps file)
10. Orographic forcing in ALADIN (ps file)

ALADIN developments during the first half of 2003

ALATNET developments during the first half of 2003

Home

ALADIN and ALATNET News ?

New rules for the Newsletter !

Sorry, no "News" part this time**.** It is of course a pity, all the more since some teams sent contributions. But the Newsletters are so late that informations became obsolete. So, why such a delay ?

There are many causes to this problem :

- more than half the contributions were late, i.e. arriving after the (already loose) deadline, with a few available only at the end of September;
- there were anyway many contributions, and very long papers;
- there was a huge editorial work for some contributions;
- there was an attempt to make everything available in-line, as some persons complained;
- the main part was available in html form from the end of September, but was not made public on the web site due to some misunderstanding;
- and afterwards there was a month of meetings and travels abroad for the editor.

However the problem is not a new one. Along the last years, the ALADIN Newsletter changed significantly, and in the right direction in my opinion, even it was sometimes proposed to suppress it (too much work for too few readers ?). This is quite clear from the following figures :

1998	2002
4 Newsletters	2 Newsletters
154 pages all together	341 pages all together
10 papers (mainly verification)	27 papers (mainly research)
PhD reports :10 pages	PhD reports : 101 pages
➢ editorial board : 1½ person	➢ editorial board : 1 person

The other topics : general informations, operational suites, ALADIN and ALATNET developments did not change that much in volume (globally).

Just the editing task now requires more than two months work per Newsletter, and there is only one person to do it (among other non negligible duties). This is too much and cannot last. In the meantime the presently used platform and tool will disappear within the end of this year, in the context of a general move to Linux.

So here is the proposal from the Toulouse Support Team to alleviate the editorial stuff. Indeed, more a requirement than a proposal.

A. The format of contributions

Up to now : ANYTHING !

- text, doc*, rtf, latex, html, latex2html, applix, pdf, ... and even more for figures
- the complexity of the format is usually independent from the content of the contribution

⇒ Editorial requirement : Use of Open Office

- free software, available on Linux and Windows
- user friendly for both *word* and *latex* fans, equations allowed (in-line or latex-like)
- new also for the Toulouse team
- anyway, no choice : Mandatory from the next Newsletter !

B. The form of contributions

⇒ Editorial requirement : Please, check English and READABILITY at home first !

- this concerns everyone, i.e. also some experienced researchers
- it should not be so difficult to have another member of the team read the contribution

C. The content of contributions

- less problematic than the two previous points, up to now
- why not a decentralized editorial board ? (instead of 1 person)

⇒ volunteers are welcome !

The present editor
Dominique Giard

1. Introduction

Changes were numerous along the last year, with the end of the common LACE operations, deep changes in Morocco and Tunisia, and a general upgrade of computers and libraries. The tables hereafter try to describe the situation at the end of September 2003, according to the informations provided to the Toulouse support team.

MODEL CHARACTERISTICS

Partner / Model	Mesh (km)	Gridpoints (C+I / C+I+E)	Grid type	SW corner (lat , lon)	NE corner (lat , lon)	Vertical levels	Coupling model
AUSTRIA-LACE	12.2	229´205 / 240 ´ 216	quadratic	33.99*N* 2.17*E*	55.62*N* 39.07*E*	37	ARPEGE
AUSTRIA-Vienna	9.6	133´117 / 144 ´ 128	quadratic	41.36*N* 5.88*E*	51.81*N* 21.84*E*	37	ALADIN-LACE Au
BELGIUM	7.0	229´229 / 240 ´ 240	linear	43.17*N* 5.84*W*	57.25*N* 17.08*E*	41	ALADIN-FRANCE
BULGARIA	12.0	79´63 / 90´ 72	quadratic	39.79*N* 20.01*E*	46.41*N* 31.64*E*	31	ARPEGE
CROATIA-LACE	12.2	229´205 / 240 ´ 216	quadratic	33.99*N* 2.18*E*	55.62*N* 39.08*E*	37	ARPEGE
CROATIA-HRn8	8.0	169´149 / 180 ´ 160	quadratic	39.00*N* 5.25*E*	49.57*N* 22.30*E*	37	ALADIN-LACE Hr
CROATIA-Dyn Adap	*2.0*	*72´72 / 80´ 80 (´5)*	*Senj, Karlovac, Maslenica,Split, Dubrovnik*			*15*	*ALADIN-HRn8*
CZECH REP.	12.2	229´205 / 240 ´ 216	quadratic	33.99*N* 2.18*E*	55.62*N* 39.08*E*	37	ARPEGE
FRANCE	9.5	277´277 / 288 ´ 288	linear	33.14*N* 11.84*W*	56.96*N* 25.07*E*	41	ARPEGE
HUNGARY	6.5	421´373 / 432 ´ 384	quadratic	34.15*N* 2.35*E*	55.3*N* 38.7*E*	37	ARPEGE

HUNGARY-Dyn Adap	*2.4*	*239´169 / 250´ 180*				*15*	*ALADIN-HU*
MOROCCO-NORAF	31	189´289 / 200 ´ 300	quadratic	1.93S 35.35*W*	44.86*N* 57.22*E*	37	ARPEGE
MOROCCO-Morocco	9	309´349 / 320 ´ 360	quadratic	17.24*N* 24.84*W*	42.46*N* 9.40*E*	37	ALADIN-NORAF
POLAND	13.5	169´169 / 180 ´ 180	quadratic	41.42*N* 5.56*E*	61.16*N* 40.19*E*	31	ARPEGE
PORTUGAL	12.7	79´89 / 90´ 100	quadratic	34.94*N* 12.42*W*	44.97*N* 0.71*W*	31	ARPEGE
ROMANIA	10.0	89´89 / 100´ 100	quadratic	41.91*N* 20.68*E*	49.80*N* 32.12*E*	31	ARPEGE
SLOVAKIA	7.2	109´79 / 120´ 90	quadratic	46.05*N* 14.69*E*	51.07*N* 25.26*E*	31	ALADIN-LACE Au
SLOVENIA	9.5	258´244 / 270 ´ 256	quadratic	34.00*N* 2.18*E*	54.82*N* 33.37*E*	37	ARPEGE
SLOVENIA-Dyn Adap	*2.5*	*148´108 / 160´ 120*	*44.57 N, 12.18 E - 46.98N 16.92E*			*17*	*ALADIN-SI*
TUNISIA	12.5	117´151 / 120 ´ 162	quadratic	27.42*N* 2.09*E*	44.16*N* 18.37*E*	41	ARPEGE

PRACTICAL IMPLEMENTATION

Partner / *Model*	Computer	Library / *Physics*	Operational applications	
AUSTRIA / *LACE*	SGI Origin 3400 20 processors	AL15 ® *CYCORA-ter*+...	· 48h forecast twice a day · synchronous 3h-coupling	· post-processing every 1h
AUSTRIA/ *Vienna*	SGI Origin 3400 20 processors	AL15 ® *CYCORA-ter*+...	· 48h forecast twice a day · synchronous 6h-coupling	· post-processing every 1h · hourly diagnostic analyses

BELGIUM/ *Belgique*	SGI Origin 3400 24 processors	AL15_02 ® *CYCORA-ter++*	· 60h forecast twice a day · synchronous 3h-coupling	· post-processing every 1h
BULGARIA/ *BG*	SUN Ultra Sparc 60	AL12 ® *CYCORA-bis*	· 48h forecast twice a day · synchronous 6h-coupling	· post-processing every 3h
CROATIA/ *LACE*	SGI Origin 3400 16 processors	AL25T1_op2	· 48h forecast twice a day · synchronous 3h-coupling	· post-processing every 3h
CROATIA/ *HRn8*	SGI Origin 3400 16 processors	AL25T1_op2	· 48h forecast twice a day · synchronous 3h-coupling	· post-processing every 3h · dynamical adaptation of wind (every 3h , 5 domains)
CZECH REP./ *CE*	NEC SX6B 4 processors	AL25T1_op4 ® *COCONUT++*	· 48h forecast twice a day · synchronous 3h-coupling	· post-processing every 1h · hourly diagnostic analyses · blending cycle (6h)
FRANCE/ *France*	FUJITSU VPP 5000 2 processors (/ 64)	AL26T1 ® *COCONUT*	· 4 forecasts a day, up to 54h, 48h, 42h, 36h · synchronous 3h-coupling	· post-processing every 1h · coupling files every 3 hours · hourly diagnostic analyses
HUNGARY/ *HU*	IBM Regatta 32 processors	AL15_03	· 48h forecast once a day · synchronous 3h-coupling	· post-processing every 1h · hourly diagnostic analyses · dynamical adaptation of wind (every 6h , 1 domain)
MOROCCO/ *NORAF*	IBM RS6000 SP	AL25T1 AL13 for assim.	· 72h forecast twice a day · lagged 6h-coupling	· post-processing every 3h · data assimilation based on O.I.
MOROCCO/	IBM RS6000	AL25T1	· 72h forecast twice a day	· post-processing every 3h

Maroc	SP		· synchronous 3h-coupling	
POLAND/ *Poland*	SGI Origin 2000 8 processors (/ 128)	AL09 (soon AL15)	· 48h forecast twice a day · synchronous 6h-coupling	· post-processing every 3h
PORTUGAL / *Portugal*	DEC Alpha XP1000	AL12 _bf02 ® *CYCORA-bis*	· 48h forecast twice a day · synchronous 6h-coupling	· post-processing every 1h
ROMANIA/ *Romania*	SUN Ent. 4500	AL15 _04 ® *CYCORA-bis*	· 48h forecast twice a day · synchronous 6h-coupling	· post-processsing every 3h
SLOVAKIA/ *Slovakia*	DEC Alpha XP1000	AL12_op6 ® *CYCORA-bis*	· 48h forecast twice a day · synchronous 6h-coupling	· post-processing every 1h
SLOVENIA/ *SI*	Cluster with 14 nodes, 22 among 26 processors used	AL25T1	· 48h forecast twice a day · synchronous 3h-coupling	· post-processing every 1h · dynamical adaptation of wind and precipitations (every 3 or 6 h)
TUNISIA/ *Tunisie*	IBM Regatta 690	AL25T1 ® *COCONUT*	· 48h forecast once a day · synchronous 6h-coupling	· post-processing every 3h

2. Changes in the operational version of ARPEGE for the first half of 2003

(more details bruno.lacroix++at++meteo.fr)

"DICORA", *20/02/2003*

See the last Newsletter for a description of the modifications.

"Longer forecast ranges", *31/03/2003*

The forecast ranges were increased, up to :

- - 102 h for the 00 UTC run,
- - 48 h for the 06 UTC run,
- - 72 h for the 12 UTC run,
- - 36 h for the 18 UTC run,

i.e. at least to 06 UTC the second day to have more diagnostics available.

"COCONUT", *15/04/2003*

See the last Newsletter for a description of the modifications.

"New geometry", *02/06/2003*

The stretching factor was reduced from 3.5 to 2.4, to attenuate the problems noticed in data assimilation. The new model resolution is T_L358 c2.4 for the forecast model, i.e. a mesh-size ranging from 23 km to 133 km, instead of 19 km - 235 km. The resolution of the outer loop of 4d-var decreased from T_L 161 to T_L149 in the meantime.

"New computer", *30/06/2003*

At first the move looked quite easy to perform (very similar computers), a parallel suite had been carefully controlled for 10 days, ... but the new machine scratched once operational !

Globally, the skill of ARPEGE was improved, even when compared to other models on large-scale scores :

COMPARAISON AVEC LE MODELE FRANCAIS
(Z500 - Echéance 72 heures - Domaine Nord20)
+ Moyenne glissante sur un an (M-5 à M+6)

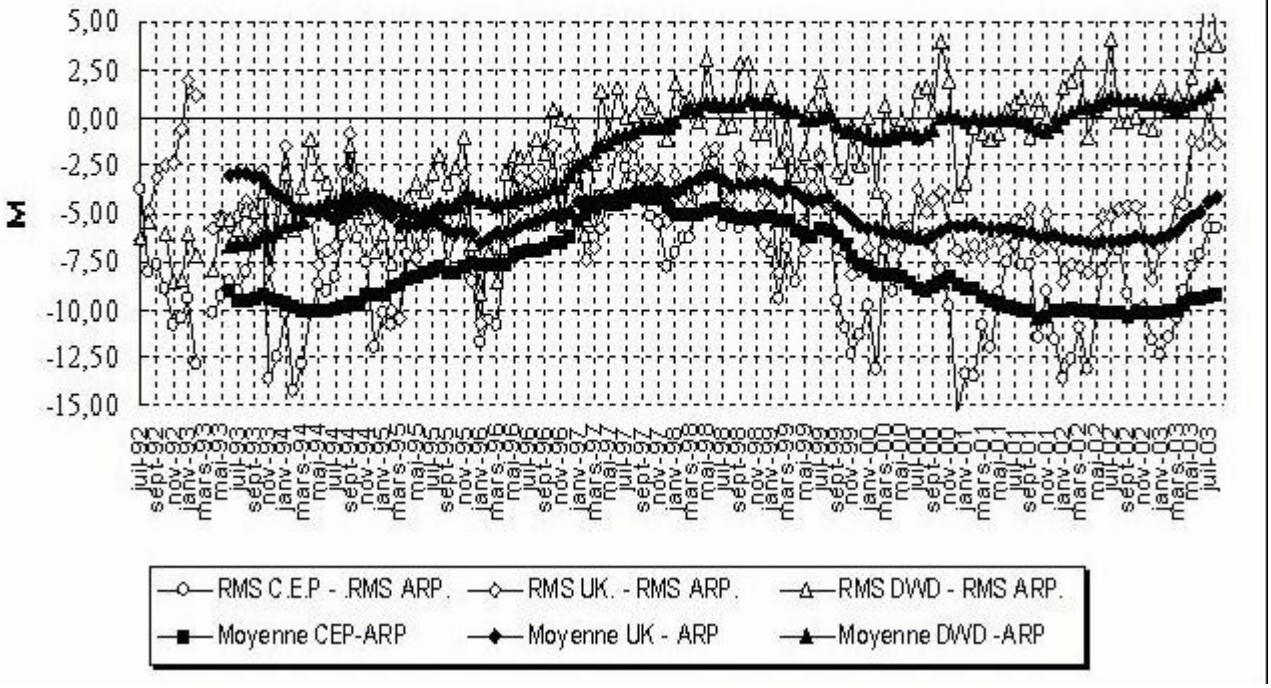

3. Operational versions in Austria

(more details thomas.haiden++at++zamg.ac.at)

Since January 2003, ZAMG is running the ALADIN model operationally on two domains, with the specifications given below. The model version currently used is AL15 (export version 03 + bugfixes).

ALADIN-LACE :

- Horizontal resolution : 12.2 km
- 37 vertical levels
- Number of gridpoints : 240 x 216 (including the extension zone)
- Time-step : 514 sec
- Coupling frequency : 3 hours (LBCs provided by ARPEGE)
- Integration time : 1/2 hour
- Availability of products : 04:00 UTC, 16:00 UTC

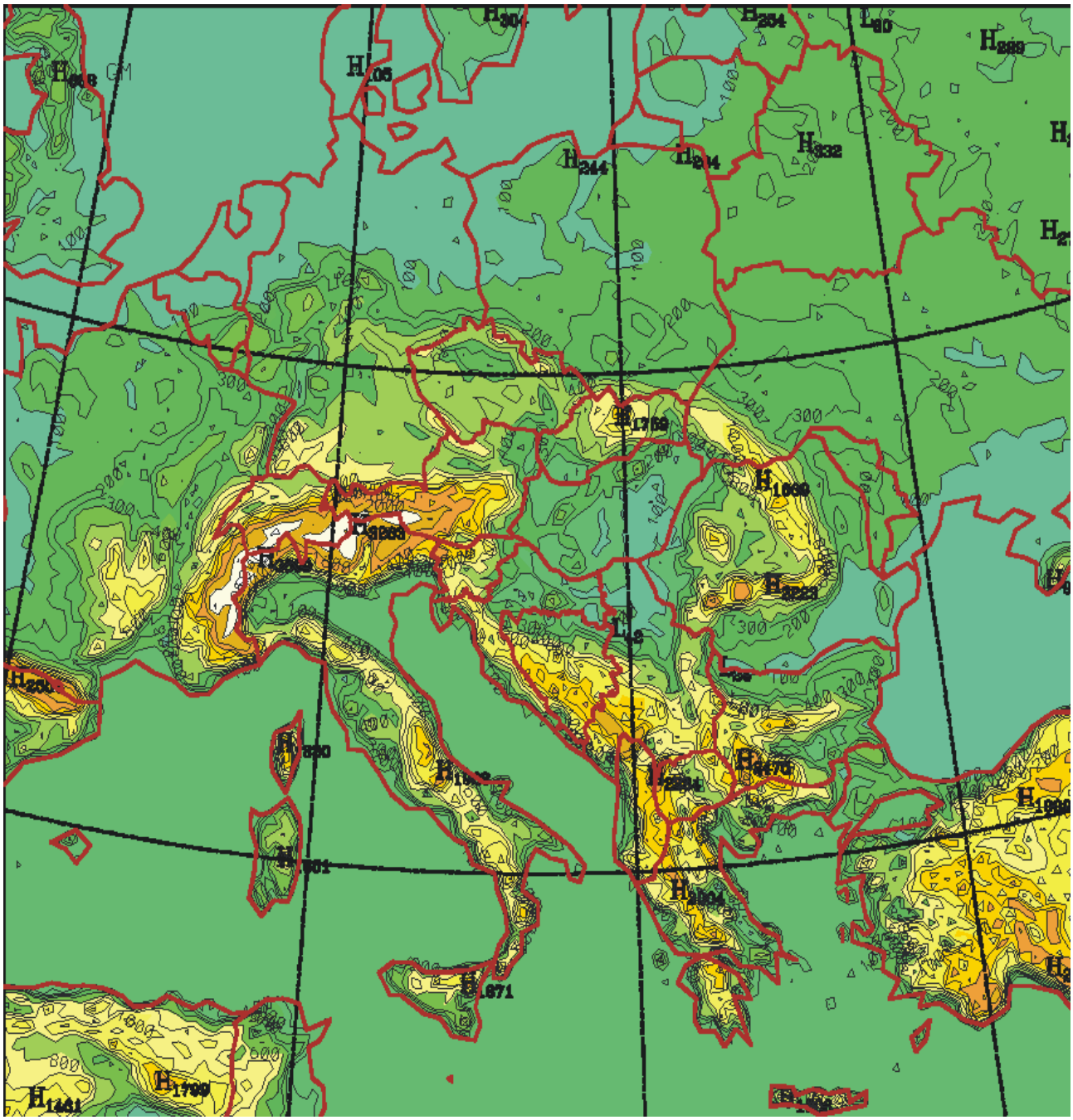

ALADIN-VIENNA :

- Horizontal resolution : 9.6 km
- 37 vertical levels
- Number of gridpoints: 144 x 128 (including extension zone)
- Time step : 415 sec
- Coupling frequency : 6 hours (LBCs provided by ALADIN-LACE)
- Integration time : 10 mn
- Availability of products : 04:15 UTC, 16:15 UTC

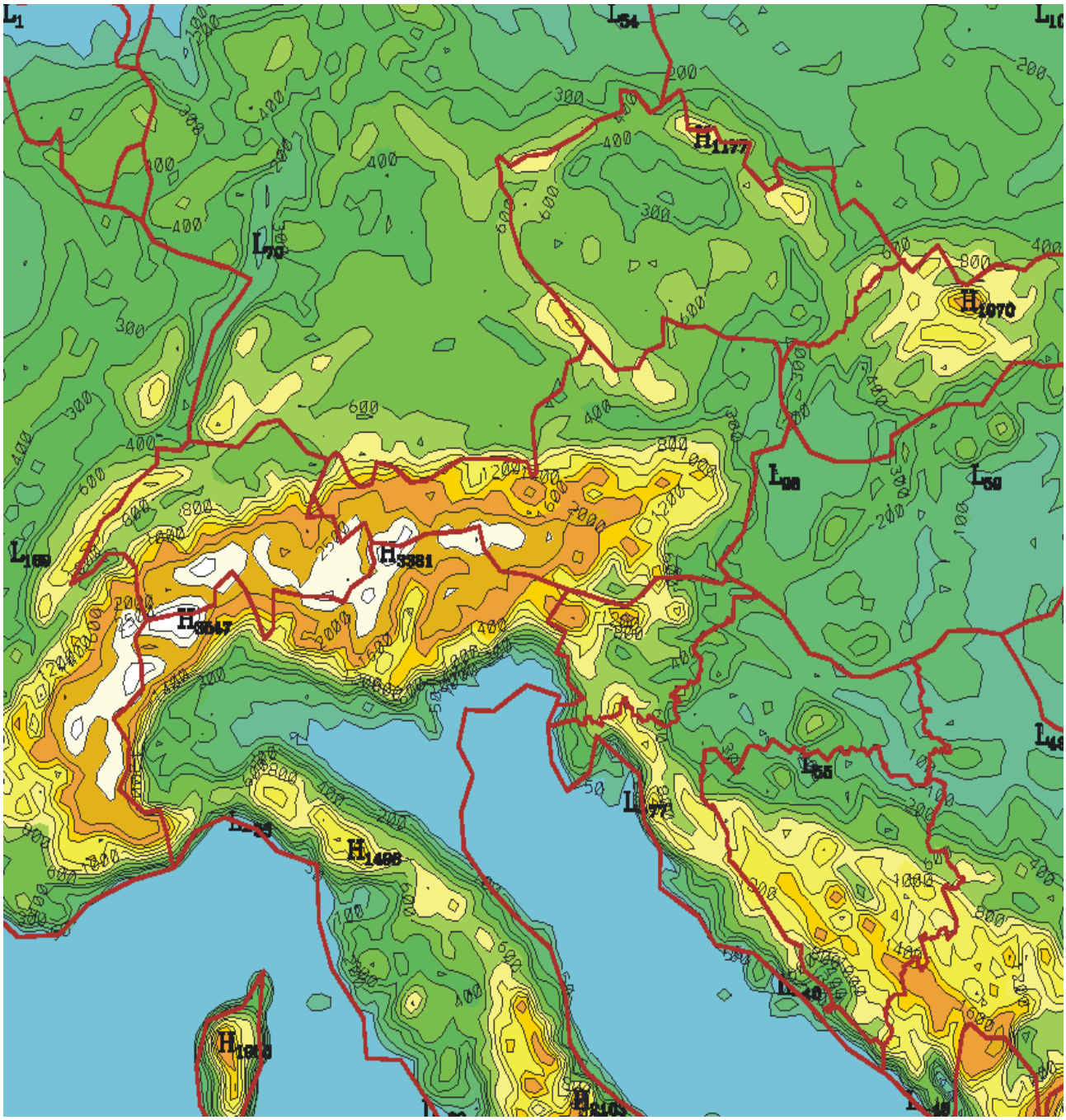

Plans for the future :

- Increasing the horizontal resolution of ALADIN-VIENNA (6-7 km)
- Data assimilation cycle for ALADIN-VIENNA using 3d-var
- See also the paper of Alexander Kann.

4. Operational version in Belgium

(more details olivier.latinne++at++oma.be)

Recently, many changes have been brought to the Belgian operational forecasts. Firstly, we have extended the forecast range up to 60 hours instead of 48. To do that, we are still using the hybrid coupling method : for the midnight run, ALADIN-Belgium is coupled to ALADIN-France for the first 54 hours, and beyond to ARPEGE, until 60 hours, while for the midday run the coupling to ALADIN-France goes up to 48 hours.

In a few weeks, the surface of the Belgian domain will also be multiplied by a factor of about five, while preserving the actual mesh-size of 7 km (see Part 1 for more details). In August, we made a request to DWD, with an aim of taking part in the project for a Multi-Model Ensemble Prediction System in Europe.

5. Operational version in Bulgaria

(more details andrey.bogatchev++at++meteo.bg)

Nothing new along the last months.

6. Operational versions in Croatia

(more details ivateks++at++cirus.dhz.hr, tudor++at++cirus.dhz.hr)

ALADIN is running operationally twice a day, for 00 and 12 UTC. Model resolutions are 12.2 km for LACE domain, 8 km for HRn8 and 2 km for dynamical adaptation domains.

Initialization of ALADIN on LACE domain is provided by Digital Filter Initialization (DFI). When the 48 hours forecast on LACE domain finishes, 48 hours forecast on HRn8 starts, without initialization, with coupling files from LACE. Coupling frequency and frequency of output files for LACE and HRn8 domains are the same, 3 hours.

In operational suite 5 domains (Karlovac, Senj, Maslenica, Split and Dubrovnik) are used for high-resolution dynamical adaptation of the wind field to orography in the lower troposphere. Four of them cover the coastal part of Croatia. Dynamical adaptation is run sequentially for each output file, every 3 hours till 48 hours.

Changes in the first half of 2003 :

From the beginning of April, the Croatian domain was enlarged from 144x120 (127x109) points to 180x160 (169x149). The domain was enlarged mostly southward and westward to cover the whole Adriatic Sea and Genoa Bay. The horizontal resolution remained the same, 8 km.

Latitudes and longitudes of new HRn8 domain:

- SE corner : 39.00°N, 5.25°E

- NE corner : 49.57°N, 22.30°E

- central point : 44.60°N, 13.00°E

Main memory on SGI was upgraded to 12288 Mbytes, because of more memory consumption by the new ALADIN version, AL25.

Speed of Internet line increased to 2 Mbytes/sec from 13th of June 2003.

RETIM2000 was installed on 16th of June, from that day comparison between transfer speeds and reliability via RETIM2000 and via Internet were performed.

From 30th of July 2003 12 UTC, operational version of ALADIN is AL25T1_op2.

Picture 1. Orography of the old (HRv8) and new (HRn8) domains

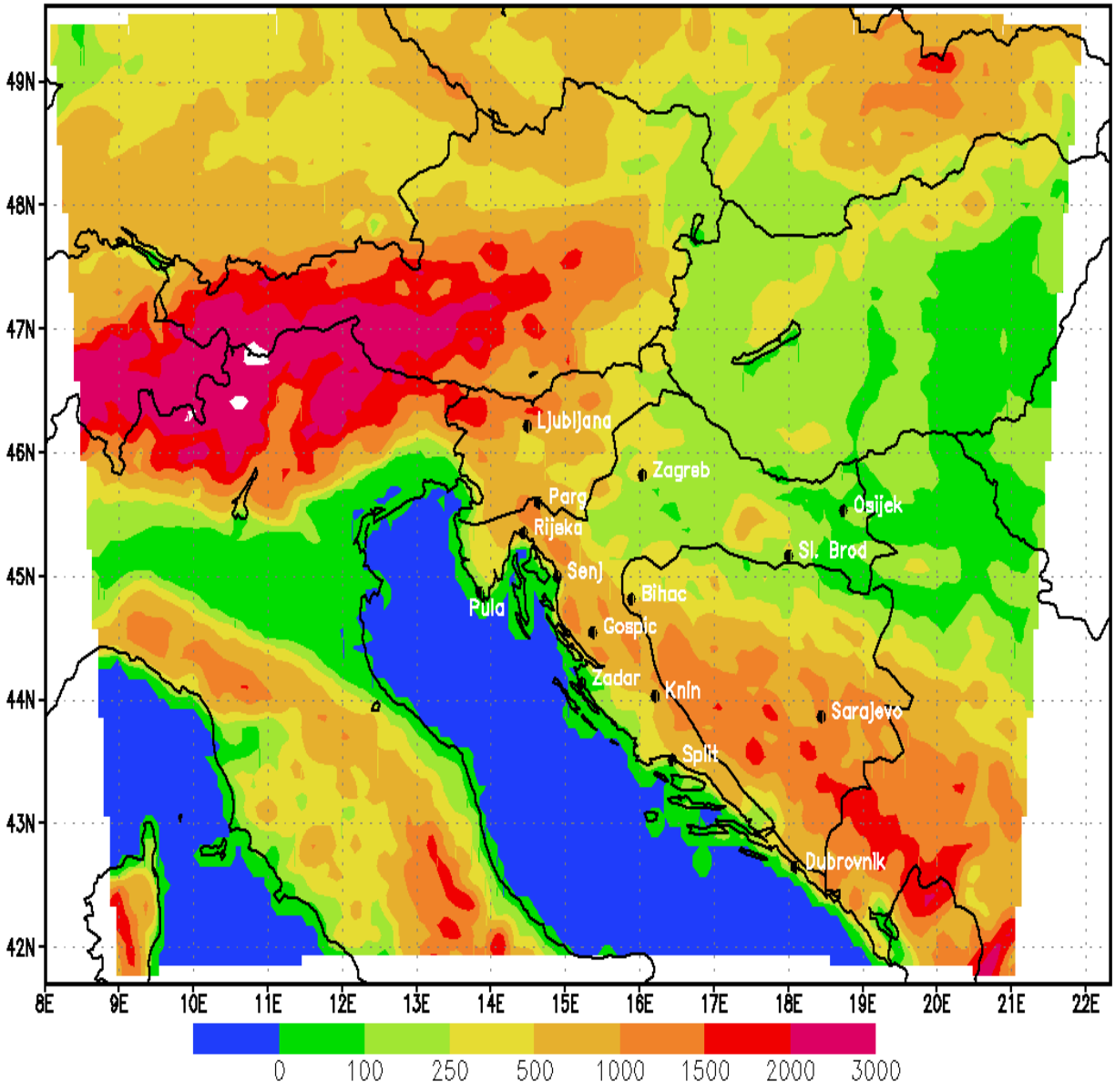
49N
48N
47N
46N
45N
44N
43N
42N
8E
9E
10E
11E
12E
13E
14E
15E
16E
17E
18E
19E
20E
21E
22E
Ljubljana
Zagreb
Pore
Rijeka
Senj
Pula
Bihac
Gospic
Zadar
Knin
Sarajevo
Split
Dubrovnik
Osijek
Sl. Brod
0
100
250
500
1000
1500
2000
3000

HRv8

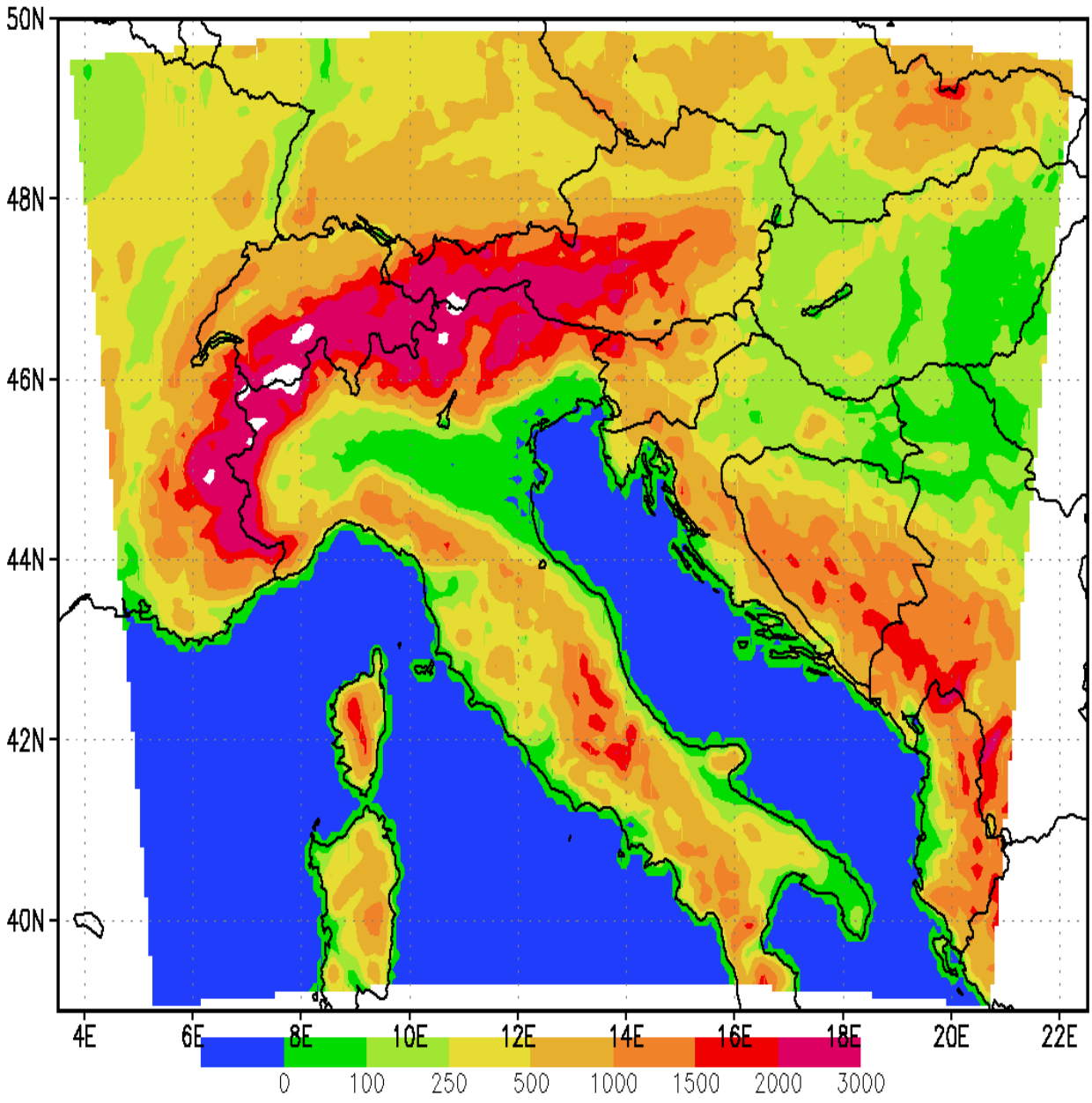
50N
48N
46N
44N
42N
40N
4E
6E
8E
10E
12E
14E
16E
18E
20E
22E
0
100
250
500
1000
1500
2000
3000

HRn8

7. Operational version in Czech Republic

(more details vana++at++chmi.cz)

Since 1st January 2003 every LACE Member exploits its own operational application of ALADIN. The recent ALADIN/LACE application operated in Prague LACE centre became the ALADIN/CE (CE standing for Central Europe) configuration of CHMI. In the beginning of 2003 it naturally kept its continuity with the previous LACE suite.

1. Evolution of the ALADIN/CE application

The ALADIN/CE suite switched to the version COCONUT+++ of the model physics :

27/05/2003 at 12 UTC network time for the production run and at 06 UTC network time for the assimilation cycle : COCONUT+++.

This physics package became operational in ARPEGE mid-April 2003. According to the original plan in Prague the switch to this model version was thought only for the end of June, together with the move to the new computer NEC-SX6 and to a higher cycle of ALADIN (AL25T1). However, with the start of warm season, the operational version CYCORA_ter+++ was not providing reasonable values of CAPE; these were extremely high. This fact together with the requirement of correct validation between the old cycle AL12 and the new one AL25T1 lead to the back-phasing of the COCONUT physics to the still operational cycle AL12 on the old computer NEC-SX4 (insufficient memory on the SX4 machine was the blocking factor). The COCONUT package was validated and gave the same results with both cycles. Meantime, already in March, the parallel testing started in comparison with the operational CYCORA_ter+++ version. These tests have shown that the COCONUT version as implemented in ARPEGE does not give completely satisfactory scores (at least neutral). For example, the bias of 2 m temperature got considerably worse, it became too cold (suite ABZ). Many other tests were made, see the description below. Finally, the satisfactory solution was found when coming back on the radiation scheme (+), on the nebulosity scheme (+) and on the horizontal diffusion coefficients (+) to the CYCORA_ter tunings.

Impact on the forecast : neutral scores, the CAPE values get reasonable compared to CYCORA_ter+++.

Technical impact : none.

The ALADIN/CE suite switched to cycle AL25T1 on new computer NEC-SX6 :

30/06/2003 at 12 UTC network time for the production run and at 06 UTC network time for the assimilation cycle : AL25T1 on NEC-SX6

In the beginning of 2003, CHMI purchased a new computer, the starting configuration is NEC-SX6/B with 4 processors and 32 Gbytes of shared memory (one node). The machine was installed in March and the acceptance tests were successfully completed on 10th June 2003. The switch of the complete ALADIN/CE suite took place on 30th June 2003, in its version COCONUT+++ on cycle AL25T1. As first future step, the resolution of ALADIN/CE will be increased.

Beside the model configurations needed for the operational suite, a considerable effort was put to the installation and validation of the ODB software. Not all ODB tools were however validated before the end of June.

Impact on the forecast : neutral.

Technical impact : important increase in the memory consumption due to the data flow, different from the

old shared memory code.

2. Parallel suites

The following parallel tests were launched to assess the impact of different modifications:

- - *Suite ABY :* It was the test of new tuning of the gravity-wave drag and orographic lift when the envelope orography is abandoned (following the study of Dunja Drvar). The scores were not satisfactory and the mean-sea-level pressure maps have shown that the drag and lift do not compensate enough the blocking effects of the envelope. Further study will take place.
- - *Suite ABZ :* It tested the COCONUT version of physics; at the same time the horizontal diffusion intensity was increased twice. The scores were not the best. There was a too cold bias of 2m temperature, computed against SYNOP observations and compared to the operational version.
- - *Suite ACA :* This test is based on the ABZ suite, but it comes back on the cloudiness scheme. The scores compared to ABZ are worse and they remain not satisfactory, compared to the operational version.
- - *Suite ACB :* This suite should have been comparable to the model version known under the name DICORA (used in ARPEGE before COCONUT). The scores were not satisfactory either. Later on it was found that there was a mistake in leaving the switch LSRCONT =.true. (it should be switched off with DICORA).
- - *Suite ACC :* This test was based on the COCONUT version (suite ABZ) however a different tuning was used for the mixing length. The goal was to find the reason of the worse scores of COCONUT. The results were not really changed by this retuning.
- - *Suites ACD, ACE, ACF :* All these tests were based on the DICORA version, adding the shear-linked convection or using various tunings. The results were not better and they did not help much to discover the reason of the bad COCONUT scores. On top, all these tests were affected by the mistake (setup of LSRCONT) made in the preparation of DICORA (suite ACB).
- - *Suite ACG :* Since the DICORA version did not lead to any improvement or to any clue on the COCONUT scores, we came back to COCONUT in this test. On top of coming back to the operational version (CYCORA_ter) for the cloudiness scheme, the same was made for the radiation scheme. This test gave reasonably neutral scores for a trial period in winter. As it was a promising configuration, it was also re-tested for a summer period, this time even with a little improvement of the geopotential score. Within the summer period test it was noticed, however, that the field structures of humidity convergence or CAPE were not as sharp as in the operational version. Therefore several single case tests were made in order to see what could cause the damping.
- - *Single test ACI, ACJ, ACK:* In these tests the convection tuning was modified (for parameters GCVPSI , GCOMOD, LSRCONT respectively) with respect to the ACG suite. The results (field structures) were almost the same as in case of ACG.
- - *Single test ACL :* This test is based again on the ACG settings, but the horizontal diffusion coefficients were set back to the values of the operational version. Indeed, too strong diffusion in ACG was the reason of too smooth fields. Therefore it was decided to keep the horizontal diffusion tuning without change. The ACL settings then became operational on 27th May and it got the name COCONUT+++ (first (+) for cloudiness scheme, second (+) for the radiation scheme and third (+) for the horizontal diffusion).
- - *Suite ACH :* This test was inspired by a study made with ARPEGE, where a better precision of computation of the semi-Lagrangian trajectory was tried (using three iterations instead of two in the trajectory computation). The test was based on the ACG suite and it was compared both with ACG and with the operational version. Surprisingly, the scores were worse in altitude, namely in bias of geopotential, which made worse also the RMSE geopotential score. This test was then left aside but perhaps some study can be later made around this issue.
- - *Suite ACM :* test of the AL25T1 cycle with the COCONUT+++ settings on the SX6 machine. It was compared to the AL12 cycle with the COCONUT+++ settings on the SX4 machine (operational version since 27th May). The scores were perfectly neutral. The comparison was confirmed by the same result obtained for the 24 h cumulated precipitation forecast with both

suites. The ACM suite became operational on the SX6 machine on 30th June 2003.

The results of parallel tests may be consulted on / pages.

8. Operational version in France

(more details bruno.lacroix++at++meteo.fr)

Mainly similar changes in ALADIN-France as in ARPEGE along these months, but no change of resolution :

"DICORA", *20/02/2003*

See the last Newsletter.

"Longer forecast ranges", *31/03/2003*

The forecast ranges were increased, up to :

- - 54 h for the 00 UTC run,
- - 48 h for the 06 UTC run,
- - 42 h for the 12 UTC run,
- - 36 h for the 18 UTC run,

i.e. to 06 UTC the second day.

"COCONUT", *15/04/2003*

See the last Newsletter.

"New computer", *30/06/2003*

With computer failures a few days after the transfer of operations to the new machine ...

9. Operational version in Hungary

(more details horanyi++at++met.hu)

During the second part of 2002 we have successfully installed a new ALADIN domain together with the switch to a direct coupling to the ARPEGE model as lateral boundary conditions (see details in the previous Newsletter). The main activities during the first half of 2003 were devoted to the further experimentation of the three-dimensional variational data assimilation scheme (3d-var) for the ALADIN model.

The most important operational activities around the local version of the ALADIN model in Budapest are detailed hereafter:

- -- The operational scripts were renewed with the help of a professional software developer team. The new scripts became very modular and systematic (however their readability had been significantly decreased).
- -- The RETIM satellite data transfer was put into use at the end of April and systematic comparison of the data transfer through RETIM and *internet-ftp* was carried out afterwards. The results showed that there is a higher reliability found in the RETIM dissemination, however the speed of the transfer is a bit slower than the speed of the *internet* capacity (detailed statistics can be provided on request for the more interested readers). Based on these measurements we have decided that we do use operationally the initial and lateral boundary files provided by RETIM (since mid-June). The *internet* solution was kept as a backup.
- -- The 3d-var data assimilation cycle was continuously running in parallel suite (with 48 forecast once per day) and the results of the double suite was systematically compared to the reference solution (dynamical adaptation). The main outcome of the comparison is briefly described in the "ALADIN developments" chapter of the same Newsletter. The classical double suite used only SYNOP and TEMP observations, nevertheless some further studies were carried out using additional ATOVS and AMDAR data in the process of 3d-var.
- -- During the spring we started to operationally monitor the performance of the ALADIN operational suite. It means that beside the graphical tool available for the operators (about the successful completion of the model run), the developers have to their disposal a laptop and a mobile phone, and a remote-login is ensured in order to make intervention in the operational suite in case of necessity.
- -- The loadleveler job scheduler was adjusted several times, nevertheless its functionality is far from being optimal, preventing the full usage of all the available resources of our IBM Regatta computer.
- -- We have introduced just very few new elements to the operational model suite: we started to make verification over the ARPEGE LBC files (for direct comparison to the ALADIN/HU version) and we have created special post-processing for the RODOS environmental application and for another dispersion model predicting low level pollution.
- -- AL25 model version was installed and partly validated, but not introduced operationally.

10. Operational versions in Morocco

(more details radi.ajjaji++at++cnrm.meteo.fr)

During the first semester of the year 2003, the Albachir suite was subjected to heavy changes. Since April 17th, 2001, the new ALADIN-NORAF (North Africa) model runs operationally, in addition to ALADIN-Morocco. ALADIN-NORAF is coupled in asynchronous mode with ARPEGE, it performs its own data assimilation with CANARI (Optimum Interpolation analysis) and it runs twice a day for 72 hours forecasts. The model resolution is 30 km and 37 vertical levels.

ALADIN-Morocco has a more finer mesh, with a resolution of 12 km. It is coupled with ALADIN-NORAF in synchronous mode with a frequency of 3 hours.

The operational cycle used for assimilation is still AL13 (because of its intensive validation in term of CANARI analysis), whereas the forecast models use AL25T1 (even if this cycle is less optimized than AL13 in term of computing performances on scalar massively parallel machines).

Validation of this configuration was done in term of verification against SYNOP and TEMP reports and also against ARPEGE analyses. The scores for the Morocco domain are unchanged despite a slight loss in geopotential field, due certainly to the asynchronous coupling with ARPEGE.

On the other hand, Casablanca organized an African seminar around ALADIN-NORAF between April 21st and May 5th in cooperation with the African Center for Meteorological Applications to Development (ACMAD). The objective of the seminar was to familiarise future African users of ALADIN-NORAF with its abilities. Twenty nationalities were present to the seminar and appreciated a lot the Moroccan/ACMAD initiative to cover North Africa by finer NWP products. For more information about this seminar, the internet web site of ACMAD (*http://www.acmad.ne*) contains a long article about it. Concerning the lectures offered by the Moroccan ALADIN team, they could be found on the intranet web site of DMN accessible from Météo-France (only!) at the address . On this site, ALADIN-NORAF products are also available in image format.

Concerning the dissemination of ALADIN-NORAF products to African countries, a list of interesting fields was decided during the seminar. The corresponding GRIB data will be available on RETIM Africa. Albachir suite will transmit GRIB files to Météo-France and the later will make them available on RETIM. The projected starting date is the end of 2003.

Due to the lack of observations over the southern part of the NORAF domain, our team is studying the possibility to use some non-conventional data (even in CANARI). In this spirit, the so-called pseudo-TEMP data were tested in ALADIN-NORAF, and their ability to localise the convection cells was examined. These data seem very promising. But the most important work that is being done around ALADIN-NORAF is concerning the use of 3d-var assimilation. An important amount of manpower is dedicated to this part. The objective is to put 3d-var in operations for ALADIN-NORAF as soon as the known theoretical problems are resolved (mass/wind balance at the vicinity of the equator, increments that cross the E-zone and reach the other opposite side of the domain, more adapted LAM screening, the best manner of cycling, etc....).

11. Operational version in Poland

(more details zijerczy++at++cyf-kr.pl)

New resources available in Cracow

In the middle of 2003 new computational resources have become available in Cracow for our ALADIN team.

First of all the SGI 2800 of the Cracow Supercomputer Center CYFRONET was upgraded. All 128 R10k and R12k processors were replaced with R14k 500 MHz ones, operational memory was enlarged up to 64 GB the and disks volume reaches now 1394 GB. For our operational purposes we are granted with 8 processors and 9 GB HDD now.

After 2-years delay we have obtained a new group server : it is a SUPERMICRO SuperServer 7042M-6 tower. Here are its main features :

- - processors : 2 x Intel Xeon 512k L2, 2.4 GHz, FSB 400 MHz
- - operational memory : 2 GB RAM, ECC DDR-200
- - disk matrix : 6 x 36 GB Ultra-160 SCSI HDD's, RAID-5
- - tape archive : DAT DDS-3, 12/24 GB
- - operating system : Red Hat Linux
- - proprietary software : Lahey Fortran 95 compiler, PV-WAVE

Due to greater available resources enhanced operational suite is under preparation.

12. Operational version in Portugal

(more details maria.monteiro++at++meteo.pt)

Nothing new along the last months.

13. Operational version in Romania

(more details banciu++at++meteo.inmh.ro)

The devoted work for improving the operational suite was performed with the aim of minimizing the availability time of the numerical forecast and for passing from lagged to synchronous mode. This transition was possible due to the SUN Enterprise 4500 platform used for running the ALADIN model. Starting from 18th of April 2003, ALADIN-Romania is integrated in synchronous mode twice per day.

Implementation of the AL15_04 version.

14. Operational version in Slovakia

(more details olda.spaniel++at++mail.shmu.sk)

Our operational configuration was not modified substantially during the first half of 2003. The most important event was the termination of the common ALADIN/LACE operational suite in Prague (December 31st 2002). Since there is still a lack of computer capacity at SHMI, it was decided to ask ZAMG/Vienna for providing an equivalent set of products (including LBCs) from their local version of ALADIN/LACE. Operational switch to ZAMG data took part at mid December 2002. During the transitional period ALADIN products were downloaded also from CHMI. It was found that time availability of ZAMG products at SHMI is comparable to that of old LACE products. Difference was usually of the order of minutes. After successful tests transfer from CHMI was stopped in February 2003. Archives for 2002 were completed with CHMI data, archives for 2003 are filled with ZAMG data.

SHMI plans to obtain sufficient computer capacity for integrating the ALADIN model on a domain of LACE size. ITT for the new "supercomputer" is in preparation, it should be announced in Autumn 2003.

Current features of the operational application ALADIN/SLOVAKIA are as follows :

· computer :

- - DEC Alpha Xp1000, EV6 processor
- - 1 GB memory
- - 36 GB HDD
- - DIGITAL UNIX V4.0
- - DIGITAL Fortran 90 V5.2

· model characteristics :

- - version: AL12_op6, CYCORA_bis
- - mode : dynamical adaptation
- - driving model : ALADIN/LACE-ZAMG
- - coupling frequency : 6 h
- - domain size : 120×90 points (extension zone included)
- - resolution : 7.18 km, 31 vertical levels
- - time-step : 337.5 s
- - forecast length : 48 hours, 2 runs per day (00 and 12 UTC)

· configurations: E001, EE927, E923, CANARI

· products :

- The variety of model products did not change. These include maps of surface fields, meteograms, vertical cross-sections, automatic forecasts and ASCII inputs for RODOS.

· visualisation :

- Pre-operational testing of integrated visualisation system Visual Weather (developed by IBL software) was almost finished. Operational usage is scheduled for autumn 2003. Visual Weather should gradually replace old visualisation tools (PAGB, CHAGAL, ...). Model forecasts are read in GRIB or GRID format.

· verification :

- Approach to verifications is unchanged. Model is verified against SYNOP, TEMP and rain-gauge measurements. Verifications are fully automatic. Results are available via intranet.

See also the ALADIN report.

15. Operational version in Slovenia

(more details neva.pristov++at++rzs-hm.si)

Tender for the new computer system on EARS (Environmental Agency of Republic of Slovenia) started mid 2002 and the new computer was installed at the end of 2002. It is a cluster system with 14 nodes (1 master and 13 computing nodes). Each node has 2 Intel Xeon 2.4 GHz processors and 2 GB of memory. All nodes are connected via gigabit fibre link through powerful Riverstone SSR 8000 gigabit switch. Users have access to 300 GB primary disk space and to additional 0.75 TB (soon to be expanded to 3.5 TB) external disks array.

Special attention has been paid to software architecture of the cluster. Cluster is running Linux OS enhanced by Score software. The Score software helps in easier maintenance of the cluster, better availability and a higher overall performance. The queuing system permits an efficient execution of the operational suite. Gang scheduling and checkpointing are some features which had been reserved for supercomputers just few years ago, but are now available on clusters as well.

A new operational suite was designed and put into operation on the new computer in the first part of 2003. During this time many various tasks needed for the suite to operate properly on the computer were completed. Those were mainly porting the ALADIN model (cycles 12, 15 and 25), compiling programs needed for the preparation of the products (PALADIN, grom, gribeuse, Harpe, etc...) and implementing SMS (Supervisor Monitor Scheduler, the ECMWF product). Together with forecasters we decided to integrate the model only for the domain which is the slightly reduced (on the northern and eastern edge) former LACE domain. The programs used in the operational suite are currently compiled with the Lahey Fortran compiler but this might be changed once tests with two other compilers (Intel and PGI) completed. A Score Cluster System Software, which is a high-performance parallel programming environment for workstation and PC clusters, was installed. We had to find the optimal way for simultaneous execution of three ALADIN configurations (the model integration, the preparation of coupling files and the off-line post-processing) on the available computer processors under the Score environment. The basis for the new operational suite inside the SMS system was our old suite and the LACE operational suite in Prague. Some changes were needed and many tests were done. Finally, on the 1st of June, we could announce that the suite became operational.

ALADIN cycle 25T1 is used in the operational suite. For the integration (e001) 22 out of 26 computing processors are used, so the remaining processors are available for preparing the boundary conditions for dynamical adaptation (ee927), the forecast fields on pressure levels (off-line Full-Pos) and the visualization of meteorological fields during the integration time. The model integration accomplishes in one hour and another one hour is needed to prepare other products.

Several applications are :

- fields written in GRIB format on a latitude×longitude regular grid, available also for one user from Italy (ARPA FVG),
- meteograms with correction of 2m temperature using Kalman filter for 36 predefined model points,
- time cross-sections using HRID on pseudo-TEMPs for 36 predefined model points,
- simulation of satellite images (pseudo-satellite movie),
- precipitation amounts needed for hydrological models,
- dynamical adaptation of surface wind and precipitation,
- vertical cross-sections for predefined directions,
- some other products for end users inside the Slovenian environmental agency (Internet) and outside users (electric companies),
- saving the selected model output for verification.

The coupling files from the ARPEGE model are transferred via Internet from Toulouse. The average time

for transferring one file is one minute (transfer rate 128 kB/s max. 153 kB/s). Files are significantly delayed (more than 2 hours) in approximately 2 % of the cases.

Characteristics of the new operational ALADIN/SI model configuration :

- 258×244 points, with extension zone 270×256 points (elliptic truncation E89×84), on a Lambert-projection domain (34.00°N; 2.18°E - 54.82°N; 33.37°E),
- 9.5 km horizontal resolution,
- 37 vertical model levels,
- 400 s time-step, range of forecast 48 hours,
- initial and lateral boundary conditions from ARPEGE,
- coupling every 3 hours,
- initial state obtained by digital filter initialization,
- integration twice per day.

Domain for dynamical adaptation of surface wind (DADA) and precipitation (PADA) are just a single one covering whole Slovenia and the most northern part of the Adriatic Sea. Characteristics are :

- 148 ×108 points, with extension zone 160×120 points (elliptic truncation E49×39), on a Lambert-projection domain (44.57°N; 12.18°E - 46.98°N; 16.92°E),
- 2.5 km horizontal resolution,
- 17 vertical model levels,
- 60 s time-step,
- initial state from ALADIN/SI,
- performed every 3 hours for the first day, every 6 hours for the second day of forecast.

Selected fields are prepared on a regular longitude×latitude grid and coded to GRIB format. The domain is smaller (36°N; 2°E - 54°N; 28°E) with 217×211 points, so the resolution in E-W direction is 0.12°, and in S-N 0.0854°.

For our forecasting visualization system VisPro many predefined raster images are prepared (around 1700 figures). Forecast fields can be also visualized with GrADS and meteograms for a selected point can be prepared on demand.

A lot of information connected with the ALADIN operational suite can be found on the internal intranet pages. The modifications and changes on computer or in the operational suite, notes about problems which appear in the operational suite with their description and solution, are listed there. Daily products can be checked; the availability of selected products is registered for each run from the start on. The ALADIN source code for cycles AL12, AL15 and AL25T1 is also available there in html format. Potential users (beginner or experienced user) can find some instructions, the missing ones will follow soon.

The old operational suite is still running on our old cluster of workstations, for backup and comparison possibility.

Our experience is that SMS monitoring system is very useful. It was worth to spend time redesigning the scripts and testing. Monitoring, testing, repeating, etc..., is much easier. We would like to thank our Czech colleagues Martin Janousek and Filip Vana for the support during the implementation of our suite in SMS.

16. Operational version for Tunisia

(more details nmiri++at++meteo.nat.tn)

During the first half of 2003, the first local implementation of the ALADIN model (cycle AL25T1) was successfully completed on the IBM Regatta pSeries 690 platform. The most important activities around that local pre-operational version of ALADIN are summarized in the following.

1. **Infrastructure job**
    - 1.1 Hardware installation (IBM Regatta pSeries 690 machine).
    - 1.2 Software update.
    - 1.3 Additional libraries installation.
    - 1.4 Creating of the ALADIN user account (operations).
    - 1.5 Disk partition.
2. **Porting of the ALADIN suite (AL25T1)**
    - 2.1 Installation of CVS (Current Version System) : an OpenSource equivalent to ClearCase.
    - 2.2 Creating the compilation procedure.
    - 2.3 Compilation time : the compilation procedure is mainly sequential; it takes 45 minutes. However, the link is very quick (few seconds). After parallelization, we hope reach 10 minutes for compilation.
    - 2.4 Installation of the whole ALADIN operational chain as running in Météo-France.
    - 2.5 Installation of the LoadLeveler job scheduling system on the IBM platform.
    - 2.6 Special transfer script was performed and tested for transferring coupling files from "delage" : The Internet transfer rates are monitored since the first day of operational application (June 26th, 2003). The reliability of this transfer is quite satisfactory for the present phase (transferring mean time of 17 coupling files from "delage" machine is equal to 80 minutes) . However, we are thinking of a new more reliable solution. It will be probably a leased line as well as the RETIM 2000 satellite dissemination system.
    - 2.7 Special post-processing (Full-Pos) script was written and tested on the IBM p690 machine.
    - 2.8 Installation of PALADIN, CHAGAL, DOMOLALO and partially GMKPAK utilities.
    - 2.9 A special script was also written to disseminate ALADIN products in their final suitable forms in order to be easily used by forecasters.
3. **Training**

    We have organized two training sessions for ALADIN team during June :

    - 3.1 Training for system administration.
    - 3.2 Training for developers.
4. **Local website**

More detailed information on "ALADIN-Tunisie" team activities are reported on the local website which can be reached using the ftp session as following :

1. In Austria

See the report on operations and the four papers from the Austrian team.

2. In Belgium

Most efforts focused on ALATNET related research or operations, and consequently are described in other parts of these Newsletters.

Forecasting peaks of extreme pollution ***(Piet Termonia)***

The operational use of the newly proposed transport index for predicting extreme peaks of pollution from the ALADIN model output has been validated in a systematic way during the first six months of 2003, taking into account the data for 3 winters (DJF) 2000-2001, 2001-2002, 2002-2003. A paper describing this application is ready.

3. In Bulgaria

An experiment to run ALADIN on a two-processor LINUX PC ***(Andrey Bogatchev*)**

The SUN workstation on which is running ALADIN-BG came to the solid age of 5 years during this summer. It is engaged not only with running the operational suite of ALADIN-BG, but also running the wind-wave model and some special applications which create files in accordance with end-users requirements and so on. In fact we reached the limit of workstation capacity with respect of running time of the operational applications. That was the main reason to start experiments to run ALADIN on another platform.

The target machine was a Linux PC with two processors INTEL XEON, of 2.4 GHz clock-rate each, 1GB memory and 100 GB disk storage. The software packages used were:

- Portland Group Workstation with trial license (FORTRAN and C);
- open implementation of MPI - MPICH-1.2.5;
- the last AL12 export version, on which is based the operational suite of ALADIN-BG.

The corresponding data for the workstation are : SUN Ultra-60, with processor clock-rate at 360 MHz, 256 MB memory and 60 GB disk storage, FUJITSU FORTRAN and C compilers, Operating System SOLARIS 9.

There were no significant problems to port the code of the model, apart from the appropriate modifications to the timing routines and the inclusion of some "*ifdef*"-s in C routines from the auxiliary library. There were no significant differences in spectral norms running the model on a single processor on PC and on workstation, which shows that the porting was done correctly.

MPICH was configured and built with shared-memory device and *romio*, using the FORTRAN90 compiler for F90 and F77, and pgCC (Portland Group C compiler) for C. The compilation of the code was done using the name of compilers used by MPICH. The values of FORTRAN, C and pre-processor flags in the makefiles are given below :

- F90=mpif90
- F77=mpif90
- CC=mpicc
- F90FLAGS=-O2 -Mfree -mp -Mnoopenmp -Mextend -DMPI -DLX86P -pc 64 -Kieee -byteswapio
- CPPDEF =-DLX86P -DLANGUAGE_FORTRAN -DLANGUAGE_FORTRAN_90
- FFLAGS =-O2 -Mnofree -mp -DLX86P -DMPI -DSCALAR -pc 64 -Kieee -r8 -i4 -byteswapio

The tests contained several runs of the model on a single processor and on two processors, using different initial conditions. In general on single processor the execution time on PC was from 2.54 to 2.9 times better than on the SUN workstation. During the runs using two processors the scalability was from 1.78 to 1.93 related to single-processor runs. It should be outlined, that the

scalability is growing with the percentage of work of the physics package. Some wall clock timing is given below :

1. SUN workstation
   - Start Tue Jun 17 11:04:01 EET DST 2003
   - End Tue Jun 17 12:29:01 EET DST 2003
2. INTEL Xeon PC : Single processor
   - Start Wed Jun 18 13:39:44 EEST 2003
   - End Wed Jun 18 14:13:29 EEST 2003
3. INTEL Xeon PC : Two processors

- Start Thu Jun 19 14:08:05 EEST 2003
- End Thu Jun 19 14:25:36 EEST 2003

Finally one can say that the Linux PC runs the model up to five times faster than the workstation. The conclusion might look like that : the multiprocessor Linux PCs may be a cheap solution for running the ALADIN model and related applications, and might be able to ensure the possibility for running of the up-to-date cycles of the model as well as to increase the number of levels and the size of the integration domain.

4. In Croatia

See the report on operations.

5. In Czech Republic

Note: all ALATNET related R & D, representing the majority of the effort, is reported in ALATNET Newsletter. Here we sum up topics which are not referred as ALATNET ones for Prague centre.

A. Parallel Suites

See the report on operations.

B. Code Maintenance

Concerning the maintenance of the code, the main effort was concentrated on the non-hydrostatic dynamics. Some technical bugs were fixed in the recent development of the new vertical divergence prognostic variable (denoted *d*4) and were reported to the phasing team in May 2003. A development branch with a new formulation of the bottom boundary condition was prepared for the autumn phasing in Toulouse.

C. Data assimilation related issues

There was no data assimilation study made in the first semester of 2003; a study on blending is scheduled for the second semester. On the other hand quite a lot of effort was put on the installation of the Observational Data Base (ODB) software and on the validation of the related tools and model configurations at the level of CY25T1. This large volume of technical work is necessary in order to restart the data assimilation research. Before the end of June 2003 some tools and configurations were validated, such as *to_odb*, *obsort*, *lamflag*, *shuffle* , screening and CANARI analysis at least with one observation. But other needed configurations were not yet working or even tested, for example *batodb*, *mandaodb*, ALADIN 3d-var.

6. In France

Note : Only non-ALATNET work is reported here. And part of the effort of the Toulouse team was dedicated to purely ARPEGE problems.

Phasing

Cycle 26T1 was completed during the spring, with the help of Andrey Bogatchev, Adam Dziedzic, Cornel Soci, Oldrich Spaniel and Piet Termonia, and a distant contribution from Gabor

Radnoti. Its content is described in a dedicated paper by Claude Fischer. The preliminary investigation of consequences of the in-depth changes scheduled by ECMWF for cycles 27 (new data flow) and 28 (automatic cleaning of interfaces) started.

Tools and code improvements

The portability of the procedure *gmkpack* was improved : see the corresponding report by Ryad El Khatib. Besides, the cleaning of the *xrd* library undertaken by Jean-Daniel Gril, together with building the portable library *PALADIN*, progresses regularly.

The cost of configuration 927 was divided by 2 after the reorganisation of I/Os in Full-Pos (Ryad El Khatib). The search for new minimization softwares to be used in configuration 131 (variational assimilation), considering that the corresponding cost-function is quadratic, has started (Karim Yessad and Gérald Desroziers).

The 1d version of ALADIN used for the validation of physics has been modified in order to allow forcing by vertical velocity, not only divergence, and use the BOMEX and TOGA datasets. For more details about the single-column model and the corresponding extraction of vertical profiles from the full 3d model, contact Eric Bazile, Yves Bouteloup or Jean-Marcel Piriou.

An experiment of intercomparison of ARPEGE and IFS forecasting systems over a 15-days winter period, starting from IFS analyses, led to an improvement of configuration 901. Whenever possible, ARPEGE (ALADIN) forecasts must use initial soil and surface prognostic fields from the ARPEGE analyses, since the differences between the two surface schemes induces a significant spin-up, spoiling forecasts especially in cold situations. Besides, this test showed that, when halving the time-step and increasing the number of vertical levels as in IFS, forecasting skills are comparable for the troposphere, ARPEGE being still worse in the stratosphere.

Martin Bellus undertook an in-depth cleaning of ARPEGE physics (`APLPAR.F90` and below), especially concerning surface (only ISBA, `LSOLV=.T.,` allowed) and cloudiness (split of `PNEBH`), removing all unused parts of the source code (even a little too much, as appeared afterwards). Then he focused on the externalization of the ISBA scheme (for further use in AROME), resuming the work started by the climate team and merging it with the above-described cleaning. This work was pursued by László Kullmann.

Operational suites

The impact of the parameterization of deep convection was examined on an "Aladinade" (i.e. the forecast of a too deep cyclogenesis) over the Mediterranean sea in May 2003. The problem disappears when changing the closure condition or using the KFB scheme, but the underlying "why" is still a mystery. Besides, along the parallel suite testing the first change of computer, an unexpected divergence was noted, due to the propagation of very small differences in SST (single versus double precision computations). Contact points : Eric Bazile and Jean-Marcel Piriou respectively.

Rashyd Zaaboul prepared parts of the new operational suites in Morocco : computing climatological files for ALADIN-NORAF and for ALADIN-Maroc at different test resolutions, implementing locally versions 25T1 of ODB and CANARI, updating the extraction of observations... He also modified the "generic" assimilation script prepared at GMAP for 3d-var or blending, to introduce the "Blendvar" and "incremental digital filter initialization" options.

Olivier Latinne prepared the move to a far larger ALADIN-Belgium domain.

Surface analysis

Adam Dziedzic and François Bouyssel designed a cheap assimilation suite to allow testing modifications related to the surface, thus impacting only the lowest levels, during long periods at a reasonable cost in ARPEGE. Note it cannot be used to test changes in orography, likely to have a large-scale impact both horizontally and vertically. The suite is based on a blending between the modified surface and low-level fields and the large-scale upperair analysis increments from the operational 4d-var assimilation suite, as follows :

assimilation steps	*surface variables*	*upperair variables*
6 h forecast	$P^{i-1}(0) \rightarrow P^{i-1}(+6)$	$P^{i-1}(0) \rightarrow P^{i-1}(+6)$, assumed close to $P^{i-1}_{op}(+6)$
soil/surface assimilation	$P^{i-1}(+6) \rightarrow A^i$	unchanged
upperair correction	unchanged	$P^{i-1}(+6)$, $A^i_{op} \rightarrow$ $A^i = P^{i-1}(+6) + FP^{-1}[FP(A^i_{op})] - FP^{-1}[FP(P^{i-1}(+6))]$
initial state	$P^i(0) = A^i$	$P^i(0) = A^i$

A^i_{op} is the corresponding operational analysis, including 4d-var upperair followed by soil/surface assimilation. The spatial filter is based on Full-Pos, with an "up-and-down" 927 to the resolution of 4d-var increments (here T298c3.5 ↔ T161c1.0).

The cost of such a simplified assimilation suite is about 8 times less than that of a full 4d-var re-assimilation. A one-week test without modification allowed to check than the resulting upperair fields didn't differ that much from the reference run (controlling large-scale balances and spin-up).

This method was used to evaluate a set of modifications proposed along the last years by Stjepan Ivatek-Sahdan, Agnesz Mika and François Bouyssel :

- spatial smoothing of soil wetness index, with a characteristic length of 15 km,
- new statistical scheme for background errors (for 2m fields),
- reduced corrections for deep soil moisture, dividing by 2 the concerned O.I. coefficients,
- excluding coastal observations in the analyses of 2m temperature and relative humidity, i.e. for the correction of soil temperature and moisture.

As expected, the resulting soil moisture looks nicer, while the scores against SYNOP observations are slightly worse than in a similar simplified suite without changes (test along June 2003).

Configuration 923

The computation of orography (Part 1) was significantly improved :

- some more cleaning, evaluation of the impact of compilation options, ...
- possibility of importing an orography of lower spectral resolution (in the reference code, no longer requiring Ryad's modsets) (*switch :* `NLISSP=1` *and* `LNORO=.T.` *in* `NAMCLA` *)*
- spectral smoothing of orography, following the formulation tested by Klaus Stadlbacher *(switch :* `NLISSP=2` *with tuning parameters* `FLISA` *and* `FLISB` *in* `NAMCLA` *)*
- management of "non-square" (`NSMAX` ≠ `NMSMAX`) domains in the optimization of orography (case of spectral smoothing or new envelope), via an improved definition of the radial wavenumber
- lower weight of the extension zone in the optimization of orography *(switch :* `SCEXT >0` *in* `NAMCLA` *)*

In the meantime, the behaviour of the two basic cost-functions ("Bouteloup" and "Jerczynski"), as the tuning parameters or the starting point of minimization change, was examined. Attempts to go further than cycles CY24T1/AL15 failed up to now. Contact points : Jadwiga Woyciechowska, Dominique Giard, and the GCO team for up-to-date scripts.

An option for "aqua-planet" models is now available. Contact point : Dominique Giard

Last but not least

Patricia Pottier and Jean-Daniel Gril corrected the ALADIN database, for 2002 and early 2003 contributions. The next update action will address the ALADIN web site, before a migration of both under Linux.

7. In Hungary

The main area of development during the first half of 2003 was the further assessment of the 3d-var data assimilation scheme used for the ALADIN/HU model version. This topic is in fact carried out in the framework of the ALATNET project, therefore the main conclusions of this work will be elaborated in the ALATNET part of this Newsletter.

The other development areas are as follows:

Gabor Radnoti validated the B-level parallelization of the ALADIN model code together with the revision of the coupling code (see detailed description in this Newsletter).

A closer collaboration started at the beginning of the year with the forecasters : they systematically evaluate the performance of the operational model and then we are trying to respond to their inquiries. This winter the performance of the ALADIN model was rather poor, especially for a period when the cold air was dominating in the Carpathian basin together with some partial snow cover. According to the preliminary investigations the main cause of the (temperature) forecast failure was the incorrect consideration of the snow at the surface (the studies will be continued and a report will be given in the next Newsletter).

Gergely Boloni, as "data assimilation working group" leader of the LACE cooperation, prepared the working plan on data assimilation of the LACE cooperation for 2003.

8. In Moldova

Nothing new.

9. In Morocco

See the report on operations.

10. In Poland

See the report on operations.

11. In Portugal

During the first half of 2003 no relevant changes have taken place, either on the Portuguese operational suite (AL12_bf_CYCORA_bis) or on the development side, since the last report.

12. In Romania

Diagnosis of horizontal variations of forecast error covariances ***(Simona Stefanescu)***

The standard deviation and zonal, meridional and 2d length-scales for temperature were computed in both spectral and gridpoint spaces. The computations were performed using the standard NMC statistics for ALADIN-Morocco. The gridpoint derivation of length-scales was done assuming that the local auto-correlation function is flat at the origin. This assumption is based on

the fact that the correlation decreases with distance on both sides of the origin and the function is continuous at the origin. No assumption related to the auto-correlation function at the origin was made in the case of spectral derivation of the length-scale. The agreement between the length-scale maps computed in gridpoint and spectral spaces suggests that the assumption of the flat auto-correlation function at the origin, in the case of gridpoint derivation, is good. The comparison between 2d maps of gridpoint and spectral standard deviations show a very good agreement. In the free troposphere, the horizontal variations of standard deviation and length-scale are much influenced by the tropics/mid-latitude contrast, while in the low levels the land/sea contrast has more influence on the horizontal variations of standard deviation and length-scale.

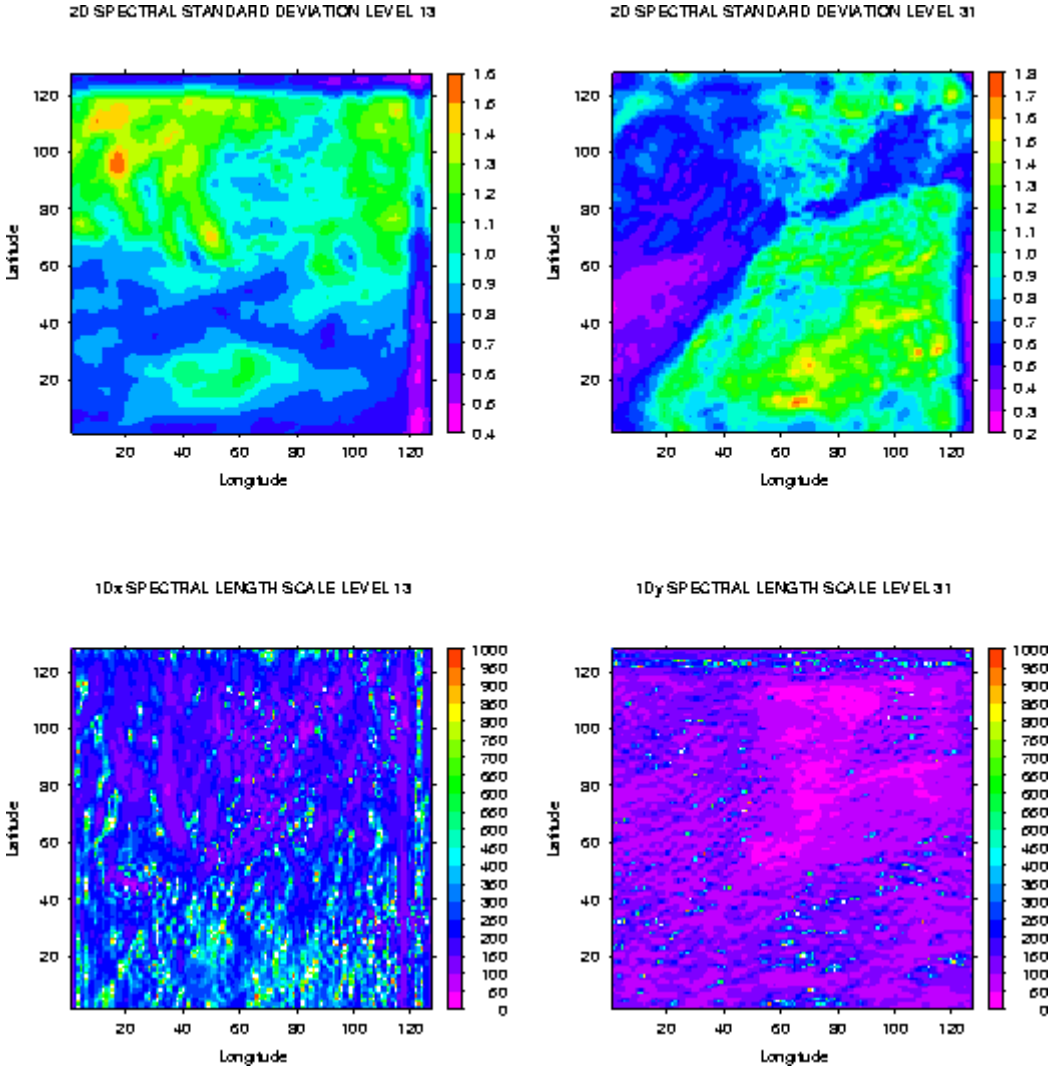

<u>Maintenance of the local aplication</u> ***(Cornel Soci and Doina Banciu)***

See the report on operations.

13. In Slovakia

Most effort was devoted to maintenance : there was very little ALADIN research carried out on SHMI. Activities can be summarized into the following points :

- A new unified framework for operational applications was created. It includes monitoring and on-line documentation. Old applications are gradually rewritten, documented and integrated into the new framework. Situation is complicated, mainly due to the fact that applications are spread among several machines. A lot of work still remains in this area.

- Versions AL15 and AL25T1 are available on DEC. An operational switch to AL25T1 is planned. Preparation of a completely new operational suite started, but the work had to be interrupted.

• Some applications using EGGX were adapted to the new geometry package and recompiled with AL25T1 libraries. In future it is planned to use PALADIN libraries for external applications, since they are independent from the model version.

• Use of CANARI to generate wind-roses in areas without observations continues. Progress is slow mainly due to the considerable time-consumption of computations needed for getting a one-year set of analyses. Dynamical adaptation of wind to 2.5 km resolution is being prepared.

• There was defended a diploma thesis studying properties of one-way Davies' coupling in a 1d linearized shallow-water model. Work started in 2001 and it was additionally inspired by presentation of Piet Termonia during the 3rd ALATNET workshop in Kranjska-Gora. Even if it deals with a set of toy problems, it might be of some interest for ALADIN community. However, the thesis was written in Slovak.

• MOS on ALADIN outputs was planned few years ago, but the work still have not started. There is a student willing to make his diploma thesis on this topic. He will investigate ability of simple MOS to improve 2m temperature forecast. Complications are expected to arise mainly from the inhomogenity of ALADIN time-series (frequent changes in operational models).

14. In Slovenia

The main ALADIN activity was the implementation of the operational ALADIN suite on the new server (see the report on Operations). The other activities focussed on the ALATNET research topics (see the ALATNET Newsletter).

15. In Tunisia

See the report on operations.

1. In Toulouse

The work of the ALATNET PhD students in Toulouse is described in separate reports, as well as other PhD reports. The summary hereafter corresponds to the joint efforts of the other visitors and the permanent staff.

1. Theoretical aspects of non-hydrostatism (NH) *(P. Bénard)*

A major step forward was achieved with the implementation of "SITRA" innovation proposed by Pierre Bénard and described in the previous Newsletter. It relies on the use of 2 different reference temperatures in the semi-implicit solver in order to stabilize both acoustic and gravity waves. And it proved quite efficient !

2. Noise control in high-resolution dynamics (*F. Vana*)

Further experiments using "SLHD" (flow-dependent gridpoint horizontal diffusion based on the dissipative properties of semi-Lagrangian interpolators) were performed : see the joint paper with A. Simon and the corresponding PhD reports.

3. Specific coupling problems

a) Blending (D. Klaric, C. Fischer, P. Riber)

A database of reference experiments on MAP IOPs was prepared and some choices re-examined. From this and careful tests in a quasi-operational framework with ALADIN-France, the potential contribution of dfi-blending to forecast skill was reassessed : very small in most situations, though quite important in some characteristic ones. Accordingly work on this topic stopped in Toulouse.

b) Tendency coupling for surface pressure (J.M. Audoin)

Further tests and retunings, based on the latest library, didn't show a significant impact of the method.

4. Reformulation of the physics-dynamics interface *(M. Tudor, J.F. Geleyn, K. Yessad)*

The methodology developed for diagnosing "sleeping" problems of nonlinear instability and/or stiffness has been applied to the new state of the operational physics package, in ARPEGE this time in order to face more situations simultaneously. At this occasion the culprit for a long-standing problem (spurious oscillations at temperatures just around the triple point) was found and corrected : a too high ratio between the assumed fall speeds of liquid and ice precipitations.

Besides work restarted around the use of RT instead of T as prognostic variable, an option to be considered when going to very high resolution and more detailed physics.

5. Adaptation of physics to higher resolution & Design of new physical parameterisations

Most of the work in this domain was dedicated to the tuning and validation of the "DICORA" and "COCONUT" packages, described in the previous Newsletter.

A reformulation of the description of drag and lift effects from unresolved orographic features, in order to be able to suppress the currently used artefact of an enhanced topography (the so-called envelope orography) was also investigated. The scheme for mountain effects was revised and the lift effect was made orthogonal to an estimate of the geostrophic wind and not any more to the wind itself. Intensive experimentation and retunings led to the conclusion that envelope orography could be removed with equal quality scores and a better description of the flow in the mountains' vicinity, with positive consequences on the rainfall forecast.

6. Use of new observations

a) Quality control and selection of observations for a mesoscale LAM (D. Puech)

The ODB (Observation Data Base) management was regularly improved, in order to take into account new observation types or new parameters (such as observation height or the statistical model for observational errors). The documentation was improved too.

b) More extensive and accurate use of conventional observations (P. Moll, M. Jurasek)

The observations of "10 m" wind received significant attention. Over sea, corrections were brought in order to use the real altitude of data (on average 7 m for buoys and 24 m for ships !). On land, the design of a careful black-listing procedure (since attempts to use directly the model information on orography for observation selection failed) allows to use them now. Besides the observation operator was improved in order to better take into account the vertical structure of the boundary layer.

c) Use of satellite data

The major step concerned the newly available MSG/SEVIRI data, provided by Meteosat Second Generation at very high spatial and temporal resolutions (5 km and 15 mn), and including informations on the variations of temperature and humidity. The whole procedure to use such observations was designed, and impact studies performed using ALADIN 3d-var assimilation, at various spatial resolutions (10 km, 2.5 km) and frequencies (from every 6 h to hourly analyses). No significant impact on the forecast of temperature was found, but the humidity and cloudiness fields are improved up to 24 h. Papers by T. Montmerle are available in the previous Newsletter and on the ALADIN web site : *http://www.cnrm.meteo.fr/aladin/scientific/2003-program.html* .

Else preprocessing and quality control procedures were designed for new, higher resolution, observations (Geowinds, locally received AMSU-A data, HIRS), and a sensitivity study performed with ALADIN. See also the PhD report of M. Szczech.

d) Progressive use of some non-conventional data

A work plan for the use of radar data was designed by F. Bouttier, M. Jurasek and V. Ducrocq. See the corresponding paper .

7. 3D-Var analysis and variational applications

a) Description of background error statistics and investigation of the problems related to biperiodicity (C. Fischer, V. Guidard, L. Berre)

Results about the use of compactly-supported functions to solve wrap-around problems are presented in the PhD report of V. Guidard.

An overview of the work performed around background error statistics in ALADIN and ARPEGE along the last year is available in the HIRLAM Newsletter n° 43, or on the ALADIN web site : *http://www.cnrm.meteo.fr/aladin/scientific/2003-program.html* .

b) Cycling strategy (V. Guidard, C. Fischer)

An alternative to blending for relaxation towards the analysis of the coupling model was proposed. It will be described in the next Newsletter.

2. In Bruxelles

The last young researcher, Martin Gera, left Belgium at the end of May.

1. Coupling problems (topics 5 & 6)

a) Monitoring the temporal interpolation (Piet Termonia)

Extra techniques for the monitoring of the coupling-update frequency have been investigated. In particular, it has been studied how a deficiency due to the temporal interpolation can be anticipated by filtering the forecast of the coupling model during the model run with a recursive digital filter.

b) Well-posed lateral boundary conditions (Chantal Moussy, Piet Termonia)

The work on an alternative formulation of the lateral boundary conditions (i.e. adapting the study of Aidan Mc Donald to a spectral model) has started, using a simple 2d shallow-water model first.

2. Refinements in physical parameterisations (topics 8 & 9)

a) Introduction of prognostic cloud water in a refined convection scheme (Luc Gerard)

The development of an integrated scheme for subgrid (convective) and resolved precipitations, implying cloud condensates as model variables, is going on. It presents an interesting auto-extinction behaviour when the reduction of the mesh-size increases the resolved contribution to precipitation and cloudiness (see Figure 1). Continuing work aims at replacing the precipitation output of the convective-updraught scheme by an output of cloud condensate, feeding the same microphysical scheme than used for estimating the resolved contributions. The new system also separates the downdraught calculation from the convective-updraught one, thus allowing them an independent life cycle, the downdraught being fed by precipitation evaporation, whichever be the origin of it. Tests in the 1d model seem to give interesting results, while the 3d implementation stays a never ending story.

b) Improved representation of boundary layer, based on a parameterization of Turbulent Kinetic energy (Martin Gera)

See the corresponding report.

c) Improved representation of orographic effects (Bart Catry)

See the dedicated paper.

3. 3D-Var analysis and variational applications (topic 11)

Wavelet representation of background error covariances (Alex Deckmyn)

Work on a wavelet representation of background error covariances was continued. Alternative transformations like "Maximal Overlap" wavelet transforms have been considered, but appeared too costly in time and memory usage. Errors caused by sub-sampling in the orthogonal wavelet transform continued to be the main hurdle, but the problem has been solved recently.

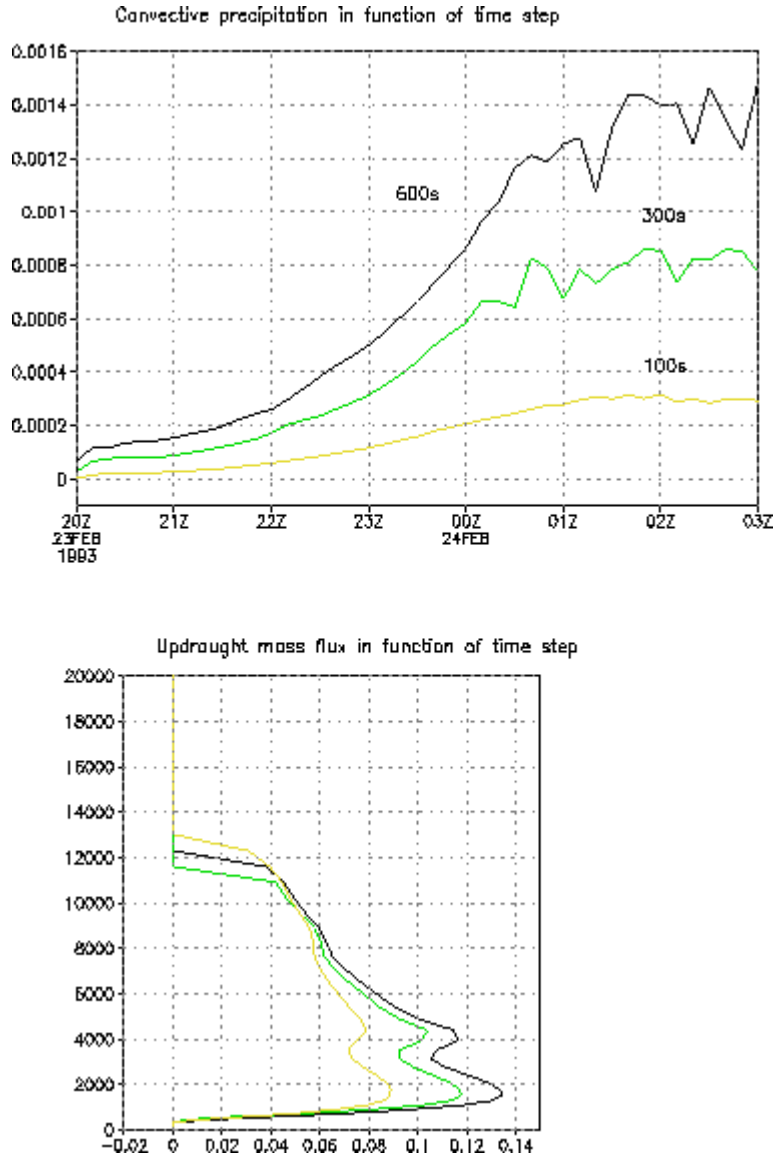

Figure 1 : Evolution of fluxes as the time-step decreases* in the 1d version of the new convection scheme, on the TOGA case. Upper part : Time evolution of convective precipitations at the surface. Lower part: Vertical profile of the updraught mass-flux.* (black : 600 s, green : 300 s ; yellow : 100 s)

3. In Prague

1 Theoretical aspects of non-hydrostatism

a) Top and bottom boundary conditions *(P. Smolíková, R. Brozková, J. Masek)*

Since the second half of the year 2001 the research on the so-called "chimney problem" has continued and it is now reaching important conclusions. As described in previous reports, the problem is manifested by a spurious standing wave above mountain tops when semi-Lagrangian advection is used. This spurious wave-pattern is called "chimney" according to its typical shape, see the example of the potential flow regime on Figure 1.

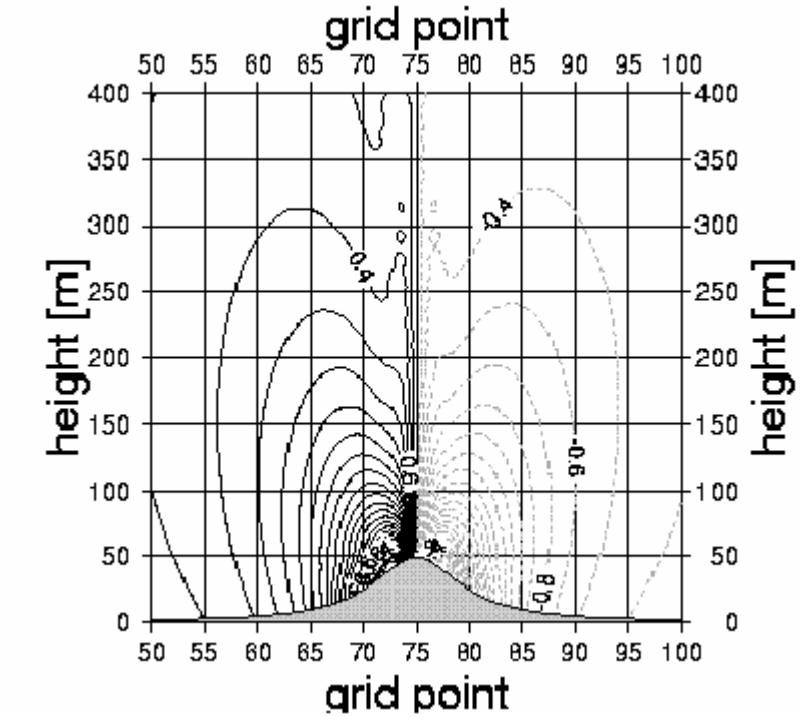

Figure 1 : Vertical velocity (w) of the potential flow regime in case of semi-Lagrangian advection. The chimney results here in a deformation of the w-isolines above the mountain top (for example the isoline of 0.4 m/s or 0.2 m/s).

Back in spring 2002, the analysis of the equations pointed to the vertical momentum equation, in particular to the fact that a "vertical divergence" type of variable is advected (C. Smith, personal communication). One hypothesis was that the advection of a vertical derivative (vertical divergence) is unstable and creates the observed noise. Another hypothesis was that the formulation of the bottom-boundary-condition term for this equation was not optimal for the semi-Lagrangian advection case. In order to cope with both plausible reasons, the advection of vertical velocity *w* was proposed instead of the advection of vertical divergence. This scheme was developed and, as expected, it provided a nice solution in the academic test environment. On the other hand this scheme is technically rather complex. The advected quantity is staggered on "half" levels of the vertical grid while the trajectories are computed at "full" levels. The change of variable is requested only for the solution of the advection, which requires the correct handling of the purely explicit part as well as of the linear semi-implicit correction part of the equation. In practice it means introducing some additional interpolation buffers carrying the linear terms of the equation (computed for the vertical divergence prognostic variable), which need to be evaluated at the origin point of the trajectory. There are some particular cases when the use of the additional buffers may be avoided, for example the case of the d_0 variable (but this variable is far from being optimal for the stability of the scheme) or two-time-level non-extrapolating scheme, usable only with predictor-corrector scheme, without decentering (J. Vivoda, personal communication). The current reference (AL26T1) code of the *"w*-advection" scheme handles only the case of the d_0 variable.

Due to the above-mentioned complications and more particularly due to the accidentally

mismanaged treatment of the linear terms in the first version of the *"w*-advection" code, the idea on a true semi-Lagrangian treatment of the bottom boundary condition emerged. In this case the acceleration term present in the bottom boundary condition is discretised in time and space like any full time-derivative, along the trajectory. Some additional interpolations are needed, too, but they remain modest, required for the lowest model level only. Then it is rather easy to handle all the required cases : all choices of the vertical-divergence variable, two-time-level or three-time-level schemes, with or without iterations, decentering or extrapolation.

The new treatment of the bottom boundary condition has been coded and tested for a large variety of options. The tests were performed with the vertical-plane version of the model for the potential flow and non-hydrostatic nonlinear regime, further with the 3d adiabatic code for the ALPIA and PYREX tests. The results were fully comparable with those obtained using either the Eulerian advection or the advection of the vertical component of the wind (i.e. without chimney wave, see Figure 2).

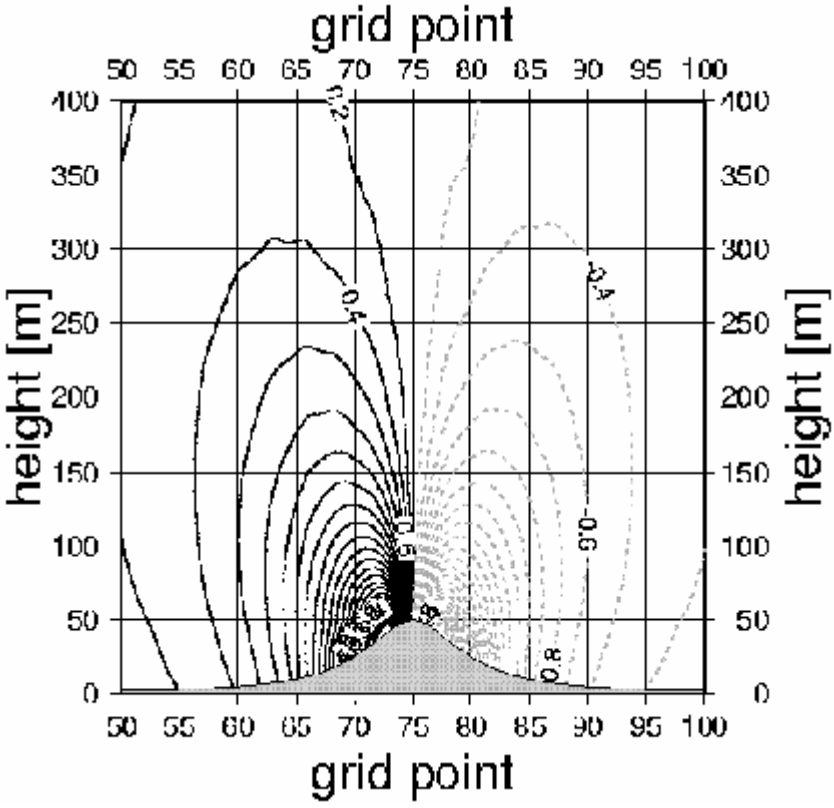

Figure 2: Vertical velocity (w) of the potential flow regime in case of semi-Lagrangian advection but with the new bottom-boundary-condition treatment. This result is fully comparable with the one obtained either when using the "w-advection" scheme or Eulerian advection (not shown).

It still remains to understand exactly the mechanism of the chimney creation. While the two schemes mentioned above (the advection of vertical velocity or the true semi-Lagrangian treatment of the bottom boundary condition) were successful in eliminating the spurious wave, it is not very clear what was the true origin (perhaps more origins) of having the chimney wave or not. Some very recent experiments carefully suggest that a dissipative operator (like interpolators or blind application of the linear horizontal diffusion) acting on the orography gradient may have similar chimney effects.

Besides the bottom boundary condition present in the vertical momentum equation, the same kind of term appears also in the horizontal momentum equation; however it seems to be less important. There was a special study to assess the influence of a different treatment of this term present in the horizontal pressure gradient computation, but the results did not show any real sensitivity to it.

A last little study was also devoted to figure out whether an alternative discretisation of the

so-called Z-term in the vertical divergence equation would bring better results (either in stability or quality). The Z-term is a working notation of the scalar product of the horizontal derivative of the vertical wind with the vertical derivative of the horizontal wind. This cross-term occurs due to the change of variable from the vertical wind to the vertical divergence. For the moment there are not yet any results which could clearly demonstrate the advantage of this or that spatial discretisation of the Z-term.

b) Predictor-Corrector scheme *(J. Vivoda)*

The general properties of the Iterative Centered Implicit (ICI) schemes were studied (the predictor-corrector scheme is an ICI scheme with one iteration). The attention was mainly devoted to the precision aspects, for example whether the propagation of the long Rossby waves is not substantially affected by the ICI. For this purpose academic systems were analysed and real case studies were also made. It can be said that the obtained results were as good as when using the classical semi-implicit scheme; however the stability of the scheme was considerably increased when using the ICI scheme. More details on this work may be found in the corresponding young researcher report.

2. Horizontal diffusion related issues *(R. Glavac-Sah, F. Vana)*

After completing the tuning of the Semi-Lagrangian Horizontal Diffusion (SLHD) parameters, which should be robust with respect to the horizontal resolution and time-step length of the model, a quite intensive experimental work took place in spring 2003. The study of the SLHD properties was extended to the non-hydrostatic dynamical kernel of ALADIN, where the ALPIA quasi-academic environment was used at resolutions of 5 km and 2.5 km. Besides the SLHD scheme was tested on some selected real cases, for example when the operational model forecast suffered from too intensive cyclogenesis. All details on the recent work on the SLHD scheme can be found in the contribution of Filip Vana in this Newsletter.

3. Physics-dynamics interface related issues *(M. Tudor)*

The first study on the general behaviour of the physics used with the Predictor-Corrector scheme took place in June. For this purpose, four nested ALPIA domains were prepared, this time not as quasi-academic environment but as real geographical domains with real mapping. The so-called climatological files were prepared for the ALPIA resolutions of 10 km (domain A), 5 km (domain B), 2.5 km (domain C) and 1.25 km (domain D). The orography used for each of the respective academic ALPIA domains was injected into these real climate files. The beginning of the study with the model physics was prepared on domain A with 10 km horizontal resolution. In the vertical, 37 levels were used alike in the recent LACE model and the coupling files were made directly from the ARPEGE analysis and forecasts. At this resolution the tests are safe with respect to the grey zone problems and the non-hydrostatic effects are also not expected to be significant. Thus the first test was meant to show a neutral behaviour of the PC scheme in ALADIN-NH with physics compared to the operationally used options (SI scheme and HPE system) or to the SI scheme in ALADIN-NH. This choice revealed to be quite wise, since many technical problems occurred when for the first time the physics was branched together with the PC scheme. It turned out that the PC scheme in ALADIN-NH was coded without any preliminary care for the buffers carrying the tendencies of the physics. An effort was made to correct the basic interface, however it is not yet quite sure that all the bugs and shortcomings were found and properly corrected. Thus the so-far obtained results are partial and will have to be confirmed.

4. Physics related issues

Effects of the orographic lift *(R. Brozkova)*

Given the encouraging results of the study made by Dunja Drvar last December, a new tuning of the orographic lift parameterization together with abandoning the envelope orography was more intensively tested. As test period the month of January 2003 was chosen since there were many typical situations with stable vertical stratification. The scores were computed for this test period and they have shown that the lift parameterisation does not sufficiently compensate the effects of

the envelope orography; for example the geopotential bias has got worse compared to the operational reference. The resulting scores may be consulted on the parallel test web page, the name of the suite is ABY. The impact of the tested configuration may be also seen quite easily on the structures of the mean-sea-level pressure in the mountainous areas : when the envelope orography is not used, the blocking effect of the mountains is clearly smaller. For the time being it was concluded that a more in-depth study on the acting of the parameterisation of the gravity wave drag and orographic lift needs to take place.

4. In Budapest

The most important ALADIN-related activities at the Hungarian Meteorological Service are concentrating on the scientific topics defined in the ALATNET research plan. Our Service was active in the following ALATNET sub-topics (in parentheses the topic number refers to the ALATNET research plan) during this semester: specific coupling problems (topic 6), design of new physical parameterisations (topic 9), use of new observations (topic 10), 3d-var analysis and variational applications (topic 11).

Hereafter the main activities in these subtopics will be briefly described.

1. Specific coupling problems

We have actively participated to the coupling mini-workshop held in Ljubljana during this spring.

Some investigations started with the implementation and tuning of explicit spectral blending for ALADIN, when a simple spectral blend is done between ARPEGE analysis and ALADIN forecast. The preliminary tuning of the blending scheme was meant as preparation for a work to be performed in Prague : systematic comparison of DFI and spectral blending (this work is still under elaboration and its outcome will be presented in the next Newsletter).

2. Design of new physical parametrisations

The only work performed on this subject was devoted to the design of the new physics-dynamics interface needed for the new generation of the ALADIN model (along a 3 months Toulouse stay).

3. Use of new observations

At the Hungarian Meteorological Service it is of great importance to apply and enhance the efficiency of the ALADIN 3d-var data assimilation scheme for the improved representation of the initial conditions of the ALADIN model. The reference version of the 3d-var scheme is using surface (SYNOP) and upperair (TEMP) observations during the assimilation process. It is of particular interest on the one hand to assess the performance of the scheme with respect to the operational dynamical adaptation scheme and on the other hand improve the scheme with the application of new types of observations : satellite (ATOVS) and aircraft (AMDAR) data. The first results using satellite and aircraft data are presented in separate articles of the Newsletter (click here or here).

4. 3d-var analysis and variational applications

Our ALATNET young researcher Steluta Alexandru continued her work with her last stay in Budapest (6 months). Her subject is "Scientific strategy for the implementation of a 3d-var data assimilation scheme for a double nested limited area model". Two reports (part 1, part 2) of Steluta can be found in this Newsletter, describing the latest results of her investigations.

With the introduction of the 3d-var scheme in the parallel suite of our Service a possibility had been opened for the systematic comparison of the dynamical adaptation (operational) scheme with the reference 3d-var version (using SYNOP and TEMP observations only). Beside the systematic comparison some case studies were also carried out in order to see, whether the 3d-var scheme is able to make improvements with respect to the operational model forecast and on the other hand doesn't destroy already successful numerical forecasts.

The main conclusions of the comparison are as follows :

♦ Case studies : two special cases were studied. For the first case (a summer heavy convective case) the 3d-var scheme brought some improvement into the poor performance of the operational model version. Unfortunately the improvement was only partial and a bit delayed, nevertheless it gave a good indication for the forecasters on the forthcoming event. The reason for this improvement was probably the application of surface observations for Hungary, which helped in the better description of the boundary-layer processes important for such a convective

phenomenon. The second case was a frontal one, which caused some floods along the Danube River during August, 2002. Already the operational forecast was reasonably good and the 3d-var governed forecast was equally good, therefore in that case data assimilation didn't make any deterioration in the already successful forecast.

♦ As far as the systematic comparison is concerned, simple statistical scores, like bias and root-mean-square errors, were computed for the operational and 3d-var model versions and compared with the help of graphics. The main conclusions of this comparison are as follows :

- The two versions are behaving rather equally, nevertheless the 3d-var forecasts provide slightly worse scores than the operational ones.
- The difference is diminishing from the surface to the higher atmosphere.
- For some fields and for some particular forecasting time some improvements can be detected.

♦ As a summary the main conclusions of the comparison can be listed as follows :

- The recently used observations (SYNOP and TEMP) provides very few additional new information with respect to the ARPEGE analysis used as initial state for the dynamical adaptation.
- The ARPEGE 4d-var scheme used to provide initial conditions for the dynamical adaptation run is providing rather good and realistic analyses resulting in an already relatively good performance of the data assimilation scheme.

Based on this study we decided to keep the 3d-var experimentation as a parallel suite and not introduce it into the operational ALADIN suite.

The work mentioned at the last Newsletter on the sensitivity studies with respect to the initial conditions of the ALADIN model continued and is described with some details in this Newsletter (click here).

Besides first experimentation started on the "singular vector" (601) configuration of the ARPEGE model. The ARPEGE configuration was tried first due to the fact that, for the LAM EPS project, first a properly targeted set of singular vectors should be computed for the global model, then the global model should run with different initial conditions modified by the relevant singular vectors and finally the limited area version (ALADIN) should be coupled by the different global model version). The first tests were technically working, however the validation of the results is not yet finished.

5. In Ljubljana

The main ALATNET event in the first half of 2003 was the mini-workshop on coupling (see the report here).

Besides the work of young researchers (Klaus Stadlbacher and Raluca Radu), described in their separate reports (K. Stadlbacher, R. Radu) , the main ALATNET topic was an extensive study of coupling and nesting performed by J. Cedilnik and G. Gregoric. For the purpose of this study the ERA reanalysis data from ECMWF was taken and an optimal coupling strategy was searched for downscaling of relatively sparse data (T159 horizontal grid with resolution about 200 km) to a typical grid resolution of today limited-area models, i.e. approximately 10 km.

The goal of performing such a regionalization of ERA data is to obtain a long series of consistent model data in order to support climatological studies which suffer from spatial and temporal inhomogenities. The optimal coupling strategy had to balance between two sources of errors: multiple nests tend to push information-providing lateral boundaries away from the region of interest and weaken constraint between innermost nest and global fields. On the other hand, no intermediate nest would cause unacceptable ratio (approx. 1:20) between the driving and coupled model resolutions.

For integration duration there is similar problem : shorter integration times tend to keep model in constant shock due to spin-up; longer-than-necessary integration on the other hand lose information from the initial state.

Our target domain was the previous operational ALADIN/SI domain. Various scenarii of coupling (single, double and triple nesting) and integration duration (6 hours to one week) were implemented and tested on MAP-SOP data. Results show that (as expected) triple coupling and week-long integrations were significantly worse than others. However, the difference between single- and double-coupled runs was surprisingly small. RMS error computed from radio-soundings data is smallest for single-coupled runs. In case of precipitation the Heidke skill-score is highest for double-coupled 48 h integration with 12 h time-lag for spin-up. This setup is now considered for runs over longer periods. Currently we are planning to perform 10 years of ERA regionalization with 2.5 km dynamical adaptations to study wind climatology.

Improvements of the compiling procedure "gmkpack"

Ryad El Khatib

Météo-France . CNRM/GMAP

The procedure "*gmkpack*" used at GMAP to compile, build archive libraries and make executables in the framework of ARPEGE/ALADIN has been recently improved in the scope of its portability. The aim is :

- first to enable its installation on any other platform than the Fujitsu machine of Météo-France ;
- second to enable an independent group of developpers to create and use complete "main" source packs with it.

While the first point looks achieved, the second one is still under progress. From now this new version is available for tests and it should become the default one by the end of the year.

New cycle CY26T1/AL26T1

Claude Fischer
Météo-France . CNRM/GMAP

Here is a brief overlook of the modified or new features in cycle 26, compared with cycle 25:

- new distributed-memory data layout for the ARPEGE/ALADIN control variable (Y. Tremolet, C. Fischer)
- ALADIN transform package is now incremental
- work in the direction of B-level and LSPLIT in ALADIN (G. Radnoti, A. Bogatchev)
- new coupling data layout, and coupling call extracted from the TAL package (G. Radnoti)
- IFS features : cleaning in NNMI
- Fullpos B-level in ARPEGE

The validation is well advanced, but some ALADIN developments remain in a shaky situation:

- NHS /*d*4 variable : problems in multi-processor, no stable test in "*mitraillette*" for the time being.

The next cycle 27 will be much more difficult for ARPEGE and ALADIN configurations, since it will concern the new data flow in the core of the model. The new data flow layout is under preparation by Mats Hamrud. It will allow for a more flexible definition of new variables, in the frame of a pre-defined Fortran90 structure, with several control keys (advected, spectrally transformed, etc...).

There will however first be a number of impacts on the ALADIN code that will require a recoding of some obsolete parts (gridpoint data coupling, NHS buffers for auxiliary variables). Some implications might not have been foreseen for the time being !

The ALADIN phasing to CY27 will probably take place over october/november 2003. In between AL26T1 and CY27, a cycle AL26T2 should be created to introduce the cleaned physics interface (MF_PHYS, APLPAR), mostly developped by M. Bellus and L. Kullmann under the supervision of J.F. Geleyn and F. Bouyssel.

Report on the present parallelization level of ALADIN code and on the re-design of coupling data stream to make it conform with "B-level" parallelization

G. Radnoti - 2003/03/16

Preliminary remark :

All the code developments and tests below in this report have been performed on AL15_03. A careful phasing will be necessary.

Introduction

ALADIN has been able to run in parallel mode using MPI for many years, but there were strong limitations in its parallelization level with respect to ARPEGE/IFS :

* In ARPEGE/IFS optionally one can use the so-called B-level parallelization. B-level parallelization means that the computational domain is distributed among processors in a two-dimensional way (in A-level parallelization all this is much simpler, distribution is done only in one dimension). The way of this two-dimensional distribution varies within the time-step and some transposition routines take care of going from one kind of distribution to the other. For example in the gridpoint space fields are distributed in the two horizontal directions. In the spectral space fields are distributed according to groups of zonal wavenumbers and along the vertical. In some parts of spectral computations (e.g. semi-implicit part), however, one needs all the vertical levels simultaneously, therefore distribution is transposed such that all vertical level are recollected and coefficients of the groups of zonal wavenumbers are further partitioned. The design of this B-level parallelization is suitable for ALADIN and in most parts of ALADIN code B-level requirements have been respected. Nevertheless this option has never worked in ALADIN. As time goes by, situation would become worse and worse because developers have no possibility to test their new developments in B-level environment, therefore sometimes they may even fully neglect these constraints. That is why we have decided that it is high time to catch up with the parallelization level of the global model.

* Situation is very similar with the so-called "*LSPLIT*" option, that intends to provide a perfect load balance for gridpoint computations both in A-level and in B-level parallelizations by allowing to break the last "latitude row" of a given A-set and to start the next A-set from this "breakpoint". An A-set in gridpoint space means a set of processors that treat the same group of latitude rows (in A-level parallelization therefore an A-set is a single processor, in B-level all the processors working on the same group of latitudes, but over different longitudinal bands belong to the same A-set).

In 2001 the spectral transformations have been externalized and put into a separate package (*tfl* for ARPEGE/IFS and *tal* for ALADIN). Since during the transformations model fields "spend some time" in all possible "model spaces", basically all parallelization-related setup has been moved to this package. In the external package one can run stand alone tests without any model computations and it gives a possibility to test the parallelization design in a much simpler environment. Therefore we decided to make the first step toward B-level parallelization and *LSPLIT* inside the *tal* package. If it works, it proves that the design and setup of B-level parallelization is perfect for ALADIN and work can be continued on the model side.

Modifications and tests on *tal* package

B-level

After some basic tests it turned out that problems occur only with the momentum fields. This immediately suggested that the specificity of ALADIN, i.e. the mean wind, is most probably not treated in a B-level-conform way. Indeed, vertical distribution was not included in the code for mean wind after reading spectral wind fields, and it was incorrectly (for B-level) distributed to all assets in direct transforms, where only the A-set holding wavenumber zero computes mean wind and it has to be distributed to all the other assets. After correcting these bugs B-level was perfectly working in the *tal* package.

Modified routines :

testtrans.F90 :	main program of stand-alone *tal* tests, vertical distribution of mean winds was included
euvtvd_mod.F90 :	B-level conform distribution of mean wind within a B-set : all A-set processors within the same B-set (set of vertical levels) must receive mean wind from the processor holding wavenumber 0)
gath_grid_ctl_mod.F90 :	a small *tfl* bug that was identified during tests (bug reported to IFS)

LSPLIT

The fact that *LSPLIT* option did not work in the package was in a way surprising because in this respect there seemed to be no principal difference between *tfl* and *tal*. However, it was easy to find that some differences exist and they are related to the ALADIN specific requirement to distinguish between C+I rows and E rows of the domain as far as computational demand is concerned. The tunable parameter called *TCDIS* is a predefined weight factor and in the ALADIN code it is taken into account when setting up gridpoint-space A-sets. This was the only reason why *tal* and *tfl* setup differed conceptually. Nevertheless this concept contradicts in *LSPLIT* case with some assumptions of the code and these contradictory assumptions (all processors have as much as possible the same number of gridpoints to treat up to the level of division modulus, i.e. a group of processors have one more point than the rest according to the modulus) and these assumptions have never been correctly replaced in ALADIN. We decided to drop the *TCDIS* concept which does not only bring us immediately to a correctly working *LSPLIT* option, but also makes the *tal* setup very close to the *tfl* one, which is a very convenient advantage.

E-zone treatment:

In the previous point I have mentioned the meaning of parameter *TCDIS*, that we have decided to drop. The solution that we have chosen instead is that we do almost the same distribution strategy as in ARPEGE with the difference that for gridpoint computations, when we distribute latitudes among A-sets we consider *NDGUX* as total number of latitudes instead of *NDGL* and at the very end we attach all E-zone rows to the last A-set (this means a very slight modification of *sumplat.F90*, *sumplatb.F90* and *sustaonl.F90* $\Rightarrow$ *suemplat.F90*, *suemplatb.F90*, *suestaonl.F90*). This is the case for gridpoint partitioning. In Fourier space, before zonal direct transforms fields are transposed to full latitude bands. Therefore a re-partitioning is performed where in principle the latitude set of each A-set may differ from that of gridpoint partitioning. This is controlled by *sumplatf.F90*. (In *LSPLIT* case this partitioning necessarily differs from that of gridpoint space, since in gridpoint space latitudes are broken, while in Fourier space they must not be). E-zone transforms are not cheaper than C+I ones, so it is reasonable to use in Fourier space the same partitioning as in

ARPEGE, i.e. not making difference between E-zone rows and C+I rows in this respect. It was tested in *tal* and it works perfectly.

We have to see that with this new solution even when *LSPLIT*=false, Fourier-space distribution differs from gridpoint one, i.e. *NDGLL=NDGENL* will not be true any more. Therefore in ALADIN code one has to be very careful with the correct usage of *NDGLL* vs *NDGENL* !

Modified routines :

suemplat_mod.F90 : *suemplatb_mod.F90* :	new versions are much closer to *tfl* counterparts than before,*TCDIS* fully dropped
suemp_trans_mod.F90 :	calls *suetaonl.F90* instead of *sustaonl.F90*, and *suemplatf.F90* instead of *sumplatf.F90*

New routine:

s*uestaonl_mod.F90* :	a slightly modified version of *sustaonl.F90*

Removed routine:

suemplatf_mod.F90

After all these modifications the transform package works for all parallelization options. Performance tests are not meaningful with the package itself because no real gridpoint computations are involved.

Further fix on the package

Later at ALADIN tests a further small bug was found and corrected within the *tfl/tal* packages, in routines *inv_trans.F90*/*einv_trans.F90*. Bug has been reported to IFS, so care is taken on its fix in further cycles.

Modifications and tests on ALADIN (configuration 001)

The fixes performed on the *tal* package provided a firm basis for starting ALADIN tests and modifications. Before starting the testing, debugging, fixing actions, I decided to re-design and re-code the coupling data-stream because it was known in advance that the original version is completely not suitable for B-level and *LSPLIT* requirements.

I. Design of a new coupling code (only technical and not scientific aspects)

I.1. Why is the original solution not good?

The way how coupling is performed in the original version of ALADIN is full of compromises that were always taken when we wanted to quickly adapt our code to the new environment, mainly coming from ARPEGE developments. The coupling code was designed in the early times to act on full latitude rows in a way that (I+E)-zone points of the given full latitude are modified by the large-scale information. For the above-mentioned reason we always kept this concept, though the present version of ALADIN code is hardly suitable for such an arrangement. This full-row concept is not only uncomfortable, but more painfully it gives unavoidable limits to optimization of performance, as far as parallelization and load balance are concerned. To see these problems we have to understand a little bit how different partitioning concepts are present in the code.

In gridpoint space, in the most general case we have latitudinal and longitudinal partitioning (B-level parallelization) and to have a perfect load balance if *LSPLIT*=true, we may even break the last latitude of each latitudinal partition (A-set). It is obvious that from such a partitioning it is not

straightforward to prepare for coupling if the full-row concept is kept. Fortunately (now I would rather say unfortunately) we could find a way out : after gridpoint computations, first one has to perform direct zonal Fourier transforms that also act on full latitudes. In the code it is done by going from the above-described gridpoint distribution to Fourier-space distribution where we have bands of full latitudes, and the other direction partitioning is replaced by vertical partitioning. At first sight this organization of arrays is suitable for coupling requirement (full rows are produced) and that is how we made our short-cut solution, but :

- we cannot use B-level parallelization since the coupling requires all vertical levels at one processor, due to semi-implicit character of coupling
- we are forced to use the same latitude-wise partitioning in gridpoint and Fourier spaces,
  $\Rightarrow$ *LSPLIT* is out of question
  $\Rightarrow$ we can't distinguish computation costs of rows in gridpoint space where there is no cost, and in Fourier space where cost of direct transforms does not depend on E-zone or (C+I)-zone.
- we were forced to call coupling from the *tal* package because the Fourier-space re-partitioning is done there

All these encouraged me to propose a new design. Below I write it down.

I.2. Skeleton of the new design

The natural location of coupling in the code is after the *"cpg, cpglag"* loops, when the *GPP* (*NPROMA,:,NGPBLKS)* arrays are filled with the result of gridpoint computations. Therefore it is natural to couple directly this array. What to do to this end ?

I.2.1 suesc2.F90

The information related to coupling is computed there.

In the new plan we should directly couple the *GPP(NPROMA,:,NGPBLKS)* arrays as they come out from *cpg*-scanning. More precisely we should at one go collect all I+E-zone points to an array and do the coupling on it. To make it easy, at the level of *suesc2.F90* we have to compute and store :

i) latitude, longitude index for *GPP*, dm-local arrays

! definition

```
NLATGPP(JPROMA,JGPBLKS)
NLONGPP(JPROMA,JGPBLKS) :
```

! global latitude and longitude index of the *(IPROMA,IGPBLKS)* element of *GPP* on the given processor; in the last block, when *IGPBLKS=NGPBLKS* usually there is rubbish in the tail, where we should put -99999 both for *NLATGPP* and for *NLONGPP*.

! computation of *NLATGPP*, *NLONGPP*

```
NLATGPP(:,:)=-99999
NLONGPP(:,:)=-99999
IPROMA=0
IGPBLKS=1
DO JGL=NDGSAL,NDGENL
  IGLG=MYLATS(JGL)
  DO JLON=1,NONL((NPTRFLOFF+JGL,MYSETB)
    ILONG=NSTA(NPTRFLOFF+JGL,MYSETB)+JLON-1
    IPROMA=IPROMA+1
    IF (IPROMA > NPROMA) THEN
      IPROMA=1
      IGPBLKS=IGPBLKS+1
    ENDIF
    NLATGPP(IPROMA,IGPBLKS)=IGLG
    NLONGPP(IPROMA,IGPBLKS)=ILONG
  ENDDO
ENDDO
```

```
      IF (IGPBLKS /= NGPBLKS) CALL ABOR1("SUESC2: CONFLICT IN NGPBLKS")
```

ii) latitude, longitude index for *GT3BUF*

! *GT3BUF* is the buffer holding large-scale values, but in packed mode, i.e. only (I+E)-zone values are stored there

```
      NEDLST:
```

! number of coupling points on the given processor like before, but computed in simpler way below

```
      NLATGT3(NEDLST),NLONGT3(NEDLST):
```

! global latitude and longitude index array of the coupling points

! computation of *NLATGT3*, *NLONGT3*

```
      NEDLST=0
      DO JGL=NDGSAL,NDGENL
        IGLG=MYLATS(JGL)
        DO JLON=1,NONL(NPTRFLOFF+JGL,MYSETB)
          ILONG=NSTA(NPTRFLOFF+JGL,MYSETB)&
          &+JLON-1
          IF (ILONG.LE.NBZONL.OR.ILONG.GT.NDLUXG-NBZONL.&
             &OR.IGLG.LE.NBZONG.OR.IGLG.GT.NDGUXG-NBZONG) THEN
! point is outside C-zone ==>it should be coupled
            NEDLST=NEDLST+1
            NLATGT3(NEDLST)=IGLG
            NLONGT3(NEDLST)=ILONG
          ENDIF
        ENDDO
      ENDDO
```

iii) The *EALFA* coupling coefficient array is computed in *suebicu.F90* (*suebicu.F90* is called before *suesc2.F90* so *EALFA* is known at this stage). However, *EALFA* is an *NGPTOT* array.

Remark :

ATTENTION *: EALFA is initialized to NBDYSZ size, but I doubt that it has an acceptable reason. Someone should revise the use of NBDYSZ, NBDYSZG in ALADIN and replace by NGPTOT, NGPTOTG wherever it is possible !!!!!!!!*
Moreover, the initialization of NBDYSZ is completely wrong in suegeo2.F90 if we keep in mind LSPLIT, B-level options!!!! This should be also revised!!!!!!! In the arpege counterpart of AL15 NBDYSZ and NGPTOT are the same (??). NGPTOT is coming from tfl, NBDYSZ from sugem1b.F90, but they are set the same way.
As I could see later on, in newer cycles NBDYSZ has been pruned, so probably my previous comments are right.)

We should perhaps not drop this *EALFA(NGPTOT,:)* definition because *EALFA* is or can be used elsewhere, but here in *suesc2.F90* we should copy the relevant part of *EALFA* to an *EALFAGT3*, i.e. only the non-zero *EALFA* coefficients ordered in the same way as the packed large-scale values. Coupling needs map factor as well (for semi-implicit part). So we introduce a *GMGT3* array to capture the relevant part of *GM*.

```
      IGPTOT=0
      IDLST=0
      DO JGL=NDGSAL,NDGENL
        IGLG=MYLATS(JGL)
        DO JLON=1,NONL(NPTRFLOFF+JGL,MYSETB)
          ILONG=NSTA(NPTRFLOFF+JGL,MYSETB)+JLON-1
          IGPTOT=IGPTOT+1
          IF (ILONG.LE.NBZONL.OR.ILONG.GT.NDLUXG-NBZONL.OR.IGLG.LE.&
             &NBZONG.OR.IGLG.GT.NDGUXG-NBZONG) THEN
! point is outside C-zone ==>it should be coupled
            IDLST=IDLST+1
            EALFAGT3(IDLST,:)=EALFA(IGPTOT,:)
            GMGT3(IDLST)=GM(IDLST)
          ENDIF
        ENDDO
      ENDDO
```

iv) The allocation part of the *GT3BUF* can remain basically as it was, just use the above-computed *NEDLST*.

v) Prune the unnecessary variables and their computation part : *NBZONLW*, *NBZONLE*, *NELOEN*, *NBZONC*

Apart from the standard coupling routines that will follow this structure, the pruned variables are used only in *erdlsgrad.F90*, consultation with Claude is necessary to adjust it to the new structure.

I.2.2 Filling GT3BUF (epak3w.F90)

i) Filling coupling buffer is done in *epak3w.F90*. The calling tree is :

```
CNT3 → ELSAC
                                        →       ELSWA3 → ——EPAK3W
CNT4,EDFI3 → ELSRW → ERLBC
```

In these calling trees only *elswa3.F90* and *epak3w.F90* have to be rewritten at this stage of cleaning.

ii) *elswa3.F90 :*

Up to the level where *ZGT3* and *ZGP* are allocated, nothing has to change. The small part calling *epak3w.F90* has to be rewritten like:

! *ZGP* is unneeded

```
ALLOCATE(ZGT3(NEDLST*IGT0))
IND=0
DO JGPBLKS=1,NGPBLKS
DO JPROMA=1,NPROMA
  IF (NLATGPP(JPROMA,JGPBLKS) > 0) THEN
    ILATG=NLATGPP(JPROMA,JGPBLKS)
    ILONG=NLONGPP(JPROMA,JGPBLKS)
    IF (ILONG.LE.NBZONL.OR.ILONG.GT.NDLUXG-NBZONL.OR.&
       &IGLG.LE.NBZONG.OR.IGLG.GT.NDGUXG-NBZONG) THEN
      IND=IND+1
      ZGT3((IND-1)*IGT0+1:IND*IGT0)=GPP(JPROMA,1:IGT0,JGPBLKS)
    ENDIF
  ENDIF
ENDDO
ENDDO
CALL EPAK3W(ZGT3,IFLDSGT0,.TRUE.)
DEALLOCATE(ZGT3)
```

iii) *epak3w.F90* :

According to the modifications in *elswa3.F90* the argument list will be :

```
EPAK3W(PDATA,KFIELDS,LDGP)
```

where :

```
REAL_B, INTENT(IN) :: PDATA(NEDLST*KFIELDS)
```

and we need a :

```
REAL_B, ALLOCATABLE :: Z00(:)
```

The part to be rewritten is the *IF (LDGP)* part : all the *JAREA*, *IZGT* part is unneeded, all *NEDLST* points are treated in one go. What will remain from the *LDGP* part is :

```
IF (LQCPL) THEN
  IF (NDD01 == 1) THEN
    GT3BUF(ISWP1+1:ISWP1+NEDLST*KFIELDS)=PDATA(1:NEDLST*KFIELDS)
  ELSEIF (NDD01 == 2) THEN
    GT3BUF(ISWP3+1,ISWP3+NEDLST*KFIELDS)=(PDATA(1:NEDLST*KFIELDS)&
     &-GT3BUF(ISWP1+1:ISWP1+NEDLST*KFIELDS))*ZRVFRCL
    GT3BUF(ISWP2+1:ISWP2+NEDLST*KFIELDS))=0
  ELSEIF (NDD01 == 0) THEN
    ALLOCATE(Z00(NEDLST*KFIELDS))
```

```
      Z00(1:NEDLST*KFIELDS) = GT3BUF(ISWP2+1:ISWP2+NEDLST*KFIELDS)&
       &*ZSQFRCL &
       &+ GT3BUF(ISWP3+1:ISWP3+NEDLST*KFIELDS)*ZFRCL &
       &+ GT3BUF(ISWP1+1:ISWP1+NEDLST*KFIELDS)
      GT3BUF(ISWP3+1:ISWP3+NEDLST*KFIELDS)=&
       &_HALF_*ZRVFRCL*(PDATA(1:NEDLST*KFIELDS)-&
       &GT3BUF(ISWP1+1,ISWP1+NEDLST*KFIELDS))
      GT3BUF(ISWP1+1:ISWP1+NEDLST*KFIELDS)=Z00(1:NEDLST*KFIELDS)
      GT3BUF(ISWP2+1:ISWP2+NEDLST*KFIELDS)=&
       &(PDATA(1:NEDLST*KFIELDS)-GT3BUF(ISWP1+1:ISWP1+NEDLST*KFIELDS)&
       &-GT3BUF(ISWP3+1:ISWP3+NEDLST*KFIELDS)*ZFRCL &
       &)*ZRVSQFRCL
      DEALLOCATE(Z00)
     ELSE
       CALL ABOR1('EPAK3W : INTERNAL ERROR NDD01')
     ENDIF
   ELSE
     GT3BUF(ISWAP+1:ISWAP+NEDLST*KFIELDS)=PDATA(1:NEDLST*KFIELDS)
   ENDIF
```

I.2.3 Coupling itself

i) According to all above, call of coupling will not be done from *tal* so all *tal* related coupling stuff has to be removed from the package and its interfaces : *LDCPL* has to be removed from the routines in *ald/transform* and down from the called package routines. Same for the *CPL_PROC* argument.

ecoupl1.F90 has to be called either from *scan2mdm.F90* or from *stepo.F90*. The former corresponds to the solution up to *AL12* the latter is closer to the *AL15* solution. Since the *AL15* solution seemed to be safe for all the configurations I would recommend and here I will develop the *stepo.F90* solution. However it can be consulted. (If *scan2mdm.F90* is chosen, the *AL12* solution would be to call coupling before session "*WRITE OUT UPPER AIR GRID-POINT DATA*"). The *stepo.F90* solution is to call coupling just before *etransdirh.F90* : remove the *LLCPL* argument from *etransdirh.F90* and introduce :

```
IF (LLCPL) CALL ECOUPL1
```

ecoupl1.F90 should be without any argument, from the global environment it must get all the information needed. (1 stands for time-level *t1*, if we decide to forget *t0*-coupling it would be nice to rename the *ecoupl1.F90, elscot1.F90, esrlxt1.F90* sequence to *ecoupl.F90, elsco.F90, esrlx.F90*).

ii) Let's see the new *ecoupl1.F90 :*

```
SUBROUTINE ECOUPL1
```

! Bla-bla-bla

```
USE ....
```

! (see from code below what is needed)

! local declarations...(see from code below what is needed, partly what is in old *ecoupl1.F90*)

! .....

```
CALL  SC2CGAP(IVORT1,IDIVT1,IUT1,IVT1,IUT1L,IVT1L &
  &,IHVT1,ITT1,IQT1,IO3T1,ILT1,IIT1,ISPD1,ISVD1 &
  &,IHVT1L,ITT1L,IQT1L,IO3T1L,ILT1L,IIT1L,ISPD1L,ISVD1L &
  &,IHVT1M,ITT1M,IQT1M,IO3T1M,ILT1M,IIT1M,ISPD1M,ISVD1M &
  &,ISVT1,ISVT1L,ISVT1M,ISPT1,ISPT1L,ISPT1M,INUL,IAT1,INUL &
  &,INUL,INUL,IFLDSGT1,IFLDSFLT,.FALSE.,.FALSE.,.FALSE.&
  &,1,NFLEVG)

ALLOCATE(ZGT1(NEDLST,IFLDSGT1))
IND=0
DO JGPBLKS=1,NGPBLKS
DO JPROMA=1,NPROMA
  IF (NLATGPP(JPROMA,JGPBLKS) > 0) THEN
    ILATG=NLATGPP(JPROMA,JGPBLKS)
    ILONG=NLONGPP(JPROMA,JGPBLKS)
    IF (ILONG.LE.NBZONL.OR.ILONG.GT.NDLUXG-NBZONL.OR.IGLG&
       &.LE.NBZONG.OR.IGLG.GT.NDGUXG-NBZONG) THEN
```

```
          IND=IND+1
          ZGT1(IND,1:IFLDSGT1)=GPP(JPROMA,1:IFLDSGT1,JGPBLKS)
        ENDIF
      ENDIF
    ENDDO
    ENDDO
    CALL ELSCOT1(GMGT3,EALFAGT3,&
      &,ZGT1(1,IUT1),ZGT1(1,IVT1),ZGT1(1,ITT1)&
      &,ZGT1(1,IQT1),ZGT1(1,IO3T1),ZGT1(1,ILT1),ZGT1(1,IIT1)&
      &,ZGT1(1,ISPD1),ZGT1(1,ISVD1),ZGT1(1,ISVT1)&
      &,ZGT1(1,ISPT1))
```

! Orography was passed but never used, so pruned here

```
    DO JGPBLKS=1,NGPBLKS
    DO JPROMA=1,NPROMA
      IF (NLATGPP(JPROMA,JGPBLKS) > 0) THEN
        ILATG=NLATGPP(JPROMA,JGPBLKS)
        ILONG=NLONGPP(JPROMA,JGPBLKS)
        IF (ILONG.LE.NBZONL.OR.ILONG.GT.NDLUXG-NBZONL.OR.IGLG.&
           &LE.NBZONG.OR.IGLG.GT.NDGUXG-NBZONG) THEN
          IND=IND+1
          GPP(JPROMA,1:IFLDSGT1,JGPBLKS)= ZGT1(IND,1:IFLDSGT1)
        ENDIF
      ENDIF
    ENDDO
    ENDDO
    END SUBROUTINE ECOUPL1
```

iii) *elscot1.F90 :*

```
    SUBROUTINE ELSCOT1 (PGM,PALFA,&
     &PUT1,PVT1,PTT1,PQT1,PO3T1,PLT1,PIT1,PSPD1,PSVD1,PSVT1,PSPT1)
```

POROG pruned, *KGL* disappeared (all *NEDLST* points treated in one go)

Otherwise everything untouched just *NEDLST* instead of *NDLON* and *NONL*

iv) *esc2r.F90 :*

Remove *KGL* from argument list of *esc2r.F90.*

```
    SUBROUTINE ESC2R(KTIMLEV,LDGP,KFIELDS,PDATA,KDIM)
```

! *KGL* disappeared

Rewriting exactly the same way as *epak3w.F90* : no need of *JAREA* business, everything goes from 1 to *NEDLST* with implicit looping.

One difference to what was done in *epak3w.F90* : for fields we cannot do implicit looping here, because *PDATA* is 2-dimensional array *(KDIM,KFIELDS)* and *GT3BUF* is 1d ==> for fields we need an explicit loop with defining offsets, i.e. the whole part after "time management" has to remain in the :

```
    DO JF=1,KFIELDS
```

loop. Then e.g. the *LQCPL* part will read as :

```
    PDATA(1:NEDLST,JF)==ZWB0*GT3BUF(ISWP0+(JF-1)*NEDLST+1:ISWP0+JF*NEDLST)&
    &+ZWB1*GT3BUF(ISWP1+(JF-1)*NEDLST:ISWP1+JF*NEDLST)&
    &+ZWB2*GT3BUF(ISWP2+(JF-1)*NEDLST:ISWP2+JF*NEDLST)
```

Similar rewriting for the other cases has to be done like in *epak3w.F90*. (So again the whole *IGT3*, *IZGT* shift is removed, everything is done in contiguous way on the *NEDLST* set, field-wise)

v) *esrlxt1.F90* :

No change is needed at all !!!!!!!!

vi) *deello.F90* :

Deallocation of arrays has to be adjusted to new and pruned arrays.

I.2.4 Memory considerations

When all the above is coded and works one has to consider the memory overhead. In the earlier solution all the coupling was done on *NDLON* slices (with the limitations described in the introduction). The above design works on the whole *NEDLST* piece.

In dm environment with many processors this is not more expensive in terms of memory. However, with a small number of processors it may become more expensive. If it is the case, it is not too dificult to introduce "chunk" loops both for the call of *epak3w.F90* and for *ecoupl1.F90*. Certainly the loop in this case has to do "chunks" according to *NEDLST* and not according to fields.

After these modifications tests were done : in A-level the code works, gives identical results as with old version. B-level tests need other debugging of ALADIN (see later in this document).

I.3 Important remarks

Adjoint aspects were not elaborated above, when everything works in the direct code, some adjoint expert should be involved.

When phasing the code according to the above it is worthwhile to do other cleaning-pruning as well. To consider e.g. if the spectral field treatment for RUBC should remain in the coupling code or it is obsolete. I hope it can be dropped, because I have not elaborated the *LRUBC* related modifications.

erdlsgrad.F90 was fully dropped because it uses the old coupling setup and it did not take into account B-level constraints at the dm-distribution involved in the routine. It should be rewritten.

The call of coupling is removed from the transform package. As a short-cut solution I pass from *stepo.F90* to *etransdirh.F90 "LLCPL=*.false.". It would be nice to prune all the *LLCPL* related stuff from the package.

II. Debugging of ALADIN in B-level with new coupling

After rewriting ALADIN coupling in the way described above I could start B-level and *LSPLIT* tests on ALADIN.

Below I list the additional modifications that I had to introduce to make ALADIN configuration 001 work in B-level / *LSPLIT* mode :

espconvert.F90 :	mis-use of *NFLEVL <--> NFLEVG*
espuv.F90 :	initializing *IVSETUV* and introducing it to calling sequence of *einv_trans.F90*
sueorog.F90 : *suecuv.F90* :	initializing *IVSETSC* and introducing it to calling sequence of *einv_trans.F90, edir_trans.F90*
euvgeovd.F90 :	mis-use of *KLEV <--> KFLSUR* + introducing *KVSETUV*
disgrid.F90 :	ARPEGE bug, reported, care taken by GMAP
etrmtos.F90 :	"mis-typing errors", trivial fixes
sump0.F90 :	remove protection of ALADIN *LSPLIT*
wrmlppadm.F90 :	mis-use of *NFLEVL <--> NFLEVG*
ewrplppdm.F90 :	introducing *KVSETUV*
suegeo2.F90 :	wrong size and definition of *NLOEN* + forcing *NBDYSZ=NGPTOT* (see earlier remark)

suemp.F90 :	2 fixes: - care had to be taken that when spectral A-sets are further splitted for SI computations, the breaking of *NSPEC2* arrays into several *NSPEC2V* arrays should not break inside a wavenumber pair, i.e. the 4 coefficients of a wavenumber pair should remain on the same processor. -wrong definition of *NDGUXL*
espnormave.F90 :	removing mean wind from norm computation : if it is to be present, code for distribution of mean wind for diagnostic purpose has to be elaborated
suspec.F90 : *suspeca.F90* : *suspeca.h* :	*AL15* code is bugged, corrected *suspeca.F90* was taken from higher cycles. *Furthermore, explicit array-bounds has to be removed from dummies to provide norm identity after suspeca (a general little bug !!!!)*

Performance tests:

After all the above-described modification B-level and *LSPLIT* options worked in configuration 001. Norm identity was guaranteed up to 6 digits in a 6 hour integration.

I made some performance tests with :

NPROC=16, NPRGPNS=NPRGPEW=NPRTRW=NPRTRV=4

on a domain with

NFLEVG=31, NDLON=240, NDGL=216

The B-level option in this configuration brings a solid 10 percent performance improvement. *LSPLIT* does not make any measurable change in performance. The effectivity of *LSPLIT* highly depends on the *NDLUXG / NPRGPNS* ratio and modulus, so tests should be repeated with several such configurations.

Toward the assimilation of radar in AROME and ALADIN : a discussion paper

F. Bouttier
Météo-France/CNRM/GMAP . September 2003

This paper has benefited from substantial contributions by M. Jurasek (SHMI), V. Ducrocq (Météo-France, CNRM/GMME) and P. Tabary (Météo-France, DSO - direction of observing systems).

1. Introduction

Radars are essential for mesoscale data assimilation, as they are the only operational network that can provide information about the structure of clouds and boundary layer in the presence of precipitation or deep convection. The assimilation of radar data is not implemented at all in the ARPEGE/IFS/ALADIN/AROME software so far, it could only be performed in a very approximate way via the retrieval of humidity or winds. Within a few years, radar data processing will be developed to a point of technical and scientific complexity similar to that of satellite radiances. This paper discusses what is the best way to go for the next few years in the ALADIN community. A strategic objective is to improve the initialization of the future AROME model with the operational radar network available over Europe and North Africa (subject to acquisition constraints) during the 2004-2010 period.

2. Which radar data ?

Radar information can be presented to the data assimilation system in several forms :

- reflectivities,
- instantaneous rain rates,
- cumulated rainfall,
- Doppler radial wind-component and related quantities (shear / turbulence),
- VAD vertical profile of wind vectors inferred from Doppler information,
- microphysical content information using multiple polarization.

Each form has advantages and drawbacks, is appropriate to different kinds of atmospheric models and analysis algorithms, and may or may not be used depending on the type of radar available.

Doppler data is relatively easy to assimilate in 3d-var is being thoroughly studied in HIRLAM, but is not available on most European sites. Hence, it will not be discussed in this paper, and the reader is referred to recent HIRLAM Newsletters to convince his/herself that radar winds would be rather straightforward to implement once available.

Multiple polarization is very useful to improve the quality and robustness of radar data at producer level but the direct use of polarization information in NWP is still rather a research topic and requires the availability of a detailed microphysics (e.g. as in the future AROME model).

Reflectivities are available almost everywhere in Europe, are not much used in 3d-var and pose some interesting problems (see Fig. 1). So it is suggested to start by concentrating on the introduction of radar reflectivities in ALADIN 3d-var. Radar networks are going to keep improving so we will go on extending the software whenever new kinds of radar data become available in a nearly operational configuration.

The physical interpretation of reflectivities is much easier if they are produced at several elevations, i.e. with volumic radar scanning. This is not available everywhere, so we should have a general

approach that will allow the use of single-elevation data ("PPI" images) as well as multiple-site data.

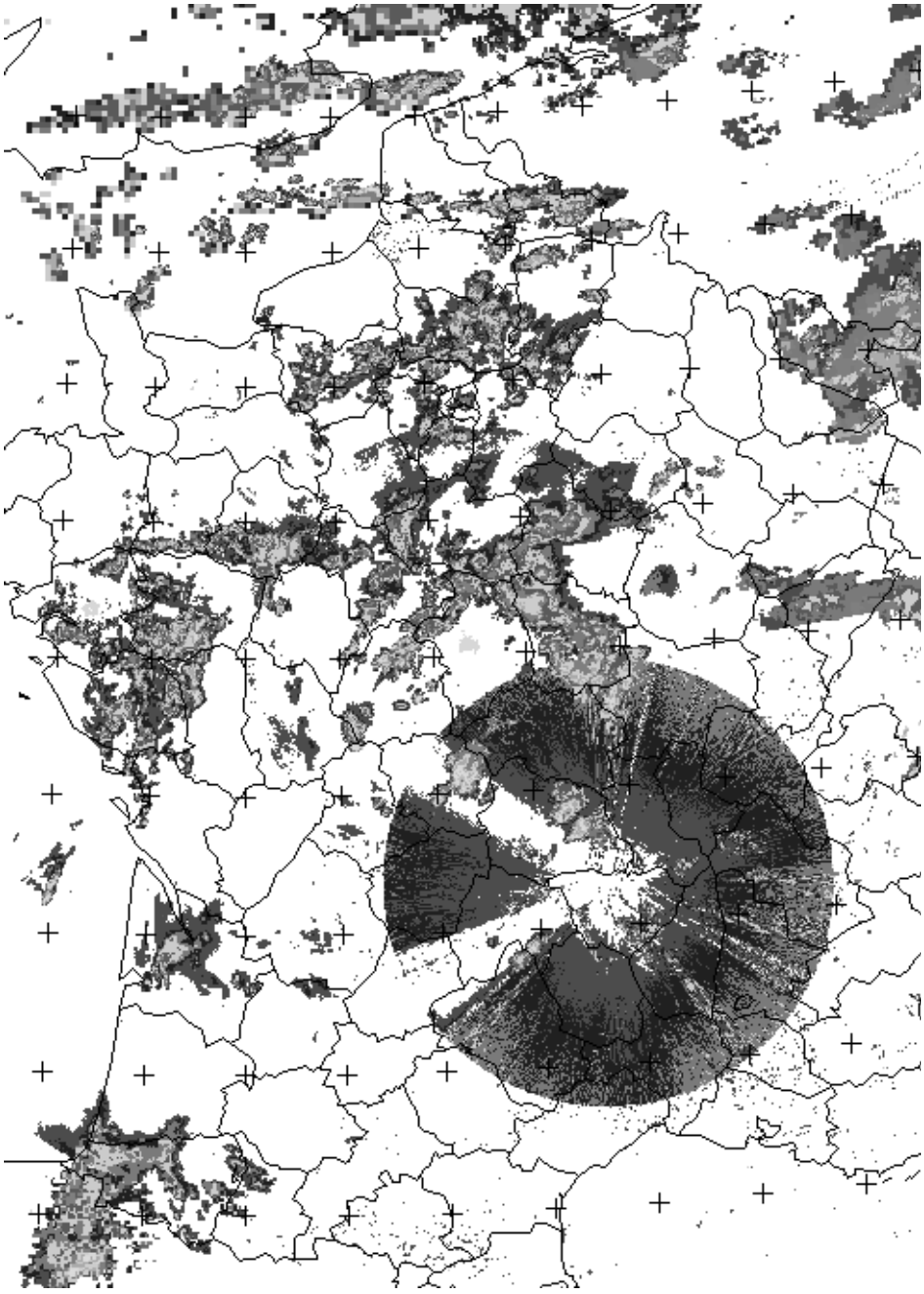

Figure 1 : International composite radar-reflectivity image over France on 28 August 2003, 13:30 UTC. The image reveals some of the problems of radar data : occurrence of gross error (electronic problem corrupting a whole radar disc), pseudo-random spurious echoes in clear areas around the Mediterranean sea, inconsistencies between the French and UK data, inconsistencies between two neighbouring radars (visible as a bow of echoes South of Paris). There are some less visible problems (orographically masked areas displayed as no-rain pixels, over- and underestimation of reflectivity depending on the distance to the radar). All these problems must be solved automatically in real time before radar data can be considered available for NWP data assimilation.

3. The philosophy : learning from satellites

The situation with radars being similar to that with TOVS radiances 15 years ago, it seems wise to try and apply the lessons learned from the TOVS community :

- The remote-sensing process is complex and nonlinear, so we should try to assimilate something close to the measured quantity (reflectivities) instead of using partial inversions to something that seems easier to assimilate in the model (rain rates or derived humidity profiles for instance). One of the reasons is that inverted data contain errors that are very difficult to correct, because they are a mixture of real data, model a-priori information, interpolation errors and empirical assumptions about the atmosphere. In 3d- or 4d-var, it is not really more difficult to use real data than inverted data.
- Assimilating reflectivities requires an observation operator that will simulate reflectivities for each radar, so the first part of the job is to develop a system to monitor radar data against model output, and ensure that the observation operator works well. Then we need to write the tangent-linear and adjoint versions of the observation operator, and check the accuracy of the linearization.
- Biases and gross errors cannot be handled by 3d- and 4d-var. We need to develop an automated software that will detect and remove the following data : corrupt, too difficult to simulate, or biased (perhaps with the help of the model and / or independent observed data, e.g. from satellites). Bias correction requires a study of the space-and-time structure of the biases between the simulated and the observed data. Each radar must be considered independently. Bias correction and gross error correction are normally done before the minimization process (e.g. in the observation preprocessing and the screening). Too dense data must also be thinned consistently with the resolution of the analysis.
- The physical process of the observation must be modelled as accurately as possible. For radars, at the planned resolutions, it means that we need to interpolate/average the model variables precisely along the radar-beam path (more on this below).
- The physics of the instrument and the interaction with the atmosphere are complex. Fortunately, many people have studied it in details, so we do not want to redo their job : we must rely on radar specialists to provide us with the physical part of the observation operator. Some interaction with them is necessary to make sure we are speaking about the same kind of instruments and resolutions (most research studies are done with sophisticated radars at very high resolutions, which are not relevant to our NWP plans). Ideally, they should write the physical part of the observation operator, and we should just plug that software into the (suitably interpolated) model fields. That is the way it already works with satellite radiances (the RTTOV software), and we shall try to make it work for radars, by international pluri-disciplinary collaboration.

4. Which model and data assimilation ?

Reflectivities are sensitive to the cloud properties, so their processing is in principle affected by the way clouds are represented in the model (e.g. subgrid-scale diagnostic clouds in large-scale physics, or detailed prognostic mesoscale microphysics). Whether cloud-related fields are part or not of the control variable may also be important to get a good impact of the data. The constraint is that we will need to work simultaneously on ALADIN and AROME for the next few years. It is not a genuine problem really, because we will anyway want to use radar data in large-scale models (ARPEGE and perhaps IFS), so we do not want the use of radar data to be too much tied to a particular set of parameterisations.

Whichever the model, it seems fair to assume that the radar observation-operator only needs to know about a few microphysical fields along the beam path (cloud and precipitation liquid water and ice, primarily) to work. The radar observation-operator does not need to know how these fields are produced, so it can be developed independently from the physics. A physics-specific piece of

software will be needed for the interface with the physics to get these fields, and to interpolate them between the model and observation geometries.

Whether the analysis corrects microphysical fields or not is not relevant for radar reflectivity simulation : we assume that the fields are provided by the physics. In the tangent-linear and adjoint observation-operators, it is not relevant either if (and only if) the fields are not part of the 3d- or 4d-var control variables i.e. if their perturbation is kept to zero. If there are microphysical fields in the control variable, which should only be done if we are confident that we will know how to correct them in the analysis, then we will have issues of size and definition of the control variable (i.e. choosing variables with a Gaussian distribution of errors), and of multivariate coupling in the background constraint term (i.e. the "Jb" balance between cloud variables and other variables such as divergence, temperature and water vapour). It is a difficult and complex issue, which can hardly be studied until we have the radar observation-operator and the prognostic cloud microphysics working in AROME : it will be studied later, probably around 2006-2008.

5. Things to do

The list of things to do before we can start radar-reflectivity assimilation experiment in ALADIN 3d-var is the following :

1. Get some radar-reflectivity data samples of reasonably good quality. This means we need to be very careful about radar data that was originally designed for human visualisation : it probably requires very strict screening of suspicious pixels.

2. Get an idea of the fields needed to simulate reflectivities. One can look at the simple radar simulation code in Meso-NH. It would be interesting to check the RSM (DWD, HIRLAM) model as well. It is essential to read a bit of scientific literature to learn what is available and what is the validity of the formulae. Discussing with the radar specialists is essential to check we are not going to start with something too silly. The Eumetnet/OPERA *web* database contains useful references and discussions on the available European radars.

3. Decide on some simple (to start with) reflectivity simulation formulae following the work in (2). Check them approximately, e.g. by applying them on current ALADIN historical files, to get an impression of the problems to solve.

4. Specify the observation-operator software completely by making a list of the necessary model fields to use (= to be interpolated for the observation operator), and of the necessary observation information (= measured data, complete identification of its expected quality, description in space and time of the relevant radar beam, all meta-data useful for the monitoring, quality control and bias correction) to be provided to the ALADIN screening and minimization. An important data access pattern is likely to be by beam, i.e. in polar form, rather than regular gridded pixels matrices as normally used for imagery. If we are confident that all along-the-beam effects (like attenuation by precipitation) are corrected before the analysis, then each pixel can be considered independently.

5. Specify carefully the technical implementation of these specifications. At this stage one can concentrate on the observation operator (leaving the screening and quality control for later) : how will the model fields be extracted from the physics and interpolated/averaged along the radar beam ? *(there are parallelization and adjoint issues to study)* How will the observed data be implemented into ODB, with specific codes and meta-data ? (*there are data volume issues to study)*

6. It is extremely important to propose code structures that will logically fit with the existing code (fields and observations). So one needs to understand very well the existing observation-operator code, to minimize the disturbance to other developers (on satellite data notably), and to think of the future by leaving room for volumic, Doppler and polarimetric

radar data, and for other similar observation operators (= with a slanted interpolation path) : GPS-occultation, limb sounders, GPS-ground slant delays, line-of-sight wind for Doppler wind lidar, radiometers with a large footprint. The aim is not to code all of them, but to think how it could be done, and to write a reflectivity-simulation code that will be compatible with them. Doppler data may become available very soon after reflectivity data (it is already the case in many countries), so it may make sense to implement Doppler data processing at the same time as reflectivities.

7. Document/write the detailed technical proposal, and have it read by the IFS /ARPEGE /ALADIN /AROME community **before** starting the heavy coding. It is usually nice to make some quick-and-dirty prototype code to see how things could work, but dirty code should **not** be merged with an official library release until it is cleaned and approved by everyone.

8. Implement the "radar data" type into the observation processing : ODB generation, screening, minimization, monitoring. At this stage, the data is simply loaded into ALADIN, but not compared with the model. Check what it costs in CPU and memory with the planned data volumes.

9. Implement the direct interpolation of model fields. This involves extracting the local gridpoint fields from the physics (or the historical fields if they are available) and interpolating them along each relevant radar path, or just at the radar pixel location if there is no effect along the path, or this effect (anomalous propagation ...) can corrected without using model fields. The beam aperture will require some consistent averaging of model fields on several levels ("beam filling" problem : at 100 km of distance, the beam may be more than 1000 m wide in the vertical). The result is model data at the time and place of each radar pixel. The code must be parallelized.

10. Convert the interpolated model data into simulated reflectivities, compute the difference with the observed data, store it into ODB and include it into the "Jo" cost function computation. The result is a computation of the "Jo" component for radar data in the screening run, and the ability to monitor the "obs-model" departures in the *ECMASCR* ODB (using *obstat* or *mandaodb*).

11. Study the monitoring statistics, and design bias correction, screening, thinning and quality control procedures. Implement them either into the screening (if requiring model fields) or in a preprocessing program. Check the speed of execution : it has to be very quick, and probably in parallel mode. This is a very interesting scientific work, and it is crucial for the success of radar assimilation.

12. Code the tangent-linear and adjoint versions of the observation operator, check the quality of the linearization in a few representative cases, check the correctness of the adjoint. The result is that you can do a 3d-var minimization that uses radar data. Check that the speed and quality of the minimization are not badly affected. Check how much closer to the data the analysis is, compared to the first guess.

13. Simulate one radar pixel, and check how it is used by 3d-var to correct to atmospheric fields.

14. Study how one analysis with radar data modifies the ALADIN and AROME (or Meso-NH) forecasts, under several situations (fronts, scattered showers, strong convection) and resolutions (10 km and 2.5 km at least). There should be some improvement to the rain and clouds. Check that the spin-up is not badly affected.

15. Run several cycles of data assimilation, to see if radar data has a cumulative (and beneficial !) effect on the forecasts : normally, they should be closer to radar (and other) data than when radars are monitored but not assimilated.

16. Retune the preprocessing and analysis parameters, improve the observation operator, test how new radar types and new physics can make the assimilation more efficient. Run tests on

field experiments to detect possible problems. Try better formulations of the background-error constraints to improve the structure of analysis increments.

6. Conclusion : the ALADIN work plan

As one can see from the above list, there is a lot of work to do so it should be shared between several people. The main work processes are :

scientific input : V. Ducrocq and her collaborators (O. Caumont, JP. Pinty, the radar labs and experts) give advice on the first simulation formulae to use. Basically, there are scalar formulae available from the Meso-NH software that can be duplicated (they will be improved by GMME, LA, etc. later but it should not change the basic data requirements that drive the design of the observation-operator software). To get a simple simulation model to start with is important, to understand the issues and do the technical prototyping work; we will upgrade ALADIN when the scientists have news methods to recommend, but we do not need to wait to start the technical work. The most simple formulae only require cloud liquid water and ice at the radar pixel location. These fields can already be taken from the ALADIN physics (the interface already exists for the ECMWF use of radiances). *contacts : V. Ducrocq, J.P. Pinty, O. Caumont, P. Tabary (at Météo-France).*

interpolation stencil : A difficult question to answer quickly is : can we use each radar pixel by using model fields at the pixel location, or does each pixel require fields along the radar beam path ? One must check with the literature and the specialists to get the right answer. If we only need pixel data interpolation is much simpler, but getting this part of the software strategy wrong may compromise the entire effort on radar data . Studying this should be first part of the work. One also needs to understand some of the science behind the development project. *(same contacts as above - some literature reading is required).*

ingestion : In parallel, one can probably start working on introducing radar data into ODB. It is a rather long and tedious work, so it is best to start early. One needs to create codes to identify potentially useful radar data and meta-data, and to design a simple layout for ODB. The new code needs to be approved at GMAP and ECMWF, and then one should develop software to write some sample radar data into ODB, and to read it from inside IFS /ARPEGE /ALADIN and from the monitoring software. *contacts : P. Caille, P. Moll, D. Puech, ALADIN ODB specialists, (E. Andersson at ECMWF for approval).*

observation operator design : The big part is the interpolation part of the observation operator. This is where most of the technical development and problems will be. The issues are (1) the parallelization : a radar beam will in general be scattered across several processors. What should be reorganized : the field data or the observation data ? (2) the memory : there will be many pixels (think of volumic scanning !). Is it best to extract the gridpoints needed to interpolate each beam, or to get all the gridpoints for a group of beams and access them directly as needed on a single processor ? (3) the efficiency : computations must be organized in an efficient way inside the model code. Current observation operators have an horizontal interpolation (using the SL code), and a vertical interpolation/physical simulator code. The optimal organization that saves both CPU, communications and memory is probably different. *contacts : the design should be done in collaboration between an ALADIN specialist (M. Jurasek at SHMI was suggested) and someone from GMAP (E. Wattrelot probably) who knows the code well. Design decisions must be checked by code experts like P. Moll, C. Fischer and M. Hamrud.*

development : The rest of the work (explained in the previous section) is rather linear once the interpolation and ODB parts are worked out. It should always involve regular contacts between

- at least one dedicated "ALADINist" (e.g. M. Jurasek but more are possible),

- at least one dedicated "GMAPist" (e.g. E. Wattrelot),
- the "radar science team" of GMME (V. Ducrocq and colleagues), who may provide contacts with other members of the science community when necessary.

collaboration : There will certainly be a long, but crucial, exchange of informations with ECMWF to reach agreements on technical aspects of ODB modifications, the new observation operator(s), and to debug the first common cycles with these modifications.

Scientific publications can be done as soon as monitoring works. Ideally the ALADIN work should start by providing quasi-operational monitoring of some radars on long periods, with code that can be validated against special test cases studied at GMME. This goal can probably be reached sometime in 2004. Then, we can start work on actual assimilation, which will provide the first experiments showing quasi-operational radar impact, probably in 2006. It is too early to foretell whether the first successful results will be found with the ALADIN-10 km model or with one of the AROME models (10 km or 2.5 km).

In parallel with the operational-oriented work, which is the priority for AROME and ALADIN, there will be some "moving target" evolution with the deployment of new radars, and the development of better observation-operator softwares (for preprocessing - e.g. propagation of radar beam - and physical simulation - e.g. interaction with microphysics). We will need to decide from time to time whether we want to continue quickly with old data/software, or whether it is more productive to redo some of the work with new and better data/software.

Comments and initiatives on these issues are welcome from all ALADIN participants who are willing to embark quickly on this complex and time-constrained project.

Orographic forcing in ALADIN

Bart Catry
Universiteit Gent . Krijgslaan 281 (S9), B-9000 Gent, Belgium

1. Introduction

As in the early eighties the resolution of the models increased, one of the most spectacular effects was the deterioration of the mean westerly flow at moderate latitudes, especially above the continents. A too strong westerly flow in the northern hemisphere in the winter and a more correct simulation in the southern hemisphere and in the northern hemisphere in the summer suggested a lack of orographic forcing.

Different methods are used to overcome this problem. One method is to increase the orography by adding an envelope (see Wallace et al., 1983). Another one uses a parameterization of the gravity waves generated by the subgrid-scale features. Both methods increase the orographic stress, thus lowering the total momentum.

These two methods are implemented in ALADIN. The envelope is created in configuration 923 (`FENVN=1` in the namelist), the parameterization of gravity waves is treated in the subroutine `ACDRAG`, giving (`PSTRDU`, `PSTRDV`), the additional zonal and meridional stress. The tuning of these effects is as fine as that the slightest change in tuning coefficients gives a much worse result. Nonetheless, the implementation of the two methods are not fully satisfactory :

1. In a number of models, the envelope has been suppressed, but ALADIN still needs it, why ?
2. When air meets a mountain, too much goes over the mountain (giving too much precipitation), too little goes around it.
3. What are the interactions between the different parameterizations (turbulence) ?
4. What happens when going to higher resolution ? ...

To study these problems, we developed a diagnostic tool that calculates the momentum budget over a certain domain. In this budget dynamical terms as well as physical parameterizations are included. So, when going from high to low resolution, there should be a shift from dynamical to physical terms. By doing this we hope to find some shortcomings in the representation of the orographic forcing in ALADIN.

2. The experiments

The chosen domain is the ALPIA domain, centred on the French Alps (45.22° N, 5.90° E). For this domain we have created the complex orography 4 times in 4 different resolutions :

Domain	points	vertical levels	resolution
A	96×96	37	10 km
B	192×192	51	5 km
C	384×384	71	2.5 km
D	768×768	98	1.25 km

A plot of the domain at the different resolutions is shown in Fig. 1.

The resolution in domain D is high enough to handle it as the "perfect" domain where all of the orographic stress is resolved. So, there is no need of a parameterization in this domain. When going to lower resolution (C, B and A), the subgrid-scale orography is not resolved any more and subgrid-scale features should be taken into account. Therefore, we have calculated (following Lott and

Miller, 1995) the variance (μ^2), the anisotropy coefficient (γ^2) and the anisotropy direction (υ) for each gridpoint in these three domains. With :

$$\mu^2 = \frac{1}{4}(h(\max) - \overline{h})(\overline{h} - h(\min)) \qquad \gamma^2 = \frac{K - \sqrt{L^2 + M^2}}{K + \sqrt{L^2 + M^2}} \qquad \upsilon = \frac{1}{2}\arctan(M/L)$$

$$K = \frac{1}{2}\left(\overline{\left(\frac{\partial h}{\partial x}\right)^2} + \overline{\left(\frac{\partial h}{\partial y}\right)^2}\right) \qquad L = \frac{1}{2}\left(\overline{\left(\frac{\partial h}{\partial x}\right)^2} - \overline{\left(\frac{\partial h}{\partial y}\right)^2}\right) \qquad M = \overline{\frac{\partial h}{\partial x}\frac{\partial h}{\partial y}}$$

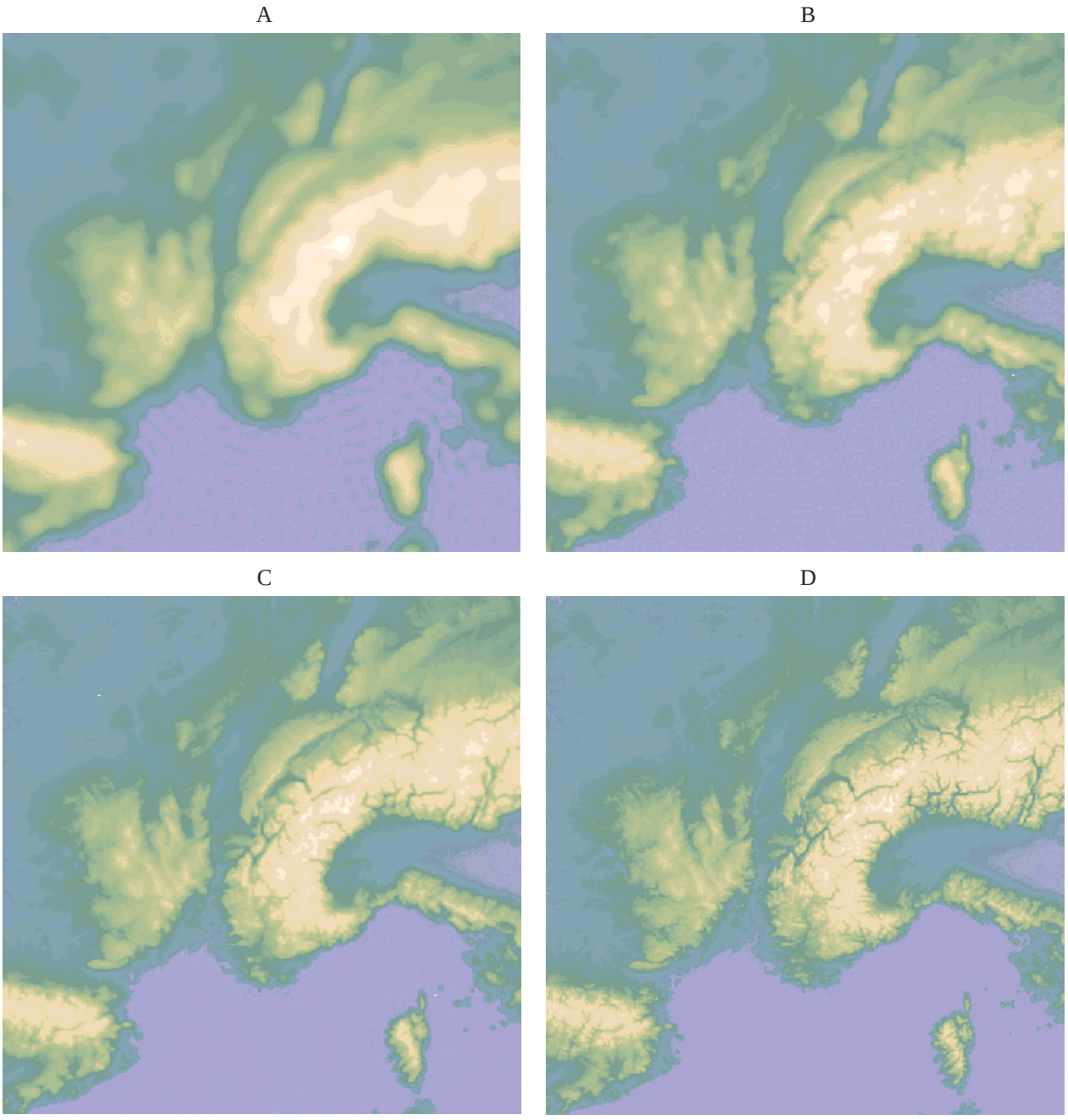

Figure 1 : The ALPIA domains : (A) 10 km resolution , (B) 5 km resolution , (C) 2.5 km resolution, and (D) 1.25 km resolution.

These three subgrid-scale features are needed for the parameterization of gravity waves. It is clear that, ideally, the effects that are not resolved any more should be taken care of by the parameterization.

The envelope was added (following Wallace et al. 1983), increasing the height by twice the standard deviation of the subgrid orography, or : *height* = *height* +FENVN ×2μ . FENVN is a tuning coefficient, where FENVN =1 stands for a full envelope and FENVN =0 stands for no envelope. However, operationally the envelope is created using only 1 times μ. Future tests will also use this value.

To study the effects over this complex orography, we chose to use an idealized flow. This flow was constructed using the ACADFA routines, which were used in previous academical studies (see for more information Bubnova, 2000). As the previous studies concentrated on the dynamics, we had to add a small physical part.

The experimental conditions are as follows : the atmosphere is dry, inviscid, in hydrostatic equilibrium and its static stability is given by a constant Brunt-Väisälä frequency N =0.01 s^{-1}. There is a constant reference flow of 24 m/s from the North-West, hence blowing more or less perpendicular on the main mountain ridge. The main flow is in geostrophic equilibrium with a constant Coriolis parameter f =0.0001 s^{-1}. The vertical levels are regularly spaced in z by 867 m for domain A, 619 m for domain B, 433 m for domain C and 306 m for domain D. Finally, the reference values of temperature and density prescribed in the middle of the domain at sea level are : $T_0 = \theta_0$ =300 K and ρ_0 =1 kg/m^3 .

As the tendency term becomes negligible after 6 hours, the forecast length was set to these 6 hours. We used the two time-level semi-Lagrangian semi-implicit approach with an ALADIN cycle-15 library. A plot (Fig. 2) has been made of the situation after 6 hours.

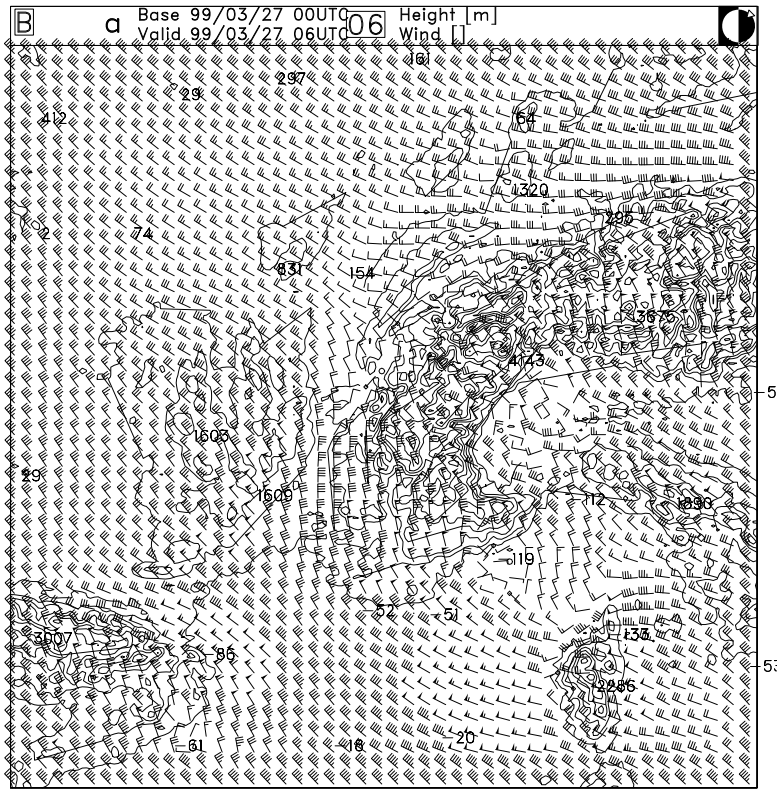

Figure 2 : The situation after 6 hours (domain B).

3. Momentum budgets

As orographic stress reduces the amount of momentum, is seems logic to look at the different components contributing to the total momentum and how they change when going to lower or higher resolutions. The components were integrated inside a box (of which the height changes from 0 to 20.000 m) over the different domains. In this box, the momentum budget should agree to the following balance equation (for the meridional case) :

$$\underbrace{\frac{\partial(\overline{\rho v})}{\partial t}}_{A}+\underbrace{\frac{\partial(\overline{\rho u v})}{\partial x}}_{B}+\underbrace{\frac{\partial(\overline{\rho v^2})}{\partial y}}_{C}+\underbrace{(\overline{\rho w v})_z}_{D}+\underbrace{\frac{\partial(\overline{p-p_{ref}})}{\partial y}}_{E}+\underbrace{\overline{\rho f u}}_{F}+\underbrace{\overline{(p-p_{ref})_h\frac{\partial h}{\partial y}}}_{G}+\text{param..}=0,$$

with

$$\tilde{Q}=\int_h^z Q\,dz \quad \text{and} \quad \overline{Q}=\frac{1}{A}\int\int_A Q\,dx\,dy,$$

where *h* denotes the orography height and *z* the height of the top. The components stand for the following :

- A: Tendency term
- B: Advection term (U-component)
- C: Advection term (V-component)
- D: Vertical flux through the top of the box
- E: Pressure gradient
- F: Coriolis term
- G: pressure drag
- Param: Parameterizations calculated by `ACDRAG` (gravity-wave stress) and `ACDIFUS` (turbulent stress)

The data needed for these integrations are abstracted from the `CPG` subroutine.

4. Tests

Going from high to low resolution

The goal of these tests is to know whether the ACDRAG routine is doing what it is supposed to do : when going from high to low resolution, there should be a shift from dynamical terms to physical terms.

When going from the C domain over the B domain to the A domain we see the following trends (see also Fig. 3) :

- The pressure drag becomes smaller. When going from B to A the decrease in pressure drag is fully compensated by an increase in gravity-wave drag (see Fig. 4). When going from C to B the decrease is partly compensated by the gravity-wave drag and partly by an increase in advection (x direction).
- There is also a steady decrease in pressure gradient (twice of the same magnitude).
- The contribution of the Coriolis effect is the same in the four domains (also D).
- There is a remarkable decrease in vertical flux when going from C to B. This decrease is negligible when going from B to A.
- The higher the resolution, the better the momentum budget is in balance. Domain C is close to being in complete balance.
- At the 2.5 km resolution the parameterization disappears.

C

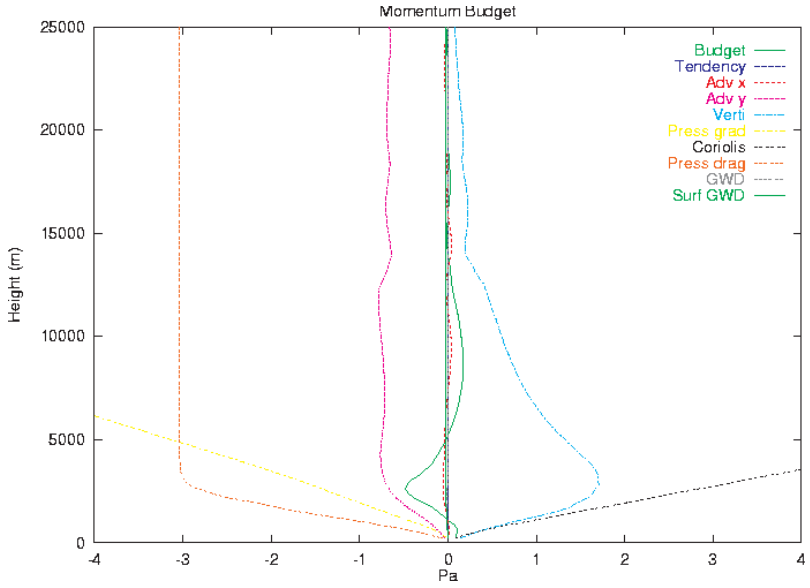

B

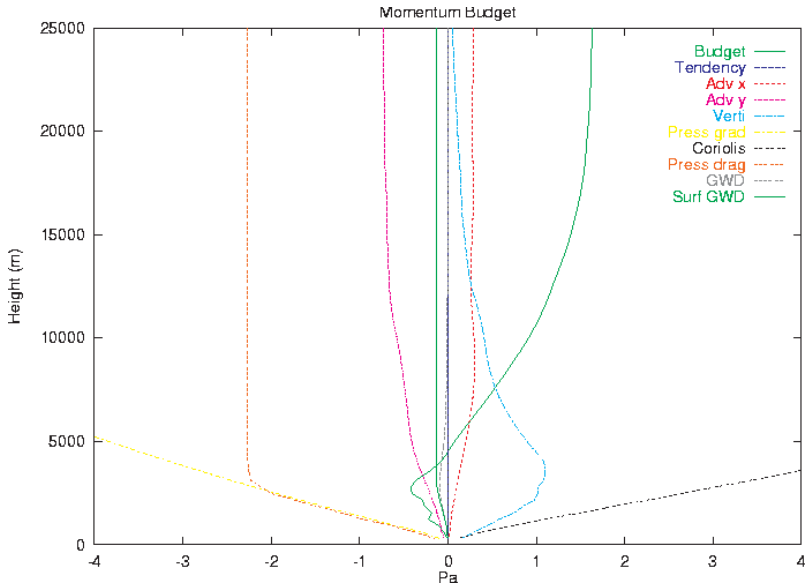

A

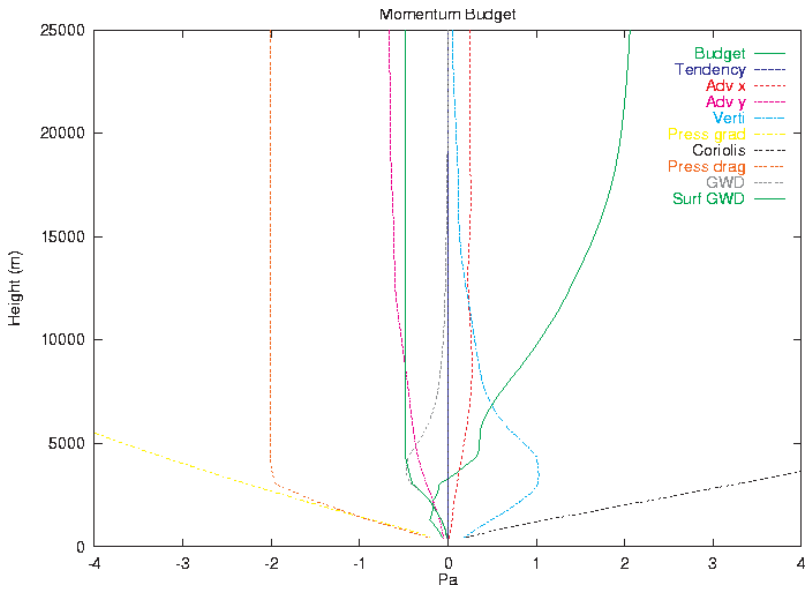

Figure 3 : Momentum budgets, going from high to low resolution : the upper figure is for domain C, in the middle for domain B and the lower figure is for domain A.

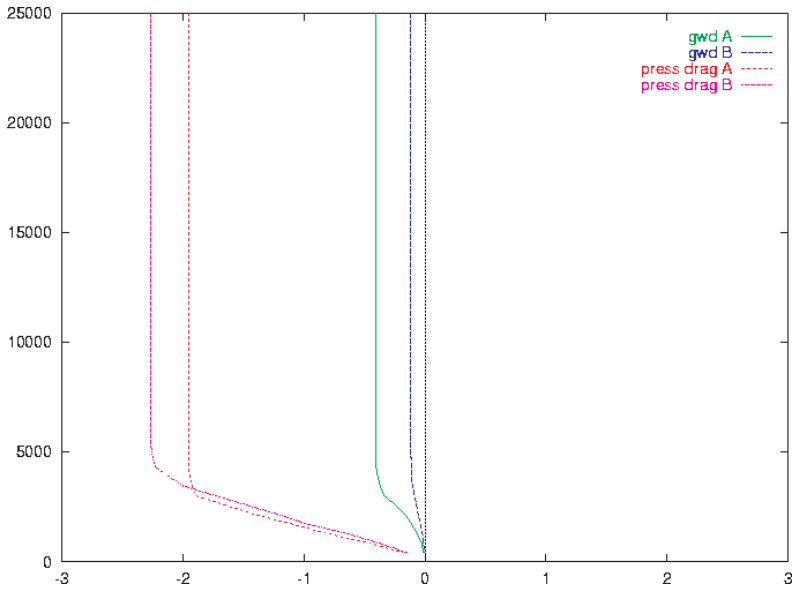

Figure 4 : When going from high to low resolution the decrease in pressure drag is fully compensated by an increase in gravity-wave drag.

Removing the envelope

Removing the envelope has always been a problem in ALADIN. ALADIN still needs it while other models can work without it. So let's see what changes in the momentum budget when we remove the envelope.

Removing the envelope actually means removing high peaks and lowering valleys. Hence it is clear that the pressure drag should decrease. An other general (logical) trend in the budget terms is that a lot of activity will take place at lower altitude. Finally, when we compare the budget it is clear that the simulation with the envelope is better than without it (the budget at lower altitude is closer to zero, see Fig. 5).

If we want the budget to move closer to zero, we must compensate the decrease in pressure drag by increasing the gravity-wave drag. Now, in the subroutine ACDRAG the nonlinear effect of blocked flow is included. This effect separates the flow in a part that goes over the mountain and a part that goes around it. The separation is arbitrarily chosen by a tuning parameter `GWDCD` which is by default set to 6. By increasing this value and hence increasing the part of the flow going around the mountain and thus increasing the stress, we can compensate for the removal of the envelope and keep our budget in balance.

We did this test for domain A, where the influence of the parameterization is high. We increased the value for `GWDCD` from 6 over (a very unrealistic) 60 to 100. The results are shown in Fig. 6. One can see clearly that by increasing `GWDCD` the momentum budget becomes better in balance, especially in the lower layers.

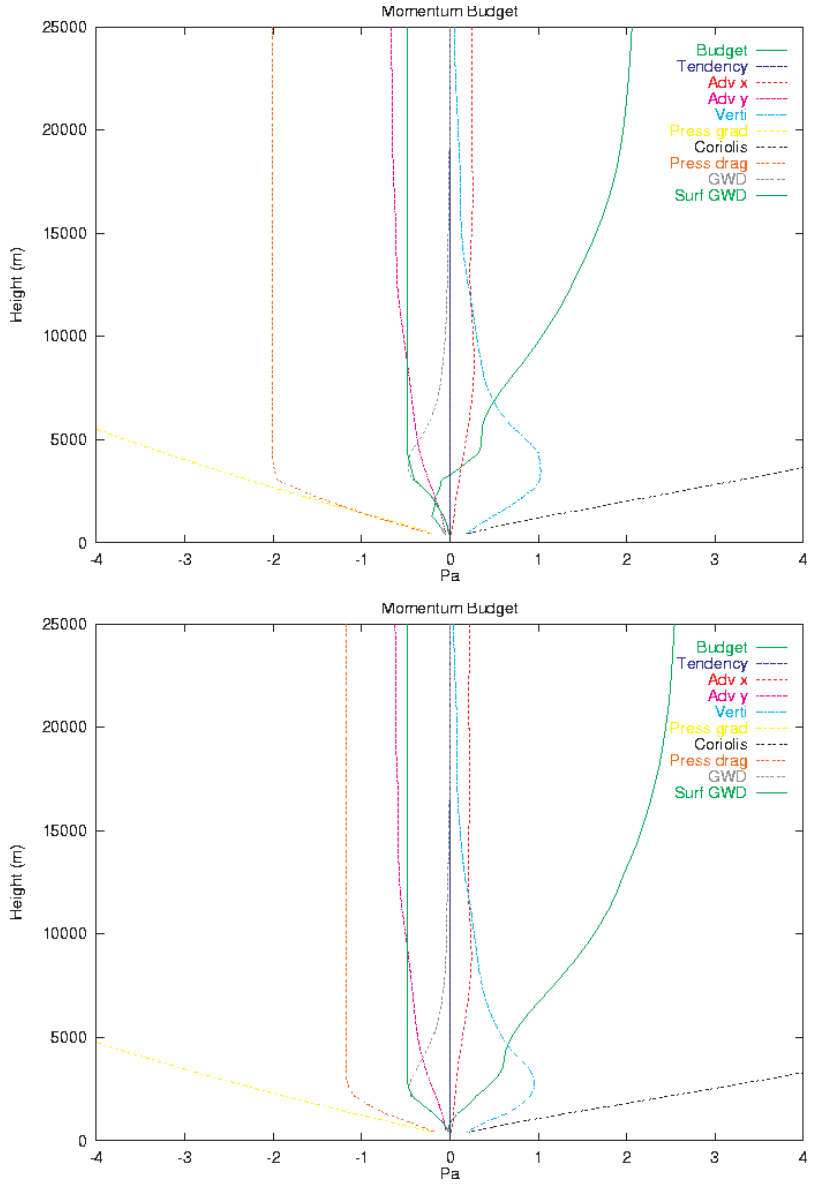

Figure 5 : Upper figure: momentum budget with envelope, lower figure: without envelope (both with GWDCD = 6).

5. Conclusions

Some preliminary conclusions concerning the change in resolution :

1. The gravity-wave drag parameterization disappears at 2.5 km resolution.
2. When going from 5 to 10 km resolution, the decrease in pressure stress is fully compensated by the increase in gravity-wave drag. So, the parameterization does what it is required to do (when a change in resolution is concerned).

Conclusions concerning the removal of the envelope :

As we can see from the momentum budgets, when installing an envelope the vertical flux is increased and spread over a larger vertical range. So when we want to remove the envelope, the parameterization should compensate for the loss of volume. As the scheme in its current form is not able to do this, we might have to think about a semi-envelope (where there is still a barrier effect, but the volume is suppressed).

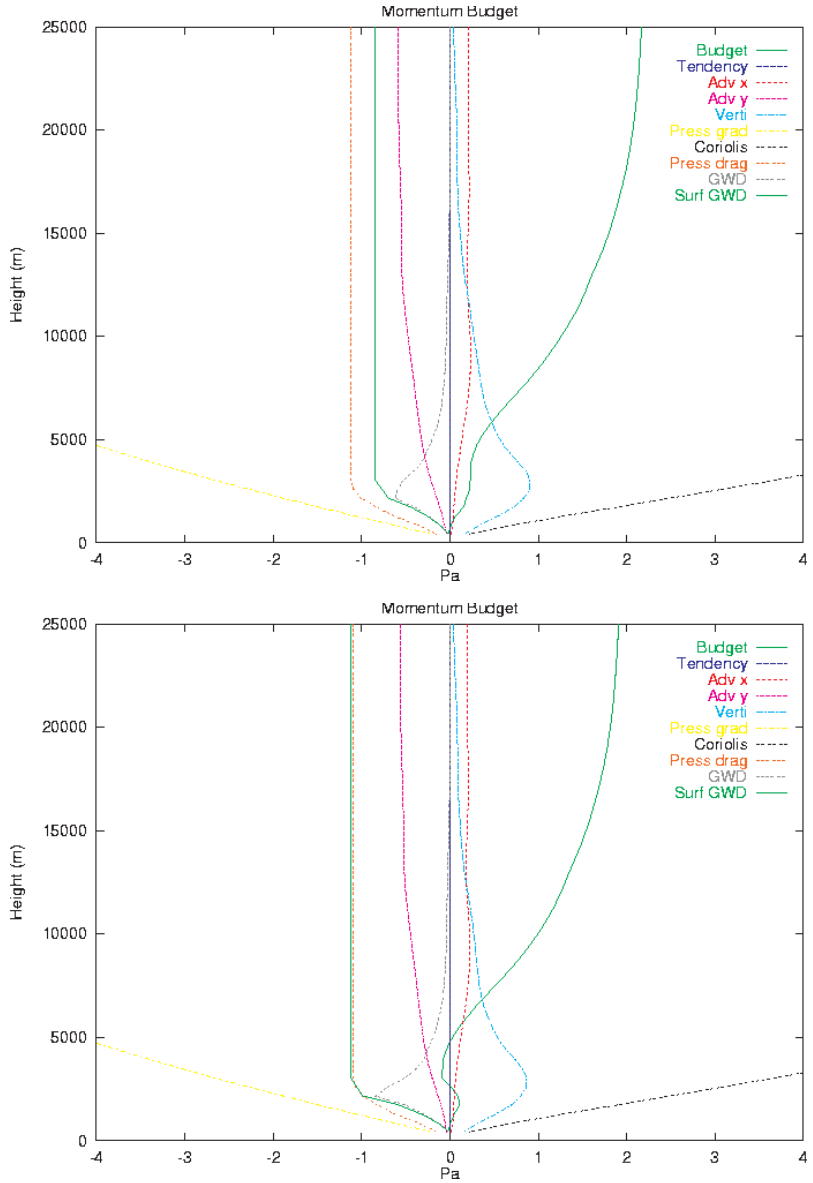

Figure 6 : Momentum budget without envelope and : upper figure : GWDCD = 60, lower figure : GWDCD = 100.

References

Geleyn J.-F. et al., 2002: Validation of ALADIN dynamics at high resolution using ALPIA, *ALADIN Newsletter*, **22.**

Gregoric G., 1997: Assesment of impact of th new low level blocking parameterization scheme on momentum fluxes over alps. GMAP *Stay Report.*

Lott F., 1999: Alleviation of Stationary Biases in a GCM through a mountain drag parameterization scheme and a simple representation of mountain lift forces. *Mon. Wea. Rev.*, **127**, 788-801 .

Lott F. and Miller M.J., 1997: A new subgrid-scale orographic drag parameterization: Its formulation and testing. *Q. J. R. Meteorol. Soc.*, **123**, 101-127.

Wallace J.M., Tibaldi S. and Simmons A.J., 1983: Reduction of systematic forecast errors in the ECMWF model through the introduction of an envelope orography. *Q. J. R. Meteorol. Soc.*, **109**, 683-717.

Beau Isabelle, 1997: Validation de paramétrisations des ondes de gravité orographiques à l'aide des données PYREX, *Thèse de doctorat*, Université Paul Sabatier, Toulouse.

Forecasting stratus formation : some insights from 1d experiments

Thomas Haiden
Central Institute for Meteorology and Geodynamics, Vienna, Austria . August 2003

1. Introduction

The ability of a model to predict low stratus crucially depends on its ability to forecast the characteristics of the vertical temperature profile. Verification studies of ECMWF and ALADIN operational forecasts have shown that both models systematically underestimate the strength and sharpness of inversions associated with stratus clouds. Most importantly, the cold air just beneath the inversion is too warm in the models, leading to an underestimation of sub-inversion cloudiness. Figure 1 shows a typical example. Below the inversion, the air is up to 5 K too warm in both models.

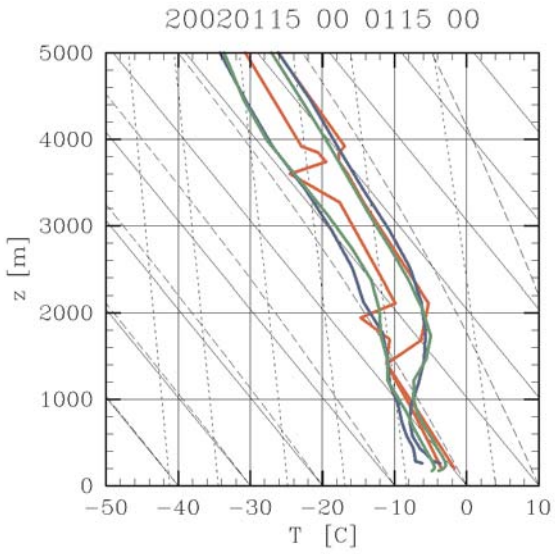

Figure 1 : Observed temperature and dewpoint temperature (red) in Vienna on a stratus day (15 Jan 2002, 00 UTC). ALADIN and ECMWF profiles are shown in blue and green, respectively. The warm bias below the inversion regularly occurs in the models during stratus episodes.

In the case of ALADIN it was found that part of the problem could be traced back to the assimilation in ARPEGE. Already at analysis time (+00 h) the model temperature structure shows a systematic deviation from the observed sounding. This happens because observed temperatures which are too far from the predicted ones are rejected. Note that this does not mean that the assimilation procedure is deficient. If the model background (the previous forecast) would be closer to reality, the assimilation would automatically keep some of the observations that are erroneously rejected now. Thus we are led back to the question of why the model does not produce the inversion structure as observed. To circumvent the problems due to assimilation we specifically investigate cases where the inversion was not present at +00 h but formed in the course of the forecast. Results of one such case study are presented here.

2. Description of the ALADIN-C model

Due to the large horizontal extent and near-homogeneity of low stratus, many aspects of the problem can be addressed using a 1d modelling approach. As a supplement to the ALADIN single column model (SCM) an off-line 1d model has been developed which incorporates selected physics subroutines of ALADIN. It is written in standard *c* and is referred to as the ALADIN-C model. The

need to develop an off-line 1d model arose from the sometimes limited flexibility of the SCM and the fact that it is almost as complex as the fully 3-dimensional ALADIN model. Also, it will be used as a framework for direct comparison of ALADIN and MESO-NH parameterizations at high vertical resolution. Up to now, ALADIN-C contains vertical diffusion and surface turbulence parameterizations (equivalent to `ACDIFUS, ACCOEFK, ACHMT`) as well as various stratiform cloudiness schemes, including one that is equivalent to `ACNEBN`. Different cycles of CYCORA can be simulated. For a description of the original ALADIN routines see Gerard (2000). The model uses a z-coordinate in the vertical, and liquid water potential temperature and total water content as dependent variables. Turbulent diffusion is computed explicitly using a small, adaptive time-step. It is planned to incorporate into ALADIN-C a number of additional routines of both ALADIN- and MESO-NH-type (e.g. radiation, a prognostic TKE scheme) in a step-wise process.

The model results shown below were obtained using a constant vertical resolution of 20 m, with the top of the domain at a height of 3000 m above ground level (= 150 layers). The coefficients related to the Richardson-number dependency of vertical diffusion are listed, since they have been re-evaluated several times during various CYCORA cycles. Following the latest recommendations we set :

```
usuric=0.175
usurice=0.5
usuricl=1.0
usurid=0.1
usuride=0.25
```

3. Cloud effects in inversion formation

The prolonged stratus episode which the example in Figure 1 refers to, started on 7 Jan 2002. After a frontal passage, synoptic-scale subsidence created a pronounced inversion in the period between 00 and 12 UTC (cf. Fig. 2). The operational ALADIN forecast (not shown) did produce the subsidence sinking but it did not generate a realistic inversion structure. To gain more insight into why the model temperature profile evolved differently from the one in the real atmosphere we performed several idealized experiments, three of which are presented here.

EXP1 : Vertical diffusion + prescribed subsidence sinking of 3 cm/s at z=3000m, decreasing linearly to zero at the surface.
EXP2 : Vertical diffusion + prescribed subsidence sinking of 3 cm/s at z=3000m, decreasing linearly to zero at z=1000m, with no subsidence below.
EXP3 : As in EXP2 but with a prescribed cloud-top cooling of 6 K/h.

For each experiment the model was initialized with the observed 00 UTC sounding, run for 12 hours, and then was compared to the 12UTC observed sounding. Surface fluxes of heat and mositure were set to zero. Figure 2a shows the result from EXP1 where the subsidence was assumed to decrease linearly towards the surface, implying horizontal mass divergence throughout the PBL. Comparison of the red and green curves shows that the forecast of the Td profile is roughly correct but the temperature is too high and the inversion unrealistically smooth. The model atmosphere is far from saturation, whereas the observed soundings indicate a layer of cloud between 500 and 1000 m above ground. The EXP1 forecast is rather similar to what the operational ALADIN model produced.

(a) EXP1 : subsidence + vertical diffusion

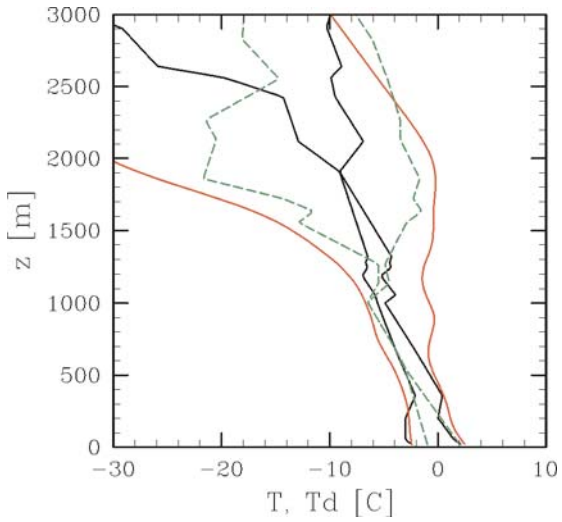

(b) EXP2 : as in EXP1, but no subsidence within PBL

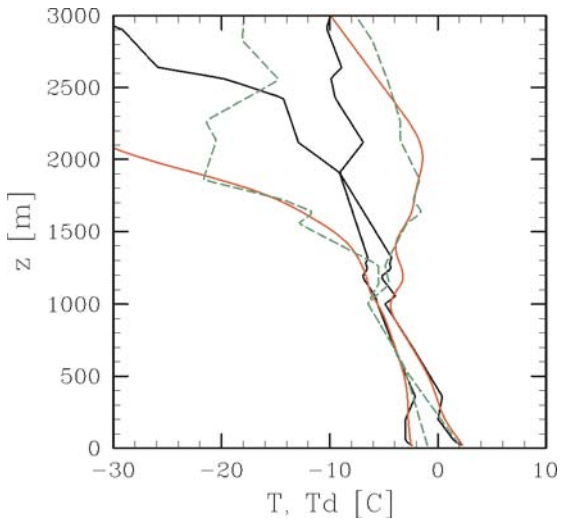

(c) EXP3 : as in EXP2 + prescribed cloud-top cooling

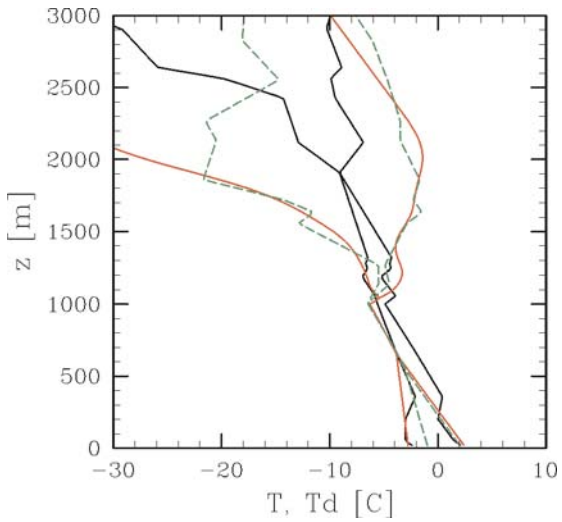

Figure 2 : Results of experiments with the ALADIN-C model. The observed Vienna sounding (T, Td) at initial time (7 Jan 2002, 00 UTC) is shown in black. The observed sounding 12 h later is shown in green. Model prediction for +12 hours is shown in red.

In EXP2 we prescribe the subsidence to drop to zero already at the top of the PBL (z = 1000 m), with zero sinking below. This generates a more realistic temperature profile, with a better defined

inversion, and air which is closer to saturation beneath it (Fig. 2b). However, in the real atmosphere the PBL has actually cooled during the 12 hours. This of course cannot be seen in EXP2 which includes vertical diffusion and subsidence warming but no diabatic effects.

To study the effect of cloud-top cooling we prescribe in EXP3 a constant diabatic cooling rate of 6 K/h at a single level (= 1000 m). With a layer thickness of 20 m this corresponds to a heat flux divergence of ~ 30 W/m², which is well within the range of values reported in the literature (Davies and Alves 1989, Ackerman et al. 1995). In this simplified experiment we do not specify explicitly whether it is radiative or evaporative cooling, or a combination of both. Figure 2c shows that the presence of the prescribed cooling brings the forecast very close to observations. The cooling gets vertically mixed throughout the PBL, creating a saturated layer between 600 and 1000 m.

Note that for all three experiments the standard vertical diffusion scheme of ALADIN was used. This proves that the scheme is in principle capable of simulating the turbulent flux structure associated with stratus, namely strong mixing within the cloud layer (due to negative buoyancy created at cloud top) and small vertical exchange directly above. Once a cloud cover of 100% is in place, and cloud-top cooling active, the model is able to maintain it. The current version of `ACNEBN`, however, does not produce 100% cloudiness, even if a layer is saturated.

The results suggest two likely causes for the inability of ALADIN to model stratus formation: (a) insufficient or absent cloud-top cooling and (b) subsidence too far down into the PBL. Whether (a) is mainly due to the cloudiness scheme or the parameterization of cloud effects in longwave radiation, is currently being investigated by H. Toth. Both (a) and (b) are probably contributing to a reinforcing feedback loop. When subsidence within the PBL keeps the air there too far from saturation, no cloud can form, hence no cloud-top radiative or evaporative cooling. The PBL, remaining too warm, does not decouple sufficiently from the flow above, allowing too much subsidence at low levels. This is further aggravated by insolation that reaches the surface because of missing cloudiness in the model and further warms the modelled PBL.

4. Conclusions

This study addresses the problem of forecasting the initiation of a stratus period, in particular the formation of the elevated inversion which is a necessary condition for this type of cloud. Comparison of observed soundings with idealized model results suggests the combined action of subsidence *above* the PBL and cloud-top cooling. An off-line 1d model (ALADIN-C) has been used to perform idealized experiments starting from observed soundings as initial condition. Different existing cloudiness schemes (`ACNEBN`, `ACNEBN`+Seidl-Kann modification, Xu-Randall, MESO-NH statistical cloudiness scheme) are currently tested within this framework, to study their effect on the stratus foreacst.

References

Ackerman, A. S., O. B. Toon, and P. V. Hobbs, 1995 : A model for particle microphysics, turbulent mixing, and radiative transfer in the stratocumulus-topped marine boundary layer and comparsions with measurements. *J. Atmos. Sci.*, **52,** 1204-1236.

Davies, R., and A. R. Alves, 1989: Flux divergence of thermal radiation within stratiform clouds. *J. Geophys. Res.*, **94,** 16277-16286.

Gerard, L., 2000: Physical parameterizations in ARPEGE-ALADIN. ALADIN report, 111 pp.

Some results of the sensitivity studies using the adjoint version of the ALADIN model

Andras Horanyi and Roland Steib

Introduction

The work presented in this Newsletter is based on the master thesis of Roland Steib, who completed his university studies as meteorologist during this summer. The main objective of the recent work was to complement and continue the work on adjoint sensitivity studies started by Cornel Soci for his PhD work. It is emphasised that the performed work gave just very preliminary results, without detailed analysis of them, due to the limitations of the framework of such a master thesis.

The main emphasis was put on the one hand to the exploration of a critical summer forecast case, when the operational ALADIN model was especially wrong, and on the other hand to the reproduction and further investigation of another case, which was already studied by Cornel Soci in his earlier ALATNET stay in Budapest. In the latter case the main further consideration was the application of the simplified and regularised physical parameterisation package in the adjoint model version as developed by Marta Janiskova.

Methodology

The applied methodology was very similar as it was used by Cornel, therefore only its main aspects and some differences are mentioned briefly :

-- The diagnostic (cost) function measuring the quality of the numerical weather prediction model's forecast (ALADIN) was computed as the quadratic difference between the model forecast and a reference analysis (the reference analysis for our case was the ALADIN 3d-var analysis; note that Cornel used the ARPEGE analysis as the true state of the atmosphere). The norm used in the experiments was the dry total energy norm.

-- The adjoint sensitivity study was performed by a nonlinear integration to obtain the trajectory needed for the adjoint model, the evaluation of the gradient at the final forecast time and then by the adjoint integration to the initial time for providing the gradient (sensitivity) fields (some target domains were used in order to concentrate only some specific areas, where the operational forecast was especially bad) with respect to initial conditions. All the simplified parameterisation schemes were tried in the course of the adjoint integration. The obtained gradients were renormalised into perturbations and then added to the original initial state providing new initial conditions for the nonlinear model run. Finally nonlinear model integration were performed and the new forecasts were compared to the original ones.

-- The ALADIN model version used was AL15 and two domains were applied : the old (extended Carpathian Basin) and new (Europe) ALADIN/HU domains (8 and 6.5 km horizontal resolution respectively). The new domain was used for the first case study and the old one for the second one.

Main results

As mentioned above two case studies were examined : the first one was related to an extremely bad ALADIN operational forecast during July 2002, the other one was an older case (June 2001), when the results earlier obtained by Cornel Soci were complemented by those ones using the simplified parameterisation schemes in the adjoint model.

1st case: 18th of July, 2002

For this summer case the operational ALADIN forecast failed to predict a heavy convective precipitation event over the middle part of Hungary already for a 6 h forecast period. At the same time a false precipitation signal appeared in the south-western part of the country. In terms of dynamical fields the most spectacular deficiencies in the operational model was found to be the forecast of the 2m-temperature field and the low-level meridional wind field. Adjoint sensitivity studies (in order to obtain 6 h gradients of the forecast-error cost function to the initial conditions) were run having the adiabatic version of the adjoint model and then several experiments were carried out using vertical diffusion, gravity wave drag, cloudiness, convection and large-scale precipitation simplified parameterisations in the adjoint model.

While examining the gradient (sensitivity) fields, one can immediately state that there was just very small advection for the given situation, i.e. the system was governed by local effects (locally triggered convection). By switching on the different parameterisation schemes in the adjoint model : the precipitation parameterisation schemes have a relatively large impact on the gradient fields (certainly it cannot be excluded that there are some numerical instabilities appearing in the gradient fields, this aspect should be further examined). The nonlinear sensitivity runs (when the initial conditions were improved by the renormalised gradients) showed that the best results were obtained, when both the large-scale precipitation and the convection scheme were switched on during the integration of the adjoint model.

As a summary it can be said that for this event, as it was anticipated, the precipitation-related parameterisation schemes had an important role and with their application in the adjoint model the forecast was successfully improved in some extent. Nevertheless it is a bit strange that the best results were obtained with the combined use of large-scale and convective precipitation, when the event was clearly a convective one (this behaviour was also noticed by Cornel Soci). Nevertheless this aspect (beside others) needs to be further investigated.

2nd case: 22nd of June, 2001

This case was already partially investigated by Cornel Soci during his ALATNET stay in Budapest : now a new model version was tried and the simplified parameterisation schemes were switched on during the adjoint model integration. Regarding the situation : a wrong precipitation forecast occurred at the south-eastern part of the country (the model erroneously gave around 15 mm precipitation to that area of Hungary, while in the reality there was just very small amount of rain). The related wind and temperature forecast was extremely bad giving for instance in some areas more than 22 m/s wind difference with the reality. While examining the sensitivity (gradient) patterns with respect to the initial conditions, first of all the strong advection is becoming clear, i.e. the meteorological system was rather a frontal one, with strong advective features. Regarding the application of the different parameterisation schemes, already the gradient of the adiabatic adjoint model version was able to correct the bad forecast and the other parameterisation schemes didn’t have any influence with respect to the adiabatic case. The main conclusion for this case was that this event was mainly conducted by dynamical forcing, when the effect of the simplified parameterisation schemes in the adjoint model were rather small.

Conclusions

The described work served just as a very preliminary investigation on the applicability of the different simplified parameterisation schemes in the adjoint model. Unfortunately we couldn’t explore with enough scientific details the obtained results, therefore at that stage it is considered that the main outcome of the work is not the deep dynamical analysis of the results, but the

demonstration of the feasibility of the applicability of the simplified schemes in the context of the adjoint model together with the hope that it can be later successfully used while computing singular vectors for short-range ensemble forecasts or in the process of four-dimensional variational data assimilation.

Acknowledgement

The authors are very grateful to Cornel Soci and Claude Fischer for their support and help during the accomplishment of the work presented in this small note.

One month parallel run of the Seidl-Kann cloudiness scheme

Alexander Kann
Central Institute for Meteorology and Geodynamics, Vienna, Austria

1. Introduction

Observing spatial and temporal evolution of temperature and moisture in the ALADIN model, deficiencies can be identified during typical wintertime periods. Although large areas are covered by a widespread low stratus layer, the model underestimates cloudiness in the lowest model levels. One source of errors is due to the treatment of observed strong inversions, which are smoothed unrealistically by the current operational data assimilation scheme if the model background is too far away from reality. Consequently, further development of the inversion strength is reduced and PBL - cloudiness cannot form.

An approach to improve the diagnosis within the cloudiness scheme is to establish a formulation that aims at typical sub-inversion cloudiness.

2. Design of Seidl - Kann stratus cloudiness scheme

A detailed description of the scheme was given in ALADIN Newsletter 22. Basically four additional criteria are introduced in subroutine *acnebn.F90* to identify low cloudiness which is connected to an inversion :

a) Quasi-saturation has to be fulfilled (currently set to 90%).

b) Coherent levels that are quasi-saturated must define a layer thicker than a critical value (currently set to 150 m).

c) Coherent inversion of critical strength must exceed a predefined value (currently 2K).

d) Distance between the lower boundary of the inversion and the upper boundary of the quasi-saturated layer must not exceed a critical value (set to 500 m).

If these four criteria are fulfilled, low cloudiness and the cloudiness of the quasi-saturated layers are set equal to one.

Comparison with the standard *acnebn.F90* and "Xu-Randall" *acnebn.F90* shows that the Seidl-Kann scheme gives results much closer to the latter with regard to inversion cloudiness.

3. One month of parallel model run

Before the modified *acnebn.F90* routine became operational in ALADIN-Vienna, a parallel run was installed and afterwards verified for the location Vienna.

From 20.12.2002 to 20.01.2003 several high-pressure systems with stratus coverage affected Central Europe, leading to differences in model output between the original *acnebn.F90* and the modified one.

Figure 1 shows an ALADIN-Vienna meteogram for the station Vienna with the original cloudiness scheme (initial time: 20.01.2003 00 UTC run). Although relative humidity often exceeds 90% in lowest model levels, only little cloud fraction is generated by the model. On the other hand, the parallel run with the modified *acnebn.F90* routine increases the cloud coverage up to 100%, which is maintained during most of the integration time (Fig. 2). The improvement of cloudiness forecasts has also positive side effects on 2 m-temperature forecasts : diurnal amplitudes are reduced due to reduced sensible heat fluxes.

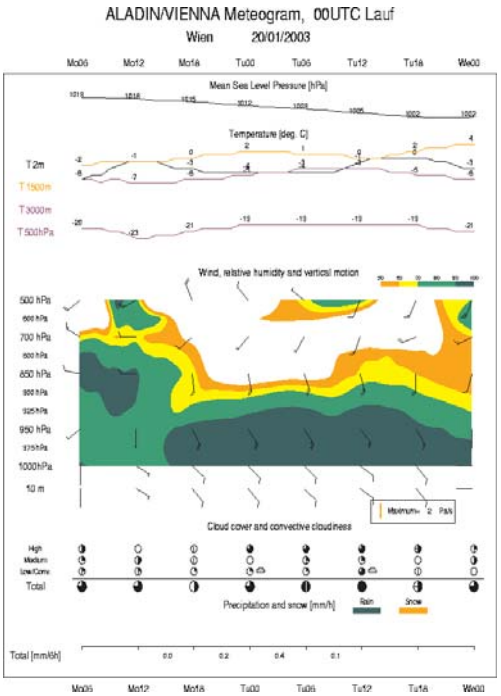

Fig. 1: ALADIN-Vienna forecast meteogram from 20.1.2003 00 UTC with original acnebn.F90

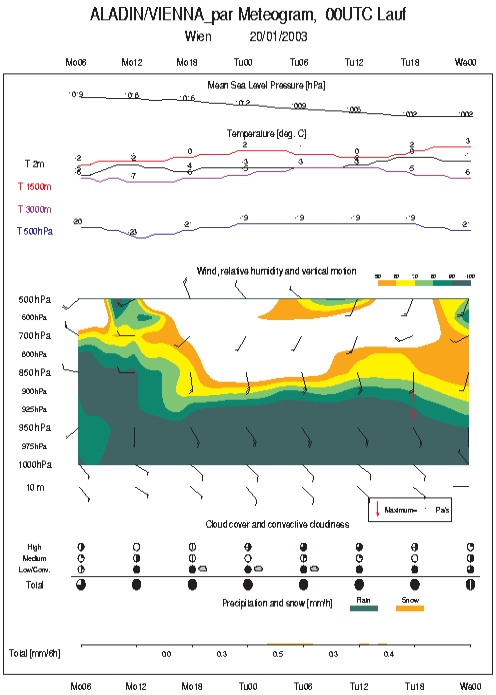

Fig. 2: ALADIN-Vienna forecast meteogram from 20.1.2003 00 UTC with modified acnebn.F90

Figure 2 points out an intensification of the vertical gradient of moisture between 850 hPa and 925 hPa as well. This is mainly based on the temporal evolution of the inversion, which becomes more pronounced in presence of low cloudiness (mainly due to cloud-top cooling).

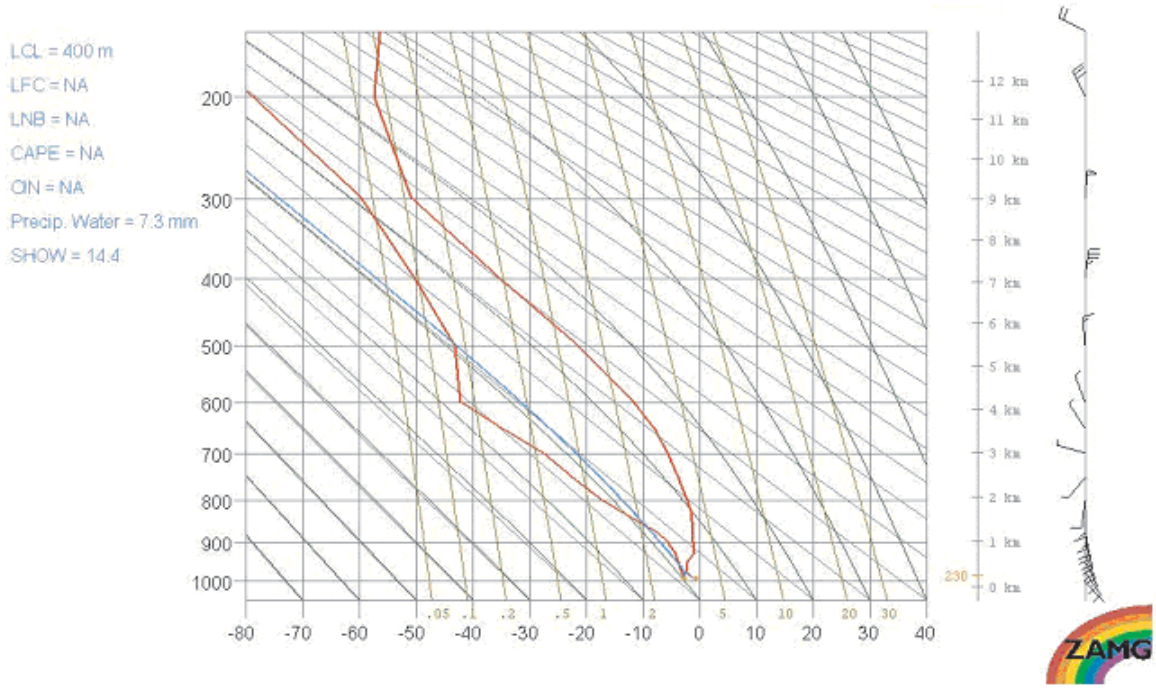

Fig. 3: ALADIN-Vienna operational model run
Date: 19.01.2003 00 UTC +12 hours forecast, location Vienna

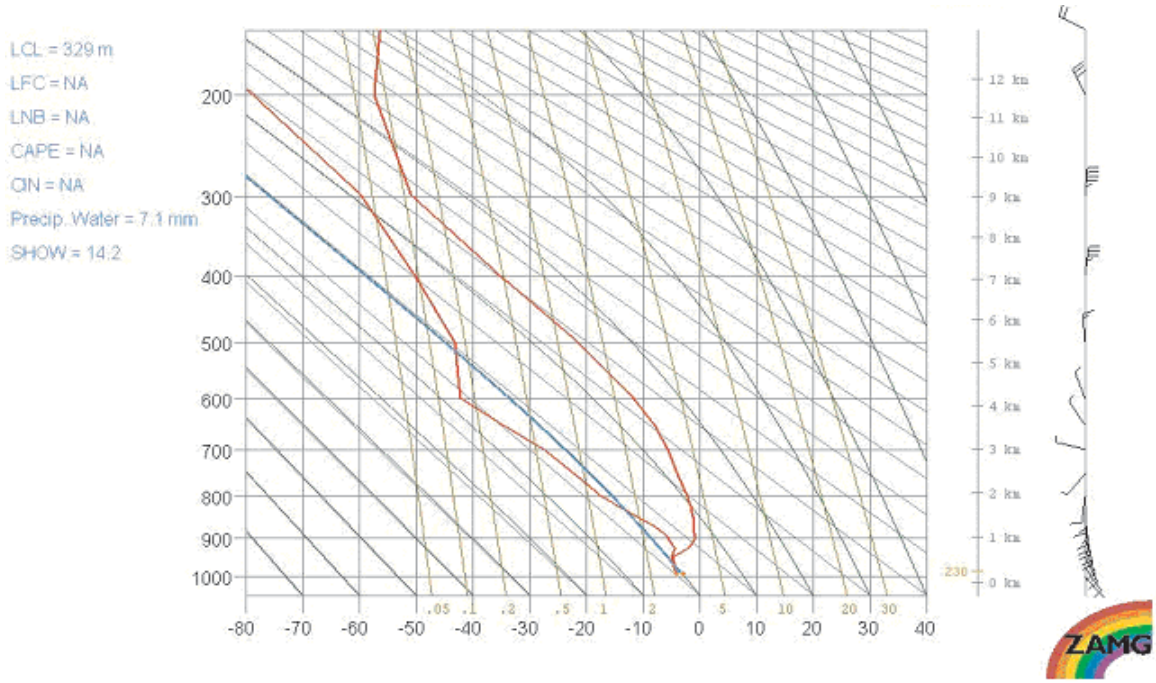

Fig. 4: ALADIN-Vienna parallel model run with *"acnebn.F90* + Seidl–Kann"
Date: 19.01.2003 00 UTC +12 hours forecast, location Vienna

This fact is confirmed in Fig. 3 (operational run, vertical profile at Vienna, 19.01.2003 00 UTC +12 hours forecast) and Fig. 4 (parallel run with modified *acnebn.F90*, vertical profile at Vienna, 19.01.2003 00 UTC +12 hours forecast) which demonstrate the formation of a more realistic stratus-type temperature and moisture profile in presence of a stratus layer.

This development was found in an other experiment as well, where low cloudiness was set equal to one regardless of the inversion strength. Cloud-top cooling and subsidence lead to a more realistic temperature and moisture profile with respect to sharpness and strength, that allows to maintain cloud coverage. Thus, a more realistic development of the vertical PBL structure seems to require the presence of a stratus-like cloudiness in the model.

The verification of one month parallel run of ALADIN-Vienna includes the parameters total cloudiness (Fig. 5) and 2 m-temperature.

Many cases in Fig. 5 show only slight changes of model output concerning total cloudiness. The vertical structure of temperature and moisture is too far away from reality, thus the four criteria (discussed in section 2) are not fulfilled. Positive values indicate an improvement using the modified cloudiness routine. The reduction of absolute errors may reach values up to 7 octa, especially during the last stratus episode, from 18.01.2003 to 20.01.2003. An overestimation of low clouds was rarely produced by the modified diagnosis within one month of parallel run. About 25% of all cases with different model output concerning total cloudiness show a slight decrease of the forecast performance, whereas 75% indicate an increased forecast quality. The mean absolute error (MAE) of total cloudiness diagnosed with the standard *acnebn.F90* is 2.0, this MAE could be reduced to 1.2 with the modification set. Note that by definition only cases with different model output of low cloudiness form the basis of MAE.

The verification of 2 m-temperature shows similar results. The mean absolute error of operational model run is about 1.8 K, the modifications in *acnebn.F90* cause a reduction to 1.5 K. 65% of all cases (= hourly observations) show improvements if forecasted with modifications, about 35% of them lead to worse forecasts.

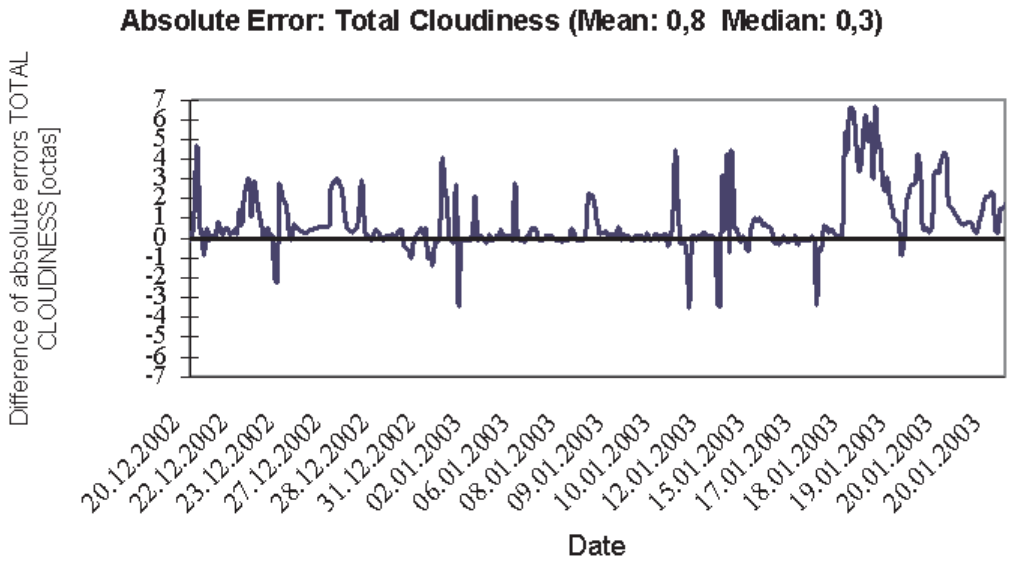

Fig. 5: Total cloudiness in octa : Absolute error of operational model output minus absolute error of parallel (=*acnebn.F90* + Seidl-Kann scheme) model run (location Vienna, interpolated). Chronological cases are chosen hourly from 20.12.2002 – 20.01.2003, and for daily 00 UTC runs (+48 hours), but only if total cloudiness at station 11035 is observed.

4. Final Remarks

The parallel run during the chosen month suggests an improved stratus forecast for the next wintertime period. Nevertheless, it should be mentioned that physical approaches with respect to a better simulation of the PBL structure are still necessary to forecast more realistic stratus-like temperature and moisture vertical profiles (improvements in the model's ability of cloud top cooling, synoptic subsidence above the PBL and tests with different cloudiness schemes, e.g. Lopez, Xu-Randall, Meso-NH schemes).

Evapotranspiration effects on mountain convection in ALADIN

G. Pistotnik and T. Haiden
Central Institute for Meteorology and Geodynamics, Vienna, Austria . August 2003

1. Introduction

Which meteorological processes determine if and where deep convection develops on a given day ? We need to address this question in order to improve the forecasting of convective precipitation. If synoptic-scale lifting mechanisms are weak or absent, meso-scale effects become important and topographically induced circulations and their convergence patterns become a major factor (e.g. Banta, 1990). With regard to the ALADIN model, this problem has been studied by Cordoneanu and Geleyn (1998). Another potentially important process is surface evapotranspiration. It partially compensates the afternoon drying of the PBL resulting from vertical mixing and thus has a direct effect on cloud base height and CAPE. Here we use the ALADIN model at high resolution (4 km) to investigate its contribution to convective rainfall in a mountainous area.

The effect of changes in Bowen ratio B=H/LE (H=sensible heat flux, LE=latent heat flux) on boundary-layer growth and convective cloud formation has been studied before (Rabin et al., 1990; Schrieber et al., 1996). It can be shown theoretically that, for a given total surface turbulent heat flux H+LE, the drier surface generates deeper convective boundary-layers and higher cloud bases (Haiden, 1997). How this affects cumulus cloud formation depends on stratification, among other things. Since the decrease in latent heat flux LE is linked to an increase in sensible heat flux H, the whole daytime boundary-layer evolution changes. Thus the specific effect of evapotranspiration as a water source cannot be isolated with this type of experiment. (It is however a very useful setup to study how deforestation affects convection, or how a prolonged dry spell reinforces itself through reduced convection.) Here we report on a different kind of experiment, where LE is set to zero only where it represents a water source for the atmosphere, but nowhere else. This is clearly an academic experiment because water gets ‘lost’ at the surface-atmosphere interface. However, it allows to directly quantify the effect of this water source on convective activity, without the complications due to a changed thermal structure, or changed flow patterns. Technically this was done by setting "`PDIFTQ(KLEV)=0`" in subroutine `ACDIFUS`.

2. Experimental setup

The area of investigation is a NW-SE running valley in Carinthia, Austria’s southernmost province. The valley was chosen because it stretches along an almost straight line (an advantage for the evolution of a nearly ideal valley wind circulation) and because it is well covered by five stations, enabling a verification of the model output by observational data. The U-shaped, rather narrow valley is surrounded by mountains reaching well above 2000 m. At its lower end, it widens into the Klagenfurt basin, a large intra-alpine basin, at a height of about 500 m. The day of investigation, 10 August 2000, has been studied before (Haiden, 2001). The synoptic situation was characterized by high pressure with a weak northwesterly flow. On the lee side, i.e. in the southern part of the Alps, undisturbed diurnal circulations could evolve. The air mass was rather stably stratified and dry, so showers and thunderstorms formed only isolated over a few (also climatologically favoured) spots along the southeastern alpine rim, none of them inside the investigation area. The case is considered representative of a large number of days during summertime when convective conditions are rather suppressed but some thunderstorms and/or showers can form locally.

Two model runs of ALADIN (AL15) were carried out at a horizontal resolution of 4 km, the first with standard settings (further referred to as the reference run) and the second with evaporation set equal to zero (referred to as the experimental run). Results of the two runs were compared,

especially with regard to the differences in the moisture patterns and simulated convective precipitation.

3. Results

In the reference run, convective precipitation starts in the late morning, around 09 UTC, and is at first strictly tied to orographical features. The first convective cells appear over the mountains framing the Klagenfurt Basin, where orographically induced convergence of the near-surface wind coincides with moisture advection from the basin. It takes two or three more hours until deep convection starts in the central parts of the Alps which do not experience humidity advection from adjacent basins or broad valleys. During the course of the afternoon, the correlation between precipitation and orographic features becomes weaker, giving way to a seemingly random precipitation pattern affecting parts of the valleys and subsiding in the evening hours. Total simulated rain amounts are low, large areas receive only some tenth of a millimeter and a few centres in the vicinity of effective "rain-producing" mountains get around 5 mm. Note that in the model much of the investigated area receives precipitation, whereas no precipitation was observed there by radar. The problem that the model generates convective precipitation too widespread and too often is well known, and is found in the operational forecasts (on 10 and 12 km resolution) as well. Figure 1a shows the areal distribution of convective precipitation generated by the reference run between 06 and 18 UTC.

In the experimental run only few areas receive precipitation (Figure 1b). This is because cloud bases are significantly higher (by up to 1 km) than in the reference run, and CAPE (not shown) almost reduced to zero. Note that the areas that still get some rainfall are close to the basin at the eastern boundary of the area, whereas in the inner-mountain areas rainfall is completely absent. Thus, the switching off of evaporation as a moisture source *everywhere* has shut down convection especially in the *inner parts* of the mountainous area. In the experimental run, the evaporation that maintains the valley's humidity excess compared to the surrounding mountains is missing as the most important humidity source. During the course of the day, boundary-layer moisture is completely mixed out by convection and not replenished. The usual structure with humid valleys and dry mountains gradually vanishes and turns into a smooth, rather homogeneous field. Reduced cumulus cloudiness allows stronger daytime heating over the mountains and intensifies the baroclinicity which drives the slope wind system. It is an interesting result that the convergence of the slope winds over the mountain tops is even slightly larger in the experimental run, and that is why also the convection's initial upward pulse is stronger. The overcompensation of this baroclinic enhancement of the convective cells by the higher condensation level is, however, sufficient to limit precipitation to those few places which offer the best conditions for deep convection.

Figure 2 shows the diurnal course of 2-meter specific humidity at the station Mallnitz (11260) situated in the upper part of the valley. The green line represents observational data and the white and red line show the results of the reference and experimental model runs, respectively. The negative bias of the reference model output is mainly due to the fact that the station height is 1185 m whereas the corresponding gridpoint in ALADIN is located at 2045 m. This is also why the operational run generates a curve with a marked single wave rather resembling a slope station whereas the observations, despite the station's rather high altitude, show weak characteristics of a broad valley with an indicated second humidity maximum in the morning. This second maximum, which was found at all stations in the valley, is due to advection of moisture by the up-valley wind. The experimental run shows a minimum late in the morning, when convective activity has mixed out the little boundary-layer moisture, before humidity increases again with the onset of the valley wind. Another interesting detail is that the model curves come close to each other again during the evening hours. A likely explanation is that the commencing mountain wind advects air from above the PBL, which has similar humidity in both experiments. Observed specific humidity, however, is

much higher in the evening, presumably because a shallow valley inversion manages to decouple from overlaying air layers. This process is not simulated by the model due to its smooth topography which gives the location the characteristics of a slope rather than a valley floor.

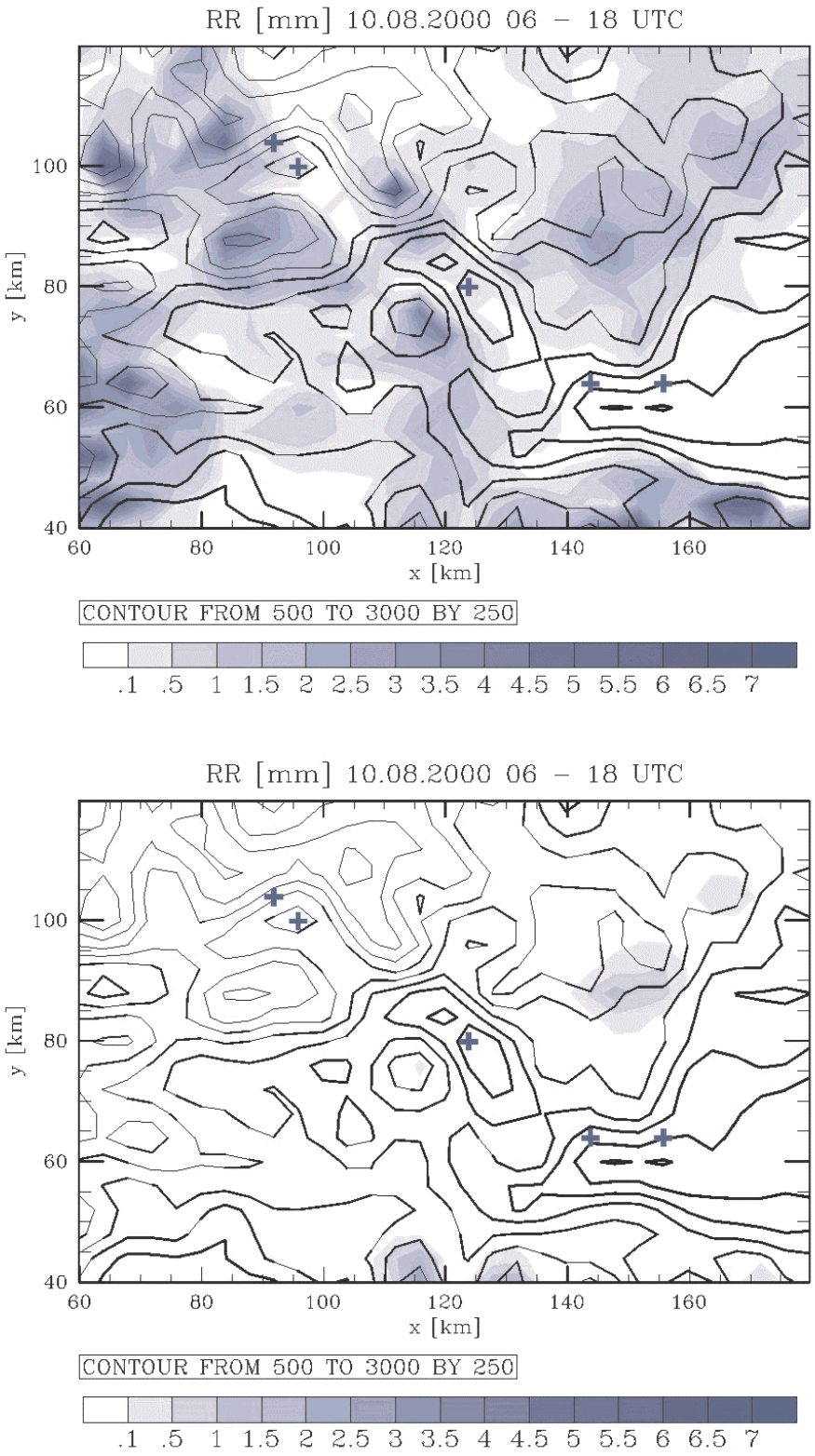

Figure 1 : Precipitation (in mm) generated by the reference model run (top) and the experimental run (bottom), on 10 August 2000 between 06 and 18 UTC. Isolines of the model topography are shown in black, the lowest being 500 m, the highest 2750 m and the spacing 250m; thicker lines represent lower elevations. The investigated valley runs from NW to SE through the area shown. Blue crosses represent the five stations covering the valley.

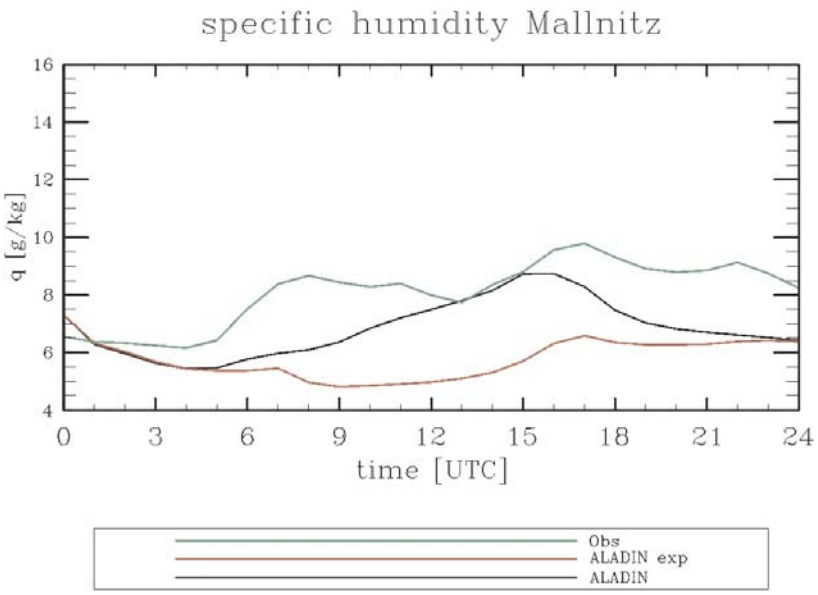

Figure 2 : Time evolution of 2-m specific humidity at the station Mallnitz (the westernmost station shown in Fig. 1), on 10 August 2000. The green line represents observational data, the black line the reference run and the red line the experimental run.

4. Conclusions

According to the model experiments, daytime surface evaporation has a large effect on convective rainfall in cases where convective activity is generally weak. Most of the areas that receive rainfall in the reference run remain dry in the experimental run. It is found that the inner, higher elevation parts of the domain are most sensitive to the lack of evaporation. With surface evaporation off, cumulus cloud bases were typically 500-1000 m higher, and CAPE decreased from 100-200 m^2/s^2 to near-zero values. The increase of 2m specific humidity during the day due to the up-valley wind is almost completely missing in the experimental run. This leads to a reduction of specific humidity in the valley of 2-3 g/kg. However, the experiment needs to be repeated (1) for a more unstable day with widespread convective activity, to see how much smaller the effect of surface evaporation is in those cases; (2) for a day where convective rainfall on the previous day has produced a distinct spatial pattern of surface evaporation that could directly affect the pattern of convective activity.

References

Banta, R.M., 1990: The role of mountain flows in making clouds. In: Blumen, W. (ed.), Atmospheric Processes over Complex Terrain. *Meteor. Monogr.*, **45**, 229-283.

Cordoneanu, E., and J. F. Geleyn, 1998: Application to local circulations above the Carpathian-Black Sea area of a NWP-type meso-scale model. *Contr. Atmos. Phys.,* **71,** 191-212.

Haiden, T., 1997: An analytical study of cumulus onset. *Quart. J. Roy. Meteor. Soc.*, **123,** 1945-1960.

Haiden, T., 2001: Orographically triggered convection: a case study. Proceedings, *10th ALADIN Workshop,* Toulouse, France.

Rabin, R. M., Stadler, S., Wetzel, P.J., Stensrud, D. J., and M. Gregory, 1990: Observed effects of landscape variability on convective clouds. *Bull. Am. Meteorol. Soc.,* **71,** 272-280.

Schrieber, K., Stull, R. B., and Q. Zhang, 1996: Distributions of surface-layer buoyancy versus lifting condensation level over a heterogeneous land surface. *J. Atmos. Sci.,* **53,** 1086-1107.

Pre-Processing of the AMDAR data at HMS

Roger Randriamampianina and Gabriella Csima
Hungarian Meteorological Service . 2003.08.28

1. Reception of the AMDAR data at HMS

The AMDAR (Aircraft Meteorological Data Reporting) telegrams contain the results of aircraft measurements. These measurements provide accurate data on wind and temperature at high levels in finer, compared to radiosonde data, time resolution. Using AMDAR data, we expect to improve the quality of the products of the ALADIN 3d-var system and, consequently, the accuracy of the forecast. We receive AMDAR data separately from each aircraft every hour or even more frequently through the Global Telecommunication System (GTS) in one or more telegrams. We store each telegram in a separate file. At present AMDAR data are saved into 1000-1500 small files per day, their number is increasing rapidly. The AMDAR telegrams are stored in two formats : ASCII and BUFR. They contain the aircraft flight number, the measurement time (days, hours, minutes in ASCII and years, months, days, hours and minutes in BUFR formats), the stage of the flight (take off, landing or other stages) and the meteorological parameters - mainly wind speed, wind direction and temperature. The ASCII telegrams contain other meteorological data like turbulence and vertical wind gust, but we do not use them in 3d-var.

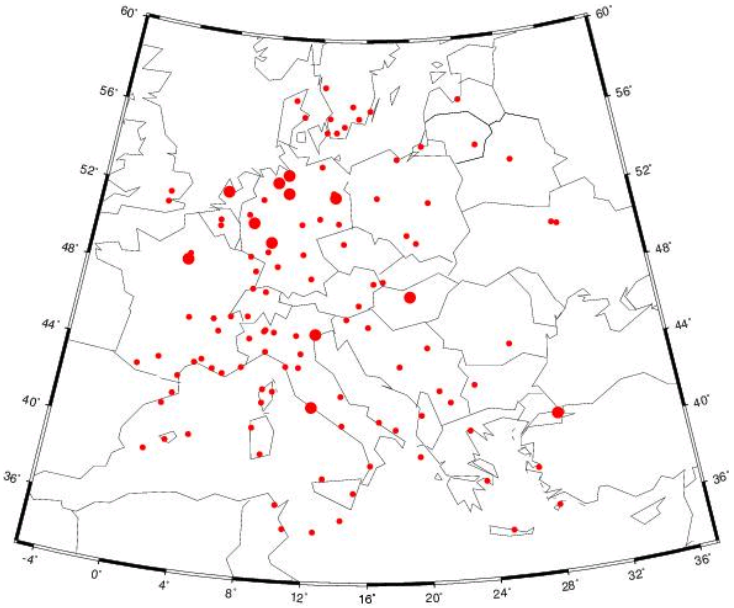

Figure 1 : Location of airports in the ALADIN-HU domain. Bold dots indicate places with big amount of AMDAR measurements.

2. Pre-processing of the AMDAR data for the 3d-var system

The AMDAR data are pre-processed for 3d-var every 6 hours. The pre-processing interval is ±3 hours. Thus, for producing the 12 h UTC analysis, for instance, we consider AMDAR data received between 9 and 15 h UTC. Figure 1 shows the airports in the ALADIN/HU domain. Bold dots indicate places (Frankfurt, Cologne, Hamburg, Berlin, Hanover, Bremen, Rome, Paris, Amsterdam, Venice, Istanbul and Budapest), where the amount of measurements during the study period (2003.02.25 - 2003.03.01) was outstandingly big. Figures 2-3 present the spatial locations of all the measurements for a 24 hours time-interval, corresponding to four (12, 18, 00 and 06 h UTC) analysis times. As can be seen in the figures, most of aircraft measurements are performed over

Western Europe. Considering the amount and spatial distribution of the aircraft data we concluded, that AMDAR data might give important additional information for the ALADIN 3d-var system. It is clear that the amount of aircraft data on the Eastern part of the ALADIN-HU domain is very small. Recently we are working on the assimilation of AMDAR data into the 3d-var system and on corresponding impact studies. We use the *"OULAN-BATOR-OBSORT-toODB"* pre-processing chain to insert the AMDAR data into ODB.

Preliminary results of the impact study on the use of AMDAR data in the 3d-var ALADIN/HU are expected until the end of this year.

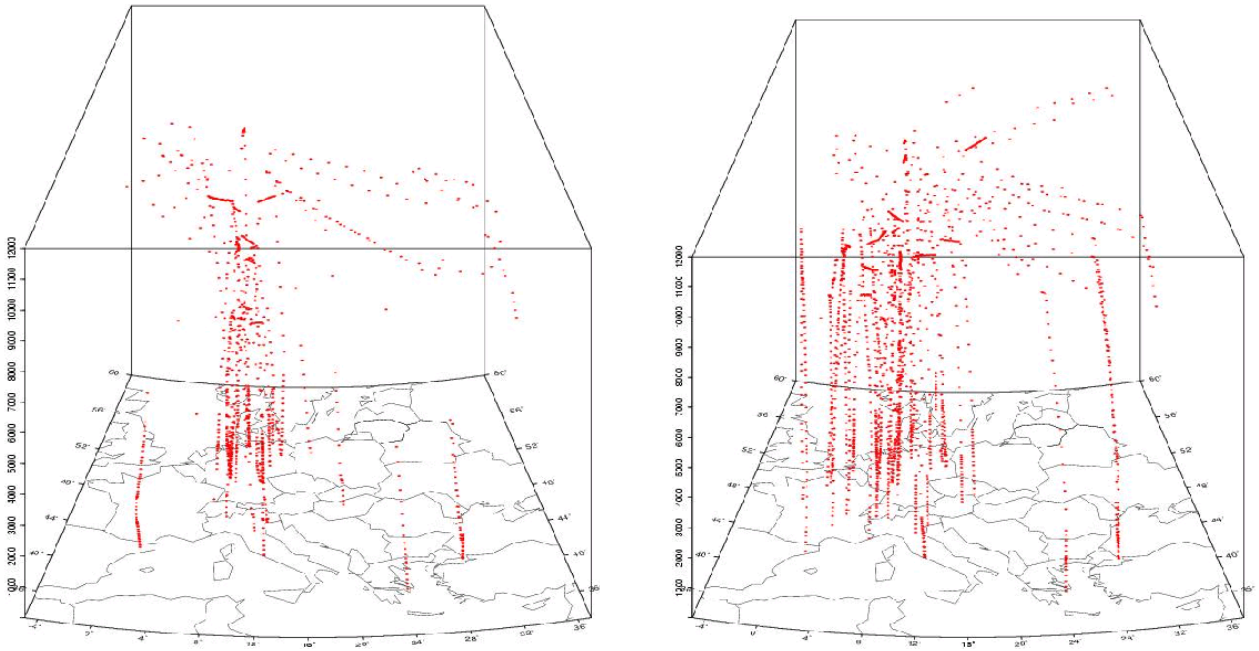

Figure 2 : Tree-dimensional distribution of AMDAR measurements (during landing and take off) over ALADIN/HU domain within a ±3 hour interval at 00 UTC (left) and 06 UTC (right) (2003.02.26) assimilation time.

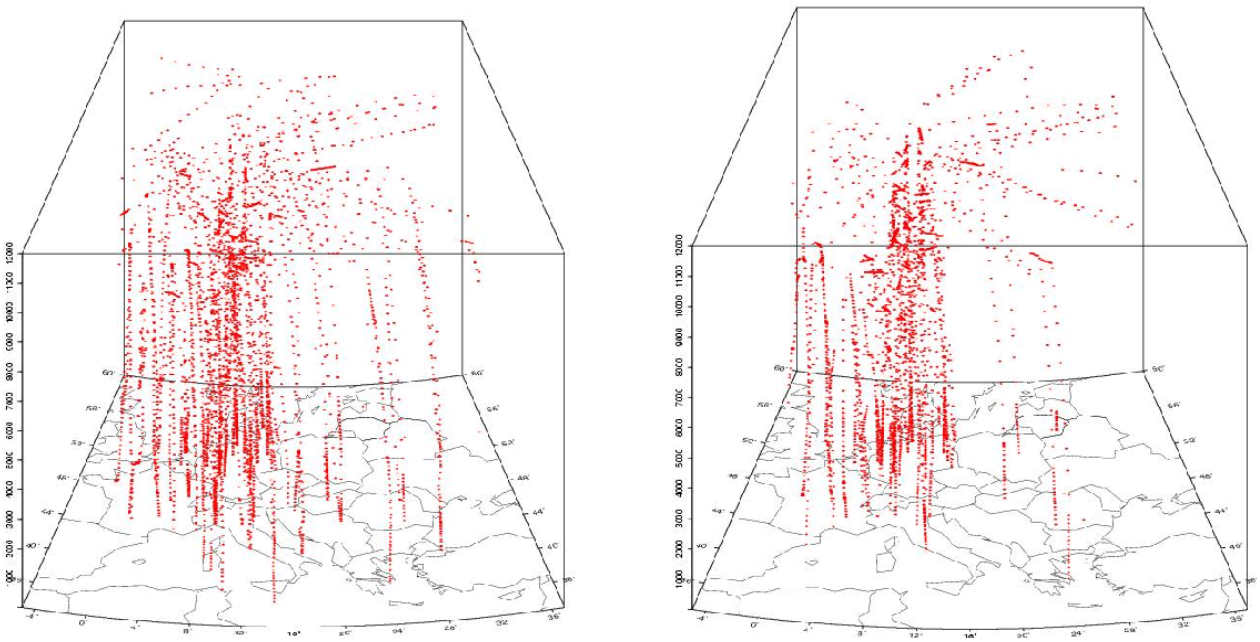

Figure 3 : Tree-dimensional distribution of AMDAR measurements (during landing and take off) over ALADIN/HU domain within a ±3 hour interval at 12 UTC (left) and 18 UTC (right) (2003.02.25) assimilation time.

Impact of the ATOVS data on the mesoscale ALADIN/HU model

Roger Randriamampianina and Regina Szoták
Hungarian Meteorological Service . 2003.08.28

1. Introduction

The pre-processing and the implementation of ATOVS data into the ALADIN three-dimensional variational (3d-var) data assimilation system at the Hungarian Meteorological Service (HMS) was described in Randriamampianina (2003). This report presents the first results of the study on the impact of ATOVS data on the analysis and forecasts of the ALADIN model.

Section 2 gives brief description of the characteristics of the ALADIN/HU model. Section 3 introduces the pre-processing of ATOVS data. Description of the experiments done for the impact study is shown in Section 4. Section 5 presents the results of the impact study, followed by some selected cases in Section 6. In Section 7 we draw some conclusions and discuss further tasks.

2. Main characteristics of the ALADIN/HU model and its assimilation system

The hydrostatic version of the ALADIN model was used in this study. The horizontal resolution of ALADIN/HU is 6.5 km. It has 37 vertical levels from surface up to 5 hPa. We use the 3d-var technique as an assimilation system. An important advantage of the variational technique is that the computation of the cost function for observations part is done in the observations space. Thus, for the assimilation of radiances, we have to be able to determine them from the model parameters. For this purpose we need a radiative transfer code. In our case (ARPEGE/ALADIN) we use the RTTOV code (Saunders et al., 1998), which uses 43 vertical levels. Above the top of the model, an extrapolation of the profile is performed using a regression algorithm (Rabier et al., 2001). Below the top of the model, profiles are interpolated to RTTOV pressure levels. Assimilation systems require a good estimation of background error covariances - the so-called "B" matrix. B matrix was computed for the new domain using the "standard NMC method" (Parrish and Derber, 1992). A 6-hour assimilation cycling was chosen, consequently the 3d-var is running 4 times a day at 00, 06, 12 and 18 UTC. We perform a 48-hour forecast once a day, from 00 UTC.

3. Data pre-processing

We receive the ATOVS data through a HRPT antenna. The AMSU-A, level 1C, data are pre-processed by the *AAPP* (ATOVS and AVHRR Pre-processing Package) package. We use the pre-processing chain *OULAN-BATOR-OBSORT-toODB* to create the ODB files. The output of the *AAPP* is read in direct way in the *OULAN* pre-processing package.

Choice of Satellite :

Because of its technical specifications, our antenna receives data from only two satellites at the same time. Data from NOAA-15 are available over the domain of ALADIN/HU at about 06 and 18 UTC, while data from NOAA-16 are available around 00 and 12 UTC. The orbit of the NOAA-17 is between the orbits of the other two satellites, a bit closer to that of NOAA-16. We know that NOAA-15 has problem not only with the AVHRR instruments but also with some microwave channels (AMSU-A-11 and AMSU-A-14). Nevertheless, NOAA-15 and NOAA-16 were chosen for the impact study, to guarantee the maximum amount of observations at each assimilation time.

Extraction of ATOVS data :

Satellite data observed and pre-processed in the interval of ±3 hours from the assimilation time are treated. The maximum number of orbits found at one assimilation time varies up to 3.

Bias correction :

The systematic error of the satellite data can be shown comparing the observed radiances with the computed (simulated) ones. The systematic error arises mainly from errors in the radiative transfer model, instrument calibration problems or biases in the model fields.

The bias-correction coefficients for data from NOAA-15 and NOAA-16 were computed according to Harris and Kelly (2001) for the study period. Note, that the bias coefficients were computed for different latitude bands. Figure 2 demonstrates the bias, computed for the same

latitude band, for NOAA-15 and NOAA-16.

Channel selection :

Analysing the bias of the brightness temperature, specific for each AMSU-A channel, inside all possible latitude bands, we decided to keep the same number of channels as in the ARPEGE model (see Table 1). Our study is interesting from the point of view of use of AMSU-A data over land (see Table 1), because the percentage of land over the ALADIN/HU domain is more than 70 %.

Observation statistics and assimilation of radiances :

It is necessary to check the efficiency of ATOVS data based on statistics (theoretical standard deviation - *rmtberr_noaa.dat* constant file) used to handle the observation in case of new data and, in our case, "new model configuration" (more examples can be seen in Randriamampianina and Rabier, 2001). The "observation (AMSU-A radiances) minus guess (computed radiances)" data were compared with the "observation minus analysis" ones for this purpose (Figs 3-6). These figures show statistics computed from a few days (2003.02.20 - 2003.02.25) of cycling. The distance between the two curves indicates how the addition of the AMSU-A data could modify the first-guess fields during the assimilation. The larger the distance the bigger the impact of the observations (so, of AMSU-A) on the analysis. These results are comparable to those computed in Randriamampianina and Rabier (2001). Another test was done before starting the experiments, which consisted in reproducing the above-mentioned experiment after reducing the theoretical standard deviation by half. We did not find any considerable changes in the results. So we decided to keep the original values of the theoretical standard-deviation at this stage, as it is used in ARPEGE.

channel number	1	2	3	4	5	6	7	8	9	10	11	12	13	14	15
over land					x	x	x	x	x	x	x	x			
over sea					x	x	x	x	x	x	x	x			
over sea ice							x	x	x	x	x	x			
cloudy pixel								x	x	x	x	x			

Table 1 : The use of AMSU-A channels. Note, that "over land" channels 5 and 6 are used when the model orography is less than 500 m and 1500 m, respectively.

4. Experiments design

In the experiments, two thinning techniques (80 and 120 km resolution) were investigated. The impact of ATOVS data was studied for a two-week period (from 2003.03.20 to 2003.03.06). Surface (SYNOP) and radiosonde (TEMP) observations were used in the control run. The impact was evaluated comparing the control run with runs using TEMP, SYNOP and ATOVS data. Examining the first results, we found that the impact of ATOVS data on analysis and forecasts depends on the way the control variables (vorticity, divergence, temperature and surface pressure, specific humidity) are handled (in particular, the assimilation of specific humidity in univariate form or with all control variables using the multivariate formulation).

The following experiments were carried out:

T8000 - TEMP, SYNOP and AMSU-A data were assimilated. The AMSU-A data were thinned at 80 km resolution. The multivariate formulation was used for all control variables.

T1200 - TEMP, SYNOP and AMSU-A data were assimilated. The AMSU-A data were thinned at 120 km resolution. The multivariate formulation was used for all control variables.

Aladt - TEMP and SYNOP were assimilated - control run. It is our 3d-var cycling running as

parallel suite. The multivariate formulation was used for all control variables.

Touhu - TEMP, SYNOP and AMSU-A data were assimilated. The AMSU-A data were thinned at 80 km resolution. The specific humidity was assimilated as an univariate control variable, whereas the other control variables were assimilated using a multivariate formulation.

12uhu - TEMP, SYNOP and AMSU-A data were assimilated. The AMSU-A data were thinned at 120 km resolution. The specific humidity was assimilated as an univariate control variable, whereas the other control variables were assimilated using a multivariate formulation.

Aluhu - TEMP and SYNOP were assimilated - control run. The specific humidity was assimilated as an univariate control variable, whereas the other control variables were assimilated using a multivariate formulation.

Dynam - Dynamical adaptation run - the operational run in Hungary.

Objective verification :

This report presents the results of the objective verification. The bias and the root-mean-square error (RMSE) were computed from the differences between the analysis/forecasts and the observations (SYNOP and TEMP).

5. Most important results

Using multivariate formulation :

- We found that AMSU-A data have positive impact on the analysis and forecasts of geopotential height when assimilating them in both 80 and 120 km resolutions. Especially, on lower levels (i.e. below 700 hPa), the impact was positive for all forecast ranges. Positive impact on the short-range (i.e. until 12 hour) forecast was observed for all model levels (see Fig. 7).
- A neutral impact on the analysis and forecasts of wind speed was observed.
- A neutral impact of AMSU-A data on the temperature profile was found.
- Regarding the relative humidity fields, a negative impact was observed.

The "stability" of the negative impact of AMSU-A data on relative humidity fields shows that its source might be in the way the humidity measurements are assimilated. We decided to separate specific humidity from the multivariate formulation and assimilate it alone (univariate form).

Assimilating the humidity in univariate form :

- The impact of AMSU-A data on the forecast of geopotential height was somewhat less, but positive, compared to the run with multivariate formulation.
- Positive impact on temperature above 700 hPa was observed from the 24-hour forecast range (see Fig. 8)
- Concerning the impact on relative humidity, an improvement could be observed (Fig. 9). It is important to mention that we found a big improvement at all model levels when assimilating the humidity data in univariate form, especially for levels around the tropopause (see Fig. 10). It can be also observed on the run without ATOVS data (see Fig. 11).
- A neutral impact was found for wind speed.

Influence of resolution :

We performed comparisons to evaluate the influence of the resolution of ATOVS data (thinning distance) on analysis and forecast. In general, the positive impact of ATOVS data on geopotential and temperature was stronger in case of finer (80 km) resolution of ATOVS data. The 120-km resolution gave "better" impact on relative humidity, wind speed and wind direction when using the multivariate formulation. Assimilating the humidity data in univariate form, the finer resolution gave "better" impact on relative humidity (see Fig. 12).

We concluded, that the positive impact was somewhat stronger in general when ATOVS data were assimilated at finer resolution, especially when the specific humidity was assimilated in univariate form.

Comparison of 3d-var and dynamical adaptation :

We can conclude that the 3d-var analysis of wind, geopotential and humidity fields was closer to the observation compared to the ARPEGE analysis (see Fig. 13), which is the initial condition for the dynamical adaptation. However the dynamical adaptation gave better results on forecasts of temperature for lower levels (see Fig. 14).

6. Selected cases

We concluded, that the impact of ATOVS data on the forecast on different parameters was slightly positive or neutral in general. In the following, we chose certain cases within the studied period to compare the runs with and without ATOVS data with a special attention on the forecast of precipitation. Exploring the reasons of the negative impact on the forecast of humidity it was ascertained, that in some cases no ATOVS data was available at all (e.g. 24 February, see Fig. 15), or the negative impact was characteristic for territories located rather far from the satellite pass (e.g. 28 February, see later). It indicates, that the negative impact may refer to the absence of ATOVS data, so that the ATOVS data did not have the possibility to correct the "bad quality" first-guess fields.

We examined what differences we receive in the spatial distribution of cumulative precipitation depending on the use (here we mean inclusion or exclusion) of the ATOVS data in the 3d-var runs. The results of this study are given in Figs 16-21.

Figures 16 and 17 show that from the synoptical point of view, there is no big differences between the maps created from results of the runs with (below) and without (above) ATOVS data. The objective verification, however, showed a positive impact (Fig. 15) of ATOVS data on humidity fields on this particular day (2 March).

Figures 18 and 19 show differences in cumulative precipitation between the runs with (below) and without (above) ATOVS data at the Eastern cost of Poland and Western part of Bielorussia. According to the real situation, presented in Fig. 19, there was some precipitation over the mentioned area. One can see that the run with ATOVS data could slightly better describe this situation (4 March).

In Figs 18 and 21 we examined a situation, when ATOVS data were available over a very small part of the ALADIN/HU domain. Analysing the 24 hour cumulative precipitation, one can say that the run with ATOVS data gave poorer results than the run without ATOVS data for cases, when the rainy territories (West-Southwest) were located far away from the satellite pass (East). Moreover, in Fig. 15 (see the 24 h forecast on Feb. 28 as an example), one can see that the impact of ATOVS data was slightly negative.

Detailed analyses of the above mentioned cases provide important additional information for the impact study compared to statistical evaluation. Thus, the indices of the objective verification sometimes might be not enough for thorough assessment of the impact of satellite data on analysis and forecast.

7. Summary, further suggestions and experiments

- The assimilation of the ATOVS data into the limited-area model ALADIN/HU gave neutral impact in general (the positive and negative impacts were slight).
- Because of the problems related to humidity, it is recommended to assimilate the humidity data in univariate form. (It would be expedient to change the assimilation of humidity from multivariate to univariate in the version of 3d-var running actually in parallel suite in Budapest.)
- The impact of the ATOVS data on the forecast of temperature was slightly negative in the lower levels. To avoid so, it is recommended to investigate the use of channels sensitive to the lower atmospheric layers (levels 5, 6 and 7), before performing any further experiments.
- Since the impact of ATOVS data with finer (80 km) resolution was somewhat "better", than that of 120 km resolution data, it is recommended to further perform the assimilation of ATOVS data at finer resolution.

• Further experiments should be done to clarify, what kind of expectations we can have in respect of assimilation of ATOVS data.

• It would be necessary to perform similar experiments for other periods as well.

• We suggest to perform further experiments to study the changes in the impact of ATOVS data on the forecast in extreme weather conditions.

Summing up, we can state that at the present stage no definite positive impact of ATOVS data on the forecast can be proved in the 3d-var data assimilation system of the ALADIN model, so it is necessary to continue the experiments.

References

[1] Harris, B. A. and Kelly, G., 2001 : A satellite radiance bias correction scheme for data assimilation, *Q.J.R. Meteorol. Soc.* , **127**, 1453-1468.

[2] Roger Randriamampianina and Florence Rabier, 2001 : Use of locally received ATOVS radiances in regional NWP. *NWP SAF report* , available at HMS and at Météo-France.

[3] Roger Randriamampianina, 2003 : Investigation of the use of local ATOVS data in Budapest, *ALADIN internal report*, 2003.

[4] F. Rabier, E. Gérard, Z. Sahlaoui, M. Dahoui, R. Randriamampianina, 2001 : Use of ATOVS and SSMI observations at Météo-France. *11th Conference on Satellite Meteorology and Oceanography* , Madison, WI, 15-18 October 2001 (preprints). Boston, MA, American Meteorological Society, pp367-370.

[5] Parrish, D. F. and J. C. Derber, 1992 : The National Meteorological Centre's spectral statistical interpolation analysis system. *Mon. Wea. Rev.*, **120**, 1747-1763.

[6] Sounders, R, M. Matricardi and P. Brunel, 1999 : An improved fast radiative transfer model for assimilation of satellite radiance observations. *Q.J.R. Meteorol. Soc.*, **125**, 1407-1425.

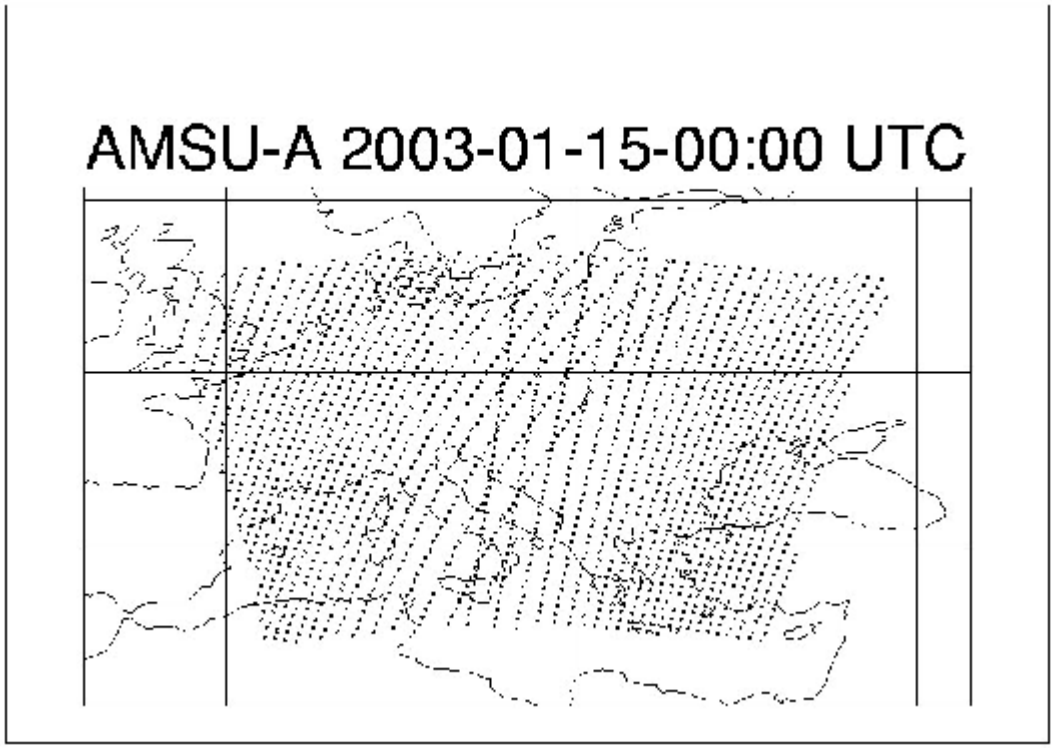

Figure 1 : Satellite data over the ALADIN/HU domain (C+I zone).

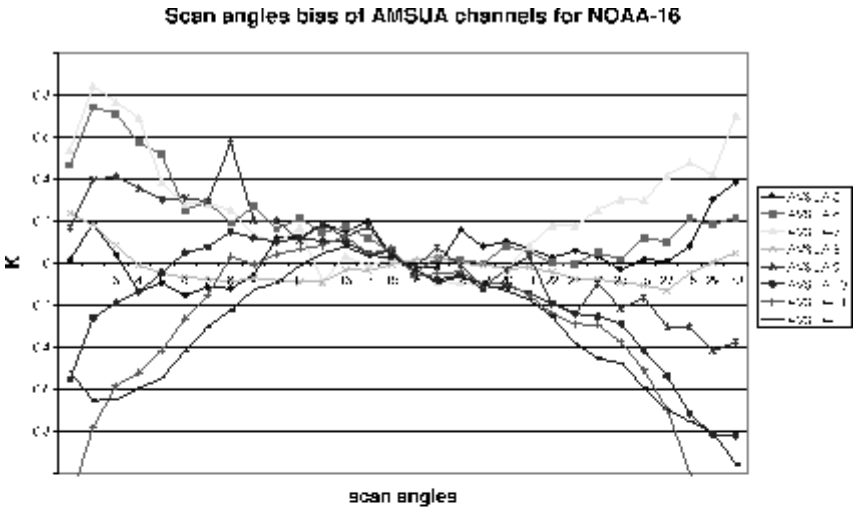

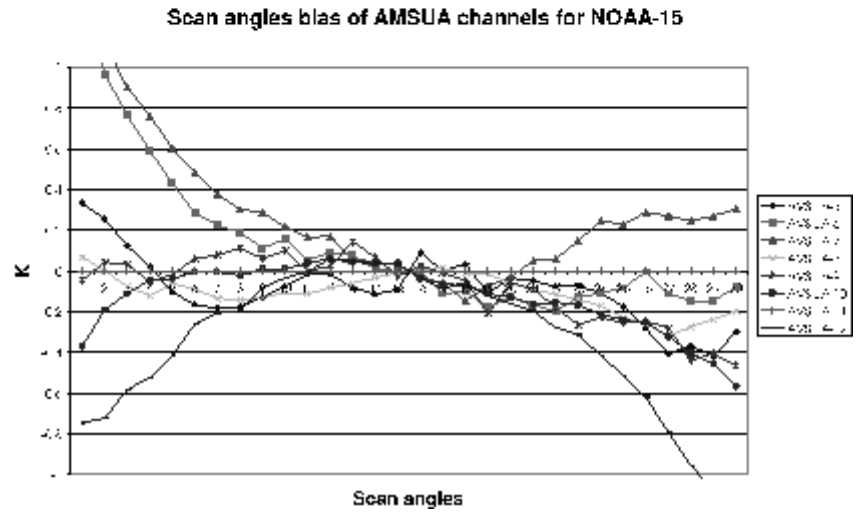

Figure 2 : Bias (in Kelvin degree) specific to the scan angles varies with latitude band. In these figures biases were computed for the same latitude band.

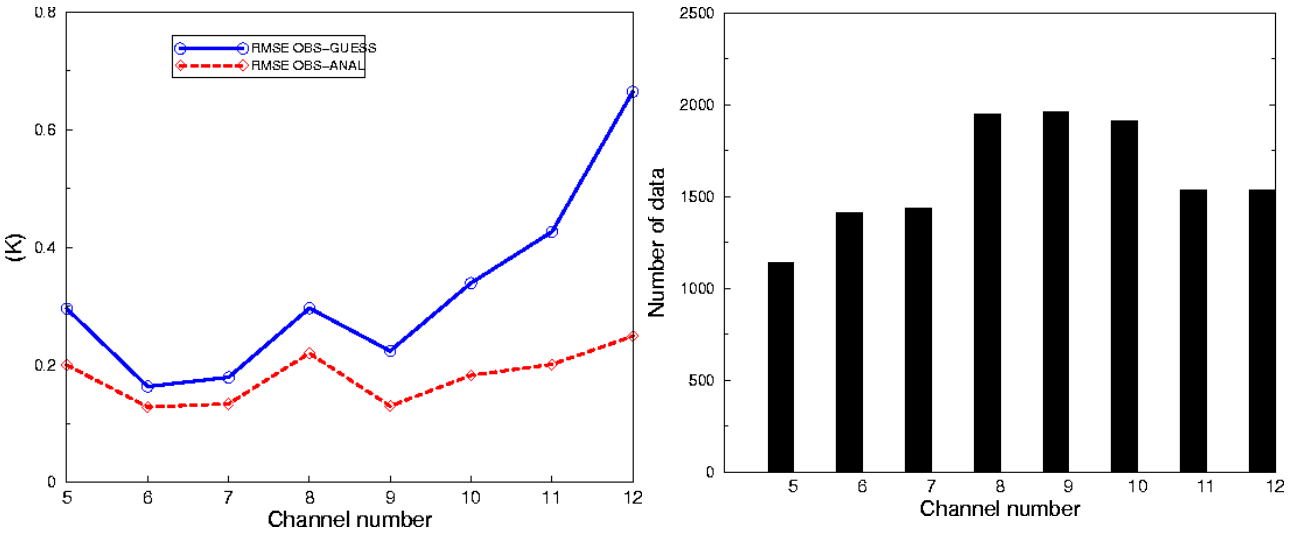

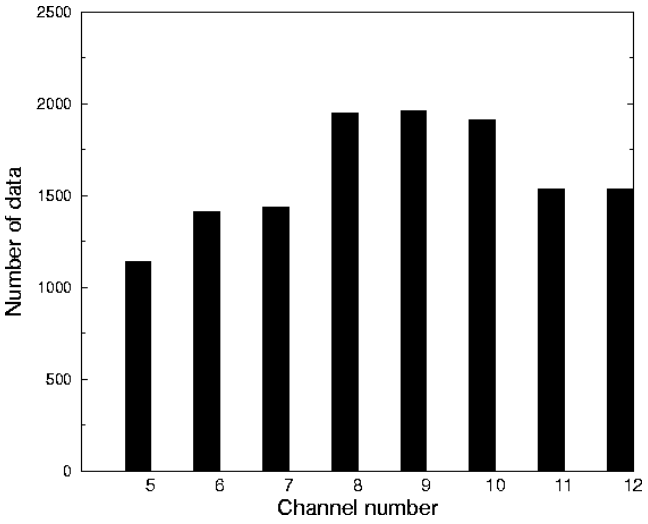

Figure 3 : Example of statistics of observation minus guess (solid line) and observation minus analysis (dashed line) for AMSU-A at 00 UTC for a five days cycling (from 2003.02.20 to 2003.0225) (left hand side). On the right one can find the number of data used in the computation of the statistics. The impact of AMSU-A is larger at higher layers of the atmosphere (channels 9-12).

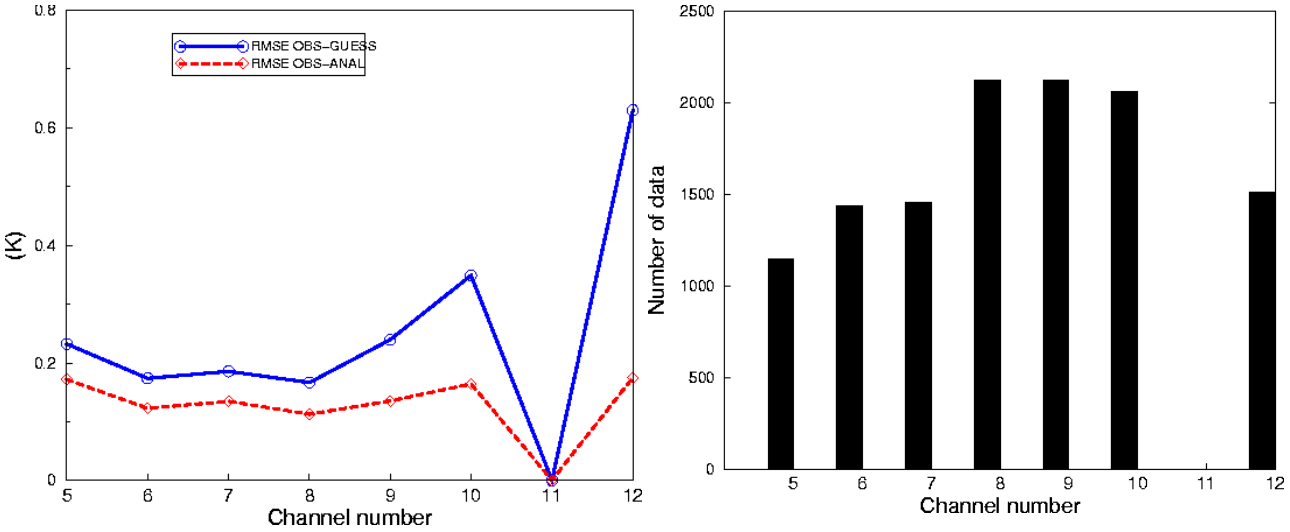

Figure 4 : Example of statistics of observation minus guess (solid line) and observation minus analysis (dashed line) for AMSU-A at 06 UTC for a five days cycling (from 2003.02.20 to 2003.0225) (left hand side). On the right one can find the number of data used in the computation of the statistics. Note, that around 06 UTC we receive data from NOAA-15, which has problem with AMSU-A channel 11. The impact of AMSU-A is larger at higher layers of the atmosphere (channels 9-12).

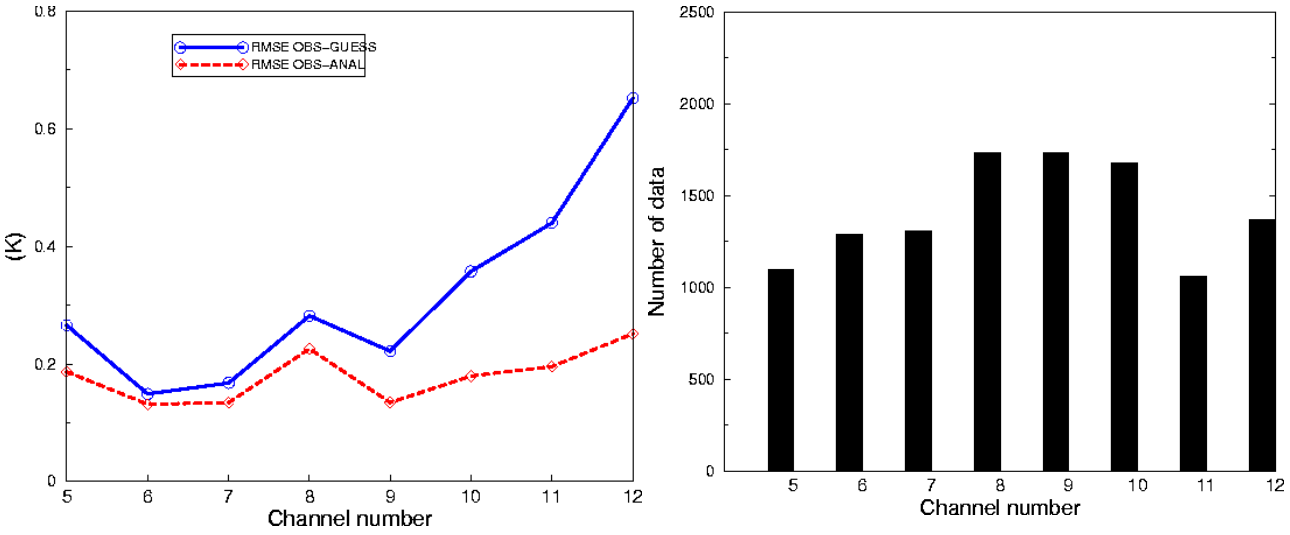

Figure 5 : Example of statistics of observation minus guess (solid line) and observation minus analysis (dashed line) for AMSU-A at 12 UTC for a five days cycling (from 2003.02.20 to 2003.0225) (left hand side). On the right one can find the number of data used in the computation of the statistics. The impact of AMSU-A is larger at higher layers of the atmosphere (channels 9-12).

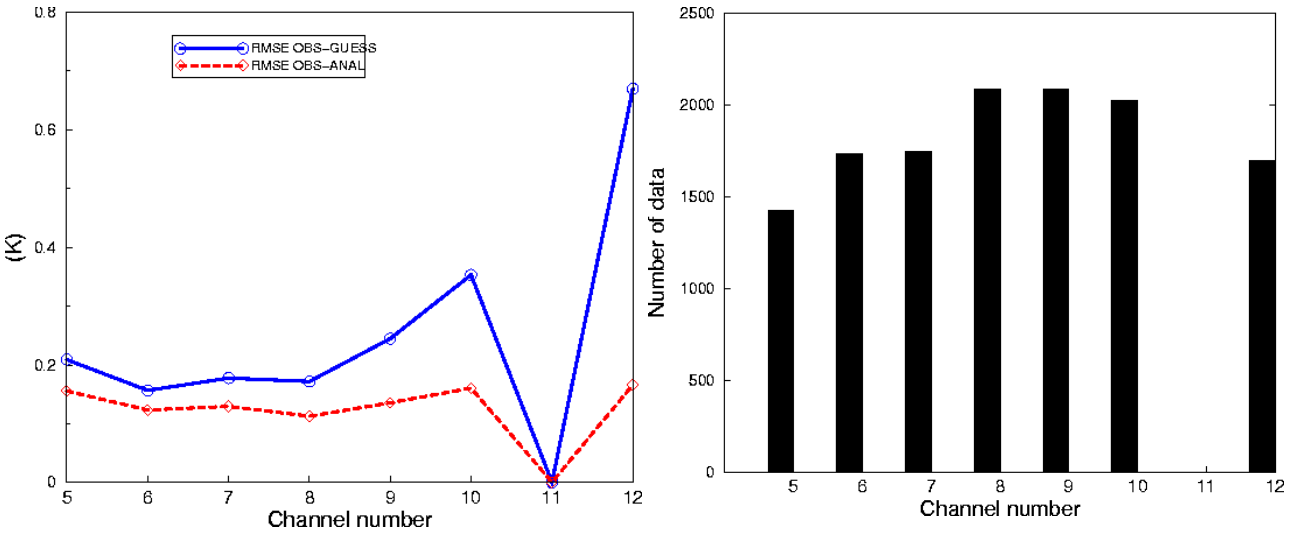

Figure 6 : Example of the statistics of the observation minus guess (solid line) and the observation minus analysis (dashed line) for AMSU-A at 18 UTC(left hand side). On the right one can find the number of data used in the computation of the statistics. Note, that around 18 UTC we receive data from NOAA-15, which has problem with AMSU-A channel 11. The impact of AMSU-A is larger at higher layers of the atmosphere (channels 9-12).

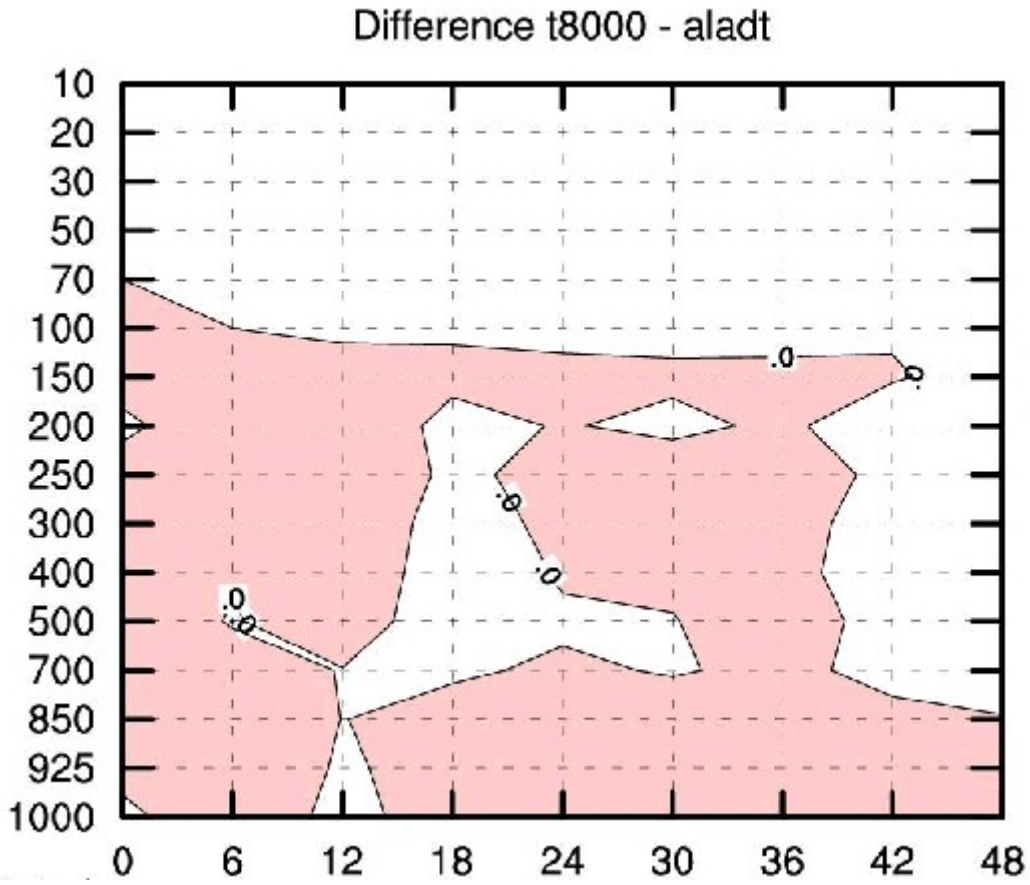

Figure 7 : Difference between the root mean square errors for geopotential height : $RMSE_{T8000}$ - $RMSE_{Aladt}$. Negative value (coloured) means that the error of run with ATOVS data is less than that of control run, thus the ATOVS data have positive impact. X and Y axes present the forecast ranges and the model levels respectively.

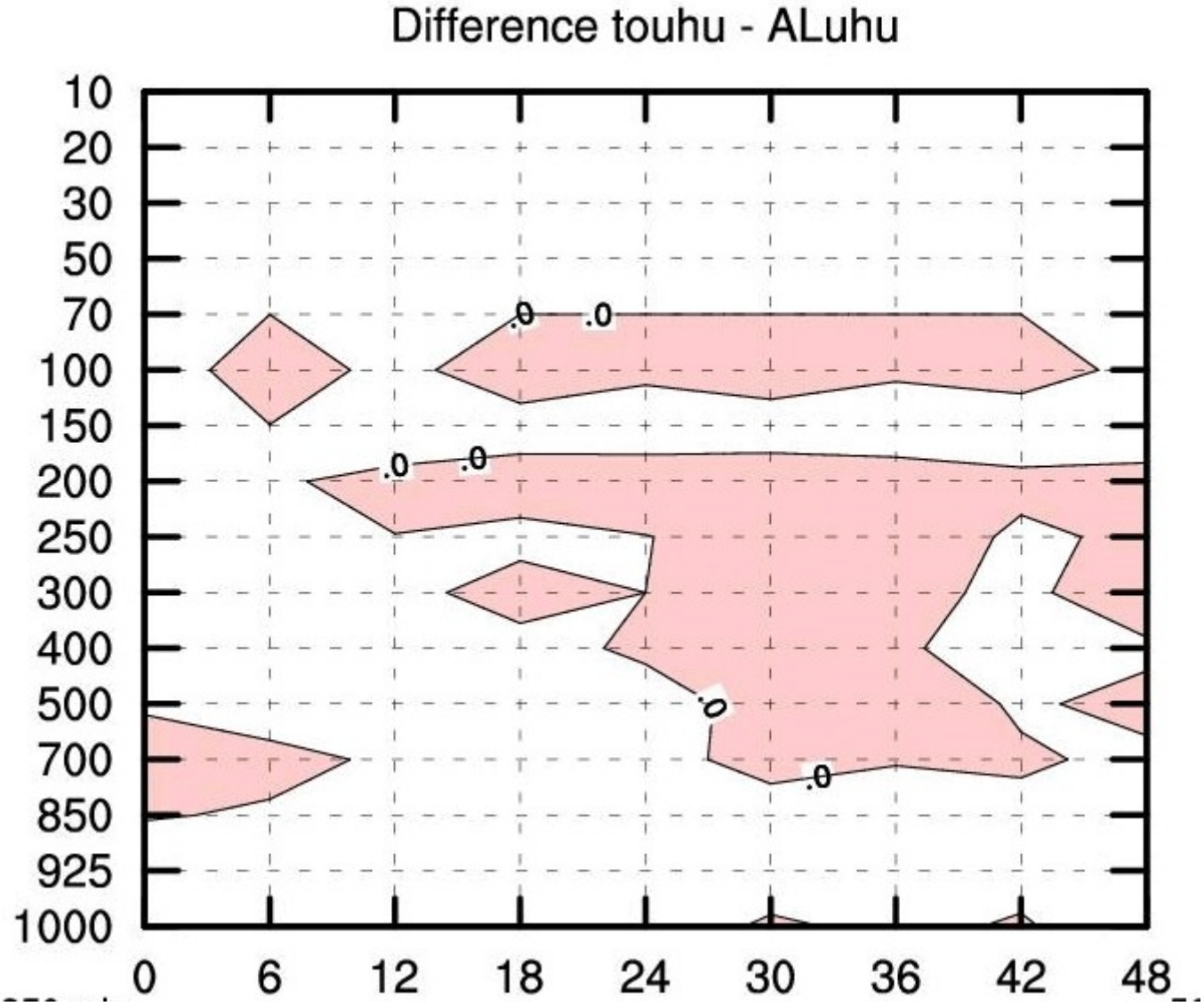

Figure 8 : Difference between the root mean square errors of temperature in case of assimilating the humidity data in univariate form : $RMSE_{Touhu}$ - $RMSE_{Aluhu}$. Negative value (coloured) means that the error of run with ATOVS data is less than that of control run, thus the ATOVS data have positive impact. X and Y axes present the forecast ranges and the model levels respectively.

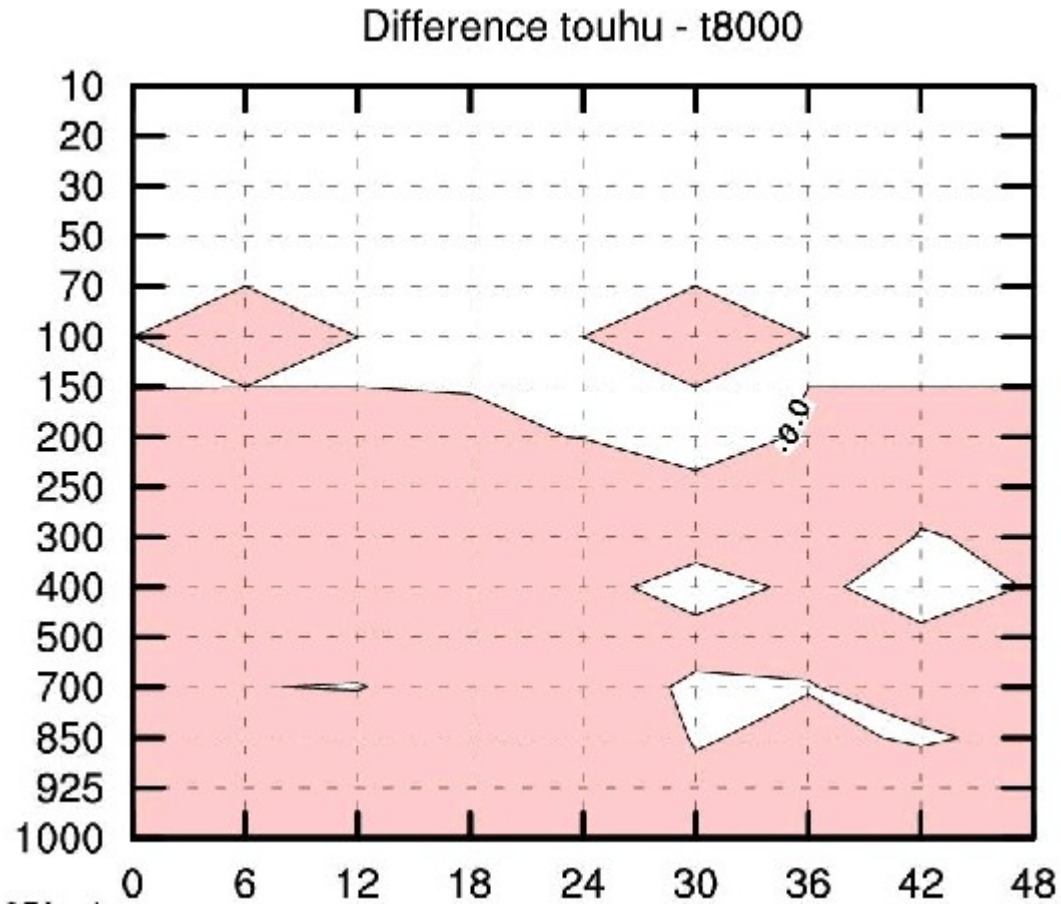

Figure 9 : Difference between the root mean square errors of relative humidity : $RMSE_{Touhu}$ - $RMSE_{T8000}$. Negative value (coloured) means that the error is reduced when assimilating the specific humidity in univarite form.

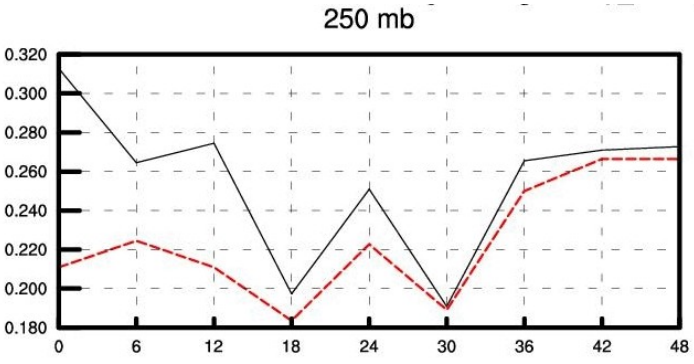

Figure 10 : Root mean square forecast errors of relative humidity (in percent) at 250 hPa level against radiosonde observation. Comparison of two 3d-var runs with ATOVS data assimilated in 80 km resolution. Solid line : when the multivariate formulation was used for all control variables (*T800*). Dashed line : when the specific humidity was assimilated in univariate form (*touhu*). X axis presents the forecast ranges in hour.

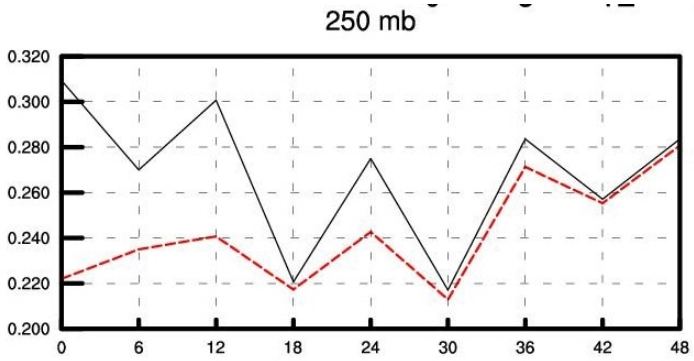

Figure 11 : Root mean square forecast errors of relative humidity (in percent) at 250 hPa level against radiosonde observation. Comparison of two 3d-var runs with TEMP and SYNOP data. Solid line : when the multivariate formulation was used for all control variables (*aladt*). Dashed line : when the specific humidity was assimilated in univariate form (*aluhu*, dashed line). X axis presents the forecast ranges in hour.

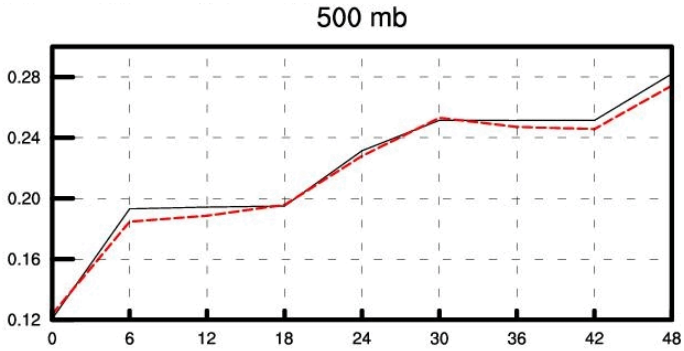

Figure 12 : Root mean square forecast errors of relative humidity (in percent) at 500 hPa level against radiosonde observation. Comparison of two 3d-var runs with ATOVS data when the humidity was assimilated in univariate form. Dashed line : thinning in 80 km (*touhu*). Solid line : thinning in 120 km (*120uhu*). X axis presents the forecast ranges in hour.

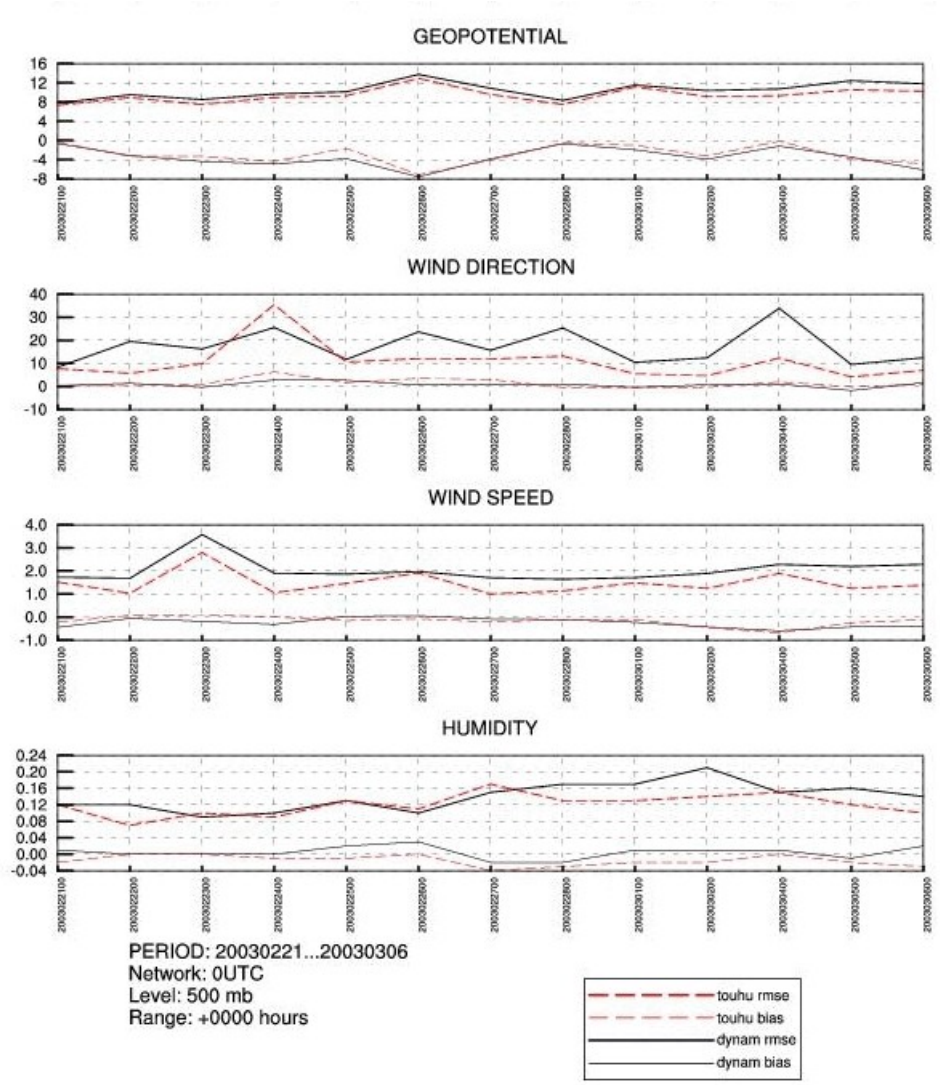

Figure 13 : Comparison of day-to-day statistics (RMSE - upper curves and bias - lower curves) of dynamical adaptation run (*dynam*, solid line) and 3d-var run with ATOVS data assilimilated in 80 km resolution (*touhu*, dashed line). The statistics correspond to 500 hPa model level.

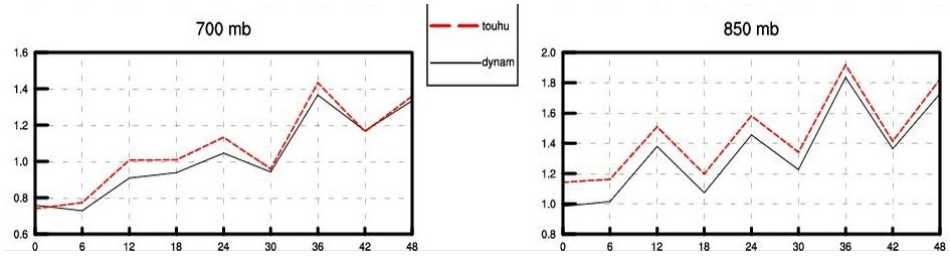

Figure 14 : Root mean square forecast errors of temperature (in Kelvin) at 700 and 850 hPa model levels. Comparison of scores of a dynamical adaptation (*dynam*, solid line) and a 3d-var with ATOVS data assimilated in 80 km resolution (*touhu*, dashed line). X axis presents the forecast ranges in hour.

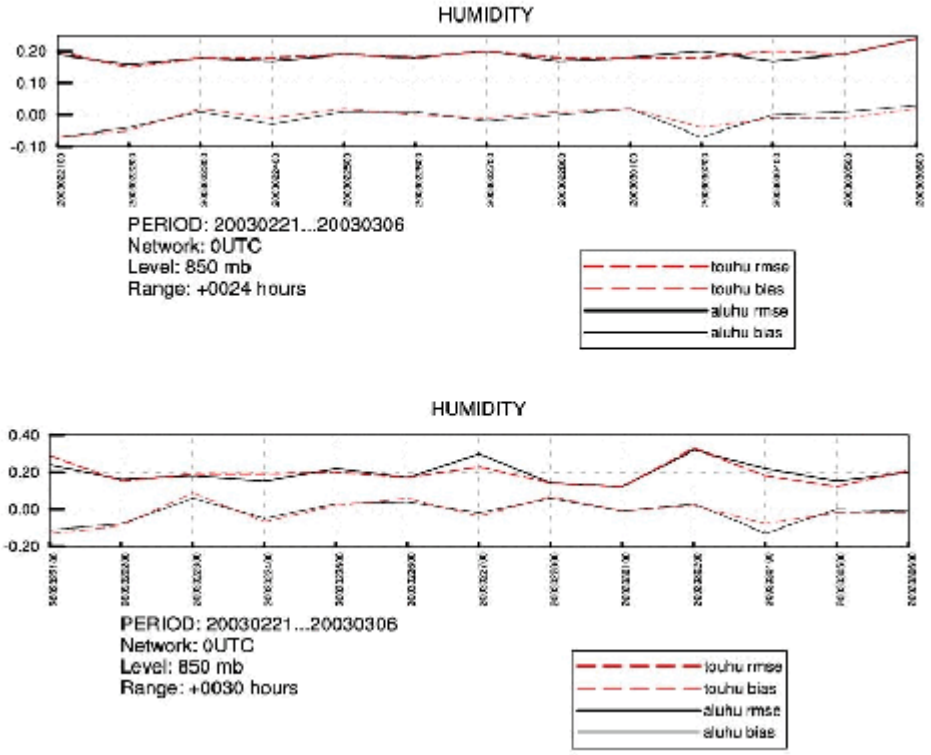

Figure 15 : Day-to-day root mean square forecast errors (upper curves) and biases (lower curves) of relative humidity at 850 hPa model level. Comparison of 3d-var run with ATOVS data assimilated in 80 km (*touhu*, dashed line) with the control one (with TEMP and SYNOP only) (*aluhu*, solid line) for 24 (upper graphic) and 30 (lower graphic) hour forecast ranges.

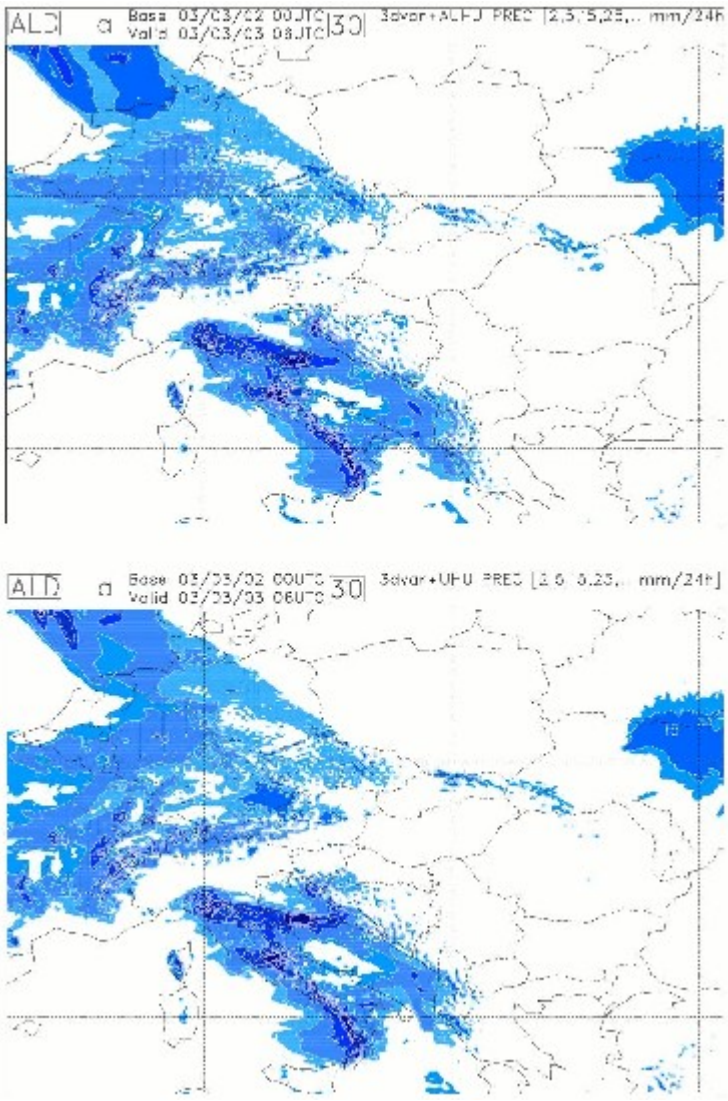

Figure 16 : The 24 hour cumulative precipitation (in mm) predicted over the ALADIN/HU domaine from 2003.03.02 00 UTC. Upper picture : control run (with TEMP and SYNOP). Lower picture : 3d-var run with ATOVS assimilated in 80 km resolution. In both runs the humidity was assimilated in univariate form. Note that the 24 hour cumulated precipitation is the difference between the cumulative precipitation predicted at 6 and 30 hour forecast ranges.

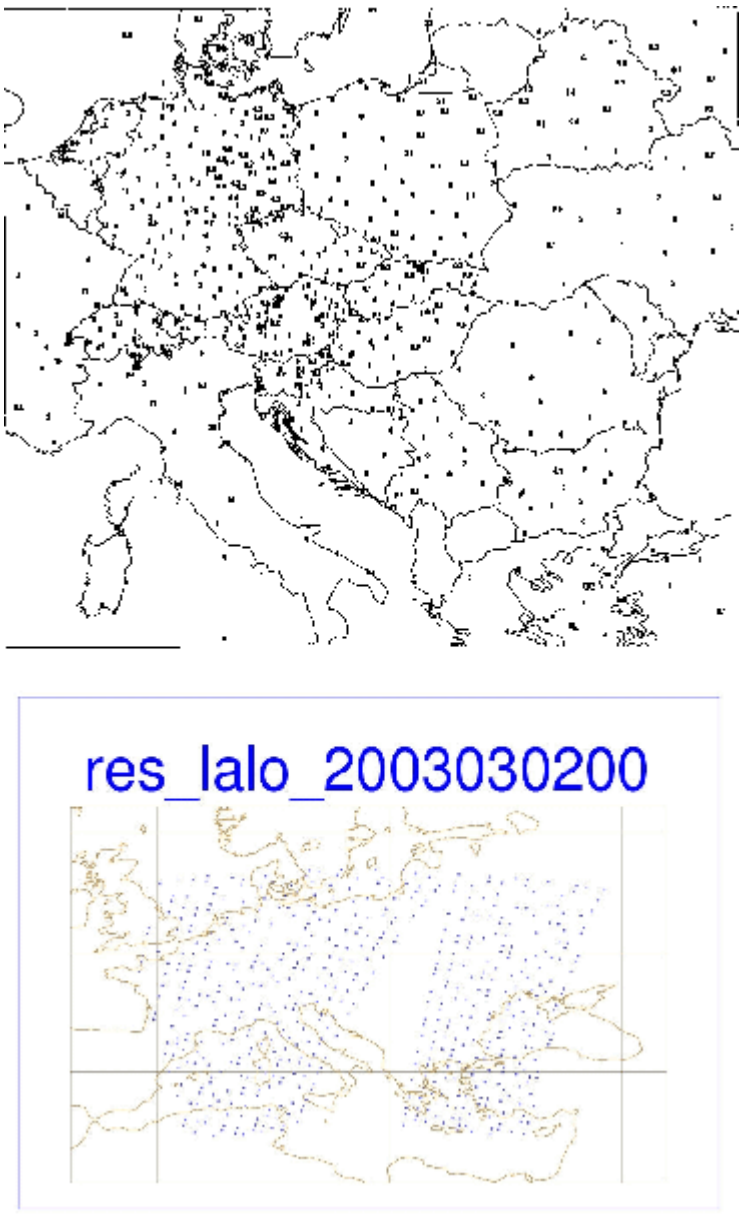

Figure 17 : The 24 hour cumulative precipitation (in mm) extracted from SYNOP telegrams for 2003.03.03 06 UTC (upper picture) and the distribution of the ATOVS pixels for 2003.03.02 00 UTC (situation after screening - active observation) (lower picture).

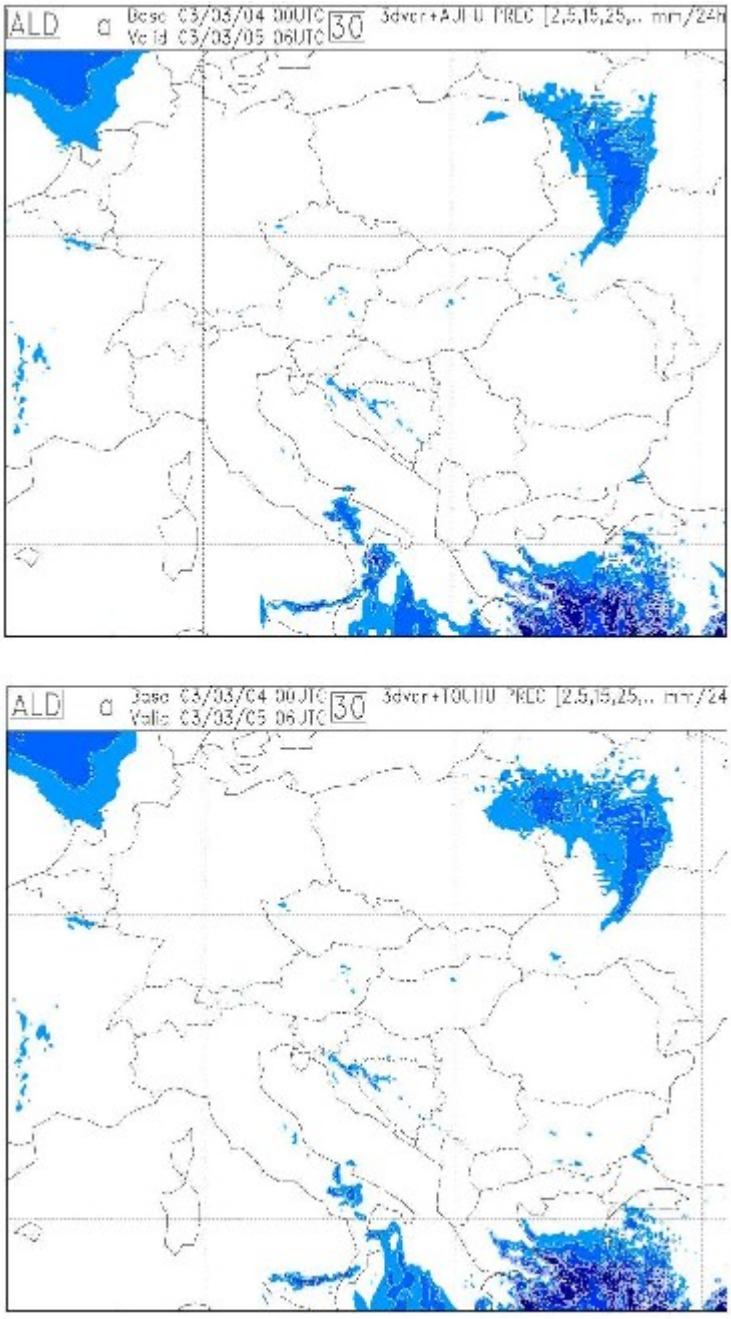

Figure 18 : The 24 hour cumulative precipitation (in mm) predicted over the ALADIN/HU domaine from 2003.03.04 00 UTC. Upper picture : control run (with TEMP and SYNOP). Lower picture : 3d-var run with ATOVS assimilated in 80 km resolution. In both runs the humidity was assimilated in univariate form. Note that the 24 hour cumulated precipitation is the difference between the cumulated precipitation predicted at 6 and 30 hour forecast ranges.

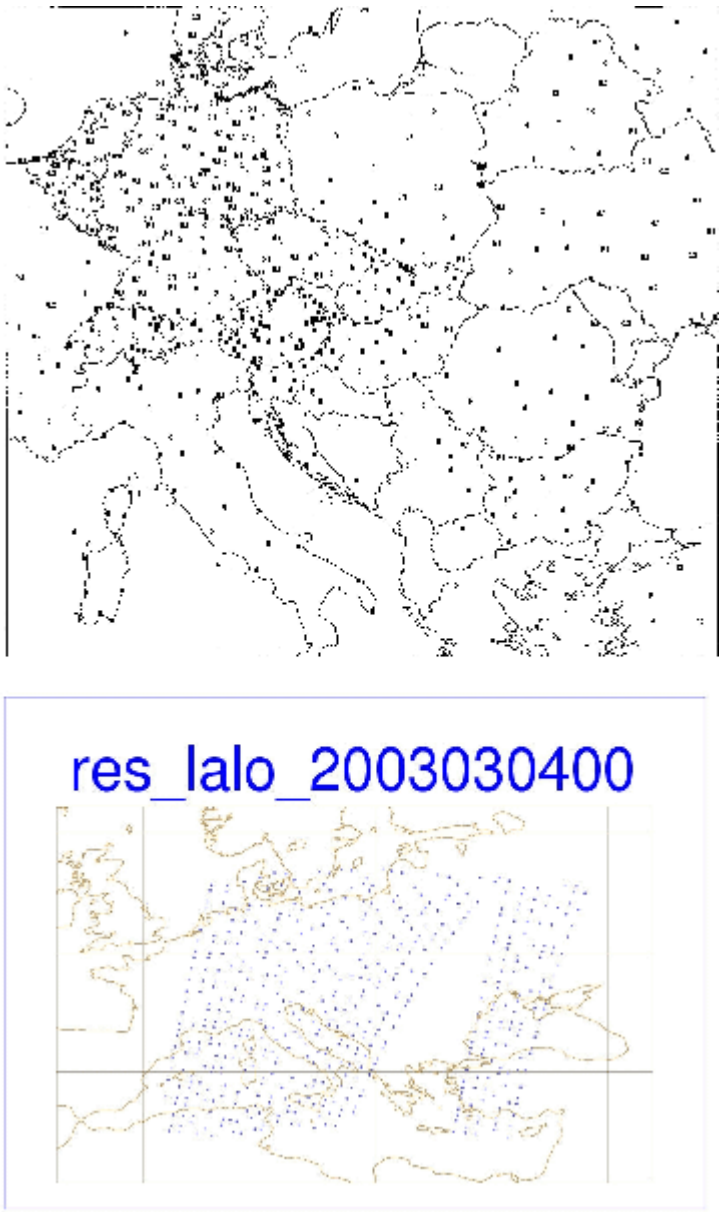

Figure 19 : The 24 hour cumulative precipitation (in mm) extracted from SYNOP telegrams for 2003.03.05 06 UTC (upper picture) and the distribution of the ATOVS pixels at 2003.03.04 00 UTC (situation after screening - active observation) (lower picture).

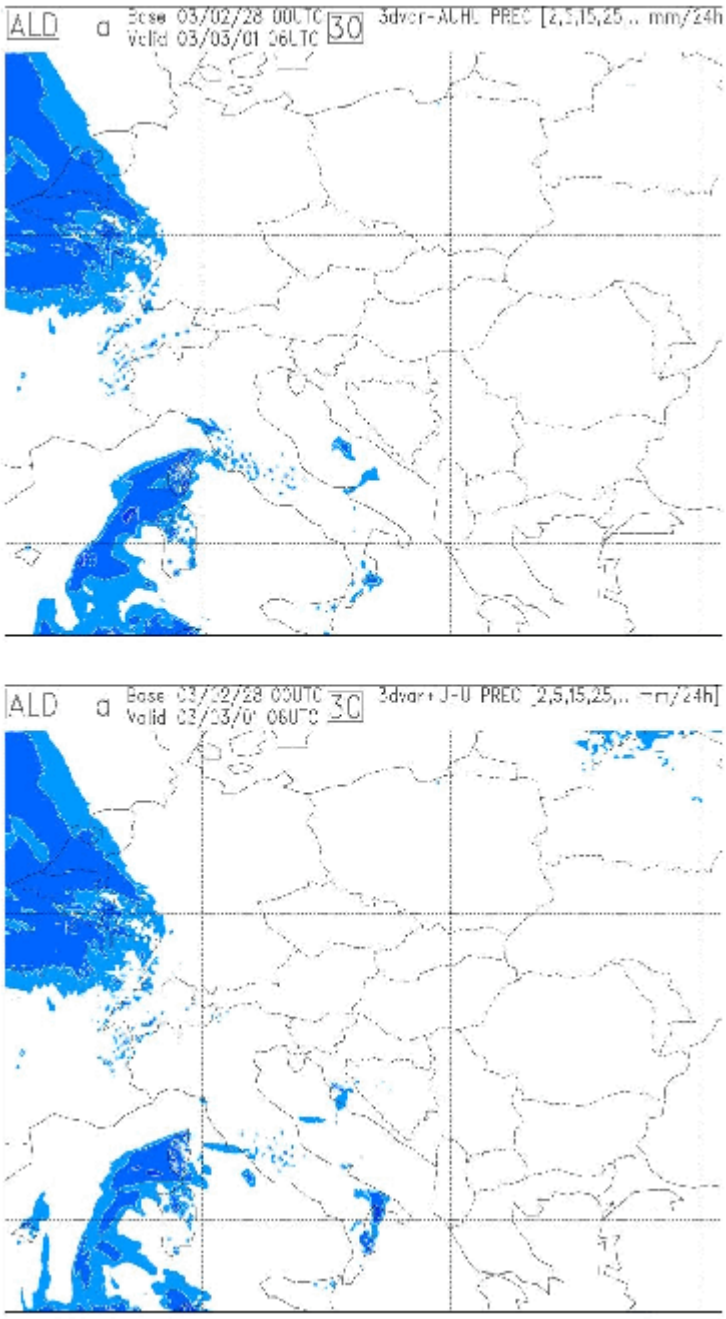

Figure 20 : The 24 hour cumulative precipitation (in mm) predicted over the ALADIN/HU domaine from 2003.02.28 00 UTC. Upper picture : control run (with TEMP and SYNOP). Lower picture : 3d-var run with ATOVS assimilated in 80 km resolution. In both runs the humidity was assimilated in univariate form. Note that the 24 hour cumulated precipitation is the difference between the cumulated precipitation predicted at 6 and 30 hour forecast ranges.

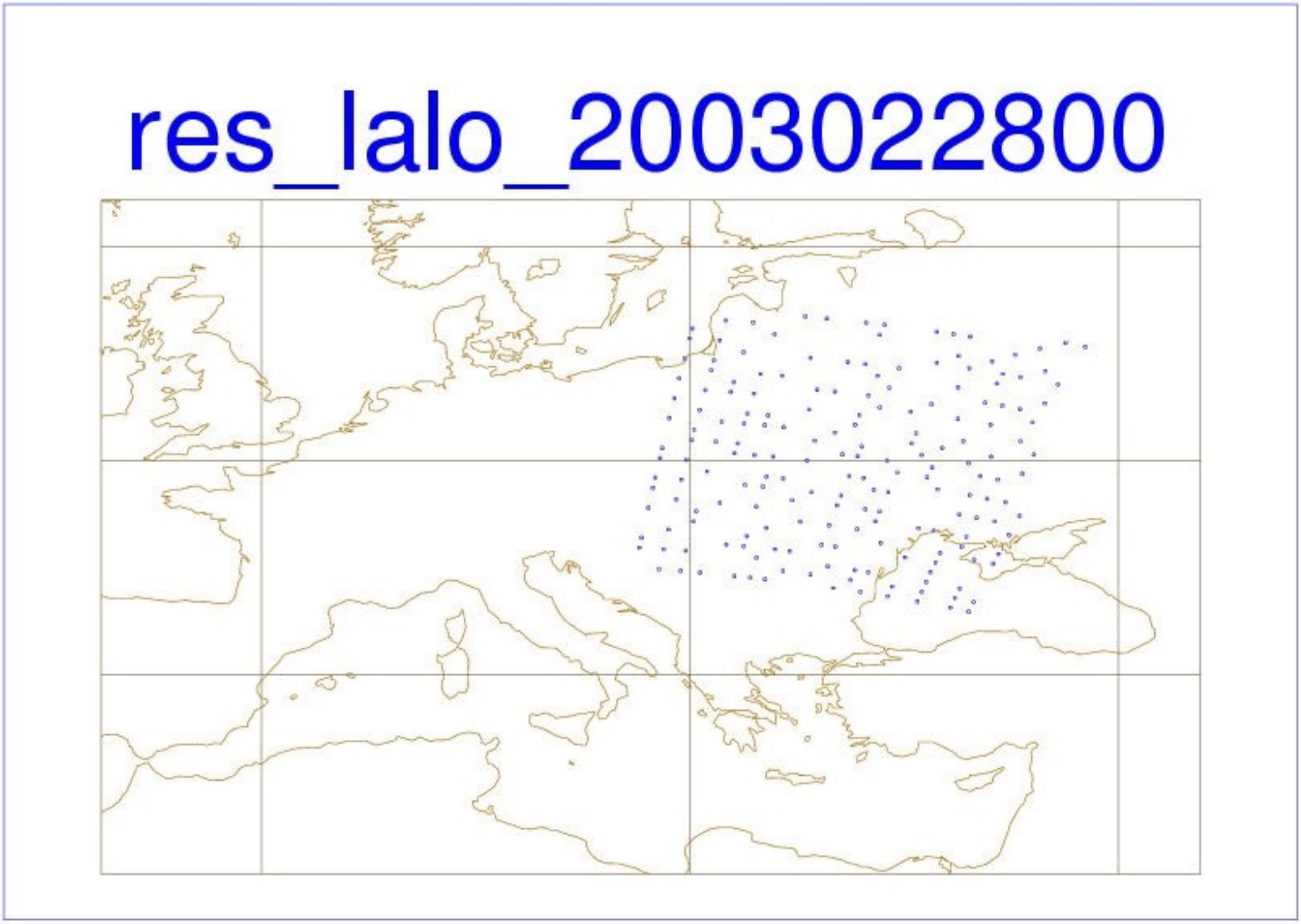

Figure 21 : The distribution of the ATOVS pixels at 2003.02.28 00 UTC (situation after screening - active observation) .

False mesoscale cyclogenesis in the ALADIN model - Sensitivity study on initial conditions, physical parameterisations and horizontal diffusion

André Simon (SHMI) and Filip Vana (CHMI)

Introduction

During the last three years, forecasts of spurious mesoscale cyclones appeared several times in the outputs of the ARPEGE/ALADIN models. This phenomenon was carefully examined within the COMPAS and GMAP teams of Météo-France (Tardy, 2003) and in the LACE centre in Prague (Vakula, 2002). However, the mechanism of creation of such small-scale storms in the model is still not entirely known and despite of some successes, e.g. with the parameterisation of shear-linked convection (Bouyssel and Geleyn, 2002), the problem of false cyclogeneses remains even in the recent operational versions of the ARPEGE/ALADIN models.

The original purpose of the study described in this paper was :

a) to evaluate the sensitivity of a false cyclogenesis to initial conditions using the adjoint of the ALADIN model
b) if possible, to perturb the initial conditions and to create a reference run without the storm prediction. The reference run will be further compared with the one producing a storm, with respect to physical fluxes and some diagnostic parameters such as the potential vorticity (PV) field.
c) according to the improved knowledge of the storm mechanism, to find ways to eliminate the storm by adjustments of physical parameterisations in the ARPEGE/ALADIN model

Short description of the selected case

The false cyclogenesis that appeared in the "20.07.2001 00 UTC" run of the ALADIN-LACE model, in the Adriatic sea, belongs to the most resistant cases. Several tests were done on physical parameterisations, that are described in the report of Vakula (2001). More recently, tests of the parameterisation of the so-called shear-linked convection (see the article of Bouyssel and Geleyn, 2002) were performed also on this situation, without significant achievements.

Looking at the forecasts of mean-sea-level pressure with a 6-hour frequency, one can follow the development of the mesocyclone, that originates from a synoptic-scale cyclone, having the centre above Northern Italy in the initial state, at 00 UTC (Fig. 1). Vertical cross-sections through this area indicate a well developed baroclinic environment according to the couple of upper and low-level potential-vorticity anomalies, where the latter shows for the troposphere unusually big values up to 4 PVU (Fig. 2b). However, the analysis of further runs shows a fast decline of the cyclone, together with the mesoscale, low-level maximum of potential vorticity. In the model run, the cyclogenesis seems to continue, reaching its peak departures from model analysis after 24 hours of integration. At that time, convection was estimated in the area of Adriatic sea (Vakula, 2001), probably connected to a shallow surface-low. However, the structure of the forecasted cyclone according to the vertical profile of potential temperature and potential vorticity seems to be unrealistic (Fig. 2c).

Adjoint sensitivity tests in the case of the so-called Adriatic storm of 20.07.2001

For the run of the adjoint of the ALADIN model, a domain with an horizontal resolution of 18 km and 37 vertical levels was chosen (the one used for the computation of boundary conditions for the operational ALADIN-LACE model). The model version used both for the reference run and for the

experiments with the adjoint of ALADIN model was *Al25T1-op2*. The adjoint run started at 21.07.2001 00 UTC and finished at 20.07.2001 00 UTC after 24 hour integration, using the simple physical parameterisation of Buizza (1993) and the so-called dry total energy as a norm (for more details about using the adjoint of the ALADIN model see the article of Soci et al., 2003). The selected target area of the storm environment is marked by a green rectangle in Fig. 1e. The reference at the beginning of the adjoint run was the model analysis valid at 21.07.2001 00 UTC.

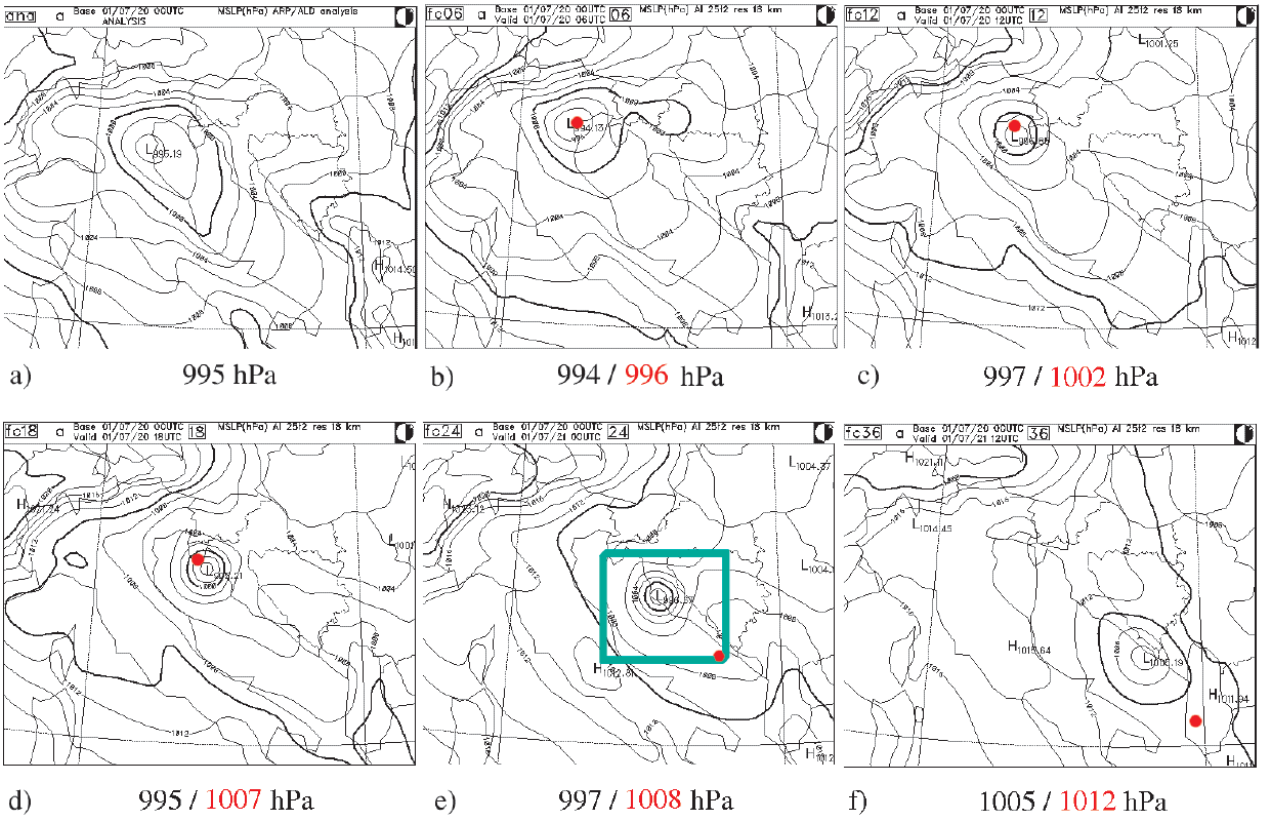

a) 995 hPa b) 994 / 996 hPa c) 997 / 1002 hPa

d) 995 / 1007 hPa e) 997 / 1008 hPa f) 1005 / 1012 hPa

Figure 1 : Analysis (a) and forecasts (b : 6 h, c : 12 h, d : 18 h, e : 24h, f : 30 h) of mean-sea-level pressure from the reference storm-creating run based on 20.07.2001 00 UTC. The experimental run was using the model version *AL25T1*, on a domain an horizontal resolution of 18 km. The values indicated below the figures compare the predicted pressure in the centre of the cyclone (black) with the value from model analysis (red). The red dots mark the position of the centre of the cyclone in model analyses. The green rectangle (e) represents the target area used for sensitivity studies.

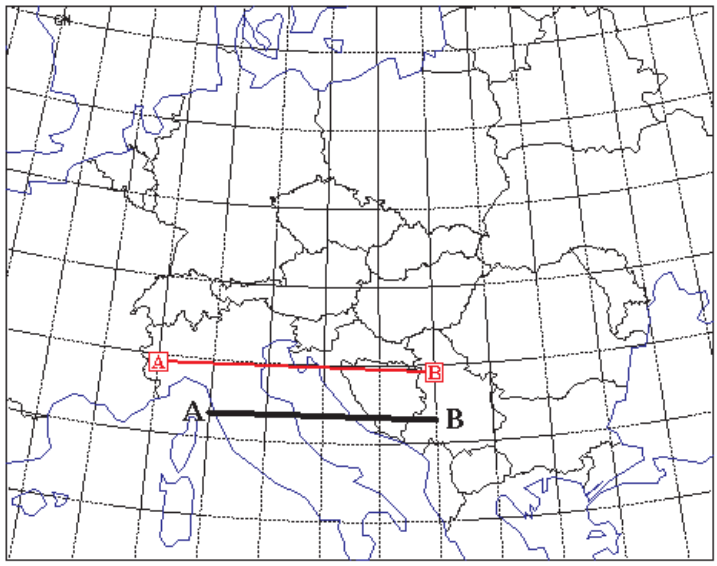

a

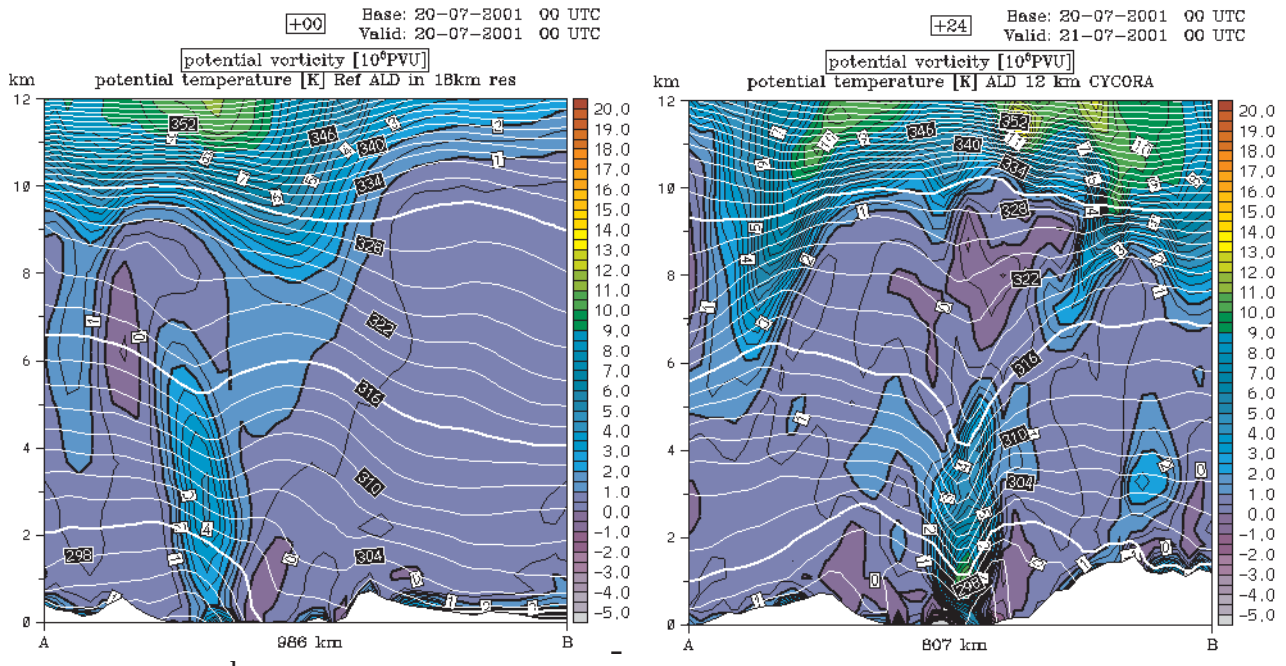

b c

Figure 2 : a) Vertical cross-section used to analyse fields in Fisg. 2b (red) and 2c (black).
b) Vertical cross-section of potential-vorticity (coloured isolines) and potential-temperature fields (white ones) in the reference analysis, valid at 20.07.2001 00 UTC. Note the well-developed low-level anomaly of potential vorticity near the centre of the cyclone and regions with dry symmetric instability (negative values of PV).
c) Vertical cross-section for the 24-hour forecast valid at 21.07.2001 00 UTC, which is using the CYCORA (CY21) package of physical parameterisations (operational in the 12-km ALADIN-LACE model in the years 2000-2001). Note the areas of exaggerated PV values in the lower troposphere, and the "warming" effect on the isolines of potential temperature in the environment of the storm.

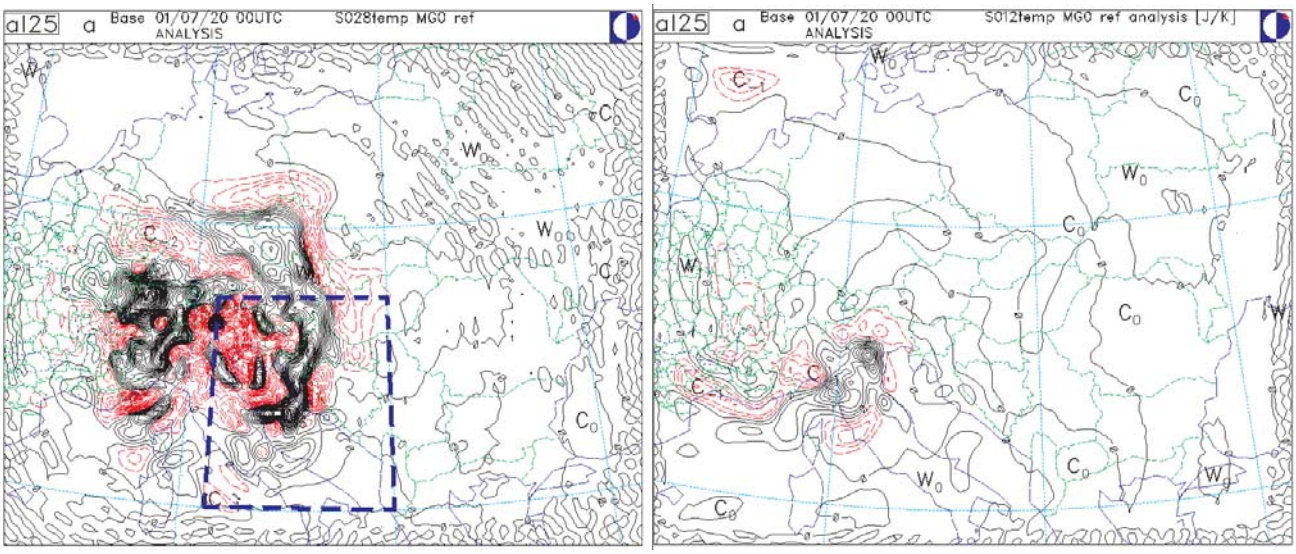

a b

Figure 3 : a) Gradients of the 24-hour forecast-error cost function, for the model run based on 20.07.2001 00 UTC, with respect to the temperature and with the dry total energy as the norm, at model levels 28 (a) and 12 (b). The result shows the sensitivity of the forecast error to the ALADIN initial conditions (according to the verifying analysis valid at 21.07.2001 and the target area marked in green in Fig.1e). The dashed blue rectangle marks the area used for the budget calculations mentioned hereafter (domain ADRI).

The gradients of the 24-hour forecast-error cost function with respect to temperature show a huge sensitivity to initial conditions. High sensitivity can be observed above all in the PBL (Fig. 3a) and

is present in a relatively wide area, concerning also places distant from the original target. In upper tropospheric levels, areas of sensitivity occur in even more distant places (on West and Northwest of the domain). However, the centre of the impact remains near the position of the low at initial time (Fig. 3b).

Model runs with adjusted initial conditions

The results of the first tests encouraged us to continue with step b), i.e. the fields of gradients of the forecast-error cost function (∇J_{t0}) were used to perturb the original model analysis, valid at 20.07.2001 00 UTC. The resulting analysis was later used for model runs with the same physical package as for the reference one, to check the impact of the perturbed initial conditions (sensitivity forecast run). The vector of the perturbation, δX_0, was computed as : $\delta X_0 = - a \nabla J_{t0}$, where α is a scaling factor, that should not exceed 1. (refer to the article of Soci et al., 2003). For our experiments, three values of *a* were used : 0.1, 0.5, 0.75 . Finally, a new initial file was creating by adding this vector (in spectral space) to the reference ALADIN analysis.

The experiment with *a*=0.1 shows a very small influence, with respect to the forecast of the storm. Sensitivity appears in the case of *a*=0.5, and by choosing *a*=0.75 one can see finally an almost entire liquidation of the storm after 24 hours of model integration (Fig. 4a).

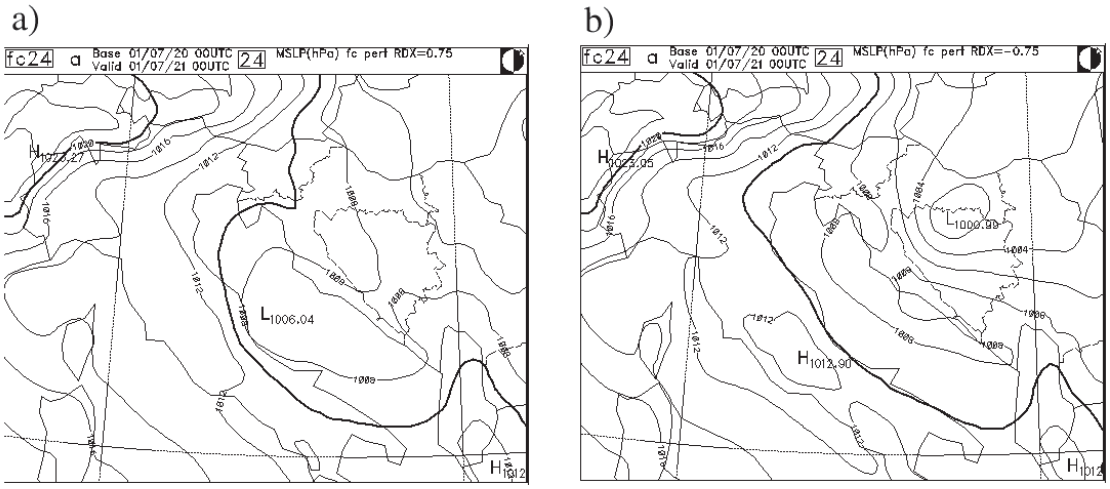

Figure 4. a) Experimental 24-hour sensitivity forecast run, valid at 21.07.2001 00 UTC and based on the original analysis perturbed by the gradient fields with the scaling factor *a*=0.75.
b) Experiment with adding the gradient fields to the initial field using the scaling factor *a*=-0.75 (opposite procedure as in the experiment corresponding to Fig.4a). Note the worse result when compared to Fig. 4a, but the relatively improved forecast of the storm when compared to the reference run (Fig. 1e) !

This result tell us some important things. First, it is possible to eliminate completely the targeted storm only by changing the initial conditions, without touching the physical parameterisation. On the other hand, the magnitude of the scaling factor used for the corresponding test is quite big : generally acceptable values are of magnitude 0.1 or even smaller.

The vertical cross-section through the centre of the cyclone at 20.07.2001 00 UTC applied to the perturbed analysis shows new structures in the potential vorticity field, mainly West from the centre of the low and below the tropopause (Fig. 5).

We get an interesting comparison between the 12-hour basic run, the 12-hour run with perturbed analysis, and the analysis valid at 20.07.2001 12 UTC. Looking at the same vertical cross-sections of potential vorticity and wind fields, one can realize that the sensitivity forecast run is not closer to the verifying analysis than the reference one (Figs. 6a-c). Nevertheless the structure of the low-level

PV anomaly in the environment of the cyclone is reorganized and, thanks to that, conditions are created for strong upslope motions, that are accompanied with the presence of vertical wind-shear. Note, that vertical wind-shear in the storm and its nearest environment is very small in the original, storm-creating run, while compensated with a strong horizontal wind-shear (Fig. 6a).

An additional experiment was performed, with the parameter *a* set to –0.75. This was meant as a contradictory experiment. If the fields of gradients are correctly computed, the sensitivity forecast run should not improve the forecast in this case. The resulting forecast from this experiment was producing the cyclone (though its position was moved), nevertheless it can be still considered as better than the forecast of the basic unperturbed run (Fig. 4b).

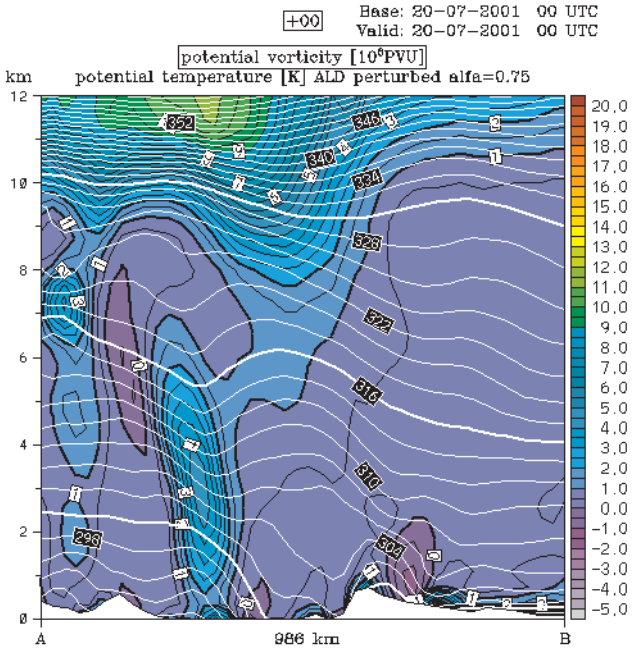

Figure 5. Vertical cross-section through the fields of potential vorticity and potential temperature, valid for the 20.07.2001 00 UTC perturbed analysis. The scaling factor for the gradient field was set to 0.75. The cross-section is the same as for the reference analysis (see Fig. 2a). Note the creation of additional PV anomaly in the far western side of the cross-section, for vertical levels between 6 and 8 km.

Diagnostics of the physical fluxes

Originally, it was supposed that a run improving the forecast (as the run with perturbed analysis using *a*=0.75) can be used as a reference for comparing physical fluxes and tendencies in the storm environment. Hence it would perhaps be possible to find ways to cancel false cyclogenesis entirely by changes in the physical parameterisations. With respect to the sensitivity gradient fields and the development of the storm, several areas were chosen to follow the differences between the sensitivity forecast run and the original, not perturbed run (domain ADRI is marked in Fig. 3a). The fluxes were computed with the help of the DDH tool (Piriou, 2001). Budgets for water vapour, temperature and energy were compared in the 24-hour period from 20.07.2001 00 UTC until 21.07.2001 00 UTC. For water vapour and temperature, the budgets for the domain ADRI show tendencies to decrease moisture and increase the temperature in the storm-producing run (Fig. 7a). The precipitation fluxes seem to have the biggest importance among the physical fluxes. However, in limited-area domains, the advection part (dynamical terms) is not negligible and can even dominate over the tendencies obtained from physical fluxes, which makes the interpretation difficult. The turbulent fluxes are important for the budget of kinetic energy, where the storm-producing run leads to bigger dissipation of energy in the PBL, due to turbulent transport. Nevertheless, this addition is compensated by strong forcing of the so-called baroclinic term

(containing the conversion of potential and internal energy to kinetic energy), that slightly increases the overall tendency of the kinetic energy in the storm-producing run (Fig. 7b).

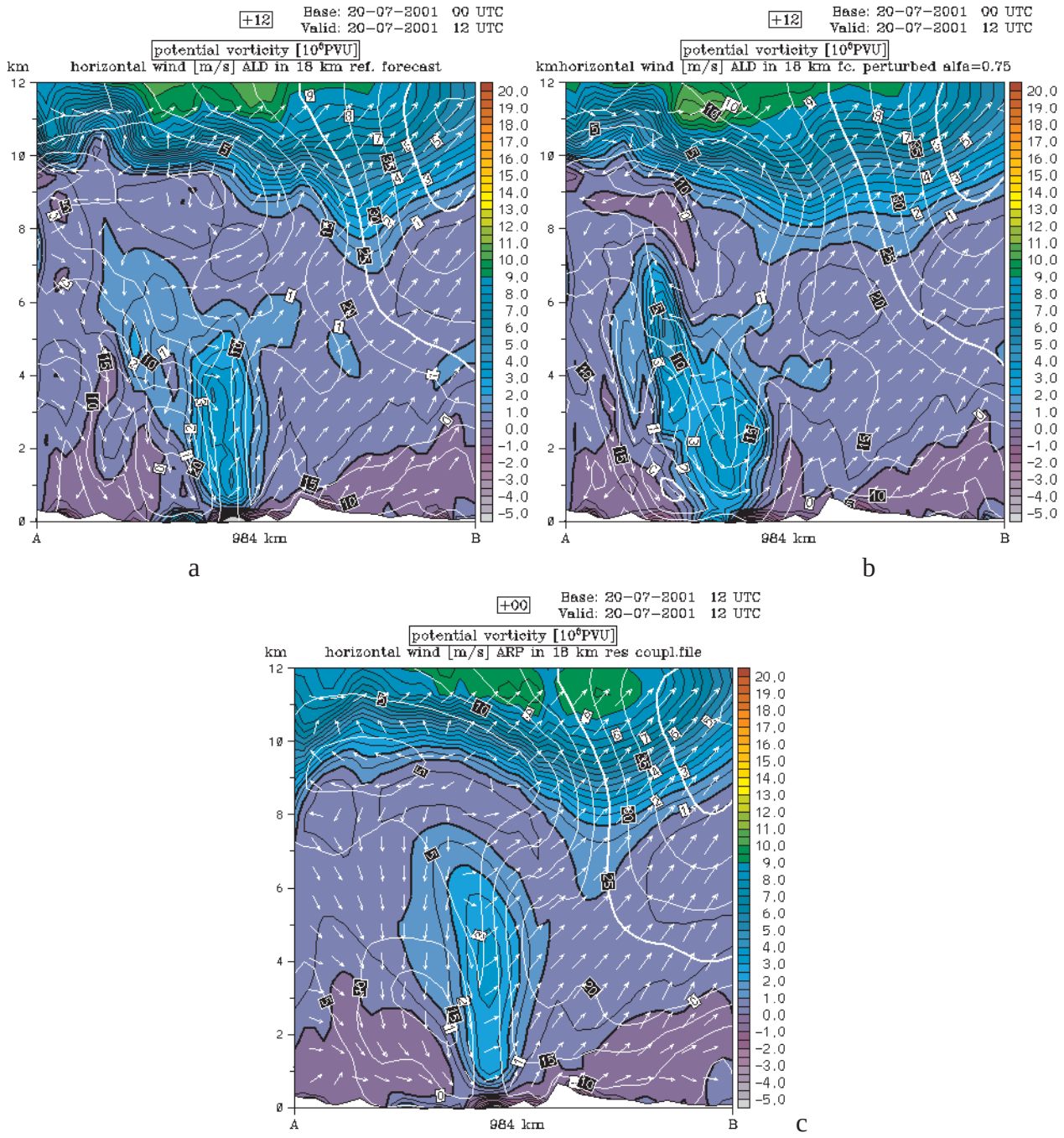

Figure 6.
a) Vertical cross-section through the fields of potential vorticity and horizontal wind in the 12-hour reference forecast, valid at 20.07.2001 12 UTC. Note the almost symmetric structure and small vertical shear of wind in the region of low-level PV anomaly (the sense of the cross-sections in Fig. 6a-c was shifted by 25' northward against the cross-section used in Fig.2b, to intersect the centre of the forecasted storm).
b) Same as in Fig. 6a but for the run with perturbed analysis (a=0.75). Note the redistribution of the PV field westward from the forecasted storm centre, causing rearrangement of the wind field (horizontal wind-shear suppressed, vertical wind-shear established). In contrary to the reference case, this environment is more favourable for slantwise up- and downdrafts, than for purely vertical motions.
c) Same as in Figs. 6a-b, but for the verifying model analysis valid at 20.07.2001 12 UTC. Note the similar structure as in Fig. 6a, but with considerably smaller amount of low-level potential vorticity above the surface-low centre.

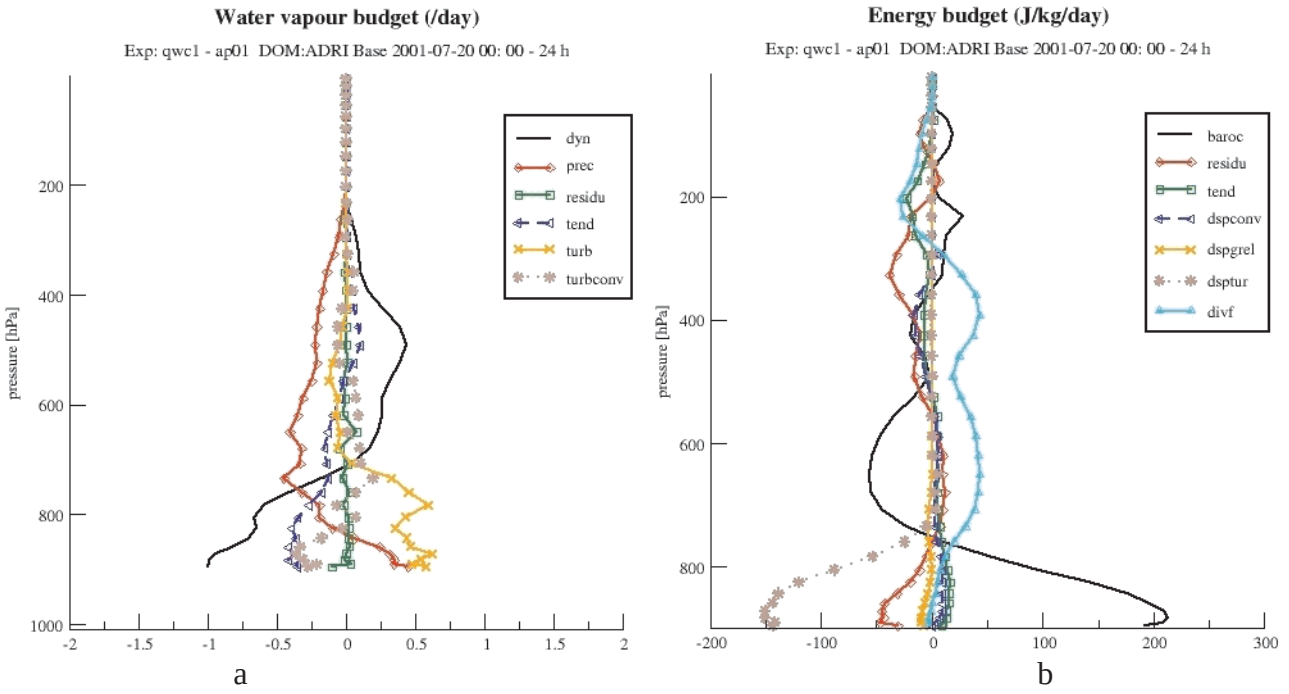

Figure 7.
a) Output of water vapour budget calculations for the differences between the basic forecast and the sensitivity forecast with perturbed initial conditions. The contribution of the terms not including physical fluxes is in black (dyn). Remarkable is the contribution of the precipitation fluxes (prec) and turbulence (turb) to the overall tendency (tend).
b) Difference of the kinetic energy budgets between the basic forecast and the sensitivity forecast run with perturbed initial conditions. The black line represents the so called baroclinic term (baroc). The residual term can contain, besides others, the contributions of the horizontal diffusion or the advection of kinetic energy. Among the physical fluxes is noteworthy the term of turbulent dissipation (dsptur).

Trials with parameterisation of dry and moist symmetric instability

Experiments with the sensitivity forecast runs cannot be taken as a true development of the atmosphere in the case of 20.07.2001. Nevertheless they show the importance of compensation processes in a symmetrically unstable atmosphere. Presence of dry or conditional instability forces slantwise (upslope or downslope) motions, and as a consequence, potential vorticity should vanish in this environment (Emanuel, 1983 and Nordeng, 1987). Actually, this is our goal in the case of the false mesoscale cyclogenesis, where the tropospheric values of PV reach abnormal values.

After the implementation of the shear-linked convection into the ARPEGE/ALADIN code, it was decided to make the vertical diffusion scheme dependent on symmetric instability as well. The adjustment of the scheme followed the work of Bennets and Hoskins (1979). A modified Richardson number was introduced to detect dry/conditional symmetric instability and to enhance the turbulent diffusion in stable PBL layers in the areas of instability. The equation for the modified Richardson number Ri_p , that replaces the original Ri, yields :

$$Ri_p = (N_w^2 / N^2)(\zeta / f)Ri - 1 \ ,$$

where N^2 / N_w^2 is the dry / moist Brunt-Väisälä frequency, ζ is the absolute vorticity and f is the Coriolis parameter. A more detailed description of the scheme can be found in the work of Simon (2003a).

For the "Adriatic storm" case from 20.07.2001, experiments with parameterisation of dry symmetric instability ($N_w^2 / N^2 = 1$), conditional symmetric instability and conditional symmetric instability coupled with shear-linked convection were performed. The most successful scheme was the first one, since improving the forecast of mean-sea-level pressure in the centre of the storm at least by

2 hPa. However, these properties are lost by application of the full scheme of conditional symmetric instability inside the vertical diffusion scheme. The application of the modified shear-linked convection scheme (Simon, 2003b) has no significant influence on the storm forecast.

Semi-Lagrangian horizontal diffusion - a possible solution ?

Recently, it was shown by Vana (2003), that an application of semi-Lagrangian horizontal diffusion, which is a kind of flow-dependent horizontal diffusion scheme, can bring a considerable progress in the case of the 20.07.2001 false cyclogenesis and also in further similar cases. The positive side of the scheme is not only the reduction of the cyclone to the depth almost corresponding to verifying model analysis. One can see on the vertical cross-sections of potential vorticity, how the originally spurious structure of the low-level PV anomaly was improved due to application of the new horizontal diffusion scheme (Fig. 8). Remarkable is that the semi-Lagrangian horizontal diffusion has in this case a huge impact also in the upper tropospheric and in the stratospheric levels, what was not expected before.

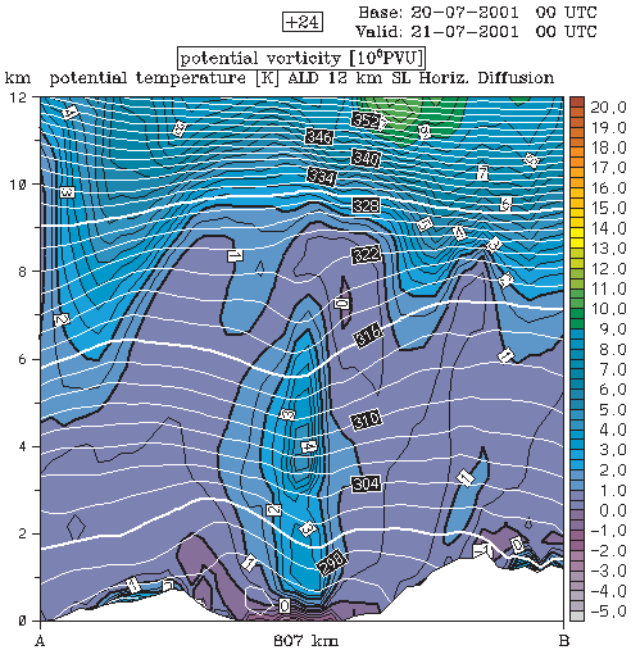

Figure 8. 24-hour forecast of potential vorticity and potential temperature, valid at 21.07.2001 and using the 12-km resolution ALADIN-LACE model, with application of the semi-Lagrangian horizontal diffusion, to be compared to the output of the reference experiment (Fig. 2c, same vertical cross-section).

Conclusion

The experiments with the adjoint of the ALADIN model showed that the process of creating the false mesoscale storm can depend on the initial conditions. Nevertheless, one need to modify considerably the initial files to get satisfying results. The diagnostics via PV field shows that the forecast of the storm is even not corrected by the way, that should fit with the corresponding model analysis.

It seems that the sensitivity gradient fields in the experiments with the adjoint model were created artificially and their computation was possibly influenced by the usage of very simple physical parameterisation for a relatively long period (24 hours).

Hence one can have doubts, whether the forecast of the storm was really a problem of initial conditions. Moreover, most recent experiment with model run based on the ECMWF analysis gave

surprisingly small differences in the forecast of the cyclone for both ARPEGE and ALADIN models, comparing to the reference storm-creating forecasts.

However, the contribution of the adjoint sensitivity tests and forecasts mentioned in this article is a larger view on the dynamics-physics interaction, that decides about the creation/cancellation of false mesoscale cyclogenesis. That means - the storm can be cancelled without changing the physical parameterisations, if the dynamics of the storm will be changed (in this case via redistribution of potential vorticity in low and mid-troposphere). This allows us to hope that a reverse process is possible as well (while the low-level PV anomalies are in fact consequences of physical processes as diabatic heating or friction). A determination, how to compensate the effects of dynamics within the physical parameterisations, is not a trivial task as one can see from the results of the DDH diagnostics in this paper. Nevertheless, recent changes in the operational physical parameterisation of the ARPEGE/ALADIN model, namely in the stratiform precipitation and vertical diffusion part (in model versions up from cycle *AL25T1-op3*), are giving already better results in number of problematic cases with false cyclogenesis.

The simulation of dry-moist symmetric instability processes either in convection or in vertical diffusion is most probably not an ultimate solution. False mesocyclones, that show an almost perfect symmetry (as in the case of the Adriatic storm predicted on 20.07.2001) are not sensitive to those schemes. The reason is that the simulated slantwise movements and turbulent exchange can start just in an environment with vertical wind shear (this works well in cases with tilted troughs or cyclones). The partial success of the dry-symmetric instability modification was caused most probably not directly (acting on the dry symmetric instabilities similar to those that appeared in the model analysis, see Fig.2).

Hence the semi-Lagrangian horizontal diffusion looks as an elegant solution to the problem of false cyclogenesis due to its selective properties (and not large effects on scores). A theory, presented in the work of Vana (2003), is telling us, that the semi-Lagrangian horizontal diffusion, although driven only by horizontal components of parameters (such as the tensor of the flow deformation), is in fact applied in three dimensions. Thus, it can simulate the effects of horizontal dissipation (in real atmosphere done by turbulence or molecular exchange) that are not present in the current one-dimensional ARPEGE/ALADIN physical parameterisation of vertical diffusion. According to the achievements of the semi-Lagrangian horizontal diffusion, we can conclude that an improved physical parameterisation of horizontal dissipation is required for correct forecasts of cyclogenesis at smaller scales.

However, further experiments will be required, concerning improved diagnostics on the effects of horizontal diffusion or a new, 3d treatment of the parameterisation of turbulent fluxes. The evaluation of some schemes of turbulent diffusion, taking into account horizontal derivatives of wind field, is currently on the way.

Acknowledgements

We would like to thank Cornel Soci, who helped us and contributed to this study, sharing his experiences and knowledge in using the adjoint of the ALADIN model.

References

Bennets D.A., Hoskins B.J., 1979 : Conditional symmetric instability a possible explanation for frontal rainbands, *Quart. J. R. Met. Soc.*, **105**, 945-962

Bouyssel F., Geleyn, J.-F., 2002 : Description of the so-called "shear-linked convection" parameterisation, *ALADIN/ALATNET Newsletters, **21/5***

Buizza R., 1993 : Impact of a simple vertical diffusion scheme and of the optimisation timer interval on optimal unstable structures. *RD Tech.Memo.*, **192**, ECMWF, 25 pp.

Emanuel K. A., 1983 : On Assessing Local Conditional Symmetric Instability from Atmospheric Soundings, *Mon. Wea. Rev.*, **111**, 2016-2013

Nordeng, T.E., 1987 : The effect vertical and slantwise convection on the simulation of polar lows, *Tellus*, **39**A, 354-375

Piriou J.-M., 2001 : Diagnostics sur Domaines Horizontaux, Guide d'utilisation et de maintenance, *Documentation*, Météo-France

Simon A., 2003a : Study of the relationship between turbulent fluxes in deeply stable Planetary Boundary Layer situations and cyclogenetic activity, *Dissertation project proposal*, Slovak Academy of Sciences, 69 pp.

Simon A., 2003b : The implementation of the vorticity into parameterisation of shear-linked convection, *Internal report*, Météo-France

Soci C., Horanyi A., Fischer C., 2003 : Preliminary results of high resolution sensitivity studies using the adjoint of the ALADIN mesoscale numerical weather prediction model, accepted to *Idöjárás*, **107**, 49-65.

Tardy M., 2003 : Les Arpegeades, power-point presentation on Atelier PREVI-GMAP, *Internal document*, Météo-France

Vana F., 2003 : Semi-Lagrangeovske advektivni schema s kontrolovanou difuzivitou - alternativni formulace nelinearni horizontalni difuze v numerickych predpovednich modelech, Doktorska disertacni prace (*Thesis*, in czech, including long abstract in english and french), 133 pp.

Vakula Z., 2001 : Adriatic storm cases, *RC LACE internal report*, 9 pp.

Vakula Z., 2002 : Adriatic storm cases, *Proceedings of the 12th ALADIN workshop*, Croatian Meteorological and Hydrological Service

Impact of the topography and LBC on the ALADIN precipitation forecast

Yong Wang (ZAMG) and Eric Bazile (Météo-France)

1. Motivation

Because of strong influence of mountain on weather processes, ALADIN have some specific problems over complex mountainous areas, especially the precipitation forecast. The aim of the work is to improve the ALADIN precipitation forecast. Special attentions are paid to investigating the impact of the model topography and LBC's on the ALADIN precipitation forecast.

2. Domains, data and meteorological situation

The domains used for the numerical simulations are shown in Fig. 1 (Ahrens *et al.*, 2001). The coarse-grid domain LACE (12.2 km horizontal resolution, 37 level in vertical, hydrostatic) is centred over Central Europe and coupled to ARPEGE. The intermediate domain VIENNA (9.6 km horizontal resolution, hydrostatic) is for the studies over the Alps and coupled to ALADIN/LACE; ALADIN/VIENNA is taken as the control run. The domain LMTA is positioned so as to include the Lago Maggiore Target Area, our most interest target area for investigation.

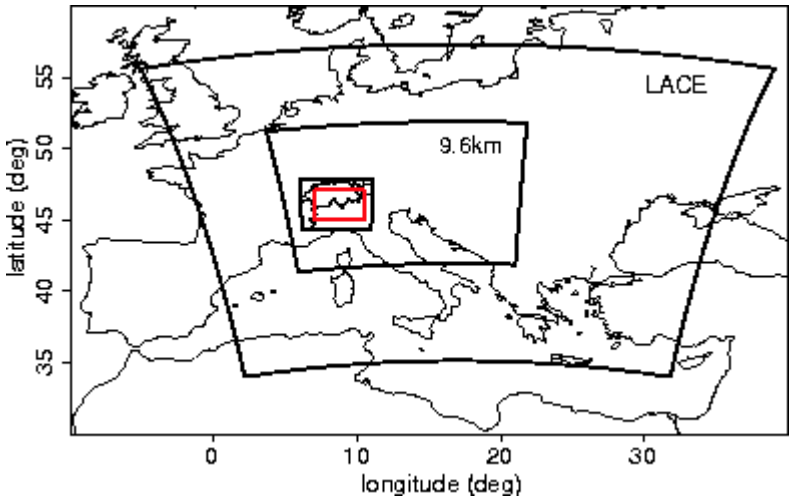

Figure 1. ALADIN domains for the numerical simulations. ***LACE*** : over central Europe, 12.2 km horizontal resolution; ***VIENNA*** : over the Alps, 9.6 km horizontal resolution; ***LMTA*** : Lago Maggiore Target Area; the sub-domain in red is used for the detailed investigation.

Heavy rainfall over the Alps occurs very often in autumn on the southern slopes of the Alps (Frei and Schär, 1998). The LMTA domain belongs to these maximums and was chosen for studying the mechanisms of persistent rain. This area is well investigated and observed within the Mesoscale Alpine Programme, MAP (Binder *et al.*, 1996, Bougeault *et al.*, 2001) and the EU Project RAPHAEL (Bacchi & Ranzi 2000). The dense operational observation network in the Alpine region was complemented during the special observation period (autumn 1999) by research instruments: ground-based and airborne radars, supplementary radio-soundings,... The dataset collected during the Intensive Observation Periods (IOPs) allows the direct study of heavy rain and the validation of fine-scale research and operational models over a mountainous area. One of the most intense rainfall episodes, IOP2b (19 and 20 September 1999), is used here for the study.

The synoptic situation of IOP2b is characterized by (details in Asencio *et al.*, 2002) : a deep cyclone located to the West of Ireland at 00 UTC on 19th Sept., and moving to France at 12 UTC on 20th Sept.; a strong stationary anticyclone over Russia, which extends by a ridge even to South of the Mediterranean Sea East of 20°E. In North Africa, a second cyclone moves from Morocco to Tunisia during the IOP2b.

An active cold front is associated with the Atlantic cyclone. At 00 UTC, it extends along an approximately North-South axis from the British Islands to Portugal. It crosses France on 19th Sept. and reaches the Alpine orography during the night. The eastwards evolution across the Po Valley during the 20th Sept. is slowed down by the stationary high pressure over Eastern Europe.

This is a typical synoptic situation for heavy rainfall over the Alps because the cold front movement will intensify the West-East pressure gradient and therefore the low-level jet ahead of it. Moreover, warm air originating from Africa crosses the Mediterranean Sea and this leads to the formation of a conditionally unstable air mass.

3. Results

For investigation of the ALADIN precipitation forecast over the complex mountainous area, the precipitation analysis (version 2.0, 25 km resolution) from ETH, Zürich, (Frei and Häller, 2001); and radar precipitation analysis provided by the MAP Data Center, Zürich, and M. Hagen, DLR, are used, which are shown in Fig. 2.

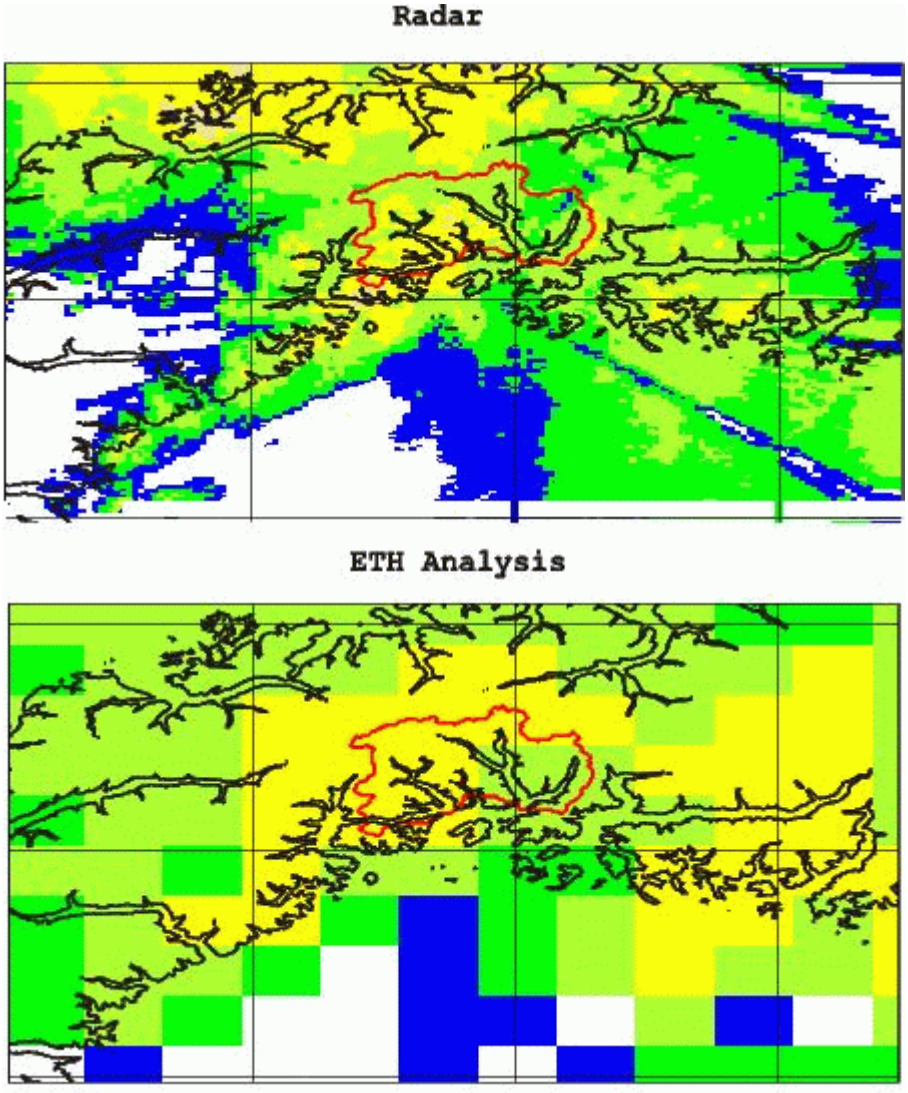

Figure 2. 24 h mean precipitation rate, in mm/h, from 06 UTC 20.09.1999 to 06 UTC 21.09.1999.

3.1 Model orography

The representation of the orography in the model plays a crucial role in the precipitation forecast. For having more knowledge about the influence of the model orography on the precipitation forecast we simulate the IOP2b case by using different model orographies in the ALADIN/VIENNA, i.e. 9.6 km horizontal resolution, coupled to ALADIN/LACE. The model orographies we have chosen are:

1. envelope orography
2. mean orography (without envelope)
3. semi-envelope orography, which is based on the variational method (Bouteloup, 1994). The underlying idea is to keep close to mean orography at the largest scales and to the usual, enhanced, envelope orography at the small scales. This is achieved simply through a modification of the cost function J minimized in the computation of the spectral orography:

$$J^{new} = J^{old} + P \sum_{n,m} \left| R_n^m - S_n^m \right|^2 / \left(\sqrt{m^2 + n^2} + 0.5 \right)^a$$

J^{old} is computed in gridpoint space so as to minimize Gibbs oscillations over sea. R and S are the spectral components of the final and mean (before any minimization) orography. a and P are tuning parameters.

The height-latitude cross-sections of the different model orographies and the original input data at longitudes 7.1°E, 8.5°E and 9.0°E are shown in Fig. 3. The mean orography is closer to the reality than the envelope and the semi-envelope ones, which increase the mass of the mountain. The comparison of the precipitation forecasts using envelope and mean orography is presented in Fig. 4. The impact of using the mean orography is positive, it reduces the precipitation maximum on the top of the mountain, and the forecast is closer to the analyses, but the other problem is still there, e.g. too dry in the lee side of the mountain. We have also compared the forecasts using full envelope and semi-envelope orographies in the model, there is indeed an improvement on the precipitation maximum, but not so evident.

One may be afraid that by introducing no envelope orography the wind forecast will be deteriorated. For this a comparison between the wind forecast with and without the envelope orography is presented in Fig. 5. This is the time-height cross-section of the averaged wind intensity. The result is very similar, and we can't conclude to any deterioration in the wind forecast by using no envelope orography. The validation of the wind intensity with the radar observations (see Asencio *et al.,* 2002) shows that the forecasted upper-level jet is weaker in intensity and few hours earlier than observed, and in the low levels the wind intensity is overestimated a bit in the period 06 UTC to 12 UTC 20.09.1999. In this period, the cold front is over the area.

3.2 Lateral boundary conditions (LBCs)

An experiment was done for investigating the impact of the coupling LBCs on the model precipitation forecast. In the simulation, the initial conditions and lateral boundary conditions, linearly interpolated in time between 6 hourly analyses (not as in the control run with a forecast), are given by the ARPEGE operational analyses. To analyse the impact, we focus on the western side of the Po Valley, and divide it into 3 areas. For the definition of those three areas, please see Asencio *et al.* (2002). The temporal evolution of the rain averaged over each area (Fig. 6) shows that the simulation with forecast as coupling overestimates the rain over Alpine slopes and Piedmont area, and is quite reasonable over central Po Valley. All of them exhibit a temporal shift. The experimental simulation is close to the radar observation in intensity over the Alpine slopes and Piedmont area, but underestimates the rain over central Po Valley. As in the control one, the temporal shift is still there.

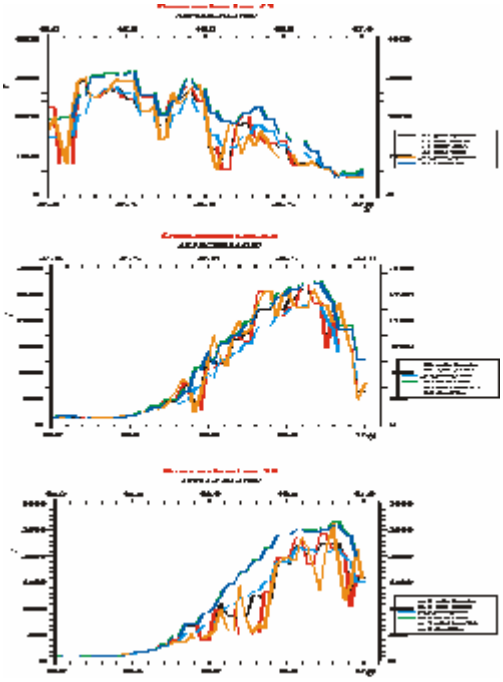

Figure 3. South-North cross-sections of the orography used in the simulations, at 7.1°E, 8.5°E and 9°E. **Grille_8proche** : average of the 8 surrounding gridpoints. **Grille_proche** : average of the 4 surrounding gridpoints. **NEW_ORO** : without envelope. **OLD_ORO** : envelope. **Relief_input923** : original input data. **Semi2Oro** : semi-envelope.

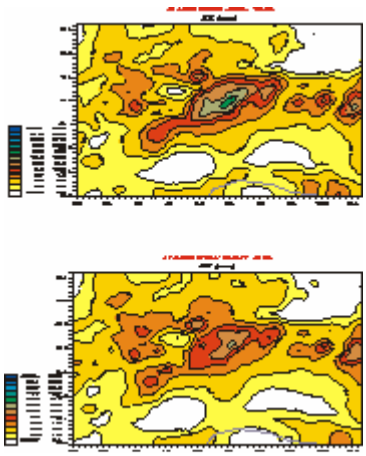

Figure 4. Comparison between the 24 h accumulated precipitation forecasts with (upper) and without (lower) envelope orography, valid for 06 UTC 20.09.1999 - 06 UTC 21.09.1999.

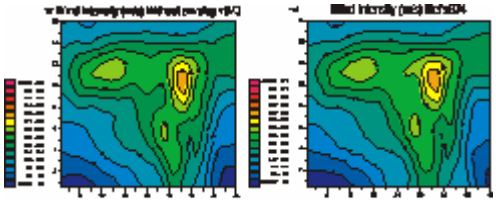

Figure 5. Time-height cross-sections of the wind intensity, in m/s. Left : forecast without envelope orography. Right : forecast with envelope. Valid from 00 UTC 19.09.1999 to 00 UTC 21.09.1999.

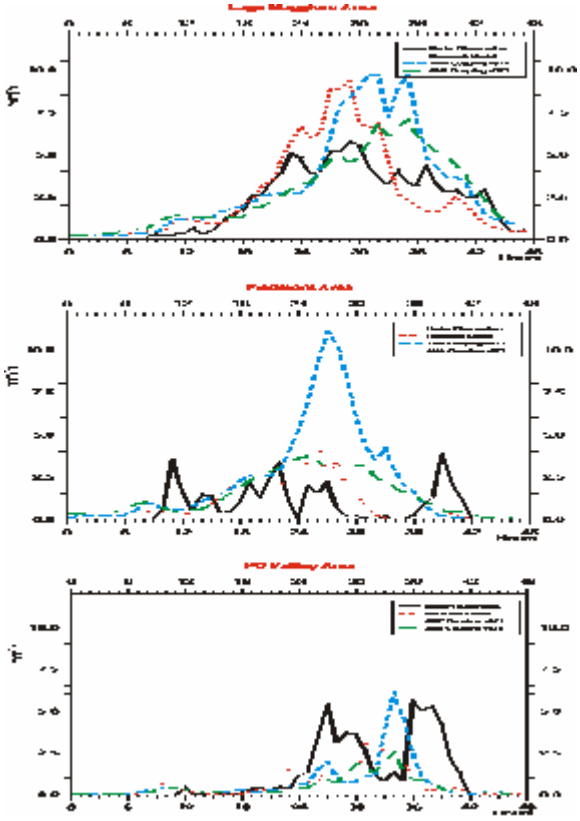

Figure 6. Time-height cross-sections of the hourly precipitation over the three areas. Black : radar analysis; red : research model Meso-NH; blue : coupled with forecast; green : coupled with analyses.

A comparison with Meso-NH, the red curves in Fig. 6, shows that ALADIN is better in intensity than Meso-NH, but the forecast timing is rather poor.

Based on the meteorological situation we consider the IOP2b case as 3 periods :

a) pre-frontal (00 UTC 19.09.1999 to 06 UTC 20.09.1999) : During this period, the cold front approaches the Po valley, the integration with analyses as coupling quite well simulates the quasi-stationary rainfall over LMTA, whereas this is not the case over the two other areas, where the duration of the rainfall episodes is more variable. In the last 6 hours of the period, the integration with forecast as coupling intensifies the rainfall too much, except over the central Po Valley.

b) frontal (06 UTC to 18 UTC 20.09.1999), it is associated with the end of rain over Piedmont, the intensification over LMTA and variable over central Po Valley. Both simulations don't recognize the timing of the rainfall and overestimate much, although the one with analyses as coupling is better.

c) the post-frontal period, the last part of 20. 09.1999, which is characterized by residual orographic precipitation and ended the whole episode. The good estimation of the rainfall over every area in both simulations is confirmed, by intensity and timing.

Again, as in Part 3.1, we have studied the wind forecast of both simulations, which is shown in Fig. 7. Both wind forecasts are alike, and in good agreement with the observations. In this aspect the model with the analyses as coupling improves the wind forecasts. However, the model overestimates the wind during the 20.09.1999 morning. In particular the simulated upper-level jet is in excess of 8 m/s compared with the observations. In the low levels, the simulation with no envelope and analyses as coupling improves the wind forecast; there is no overestimation of the wind intensity any more.

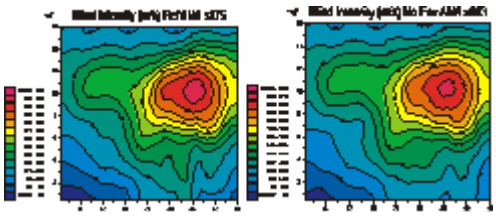

Figure 7. As in Fig. 5, but with ARPEGE analyses as coupling. Left : wind forecast with envelope orography. Right : forecast without envelope.

4. Conclusion

We have studied the MAP IOP2b case for investigating the possibilities of improvement on the ALADIN precipitation forecast over complex mountainous areas. This case is typical for heavy precipitation in the Alpine region. The emphasis has been put on the Lago Maggiore area in the Alps because of the dense observations collected by research and operational measurements during the MAP IOPs. ALADIN simulations with different orographies and coupling strategies have been carried on. The main conclusions of this work are summarized in the following :

Mean orography in the model does improve the precipitation forecast, and doesn't deteriorate the wind prognoses.

The best result for rainfall and wind forecast we get is by using the ARPEGE analyses as coupling LBCs, which indicates that obtaining a good ALADIN forecast largely depends on the quality of the coupling model.

Further works on this subject are still to be done, especially on the influence of the microphysics and the data assimilation for the initial state of the model. Mesoscale predictability of the quantitative precipitation forecast over complex mountainous area is another aspect of the future investigation.

Acknowledgement

We acknowledge D. Giard and F. Bouyssel for advice and technical help. This project has received funding from the *Österreicher Austauschdienst* (ÖAD), Republic of Austria. Cooperations with the *Institut für Meteorologie unf Geophysik, Universität Wien* and the MAP archive are kindly acknowledged.

References

P. Binder and C. Schär (eds) 1996, MAP Design Proposal,

P.Bougeault, P. Binder, A. Buzzi, R. Dirks, R. Houze, J. Kuettner, R. B. Smith, R. Steinacker, and H. Volkert 2001, The MAP Special Observing Period, *Bull. Am. Meteor. Soc.* **82**, 433-462.

C. Frei and C. Schär 1998, A precipitation climatology of the Alps from high-resolution rain-gauge observations, *Int. J. Climatol.* **18**, 873-900.

C. Frei and E. Häller 2001, Mesoscale precipitation analysis from MAP SOP rain-gauge data, *MAP newsletter* **15**, 257-260.

B. Ahrens, Y. Wang and K. Jasper 2001, On ALADIN quantitative precipitation forecasts in Vienna. *ALADIN Newsletter*, **19**, 64-68.

Y. Bouteloup 1994, Improvement of the spectral representation of the earth topography with a variational method, *Mon. Wea. Rev.*, **123**, 1560-1573

N. Asencio, J. Stein, M. Chong and F. Gheusi 2002. Analysis and simulation of the local and regional conditions for the rainfall over Lago Maggiore Target Area during MAP IOP2B. Submitted to *Q. J. R. Meteor. Soc.*

1. Radi AJJAJI : "Incrementality deficiency in ARPEGE 4d-var assimilation system"

This contribution is very long, since presenting a synthesis of the work achieved along the 3 last years.

Explanation of cases of erroneous humidity analysis in ARPEGE 4d-var

The three following papers (with a fourth one in the next Newsletter) try to understand erroneous humidity analyses noticed in punctual cases over some mountainous areas and in the desert. Two selected cases are thoroughly examined, one situation over Sahara region (June 26th, 2000), where 4d-var assimilation introduced a great fictitious moistening, and one over northern Spain, where the 4d-var analysis was far drier than the reality (April 24th, 2001).

The first paper tries to find an explanation in the incremental approach (more precisely the multiple-truncation incremental scheme used operationally in France). A series of experiments consisting in running several 15-days assimilation suites with changes in the different ingredients involved in 4d-var (with the French ARPEGE setups : incremental, multi-incremental, non incremental, simplified physics in the last inner loop, simplified physics in all loops, adiabatic runs, etc...). The results suggest that the problem of wrong humidity analysis is somewhere else. A number of hypotheses are expressed, which require more experimental studies.

The second paper tries to formulate the dynamics of the Eulerian tangent-linear model used in the minimisation. This theoretic formulation shows the potential terms likely to be responsible, in the adjoint model, for the large humidity increments. These terms are then carefully examined in terms of order of magnitude. They allow to explain partly the problem by indicating strange magnitudes for some fields, such as pressure gradients over mountainous areas and vertical velocities over southern Sahara.

The third paper tries to find an explanation in the B covariance matrix used in 4d-var, by examining the order of magnitude of the implied background-error standard deviations, in terms of the different control variables, focusing on specific humidity. This study shows reasonable values at the beginning of the assimilation window.

PAPER I

Radi Ajjaji

Abstract

This paper discusses a problem observed since the very beginning in the 4d-var assimilation system at Météo-France. Precipitations over the Sahara desert are extremely overestimated in forecasts having as initial state a multi-incremental 4d-var analysis (Veersé and Thépaut, 1998). This problem is observed frequently during the summer period (June, July, and August). Several investigations had been done to diagnose and fix this problem which constitutes a serious source of weakness in ARPEGE assimilation system used at Météo-France since June 2000. As a first try to solve the problem, it has been decided to apply an incremental semi-external digital filter initialization at the end of the assimilation process to further filter model fields, especially humidity, at full resolution and consistently with the physics. This weakened slightly the problem but didn't solve it definitively.

The first ingredient suspected was the simplified physics introduced in the last inner loop, then the multi-truncation incremental approach. The different results showed that the overestimated rainfall is not caused by these two ingredients. A last experiment showed that the abnormal humidity increments associated to the large amounts of precipitations in the subsequent forecast over Sahara are caused by a strange feature of the tangent-linear dynamics, causing an abnormal nonlinear evolution of the increments during the minimization process.

1. Introduction

Four-dimensional variational assimilation (4d-var) has been operational at Météo-France since June 20th, 2000. The basic characteristics of this system are similar to those of the ECMWF 4d-var, with some specific components including the multi-incremental technique, a weak constraint based on digital filtering, the use of another set of specific simplified physical parameterizations based on Météo-France full physics package, and later an additional incremental semi-external filtering.

At the date of writing, minimization was based on three successive outer and inner loops. The first, second and third inner-loop minimizations are performed at spectral truncations T42, T63 and T95 respectively: This is cheaper than a pure incremental technique performed at resolution T95 (Veersé and Thépaut, 1998). The model resolution in the outer loops (and in forecasts) is T199, with a stretching factor of 3.5 and 31 vertical levels.

Noise is controlled inside the minimization process through a weak constraint based on a incremental digital filtering (Gauthier and Thépaut, 2000). A semi-external digital filtering is added to the system.

The last minimization (at truncation T95) is performed using diabatic tangent-linear and adjoint models containing simplified (regular) physical parameterizations : linear vertical diffusion, gravity wave drag, large-scale precipitations, radiation and deep convection (Janiskova et al., 1999).

This system configuration has been validated on several periods of parallel runs and the results were compared to the operational 3d-var system. However, on the Sahara area, the scores were bad, especially those concerning humidity field. This leads to a great overestimation of precipitation parameter over this zone.

Our investigations concerns the system described hereabove. The experiments concern a period of 10 days of variational assimilation from June 1st to June 10th, 2000. During this period, which corresponds to the beginning of operational 4d-var assimilation at Météo-France, frequent abnormal cases of precipitation overestimation over Sahara were observed.

In the second section, a brief description of the problem will be presented, followed by a description of the first solution tried to weaken it : the so-called semi-external digital-filter initialization. The third section will be dedicated to the investigations made to show the impact of the simplified physics introduced in the last inner loop. The fourth section will discuss the impact of a multi-truncation against a mono-truncation incremental approach. The problem will then be diagnosed in section 5 by studying some conceptual deficiencies in the derivation of TL/AD dynamics which may cause, among others, a bad behaviour of humidity increments.

2. Precipitation overestimation by ARPEGE forecast

Specific humidity, which is one of the 4d-var control variable, shows large positive analysis increments in the lowest model levels, over some subtropical land areas : Saudi Arabia, Sahara, Mexico, southern United States, ... (Fig. 1). Theses areas are characterized by high temperatures and dry conditions. Moistening could be as high as 10 g/Kg, and then it causes more and more humid subsequent forecast.

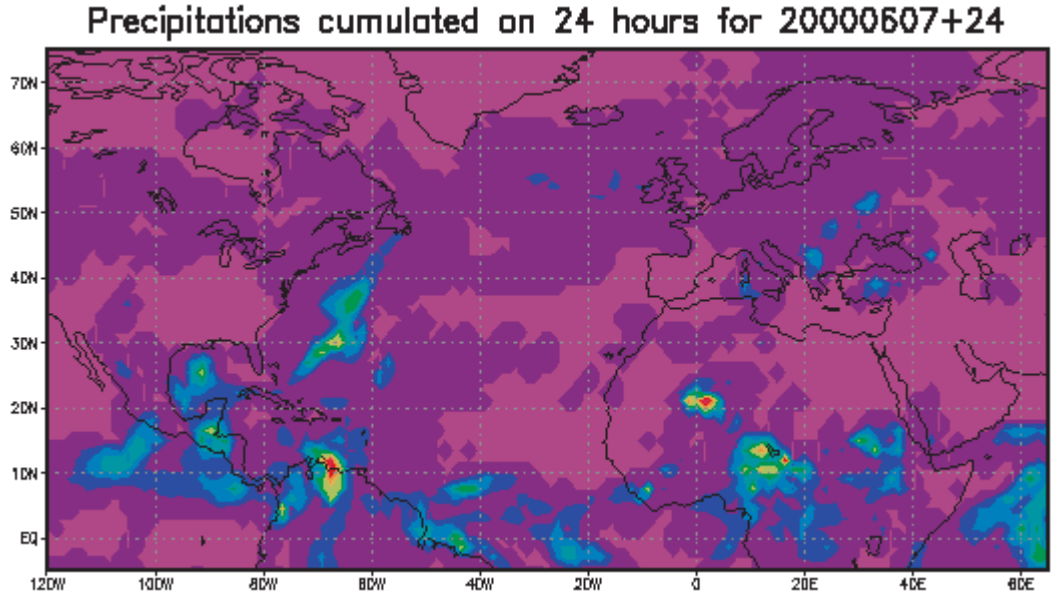

Figure 1 : 24-hours convective precipitation given by an ARPEGE forecast based on a 4d-var analysis. Precipitations localized at [20°N, 5°E] are completely fictitious.

The main observational data used by humidity analysis are TEMP specific humidity, SYNOP 2 m relative humidity and TOVS radiances in channels HIRS-10, 11 and 12. Several other TOVS channels also have a slight influence on humidity. There may also be a weak influence on the humidity analysis from surface pressure data and radiosonde geopotential data through, at least, virtual temperature effects.

As a first solution suggested and applied to cure this wrong behaviour quickly and easily, a "semi-external" digital filtering (based on finalization) was applied. It is added to the system with almost no extra cost, as it uses model integrations which have to be performed anyway during 4d-var : observation screening, computation of the last model trajectory at the end of the minimization. As it is shown on Fig. 2, this solution has no great effect on our problem.

In an assimilation system like the operational one at Météo-France, multiple ingredients could be at the origin of a bad humidity analysis : simplified physics, multiple-truncation incremental approach, incremental approach itself, something wrong in the conception of TL/AD models, bad use of some

observation types, use of incoherent background specific humidity structure functions. They were examined afterwards.

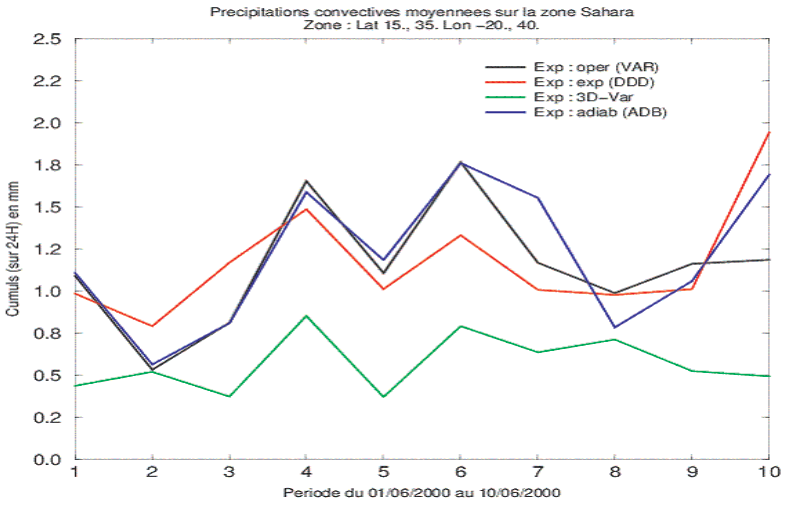

Figure 2 : 24-h convective precipitations amounts averaged over Sahara [15°N, 35°N]×[20°W, 40°E] for operational context [VAR], operational context with semi-external DFI [DDD], adiabatic context [ADB]. Forecasts based on 3d-var are taken as references.

3. Impact of simplified physics on humidity analysis over Sahara

A set of simplified and regular physical parameterizations as well as its tangent-linear and adjoint versions has been implemented in the ARPEGE data assimilation system. The main objectives are not only to be realistic enough, but mainly to be simple and regular for the efficiency of minimization in 4d-var. The package contains a simplified computation of radiative fluxes, vertical turbulent diffusion, orographic gravity waves, deep convection and stratiform precipitation fluxes (Janiskova et al., 1999).

In the operational version, this physics package is switched on only during the last inner loop, at resolution T95. At this truncation, the resolution is considered to be sufficiently high so that an inclusion of some physics becomes necessary. But this could have a bad impact on the humidity increments computed during the two first adiabatic inner loops. To investigate this aspect, two experiments were performed.

3.1 Applying simplified physics in all inner loops

In principle, this should produce more consistent increments, the impact of simplified physics affecting the increments since the beginning of the minimization, at truncation T42. But no significant effect on humidity increments can be observed, and the forecast scores keep unchanged. Such a study was already done by (Janiskova et al., 1998) where more investigations were carried out and extended to all other fields. Here the study focuses on humidity and temperature fields.

The shape of the cost-function decrease confirms the results obtained by (Thépaut et al., 1999). The introduction of simplified physics in all inner loops causes a less convergence ratio at the same number of iterations.

A single-observation experiment (one individual observation of specific humidity at 850 hPa is introduced somewhere over Hoggar mountains) shows a little difference, for humidity and temperature increments, between the experimental and operational configurations. Humidity increments look more noisy at resolutions T42 and T63, which reflects the impact of physics.

So, as a conclusion, we can say definitely that applying simplified physics only in the third inner loop is consistent and not responsible for humidity troubles.

3.2 No physics in the assimilation system : adiabatic inner loops

The aim of this experiment is to quantify the impact of simplified physics on the humidity increments. This is the only experiment that will confirm or not an eventual responsibility of simplified physics.

The scores and all the diagnostics presented on Figs. 3a-b show that the problem of big positive humidity increments keeps unchanged in the adiabatic assimilation experiment. One can also notice the quasi-neutral effect of the simplified physics on the forecast quality over this Sahara region. This is consistent with (Thépaut et al., 1999) where this neutral effect was also shown for all the tropical and subtropical regions.

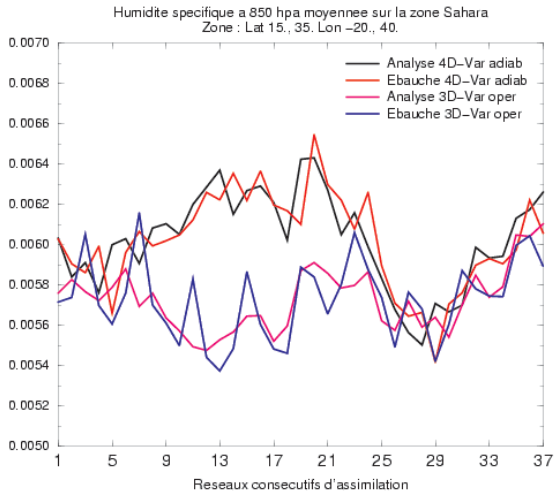

Figure 3a : Specific humidity averaged in space on Sahara [15°N, 35°N]×[20°W, 40°E] in a 10-days adiabatic 4d-var suite

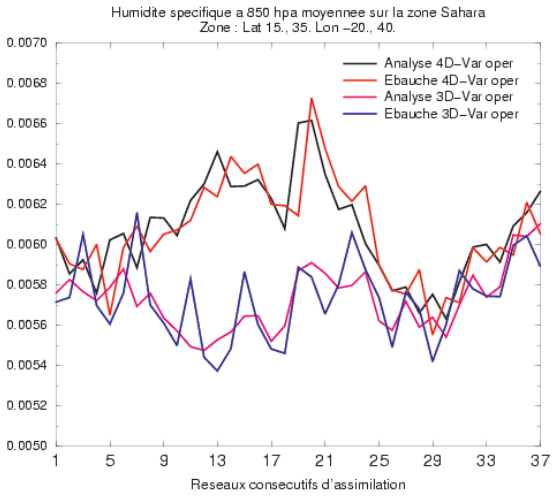

Figure 3b : Same as Fig. 3a, but for the operational context

4. Impact of minimization truncation on the humidity-increment field

Two assimilation configurations are studied : mono-truncation incremental and non incremental experiments are compared to the operational multiple-truncation incremental one. The simplified physics is still introduced in the last inner loop, in all cases.

4.1 Mono-truncation incremental case

The minimization truncation is the same (T95) during all the three inner loops; 25 iterations are allowed for each inner-loop minimization. This configuration is then rather similar to a simple incremental configuration with 75 iterations. But it is not exactly the same because simplified physics is not switched on since the beginning.

The results are shown on Figs. 4a-b. One can notice that a little improvement is obtained : the humidity-increments mean profile shows smaller values near the surface, i.e. along the layers between 1000 hPa and 700 hPa. But the increments still not realistic compared to those resulting from 3d-var assimilation, and the forecast scores are still very bad.

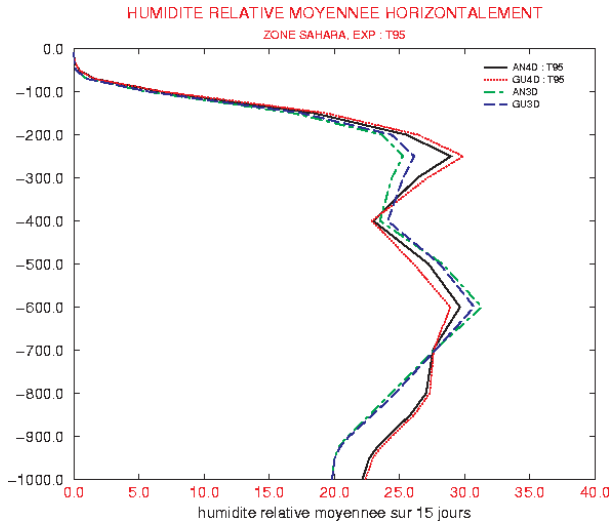

Figure 4a : Relative-humidity zonal mean profiles averaged over a 10 days 4d-var suite in a mono-truncation context. The corresponding 3d-var experiment is taken as reference.

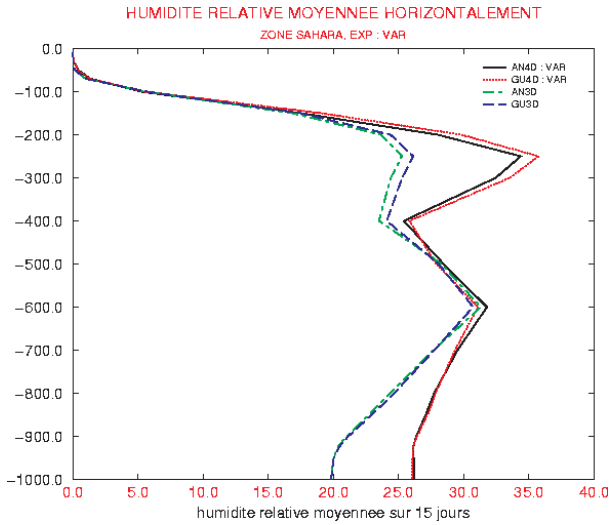

Figure 4b : Same as Fig. 4a, but in the operational (multi-truncation) context

On the single-observation experiments (Fig. 5a) the isolines for specific-humidity increments, during the two first inner loops, seem sparser and with a greater magnitude compared to the operational case (differences are shown in Fig. 5b). The second and third inner loops show no significant difference compared to the first inner loop. This could be explained by the fact that the convergence is quickly reached during the first inner loop.

4.2 Impact of incrementality

The main practical problem to be solved for an operational implementation of 4d-var is the reduction of the great computational resources needed. One important approach to achieve this goal is the incremental formulation (Courtier et al., 1994). This formulation allows the minimization to be performed at lower resolution and with a simplified linear model whereas the atmospheric state remains transported by the nonlinear direct diabatic model.

The direct nonlinear model used at high resolution in the so-called outer loops is the T199 ARPEGE one. An outer loop consists mainly in calculating observation departures at high resolution in an environment of realistic physics and dynamics. This information is then used as a forcing ingredient during the inner loops to keep the integrations involved along the minimizations close to the atmospheric "reality".

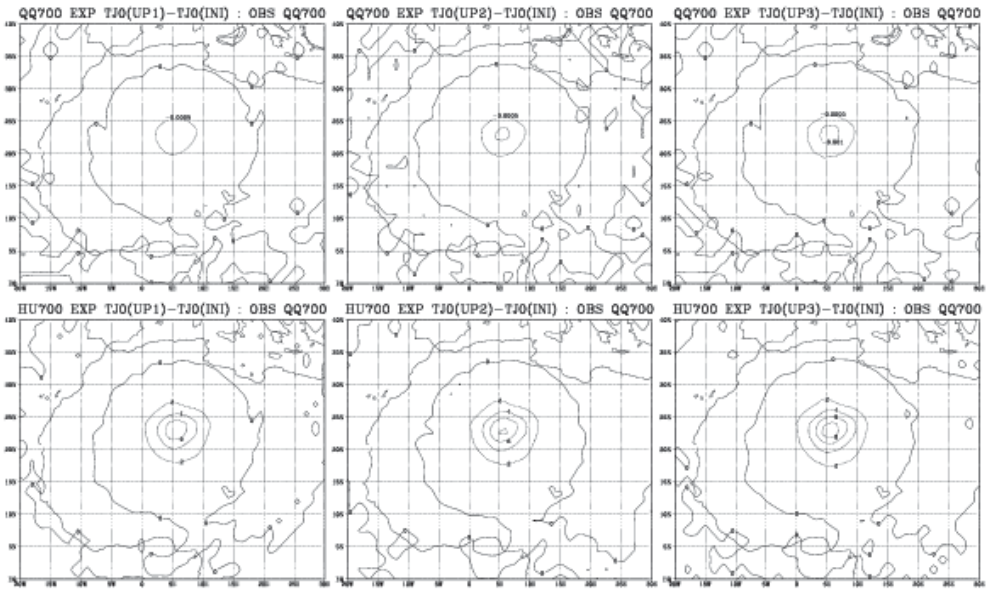

Figure 5a : Increments obtained in a single-observation experiment for specific and relative humidity during the three 4d-var minimization updates. The same truncation is used for all the inner loops.

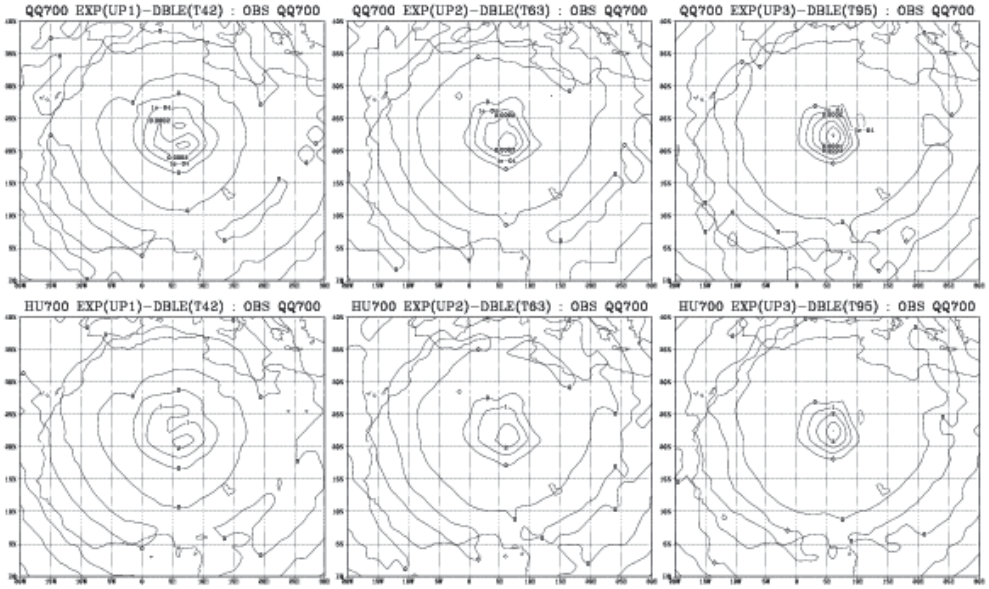

Figure 5b : Difference between the increments described in Fig. 5a and those obtained in an operational context.

The tangent-linear and adjoint models used during the minimizations are in fact the direct consequences of the incremental technique. They are introduced to approximate a real, more complex and heavier, calculation of the cost function and its gradient. The former becomes quadratic and thus the convergence of the algorithms used for minimization is guaranteed.

As a consequence, non-incremental experiments consist, in fact, in using the same resolution for inner and outer loops, and especially in minimizing the complete cost function of 4d-var, which requires the adjoint of the full nonlinear model. This is, of course, very difficult to achieve.

To simulate a non-incremental experiment in the context of our studies, we just forced the same horizontal resolution T95 both in outer and inner loops. The tangent-linear model and its adjoint are kept during minimizations. The forecasts are done at truncation T95.

The results show non significant changes. The phenomena remain non sensitive to this handling. But this doesn't mean that incremental technique is not responsible of the anomaly. It is perhaps indirectly involved in it, at least by the use of TL/AD approximations of the forecast model and observation operators. This will be discussed in the next section.

5. TL/AD formulation aberration

Thanks to François Bouttier (personal communication), sensitivity experiments, executed without specific humidity in the cost function, revealed the presence of a non-zero gradient with respect to this variable. So it turns out that there is something annoying in the TL/AD formulation of the dynamics. The specific-humidity increments are caused by the linearization of three terms in the dynamics:

$$Cp = q \cdot Cp_v + (1-q) \cdot Cp_d$$

$$R = q \cdot R_v + (1-q) \cdot R_d$$

$$\delta(RT) = T \cdot \delta R + R \cdot \delta T$$

Indices *"v"* and *"d"* stand for "vapour" and "dry" respectively. R is the air gas-constant, R_v the vapour one, R_d the dry air one. Cp, Cp_v, and Cp_d are the specific heats at constant pressure for air, water vapour and dry air respectively.

Experiments done by F. Bouttier also revealed that more than 90% of the humidity increments are caused by the adjoint of the third equation hereabove.

This fact happens, for example, in Sahara region because, apparently, there is a combination of high temperatures and large horizontal gradients of RT on the model surfaces. One must keep in mind that this is not due to an incorrect adjoint formulation : this is a feature of the dynamical equations. It seems that a solution of the problem could be the introduction of some extra-terms into the TL/AD models, to prevent large local derivatives. The problem is probably not limited to the humidity field.

As a first confirmation of this investigation, an experiment consisting in forcing R_v by R_d along the 4d-var minimization is performed. There should be a noticeable impact on increments since :

$$\delta(RT) = (R_v - R_d) \cdot T \cdot \delta q + ...$$

$$\delta(\nabla q) = (R_v - R_d) \cdot T \cdot \delta(\nabla T)$$

As it can be seen on the figures below, the problem disappears completely. But putting "R_v=R_d" is not the solution of the problem, it is just a mean to confirm the importance of local derivatives in the TL/AD part. More investigations are still be done to find a scientific reasonable cure.

From Figs. 6, 7 and 8, one can notice that, when compared to 3d-var, the experiment with R_v forced to R_d is the better one, indicating that the formulation of the TL/AD of dynamics still needs some modifications to work correctly.

This abnormal feature was present within the previous ARPEGE/IFS 3d-var assimilation. The conclusion at that time was that there was a problem with the specification of humidity background-errors in hot and dry conditions (Rabier et al. 1998). But this was significantly amplified by the change to 4d-var, from the very beginning, and some other problems appeared more recently, such as the April 24th, 2001, case (Figs. 9a-b). At 18 h UTC, the 4d-var assimilation introduced a strong drying over a large area, from Spain to Germany, not justified at all by observations. Six hours later, the reverse correction was introduced, going back to reasonable fields.

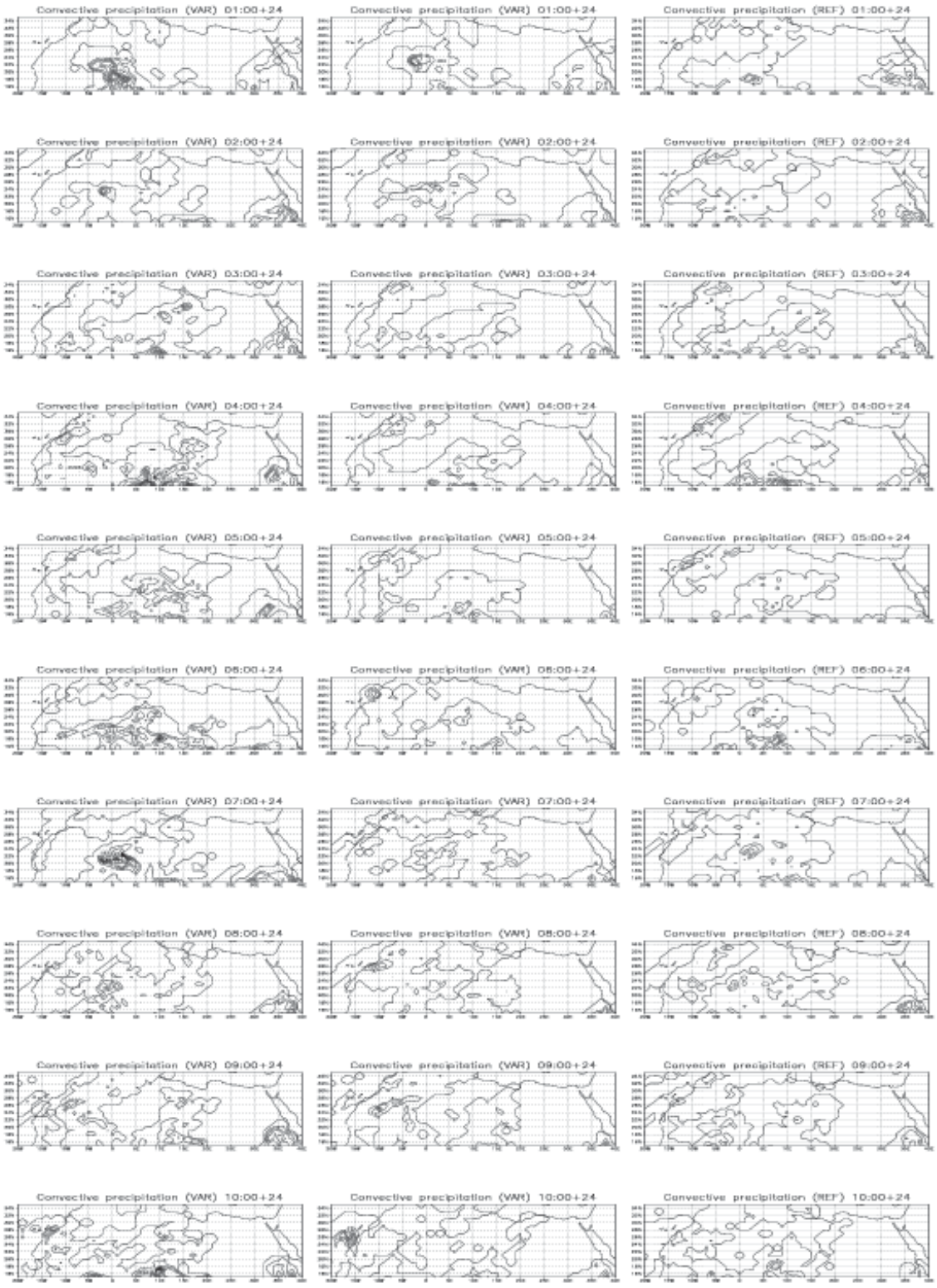

Figure 6 : Charts of convective precipitations (00 + 24 h) over Sahara, for the period between 01/06/2000 and 10/06/2000. Right column: operational suite. Left column: 3d-var reference. Middle column: results when forcing R_v to R_d in 4d-var.

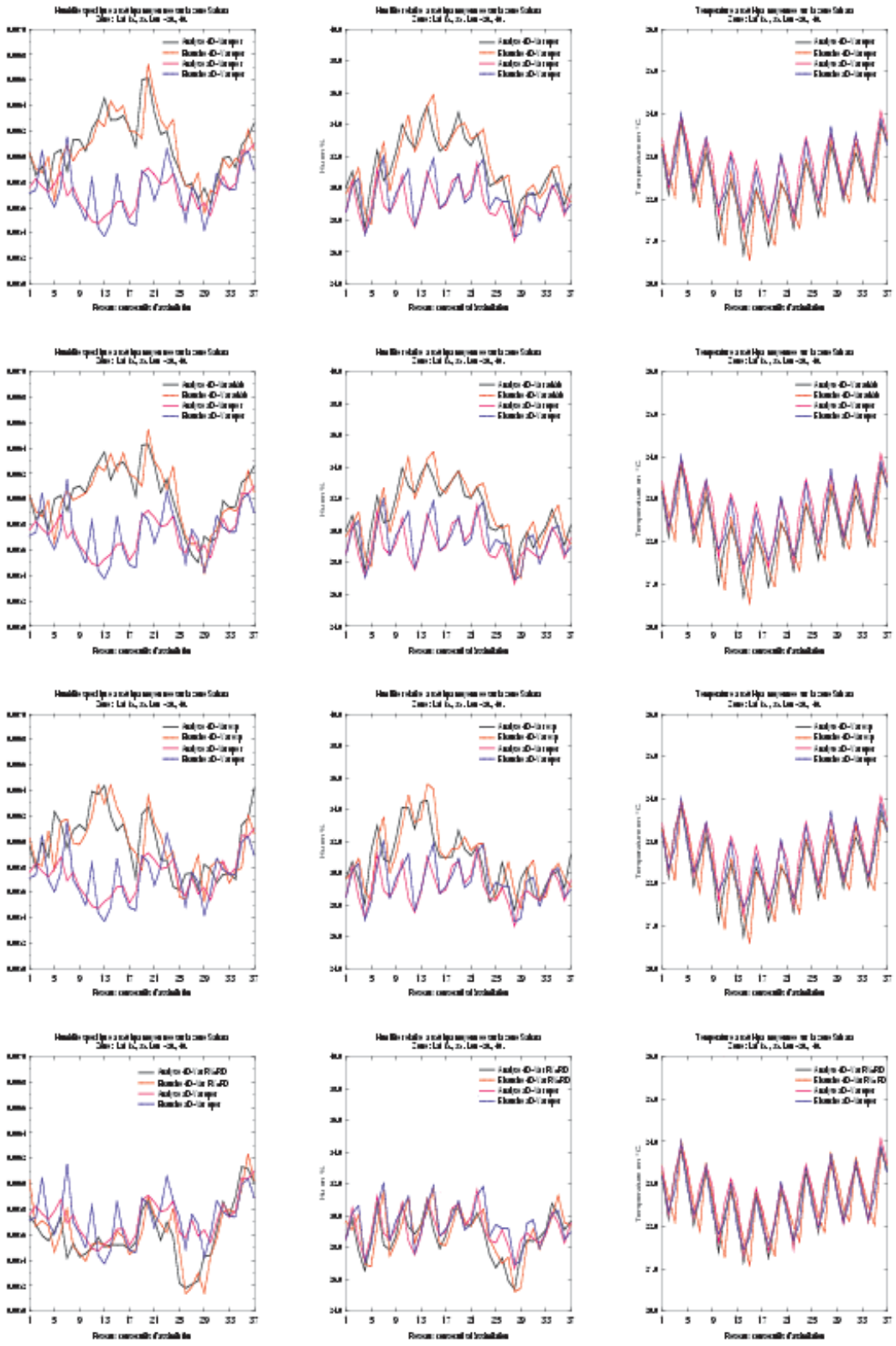

Figure 7 : Zonal means of specific humidity (right), relative humidity (middle) and temperature (left).
From top to bottom : operational 4d-var against 3d-var, adiabatic 4d-var against 3d-var, mono-truncation incremental 4d-var against 3d-var, experiment "R_v=R_d" against 3d-var.

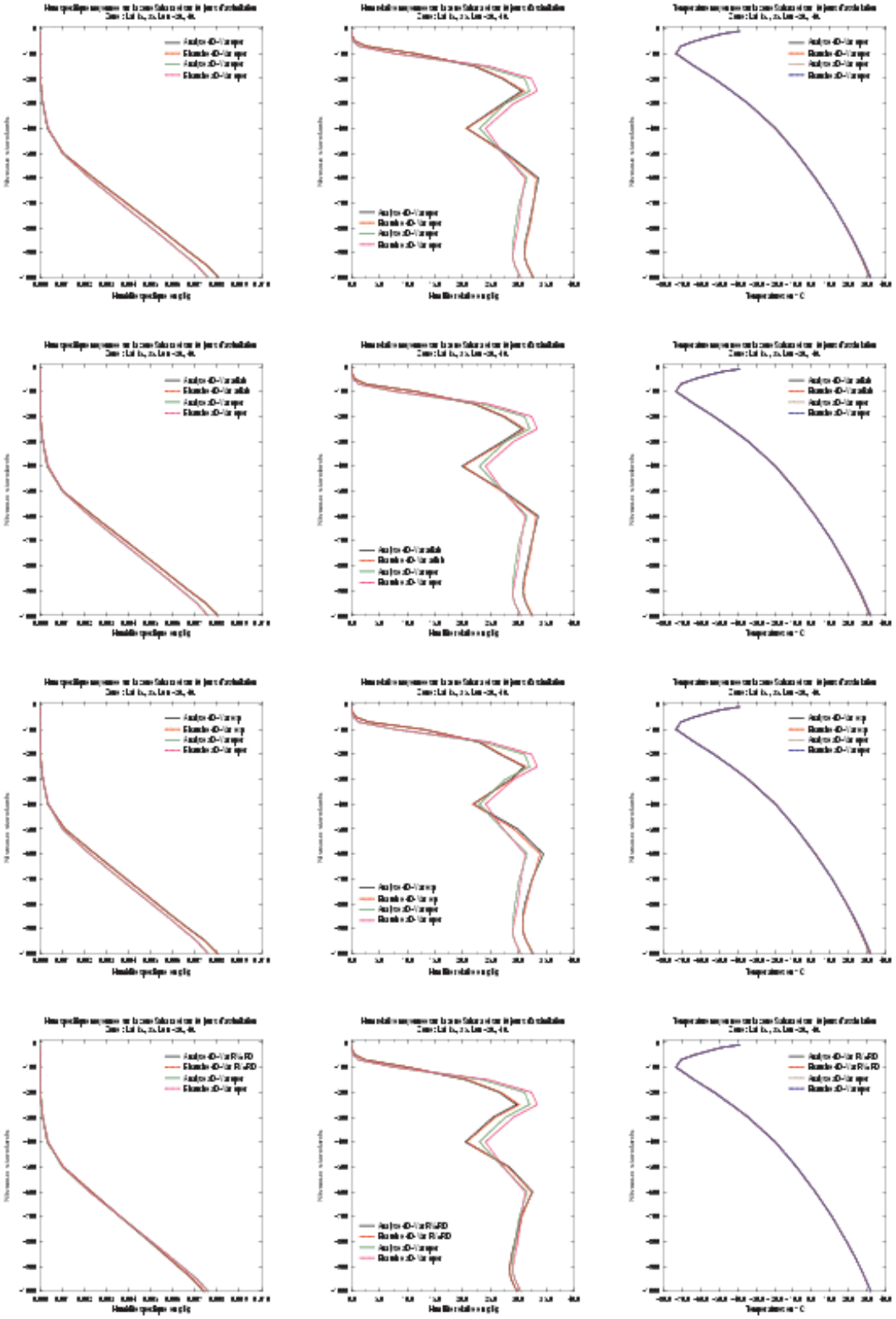

Figure 8 : The same as Fig. 7, but for zonal means averaged on standard levels over a 10-days assimilation experiment

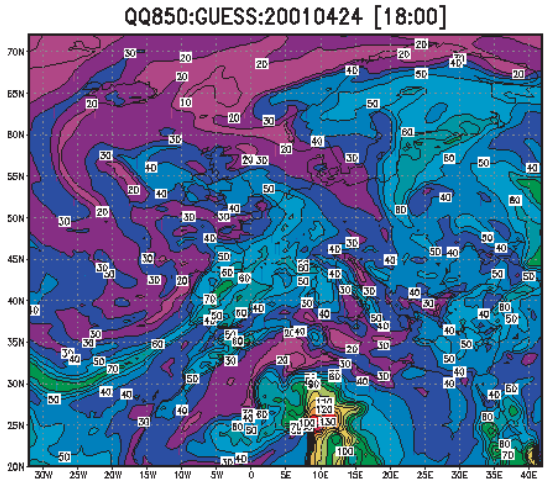

Figure 9a : 850 hPa specific humidity; first guess, 18 UTC

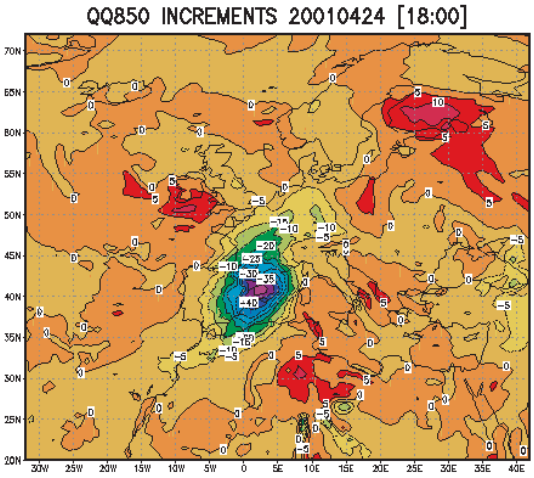

Figure 9b : Specific-humidity increments at 850 hPa.

On the April 24th, 2001, case, a detailed investigation of the impact of observations led to the following remarks :

- No TEMP is available, within 300 km of the maximum increment, along the 6 hours assimilation window (missing observation at that time);
- The anomaly is suppressed by adding an artificial TEMP observation (derived from the forecast) (Fig. 10)
- Suppressing AIREPs and/or SYNOPs suppresses the anomaly.
- 2 AIREPs around Baléares are likely to be at the origin of most of the problem;
- The problem on q is replaced by a problem on T, if suppressing the temperature observation in these 2 AIREPs.
- The impact of simplified physics, multi-truncation, ... is neutral.
- Applying the "R_v=R_d" trick suppresses the anomaly entirely.
- Sensitivity experiments, executed with no specific humidity in the cost function, reveal the presence of a non-zero gradient with respect to the specific humidity variable (Fig. 11)

Some other tests were performed, such as : "R_v=R_d" trick, "R_v=R_d" trick but not in the observation operators, impact of horizontal diffusion, etc ... The evolution of the problem along all the steps of 4d-var was carefully examined. This led to the following diagnostic :

The multivariate assimilation tries to fit observations by adjusting q first, even with very strong increments, especially when there are very few observations of humidity to constraint it. This happens since the very first integrations of the TL and AD models, as shown on Fig. 11, at the lowest resolution, and increases regularly along the minimization steps.

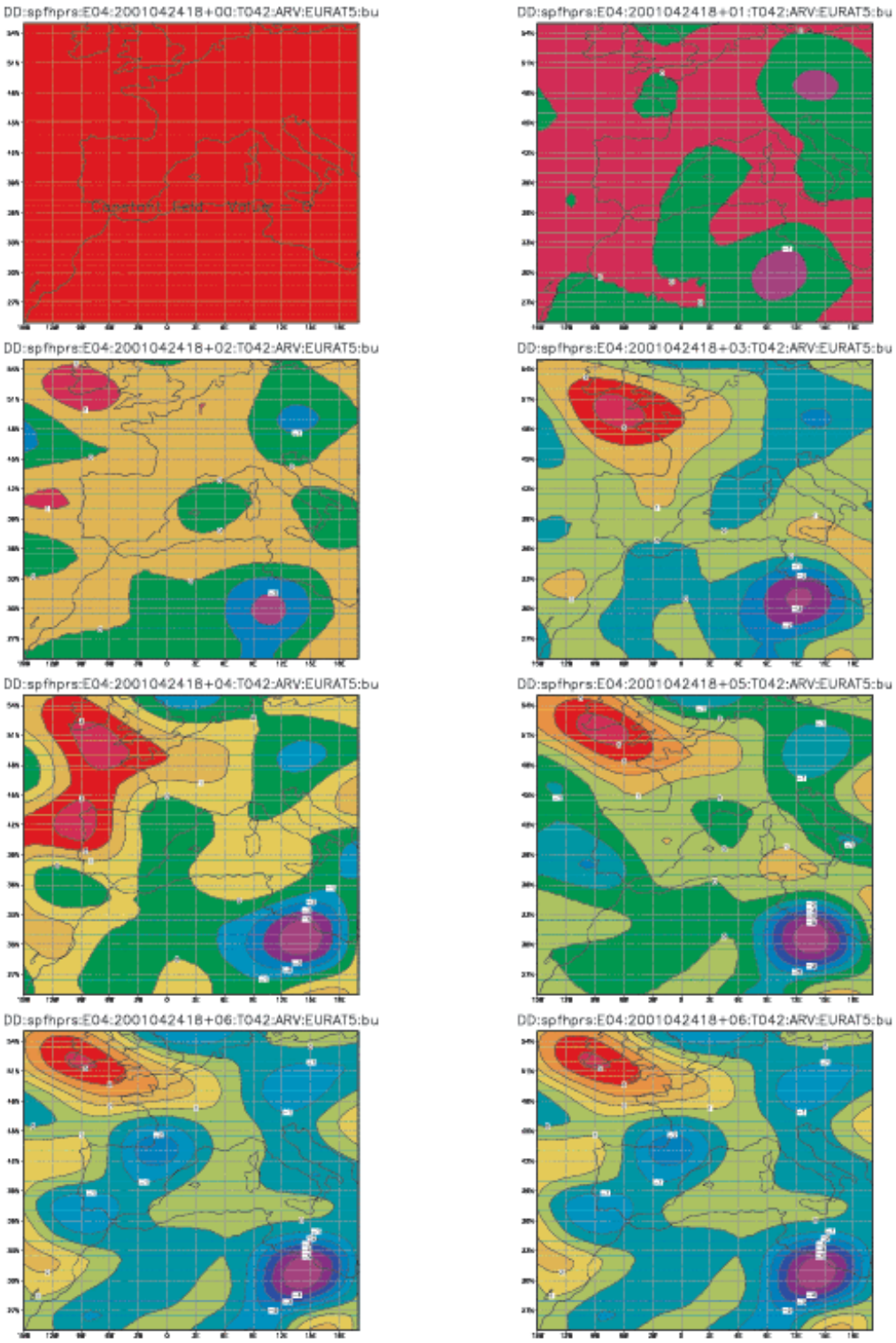

Figure 10 : Difference between the operational and experimental cases for tangent-linear evolution of T42 analysis increments along the assimilation window (6 hours). The experimental case consists in a simulated TEMP observation introduced at the vicinity of the anomaly. The anomaly disappearance gives evidence about the importance of humidity observations.

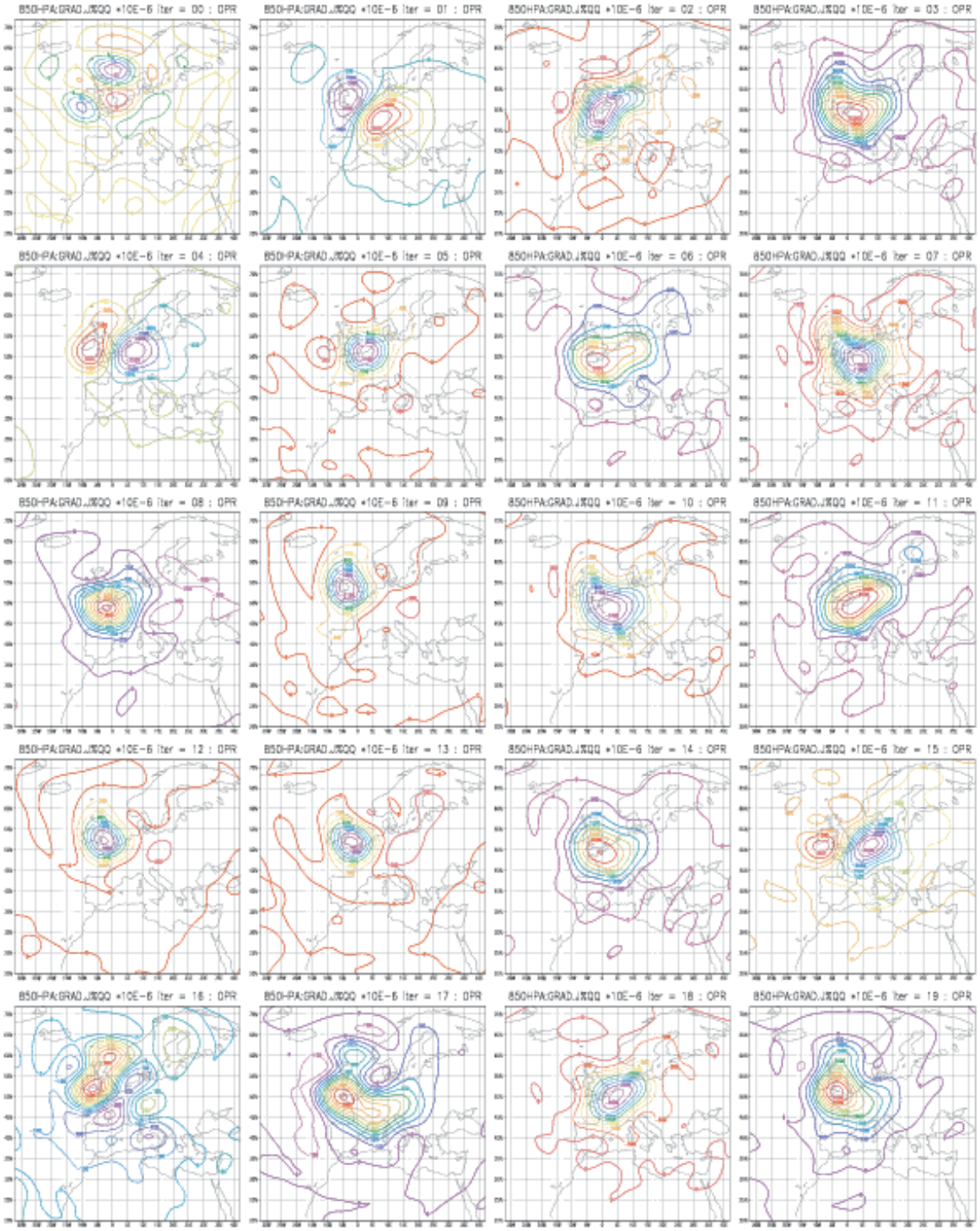

Figure 11 : Cost-function gradient with respect to specific humidity, computed at the beginning of the assimilation window at the end of each iteration during the first (T42) inner loop. Specific humidity is not included in the cost function.

These multivariate aspects of 4d-var could be illustrated in a simple context as follows.

If we suppose that the nonlinear direct prognostic model equations read:

$$\frac{d\mathbf{v}}{dt} = -f\,\mathbf{k}\times\mathbf{v} - \nabla\phi - RT\cdot\nabla\ln(p) + \mathbf{F}_v \qquad \mathbf{v} = (u,v)$$

$$\frac{dT}{dt} = \frac{RT}{Cp}\cdot\frac{\omega}{p} + F_T$$

$$\frac{dq}{dt} = 0 + F_q$$

Then, the associated tangent-linear model in the vicinity of a given model state reads :

$$\left(\partial_t + U_b\partial_x + V_b\partial_y\right) u' = -\partial_x U_b u' + (f - \partial_y U_b)v' - \partial_x\phi' - \frac{R_b T_b}{P_b}\,\partial_x p' - \partial_x\ln(P_b)\cdot R_b T' - \partial_x\ln(P_b)\cdot T_b(R_v - R_d)q'$$

a similar equation for $(\partial_t + U_b\partial_x + V_b\partial_y)v'$

$$\left(\partial_t + U_b\partial_x + V_b\partial_y\right) T' = \frac{A_b}{\omega_b}\,\omega' + \frac{A_b}{T_b}T' - \frac{A_b}{P_b}P' + \frac{A_b}{R_d}(R_v - R_d)q' - \frac{A_b}{Cp_b}(Cp_v - Cp_d)q'$$

$$\left(\partial_t + U_b\partial_x + V_b\partial_y\right) q' = 0 \qquad\qquad A_b = \frac{R_b T_b \omega_b}{Cp_b P_b}$$

Index "*b*" indicates basic-state fields, in the vicinity of which tangent-linear calculations are done. The primed variables indicate the perturbations transported by the tangent-linear model. *U*, *V*, *u*, *v* indicate wind variables, *T* temperature, *q* specific humidity, *P* and *p* pressure.

If we consider only the important terms related to R_v and R_d, these equations could then read:

$$u'(t+1) = -\partial_x\ln(P_b)\cdot T_b(R_v - R_d)q'(t) + u'(t) + \ldots$$

$$v'(t+1) = -\partial_y\ln(P_b)\cdot T_b(R_v - R_d)q'(t) + v'(t) + \ldots$$

$$T'(t+1) = A_b[(R_v - R_d)/R_b - (Cp_v - Cp_d)/Cp_b]q'(t) + T'(t) + \ldots$$

$$q'(t+1) = q'(t) + \ldots$$

The adjoint equation for specific humidity could then read:

$$q^{ad}(t+1) = -\partial_x\ln(P_b)\cdot T_b(R_v - R_d)\cdot u^{ad}(t) - \partial_y\ln(P_b)\cdot T_b(R_v - R_d)\cdot v^{ad}(t) + A_b[(R_v - R_d)/R_b - (Cp_v - Cp_d)/Cp_b]\cdot T^{ad}(t) + q^{ad}(t) + \ldots$$

In this adjoint equation, it is clear that specific humidity (*q*) will be modified to fit wind and temperature observations, unless R_v and R_d are kept identical. The suggested trick of setting artificially R_v to R_d in the TL and AD models was very efficient in reducing problems, as illustrated by the above figures. But that is not a long-term solution, since not scientifically based.

Setting "R_v=R_d" everywhere may be not necessary and even detrimental, since :

- useless for observation operators,
- dangerous in equations for *T*, because of the balance with (Cp_v-Cp_d),
- *q* is perhaps not the only control variable concerned.

6. Conclusion and discussion

The incremental approach proposed by Courtier et al. (1994) reduces the computational cost of the original 4d-var algorithm. An approximation of the solution is found iteratively by solving several quadratic cost functions, approximations of the original one obtained by linearization of the model and the observation operators at lower spectral truncations. The solutions at low resolution are used as a correction to update the initial state at high resolution. The constant term of the linearization represents the model equivalent at observation points and is always computed at full resolution. In this way nonlinearities are taken into account indirectly.

At low resolution, the tangent-linear version of the model is used to transport the errors (instantaneous increments) along the assimilation window. This linearized version of the model must take into account not only the dynamic, but the physics as well.

However, physical processes such as condensation, convection, vertical diffusion, gravity wave drag, etc ... , are highly nonlinear and often discontinuous with threshold effects, which may cause serious convergence problems in the minimization. As a consequence, in the incremental 4d-var framework, the errors (increments) are transported by a tangent-linear model including a linearization of a regular simplified physics package.

The operational 4d-var at Météo-France uses a multiple-truncation incremental approach consisting in doing three minimizations at different truncations (T42, T63 and T95, the forecast model being run at resolution T199 with stretching).

Some problems of unrealistic precipitation over Sahara, which were already present in the 3d-var ARPEGE version, are amplified with the 4d-var implementation. This paper tried to understand this problem in the framework of incremental 4d-var.

Several 4d-var assimilation suites were run over a period of 10 days (June 2000) corresponding to overestimated precipitations in the operations. An individual remarkable case (April 24th, 2001) in a temperate area (Spain) is also studied. The main results may be synthesized as follows:

- When using a tangent-linear model with and without (adiabatic mode) linearized simplified physics, the problem remains the same. This does not mean, however, that there is nothing to do (perhaps to tune) in the simplified physics.
- Applying or not semi-external digital filtering has the same neutral effect.
- When performing a multiple-truncation incremental 4d-var in which the three resolutions are the same and equal to the higher one (T95), 24-h cumulated precipitations over Sahara area are reduced by a non negligible factor.
- Sensitivity experiments, executed with no specific humidity in the cost function, revealed the presence of a non-zero gradient with respect to specific humidity.

As a first conclusion, we can suppose that the multi-incremental approach has a relatively bad impact over tropical areas. In the concept of this approach, a lot of combined factors are present and could explain this fact :

- The hypothesis saying that large scales force the shorter ones could be not valid at the vicinity of the tropics.
- There is a large difference between the resolution of the direct full model, used to compute the model equivalent observations, and the minimization resolutions.
- Some physical processes (related to humidity) are not taken into account in the tangent linear model. Theses processes, if present, could compensate some bad features of the multivariate implicit aspect of 4d-var.
- There exist situations where the 4d-var minimization finds it easier to fit height (or wind) data through a change of specific humidity than through a change of temperature, even if specific humidity change has to be substantial in magnitude to achieve this goal.

To avoid this bad 4d-var behaviour, several solutions may be suggested :

- Enriching observation information by more and more humidity data. This will constraint the implicit adjustment done during minimizations to be more consistent. The humidity increments could then remain close to the reality.
- Background structure-functions must be tuned so that more reliability still given to the guess information, at least over poor regions in term of observations.
- Using more complete regular physics for TL/AD models. This will compensate certainly the bad features of multivariate implicit aspect.
- Specific humidity increments could be constrained to remain realistic by imposing analytic or statistic relationships between errors for humidity and for the other variables.
- Using artificial compensating extra terms to weaken the gradients calculated with respect to specific humidity, during the minimization process.
- Taking into account second order terms neglected in the TL/AD formulation. Theses terms could be non negligible in a context when TL/AD are used on longer assimilation windows (Tanguay et al., 1996), and especially when the atmospheric situation is highly baroclinic.

References.

Courtier, P., J.-N. Thépaut, and A. Hollingsworth, 1994 : A strategy for operational implementation of 4D-Var, using an incremental approach. *Quart. J. Roy. Meteor. Soc.*, **120**, 1367-1387.

Gauthier, P. and J.-N. Thépaut, 2001 : Impact of the digital filter as a weak constraint in the preoperational 4D-Var assimilation system of Météo-France. *Mon. Wea. Rev.*, **129**, 2089-2102.

Janiskova, M., J.-N. Thépaut and J.-F. Geleyn, 1999 : Simplified and regular physical parameterisations for incremental four-dimensional variational assimilation. *Mon. Wea. Rev.*, **127**, 26-45.

Jarvinen, H. , J.-N. Thépaut, P. Courtier, 1996 : Quasi-continuous variational data assimilation. *Quart. J. Roy. Meteor. Soc.*, **122**, 515-534.

Tanguay, M., P. Bartello and P. Gauthier, 1996 : Four-dimensional data assimilation with a wide range of scales. *Tellus*, **47A**, 974-997.

Thépaut, J.N., P. Caille, V. Cassé, J.-F. Geleyn, P. Hautie, M. Janiskova, P. Moll, J. Pailleux, F. Taillefer, F. Veersé, 1997 : 4D-Var developments at Météo-France. In *Proceedings of ECMWF workshop on non-linear aspects of data assimilation*. ECMWF, Reading, 9-11 September 1996, 469-491.

Rabier, F., E. Andersson, J. Haseler, P. Unden, P. Courtier, G. Kelly, D. Vasiljevic, C. Brankovic, C. Cardinali, C. Gaffard, A. Hollingsworth, C. Jakob, P. Janssen, E. Klinker, A. Lanzinger, M. Miller, A. Simmons, B. Strauss, J.-N. Thépaut, P. Viterbo, 1998: The ECMWF implementation of three-dimensional variational assimilation (3D-Var). III: Experimental results. *Quart. J. Roy. Meteor. Soc.*, **124**, 1831-1860.

Veersé, F. and J.-N. Thépaut, 1998 : Multiple-truncation incremental approach for four-dimensional variational data assimilation. *Quart. J. Roy. Meteor. Soc.*, **124**, 1889-1908.

PAPER II

Radi Ajjaji

Introduction

In this paper, a detailed theoretical study is made to determine the exact terms in the tangent-linear model (TL) and its adjoint (AD) which are responsible of the mutual influence existing between prognostic and diagnostic model variables in a four-dimensional variational analysis. These terms are then quantified in experimental investigations aiming at the determination of the synoptic ingredients responsible for some abnormal features like the over/under-estimation of specific humidity increments.

The first section is dedicated to the nonlinear, tangent-linear and adjoint theoretical formulations. The second interprets some experimental investigations performed with complete and partial sets of observations and tries to link the interpretations to the expressions found for the above-mentioned terms.

1. Eulerian tangent-linear formulation of the primitive model equations

To understand the multi-variate effects in a 4d-var assimilation system, which uses the model dynamics and physics as information sources (among others) to find the best linear unbiased estimate (BLUE), the hydrostatic primitive equations of ARPEGE/IFS are described in a humid adiabatic context. Then a linearized form of these equations at the vicinity of a basic nonlinear model state is presented; this will underline the different terms that govern the behaviour and magnitude of the gradients of the different control variables. This will show, in particular, the terms influencing the specific humidity adjoint calculations.

The framework is assumed as Cartesian. This greatly simplifies the form of horizontal spatial operators (as e.g. horizontal derivatives). But, this does not change at all the essence of all the features discussed in this paper, compared to the way they appear in the real (non Cartesian) model. The vertical coordinate is the same as in the numerical model; it is the hybrid pressure coordinate η ($\eta \in [0,1]$), which is defined implicitly from two (arbitrary) functions A and B by :

$$P(x, y, \eta, t)=A(\eta)\, P_{00} +B(\eta)\, P_s(x, y, t)$$

where P is the hydrostatic pressure and P_s the surface hydrostatic pressure. The following boundary conditions are imposed for A and B :

$$A(0)=B(0)=A(1)\ B(1)=1.$$

1.1 The nonlinear system equations

Two versions of the equations are used for the dynamics in ARPEGE/IFS : the Eulerian version and the semi-Lagrangian one. All the experiments described below are achieved in a 4d-var setup using Eulerian formulation both for trajectory and TL/AD integrations. That's why all the equations are expressed in Eulerian form.

The Cartesian humid adiabatic system for Eulerian 3d rotating atmosphere directly reflects the corresponding nonlinear equations in the numerical model :

$$\frac{\partial \vec{u}}{\partial t} = -\vec{u}\cdot\vec{\nabla}\vec{u} - \dot{\eta}\frac{\partial \vec{u}}{\partial \eta} + 2\vec{\Omega}\times\vec{u} - RT\vec{\nabla}(\ln(P)) - \vec{\nabla}\phi$$

$$\frac{\partial T}{\partial t} = -\vec{u}\cdot\vec{\nabla}T - \dot{\eta}\frac{\partial T}{\partial \eta} + \frac{R}{C_p}T\frac{\omega}{P}$$

$$\frac{\partial q}{\partial t} = -\vec{u}\cdot\vec{\nabla}q - \dot{\eta}\frac{\partial q}{\partial \eta}$$

$$\frac{\partial P_s}{\partial t} = -\vec{\nabla}\cdot\int_0^1 \frac{\partial P}{\partial \eta}\vec{u}\,d\eta$$

where T is the temperature, the vector Ω represents the earth rotation, $\vec{u}$ the horizontal wind vector, ϕ the geopotential, q the specific humidity, R the air perfect-gas constant and Cp the specific heat at constant pressure. "∇ " and "$\nabla\cdot$" stand respectively for the horizontal gradient and divergence operators.

We have also the following diagnostic relationships :

$$\phi = \phi_s + \int_\eta^1 \frac{RT}{P}\frac{\partial P}{\partial \eta}d\eta$$

$$\frac{\partial}{\partial t}\left(\frac{\partial P}{\partial \eta}\right) + \vec{\nabla}\cdot\left(\vec{u}\frac{\partial P}{\partial \eta}\right) + \frac{\partial}{\partial \eta}\left(\dot{\eta}\frac{\partial P}{\partial \eta}\right) = 0$$

$$\frac{\partial P}{\partial \eta}\dot{\eta} = \mathrm{B}(\eta)\int_0^1 \vec{\nabla}\cdot\left(\frac{\partial P}{\partial \eta}\vec{u}\right)d\eta - \int_\eta^1 \vec{\nabla}\cdot\left(\frac{\partial P}{\partial \eta}\vec{u}\right)d\eta$$

$$\omega = \vec{u}\cdot\vec{\nabla}(P) - \int_0^\eta \vec{\nabla}\cdot\left(\frac{\partial P}{\partial \eta}\vec{u}\right)d\eta$$

The first one can be obtained by vertical integration of the hydrostatic equation; the second one is a form of the continuity equation, while the two last ones are obtained by vertical integration of the surface pressure equation.

The pressure-force term in the momentum equation " $RT\nabla\ln(P)+\nabla\phi$ " includes a contribution due to the horizontal pressure gradient and another one given by the geopotential gradient. This term is very important in the discussions below. It depends on almost all the prognostic variables (q via the air perfect-gas constant $R=(1-q)R_d + qR_v$ where R_v and R_d are respectively the water vapour and the dry air constants, T, P and P_s), it implies a vertical integration and an horizontal pressure gradient. It constitutes a dynamic term allowing multi-variate mutual influences for these fields. It will be studied in details when formulating its linearized expression.

Another important term, with a similar impact, is the conversion term which appears in the thermodynamic equation "$RT/C_p\cdot\omega/P$". R and $Cp = (1-q)Cp_d + qCp_v$ (where Cp_d and Cp_v are the specific-heat constants for dry air and water vapour respectively) depend both on specific humidity;

ω is a diagnostic function of wind components and pressure. It appears, then, that this term is also responsible for mutual influence between variables during a 4d-var assimilation process.

The other terms which are mainly the horizontal and vertical advections and Coriolis force play also the same role, but in a less important way.

1.2 Linearized form of the primitive Eulerian hydrostatic equations.

There can be several different forms for the linearized versions of the unique original hydrostatic primitive adiabatic system. This comes from the fact that the basic state can be chosen in several ways. In the context of 4d-var analysis, the linearization is done in the vicinity of a basic state called "trajectory" obtained by integrating the nonlinear model in parallel with its linear integration. This linearization integration is then called the tangent-linear one.

When linearizing model equations, one assumes that all terms implying the products of perturbations are very small, and then could be neglected. This is correct only if the time integration is short and the model trajectory doesn't cover a rapid baroclinic atmospheric situation.

The prognostic variables used in the TL/AD versions of the forward nonlinear model are the perturbations u', T', q' and P_s' of momentum, temperature, specific humidity and surface pressure.

The linearized equations will be written in a form implying only these variables; the diagnostic parameters such as ϕ, ω and ψ will be linearized first, and expressed using the prognostic perturbations.

The RT term which depends on both temperature and specific humidity will be considered as one variable renamed Z. We have : $Z'=(R_v - R_d)Tq'+RT'$

The nonlinear hydrostatic equation takes the expression $\partial_\eta \phi = Z \cdot \partial_\eta \ln(P)$, with horizontal gradient :

$$\frac{\partial}{\partial \eta}\left(\vec{\nabla}\phi\right) = Z\frac{\partial}{\partial \eta}\left(\vec{\nabla}\ln(P)\right) + \vec{\nabla}Z\frac{\partial \ln(P)}{\partial \eta}$$

The linearized form of this equation is then :

$$\frac{\partial}{\partial \eta}\left(\vec{\nabla}\phi'\right) = \left[\frac{\partial}{\partial \eta}\left(\vec{\nabla}(\ln P)\right) + \frac{\partial \ln(P)}{\partial \eta}\vec{\nabla}\right]Z' + \left[\vec{\nabla}Z + Z\vec{\nabla}\right]\frac{\partial}{\partial \eta}\left(\frac{P'}{P}\right)$$

The only boundary-condition required for integrating vertically this equation is the horizontal gradient of the surface-geopotential perturbation which is assumed to be zero. This leads to :

$$\vec{\nabla}\phi' = \int_\eta^1 \left[\frac{\partial}{\partial \eta}\left(\vec{\nabla}(\ln P)\right) + \frac{\partial \ln(P)}{\partial \eta}\vec{\nabla}\right]Z' d\eta + \int_\eta^1 \left[\vec{\nabla}Z + Z\vec{\nabla}\right]\frac{\partial}{\partial \eta}\left(\frac{P'}{P}\right)d\eta$$

On the other hand, if we assume : $\partial_\eta P = m$, then : $m' = \partial_\eta P'$. The linearized expression of $\dot{\eta}$ is a function of $\vec{u}'$ and P'. After this change of variable, it reads :

$$\dot{\eta}' = -\frac{\dot{\eta}}{m}m' + \frac{B(\eta)}{m}\int_0^1 \vec{\nabla}\cdot(m'\vec{u})d\eta - \frac{1}{m}\int_\eta^1 \vec{\nabla}\cdot(m'\vec{u})d\eta + \frac{B(\eta)}{m}\int_0^1 \vec{\nabla}\cdot(m\vec{u}')d\eta - \frac{1}{m}\int_\eta^1 \vec{\nabla}\cdot(m\vec{u}')d\eta$$

The linearized momentum equation can then read :

$$\frac{\partial \vec{u}'}{\partial t} = \left[-\vec{u}' \cdot \vec{\nabla}\vec{u} - \vec{u} \cdot \vec{\nabla}\vec{u}' - \dot{\eta}\frac{\partial \vec{u}'}{\partial \eta} + 2\vec{\Omega}\times\vec{u}' - \frac{1}{m}\frac{\partial \vec{u}}{\partial \eta}\mathrm{B}(\eta)\int_0^1 \vec{\nabla}\cdot(m\vec{u}')d\eta + \frac{1}{m}\frac{\partial \vec{u}}{\partial \eta}\int_\eta^1 \vec{\nabla}\cdot(m\vec{u}')d\eta \right] +$$
$$\left[-\mathrm{Z}\vec{\nabla}\left(\frac{P'}{P}\right) - \int_\eta^1 (\vec{\nabla}\mathrm{Z} + \mathrm{Z}\vec{\nabla})\frac{\partial}{\partial \eta}\left(\frac{P'}{P}\right)d\eta - \frac{1}{m}\frac{\partial \vec{u}}{\partial \eta}\mathrm{B}(\eta)\int_0^1 \vec{\nabla}\cdot(m'\vec{u})d\eta + \frac{1}{m}\frac{\partial \vec{u}}{\partial \eta}\int_\eta^1 \vec{\nabla}\cdot(m'\vec{u})d\eta \right] +$$
$$\left[-\int_\eta^1 \left(\vec{\nabla}(\ln P) + \frac{\partial \ln P}{\partial \eta}\vec{\nabla} \right)\mathrm{Z}'d\eta - \mathrm{Z}'\vec{\nabla}(\ln P) \right]$$

The last term includes contributions of both q' and T'. It is equal to the following expression :

$$(R_v - R_d)\left[-\int_\eta^1 \left(\vec{\nabla}(\ln P) + \frac{\partial \ln P}{\partial \eta}\vec{\nabla} \right)(Tq')d\eta - T\vec{\nabla}(\ln P)\cdot q' \right] +$$
$$\left[-\int_\eta^1 \left(\vec{\nabla}(\ln P) + \frac{\partial \ln P}{\partial \eta}\vec{\nabla} \right)(RT')d\eta - R\vec{\nabla}(\ln P)\cdot T' \right]$$

This form shows a linear evolution of $\vec{u}'$ depending on $\vec{u}'$, P', T' and q' as :

$$\frac{\partial \vec{u}'}{\partial t} = A_{\vec{u}}\vec{u}' + \vec{B}_{\vec{u}}T' + \vec{C}_{\vec{u}}q' + \vec{D}_{\vec{u}}P'$$

The linearized thermodynamic equation reads :

$$\frac{\partial T'}{\partial t} = \left[-\vec{u}'\cdot\vec{\nabla}T + \frac{\mathrm{Z}}{PCp}(\vec{\nabla}P)\cdot\vec{u}' - \frac{\mathrm{Z}}{PCp}\int_0^\eta \vec{\nabla}\cdot\left(\frac{\partial P}{\partial \eta}\vec{u}'\right)d\eta - \frac{\partial T}{\partial \eta}\frac{1}{m}\mathrm{B}(\eta)\int_0^1 \vec{\nabla}\cdot(m\vec{u}')d\eta + \frac{1}{m}\frac{\partial T}{\partial \eta}\int_\eta^1 \vec{\nabla}\cdot(m\vec{u}')d\eta \right]$$
$$+\left[-\frac{\mathrm{Z}\omega}{P^2Cp}P' - \frac{\mathrm{Z}}{PCp}\int_0^\eta \vec{\nabla}\cdot\left(\frac{\partial P'}{\partial \eta}\vec{u}\right)d\eta + \frac{\mathrm{Z}}{PCp}(\vec{\nabla}P')\cdot\vec{u} - \frac{1}{m}\frac{\partial T}{\partial \eta}\mathrm{B}(\eta)\int_0^1 \vec{\nabla}\cdot(m'\vec{u})d\eta + \frac{1}{m}\frac{\partial T}{\partial \eta}\int_\eta^1 \vec{\nabla}\cdot(m'\vec{u})d\eta \right]$$
$$+\left[-\vec{u}\cdot\vec{\nabla}T' + \frac{\omega}{PCp}\mathrm{Z}' - \frac{\mathrm{Z}\omega}{PCp^2}C'p \right]$$

The last term in this equation could be divided in two parts depending respectively on q' alone and T' alone as :

$$\left[-\vec{u}\cdot\vec{\nabla}T' + \frac{\omega R}{PCp}T' \right] + \frac{RT\omega}{PCp}\left[\frac{R_v - R_d}{R} - \frac{Cp_v - Cp_d}{Cp} \right]\cdot q'$$

Thus the linear evolution of T' is expressed as :

$$\frac{\partial T'}{\partial t} = \vec{A}_T\vec{u}' + B_T T' + C_T q' + D_T P'$$

The linearized equation for specific humidity is simpler as it consists only in linearizing the corresponding horizontal and vertical advections terms :

$$\frac{\partial q'}{\partial t} = \left[-\vec{u}' \cdot \vec{\nabla} q - \frac{\partial q}{\partial \eta} \frac{1}{m} \mathrm{B}(\eta) \int_0^1 \vec{\nabla} \cdot (m\vec{u}') d\eta + \frac{1}{m} \frac{\partial q}{\partial \eta} \int_\eta^1 \vec{\nabla} \cdot (m\vec{u}') d\eta \right] - \left[\dot{\eta} \frac{\partial q'}{\partial \eta} + \vec{u} \cdot \vec{\nabla} q' \right]$$

$$+ \left[-\frac{1}{m} \frac{\partial q}{\partial \eta} \mathrm{B}(\eta) \int_0^1 \vec{\nabla} \cdot (m'\vec{u}) d\eta + \frac{1}{m} \frac{\partial q}{\partial \eta} \int_\eta^1 \vec{\nabla} \cdot (m'\vec{u}) d\eta \right]$$

This may be written as :

$$\frac{\partial q'}{\partial t} = \vec{A}_q \cdot \vec{u}' + 0 \cdot T' + C_q q' + D_q P'$$

Finally, the last equation to linearize is the evolution of the pressure field. The 3d-pressure perturbation may be deduced from the perturbation of surface pressure by : $P' = \mathrm{B}(\eta)\, P'_s$. The linearized form of the equation for pressure is then :

$$\frac{\partial P'}{\partial t} = -\mathrm{B}(\eta) \vec{\nabla} \cdot \int_0^1 \frac{\partial P'}{\partial \eta} \vec{u} d\eta - \mathrm{B}(\eta) \vec{\nabla} \cdot \int_0^1 \frac{\partial P}{\partial \eta} \vec{u}' d\eta = \vec{A}_P \vec{u}' + 0 \cdot T' + 0 \cdot q' + D_P P'$$

The following system summarises the four prognostic linearized equations :

$$\begin{pmatrix} \frac{\partial \vec{u}'}{\partial t} \\ \frac{\partial T'}{\partial t} \\ \frac{\partial q'}{\partial t} \\ \frac{\partial P'}{\partial t} \end{pmatrix} = \frac{\partial}{\partial t} \begin{pmatrix} \vec{u}' \\ T' \\ q' \\ P' \end{pmatrix} = \begin{pmatrix} A_{\vec{u}} & \vec{B}_{\vec{u}} & \vec{C}_{\vec{u}} & \vec{D}_{\vec{u}} \\ \vec{A}_T & B_T & C_T & D_T \\ \vec{A}_q & 0 & C_q & D_q \\ \vec{A}_P & 0 & 0 & D_P \end{pmatrix} \begin{pmatrix} \vec{u}' \\ T' \\ q' \\ P' \end{pmatrix}$$

By transposing the matrix appearing on the right-hand-side of this system, we obtain the adjoint form of the linearized equations.

$$-\frac{\partial}{\partial t} \begin{pmatrix} \vec{u}^{ad} \\ T^{ad} \\ q^{ad} \\ P^{ad} \end{pmatrix} = \begin{pmatrix} A_{\vec{u}} & \vec{A}_T & \vec{A}_q & \vec{A}_P \\ \vec{B}_{\vec{u}} & B_T & 0 & 0 \\ \vec{C}_{\vec{u}} & C_T & C_q & 0 \\ \vec{D}_{\vec{u}} & D_T & D_q & D_P \end{pmatrix} \begin{pmatrix} \vec{u}^{ad} \\ T^{ad} \\ q^{ad} \\ P^{ad} \end{pmatrix}$$

When neglecting the temporal time-step (or forcing it to one second - 1.-), the specific humidity

gradient is given by the following equation :

$$Grad(q)_{t-1} - Grad(q)_t = \vec{C}_{\vec{u}} \cdot Grad(\vec{u})_t + C_T \cdot Grad(T)_t + C_q \cdot Grad(q)_t$$

$$Grad(q)_{t-1} - Grad(q)_t = (R_v - R_d)\left[-\int_{\eta}^{1} \left(\vec{\nabla}(\ln P) + \frac{\partial \ln P}{\partial \eta} \vec{\nabla} \right)(T \bullet) d\eta - T\vec{\nabla}(\ln P) \cdot \bullet \right] \cdot Grad(\vec{u})_t$$

$$+ \frac{RT\omega}{PCp}\left[\frac{R_v - R_d}{R} - \frac{Cp_v - Cp_d}{Cp} \right] \cdot Grad(T)_t$$

$$+ \left[\dot{\eta} \frac{\partial \bullet}{\partial \eta} + \vec{u} \cdot \vec{\nabla} \bullet \right] \cdot Grad(q)_t$$

When we assume dry TL/AD integrations (and the same for the corresponding trajectory) by considering that $R = R_d$ (or $R_v = R_d$), we eliminate the impact of C_u and we simplify C_T.

In the ARPEGE/IFS setups, Cp_v and Cp_d are set as :

$Cp_v = 4.\ R_v$ and $Cp_d = 3.5\ R_d$.

Then,

$Cp_v = 8./7.\ Cp_d$ and $Cp = (7.+q)/2.\ R = (7.+q)/7.\ Cp_d$,

$R/Cp = 2./(7.+q) \approx 2./7.$ and $(Cp_v - Cp_d)/Cp = 1/(7.+q) \approx 1./7.$,

so that :

$RT/C_p \cdot \omega / P \cdot [\ (R_v - R_d)/R - (Cp_v - Cp_d)/Cp]$ is reduced to : $-2.T\omega / P / (7.+q)^2 \approx -2./49.\ T\omega / P$.

But, when we put $R_v = R_d$ at the level of CVA1 (under key LDRYTL), the setups are already done. In this case :

$RT/C_p \cdot \omega / P \cdot [\ (R_v - R_d)/R - (Cp_v - Cp_d)/Cp]$ is reduced to $R_d\, T\omega / P \cdot (4.R_v - 3.5\ R_d)/[4.\ qR_v + 3.5\ (1-q)R_d]^2$.

The effect of C_T is still present but, due to its sign, it affects the specific humidity increments in the opposite way.

In the real case, where $R = (1-q)R_d + qR_v$ and $Cp = (1-q)\ Cp_d + qCp_v$ we have :

$$[(R_v - R_d)/R] \ / \ [(Cp_v - Cp_d)/Cp] \approx 0.725\ (1+0.23\ q) \approx 0.725$$

where q is considered to be dimensionless. That is, we have : $(R_v - P_\delta)/P \leq (Cp_v - Cp_d)/Cp$.

To have an idea about the trajectory parameters that contributes in the anomaly, we can compare the values of C_T before and after applying $R_v = R_d$. If we denote them $C_{T(bef)}$ and $C_{T(aft)}$ respectively, then at the beginning of the assimilation window we have :

$$C_{T(bef)} - C_{T(aft)} = (R_v - R_d) \cdot T\omega / P \cdot Cp_d / Cp^2 \approx (R_v - R_d) / Cp_d \cdot T\omega / P = 0.17\ T\omega / P$$

This difference is large in an atmosphere characterized by high temperatures, strong vertical motions, low pressures. This context is typical of highly baroclinic atmosphere.

The adjoint model integration is a backward one having as initial state the last tangent-linear forecasted perturbation on the assimilation window, transported to the observation space thanks to the observation operators, then normalized by the observation errors and returned back to the physical space by the adjoint of the observation operators, as could be seen on the analytical expression of the cost-function gradient :

$$\nabla J = (B^{-1} + \sum_{i=0}^{N} M'^{T} H'^{T} R_i^{-1} H' M') \cdot \delta x - \sum_{i=0}^{N} M'^{T} H'^{T} R_i^{-1} d_i$$

where B is the matrix of model error covariances, R_i the matrix of observation error covariances for time-slot "i", H' and M' the tangent-linear versions of the observation operator and the nonlinear model respectively (^{T} indicates the transposition of the matrixes), and d_i is the innovation vector.

The process of TL/AD integrations is iterated several times, but the trajectory is calculated only once. That means that the coefficients of the matrixes involved in the TL/AD models are computed once, whereas the perturbations δx are iterated several times as required by the minimizing process.

2. Experiments achieved to go further in the investigations of the specific humidity analysis anomaly for the situation of April 24th, 2001, at 18:00 UTC

2.1 Description of the experiments

The first experiments, described in Paper I, consisted in determining which observation types contributed the most to the anomaly. The aim was to identify minimum degrees of freedom in order to be able to interpret easily the difficult 4d-var assimilation processes involved in an experiment. This sensitivity study showed a great impact of AIREP and SYNOP types. Each of these two types is responsible for about 50% of the large negative specific humidity increments (Figs 2a-b and 5a).

More precisely a single SYNOP observation of surface geopotential at 18:00 UTC is found to be responsible for about 30% of the anomaly caused by all the SYNOPs. The corresponding station is an automatic one, identified as 08233, localized at [40.93°N,-1.30°W]. Two AIREPs, EU4593 and EU1456, are also concerned.

The experiments below will use this single SYNOP geopotential observation to diagnose the anomaly and to quantify the several terms involved in the computation of the specific-humidity increments. The strategy that will be followed consists in quantifying the magnitudes of each term (C_u, C_T, C_q), and then deduce in which context this problem could happen knowing the ingredients (in the trajectory or in the perturbations) that are responsible for the magnitude of the main term among these three.

This will lead to more visibility on the context causing this kind of anomaly. Thus, we could identify and handle efficiently the real cause of the problem.

2.2 Increments from a single observation : theoretical aspects

In case of a single observation, situated at time-slot $i > 0$, the incremental cost-function has the following form :

$$J(\delta x) = \tfrac{1}{2}\, \delta x^{T} B^{-1} \delta x + \tfrac{1}{2}\, (d_i - H' M'_{t0 \to ti} \delta x)^{T} R_i^{-1} (d_i - H' M'_{t0 \to ti} \delta x)$$

Here $d_i = D$ and $R_i^{-1} = \sigma_0^{-2}$ are reduced to scalar values.

The analysis increment δx_a is obtained for $\nabla J = 0$. After some rearrangements, and if we suppose that the observation is situated at the gridpoint corresponding to the mth element of the analysis vector, then it is expressed as :

$$\delta x_a = x_a(t_0) - x_b = \frac{y - x_a(t_i)_m}{\sigma_0^2} \begin{pmatrix} (BM^T_{t_0 \to t_i})_{1,m} \\ (BM^T_{t_0 \to t_i})_{2,m} \\ \dots \\ (BM^T_{t_0 \to t_i})_{N,m} \end{pmatrix}$$

It is now clear that the analysis increments at the beginning of the assimilation window are obtained from the normalized analysis increments at time-slot i, transported by the adjoint model to time-slot 0, and then normalized by the model errors.

This preliminary theoretical study shows that if one wants to analyse the behaviour of TL/AD in 4d-var in the context of a single observation, this later must not be situated at the beginning of the assimilation window. In this case only observation operators would act in the minimization, and the problem would be a 3d one.

In the experiments described here, the observation is situated at the middle of the assimilation window and the increments are evaluated and visualized at the beginning of this window. Let's remember that the abnormal drying introduced by the operational analysis in this situation concerns all the time-slots between 15:00 and 21:00 UTC.

If we analyse the increments at the middle of the window, their expression is given by :

$$M_{t_0 \to t_i} \delta x_a = \frac{y - x_a(t_i)_m}{\sigma_0^2} \begin{pmatrix} (M_{t_0 \to t_i} BM^T_{t_0 \to t_i})_{1,m} \\ (M_{t_0 \to t_i} BM^T_{t_0 \to t_i})_{2,m} \\ \dots \\ (M_{t_0 \to t_i} BM^T_{t_0 \to t_i})_{N,m} \end{pmatrix}$$

This case is similar to a 3d-var case, where the background cost-function (distance to the guess) implies the matrix MBM^T. It is then clear, that in presence of rapidly evolving atmospheric phenomena the model errors may be greatly amplified by the tangent-linear model. Thus, assimilation will rely more on the observation ingredient. This will be the only information governing the assimilation.

The absence of specific-humidity observations combined with the above-mentioned fact could lead to abnormal analysis structures.

2.3 Contribution of SYNOPs and AIREPs to the specific-humidity increments.

The parameters from SYNOPs used in the upperair analysis are 10-m wind and geopotential. The other surface parameters are not used. The observed surface-geopotential gives information on temperature and pressure via the observation operators. So, introducing a SYNOP geopotential is similar to using an observation of temperature and pressure. The signal on temperature is then converted to a specific-humidity increment by the strong multi-variate property of 4d-var (Fig. 5).

The parameters used from AIREP reports are horizontal wind and temperature. In this situation, AIREPs were very dense on Western Europe along the assimilation window, as shown on Fig. 1.

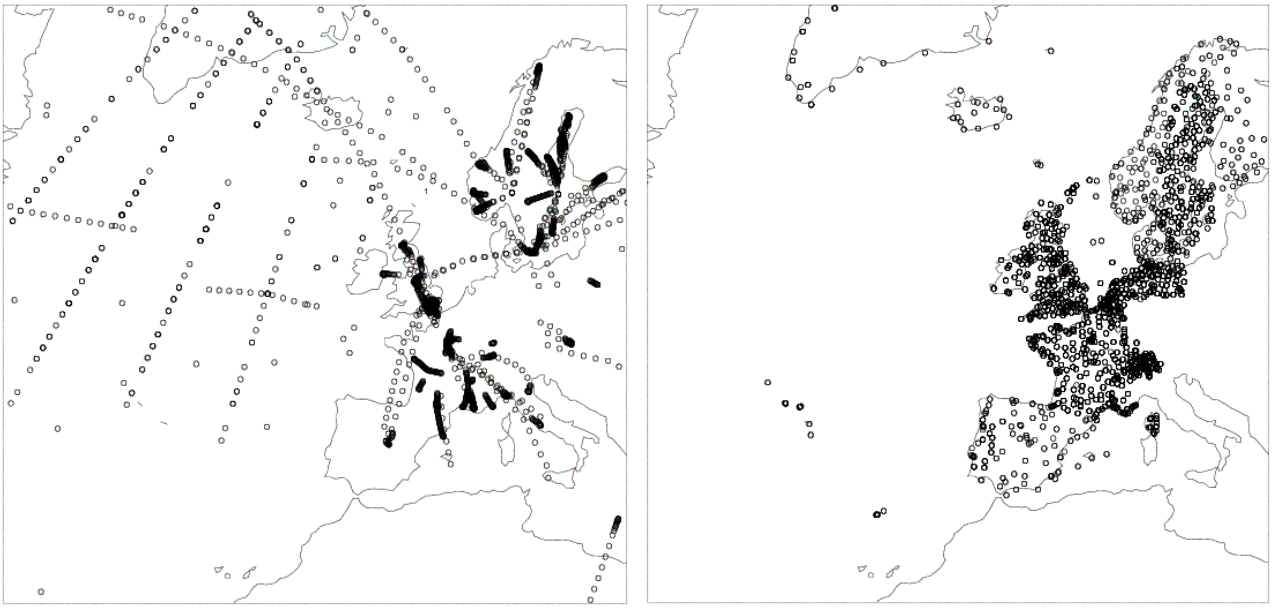

Figure 1 : Geographic localization of AIREPs (left) and SYNOPs (right) between 15:00 and 21:00 on April 24, 2001

2.4 Impact of AIREP reports on specific-humidity increments for April 24th, 2001, at 15:00

An experiment consisting in running 4d-var assimilation with only AIREP reports showed that this observation type contributed a lot in creating large specific-humidity increments (up to 15. 10^{-4}) along a band including the anomaly zone (Fig. 2a). AIREPs caused also another area of large specific-humidity increments (up to 13. 10^{-4}) North-East of the anomaly zone.

When combining TEMP and AIREP reports into one same experiment, the North-East part of the band of large specific-humidity increments disappears entirely. This fact is associated to the presence in this region of 3 TEMPs as shown in Fig. 3b. Let us remember that along the assimilation interval there is no TEMP reports in the entire anomaly area over Spain. TEMP reports are the only observation types informing on upperair humidity.

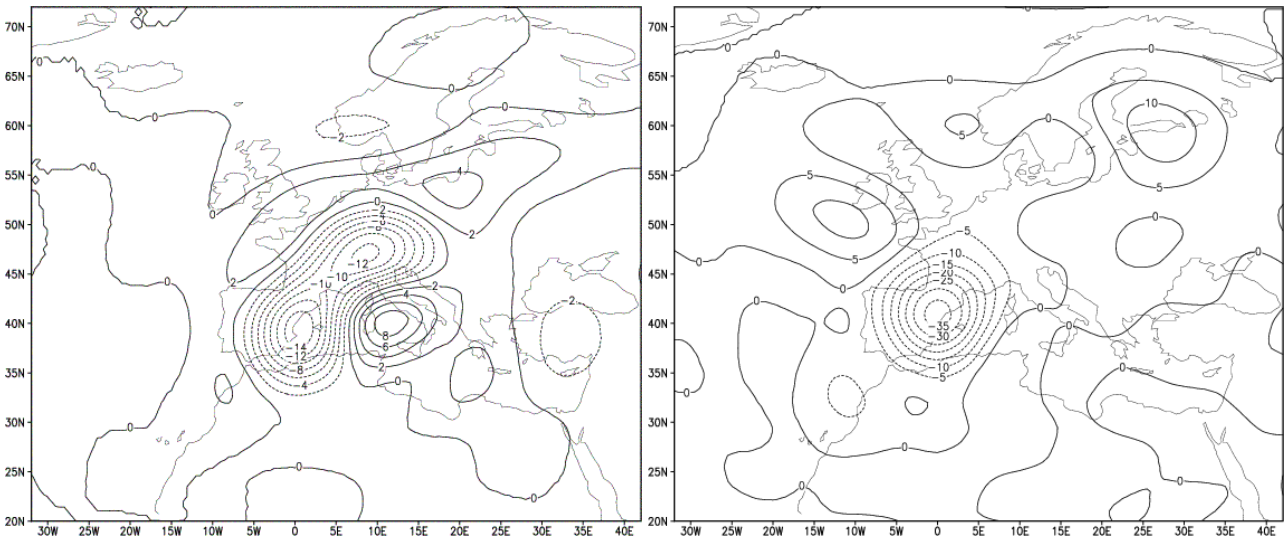

a b

Figure 2 : 850 hPa specific-humidity increments at 15:00 UTC, obtained using : a) AIREPs only b) a complete set of observation types. The values are multiplied by 10^4.

On the other hand, unexpectedly, the AIREP parameter associated to specific-humidity increments anomaly is not temperature, but wind (Figs 4a-b). As can be seen from the equations presented in part 1.2, the term acting here is $C_u^{\cdot}\ u^{ad}$.

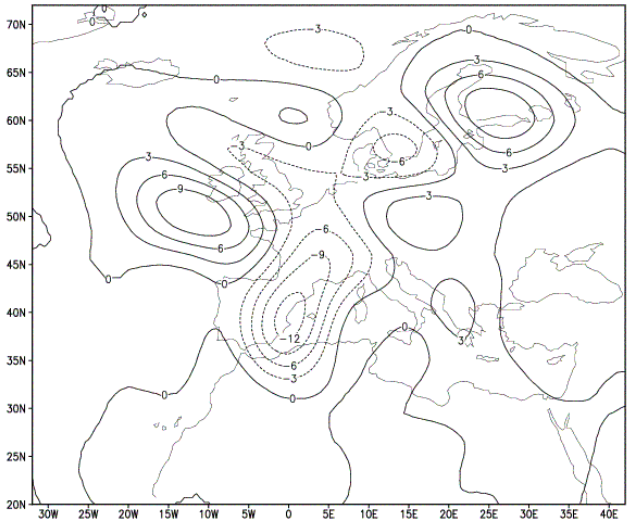

a

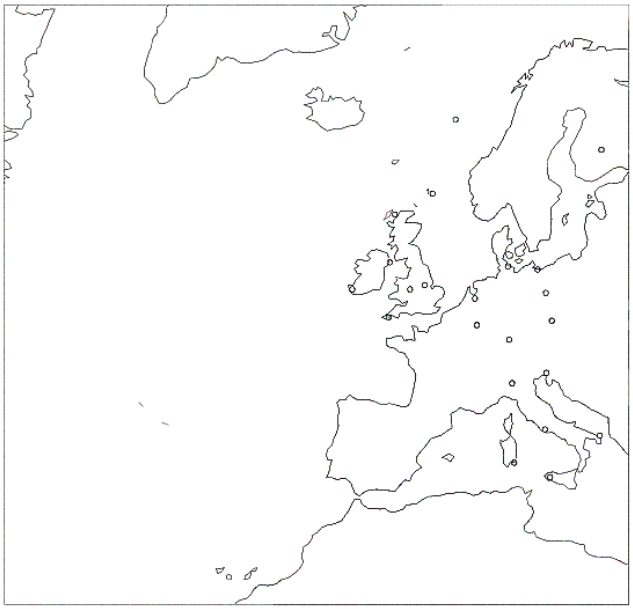

b

Figure 3a : Impact of AIREPs and TEMPs when used both in analysis. One can notice the disappearance of the band of large specific humidity increments on Southern Germany showed in Fig. 2a.

Figure 3b : The circles indicate the localization of the few TEMP reports available on Europe region along the assimilation window, between 15:00 and 18:00 UTC.

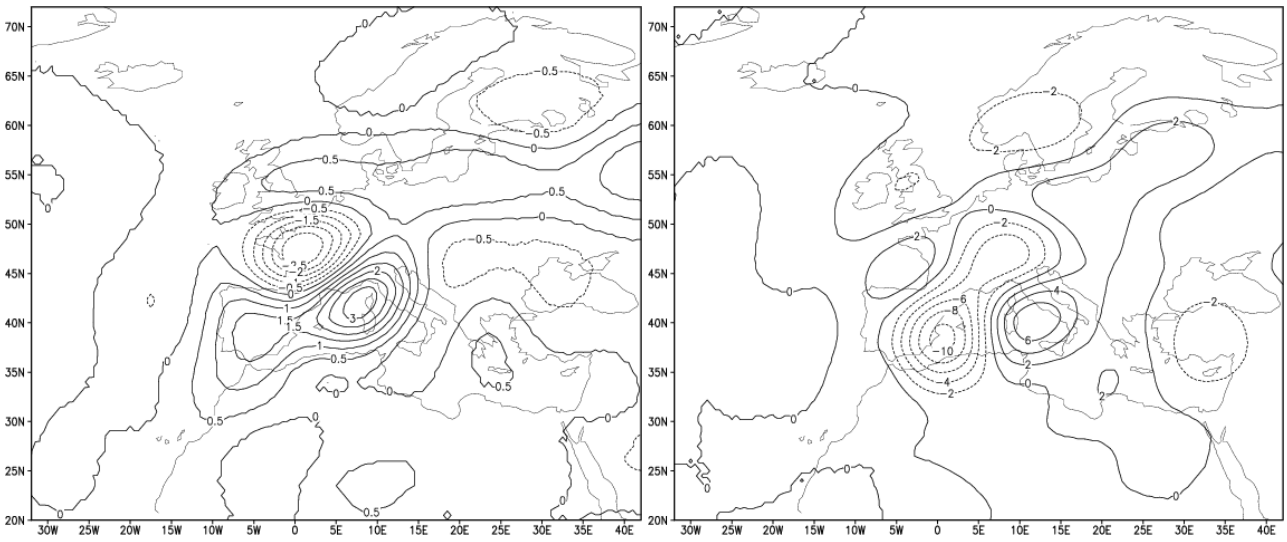

Figure 4 : Contribution of AIREP data to the anomaly : a) temperature, b) winds . The values are multiplied by 10^4 .

2.5 Impact of SYNOPs on specific-humidity increments for the situation of April 24th, 2001

An experiment consisting in using only SYNOPs in the cost function has been performed. As shown on Fig. 5a, the impact on specific-humidity increments is also large (about $15.\ 10^{-4}$) and corresponds to the anomaly zone. The parameter responsible for that is mainly the geopotential (by 99 %); 10-m wind has a far smaller impact (Fig. 5).

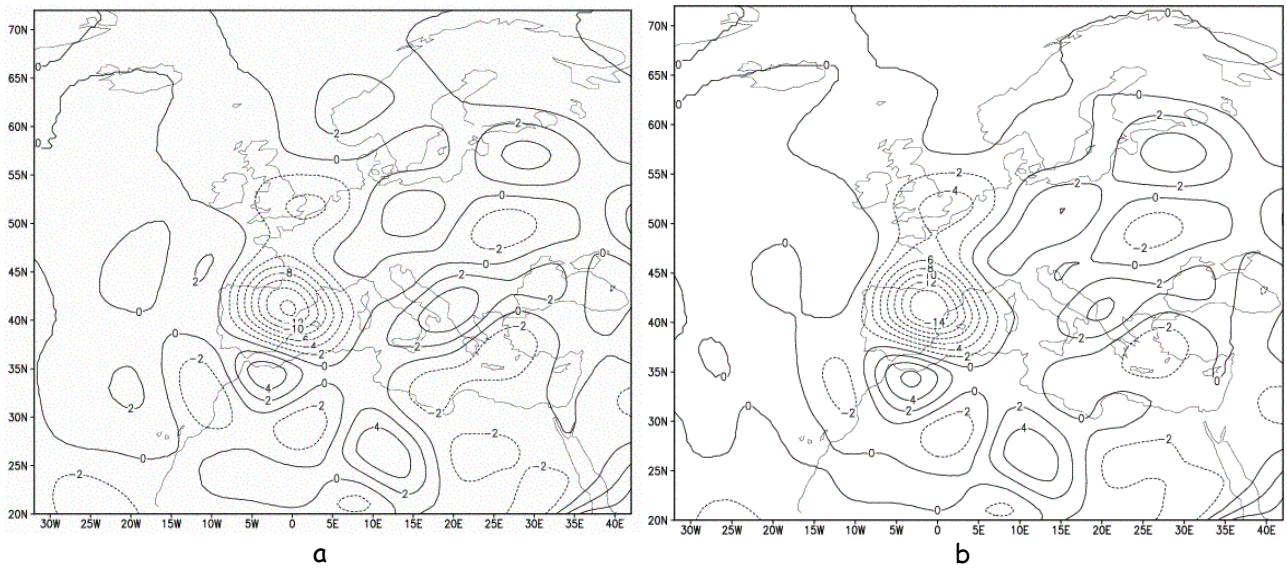

Figure 5 : Contribution of SYNOP information to the specific-humidity increments : a) all data, b) only geopotential data . The values are multiplied by 10^4. Fields at 850 hPa are shown, as for the the other plots of increments.

Since 10-m wind has a neutral effect on humidity analysis, and surface geopotential acts as an observation of temperature, the adjoint term that is involved in the amplification of humidity

increments here is mainly $C_T \cdot T^{ad}$.

These diagnostic experiments show that the anomaly is caused by two separate ingredients associated to AIREPs and SYNOPs. In the following, the impacts of single-observation experiments involving these two types are shown.

2.6 Impact of a single SYNOP geopotential observation on specific-humidity increments.

The following table gives the characteristics of the concerned SYNOP geopotential observation :

Identifier	Latitude	Longitude	Altitude	OMF	VAR	PPP
08233	40.93 °	-1.30 °	902 m	28.6	8845.6	91170.0

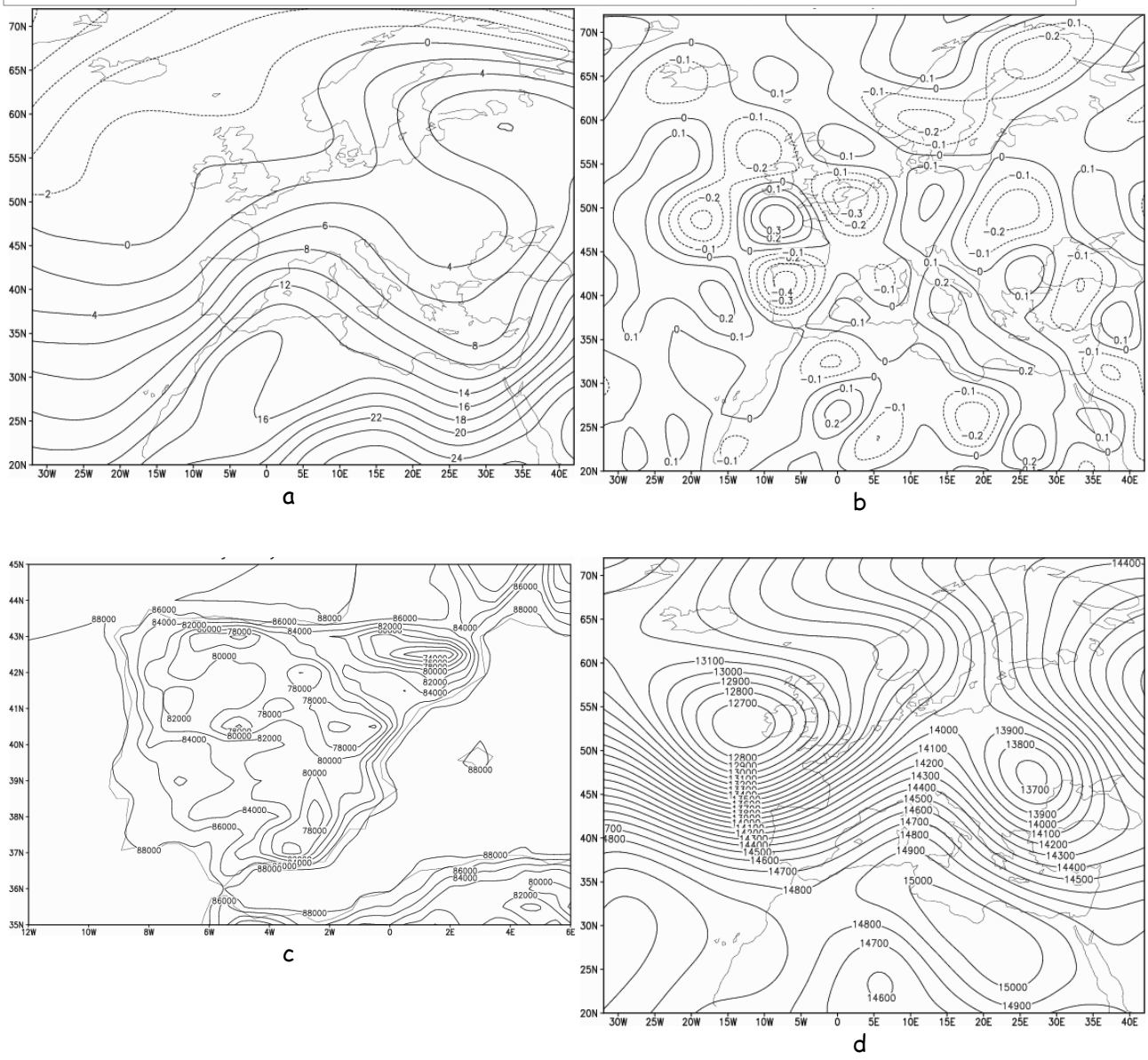

Figure 6 : Initial trajectory fields at 850 hPa for : a) temperature, b) vertical velocity, c) pressure, d) geopotential. These fields are the same in all experiments, they correspond to the guess fields at low resolution.

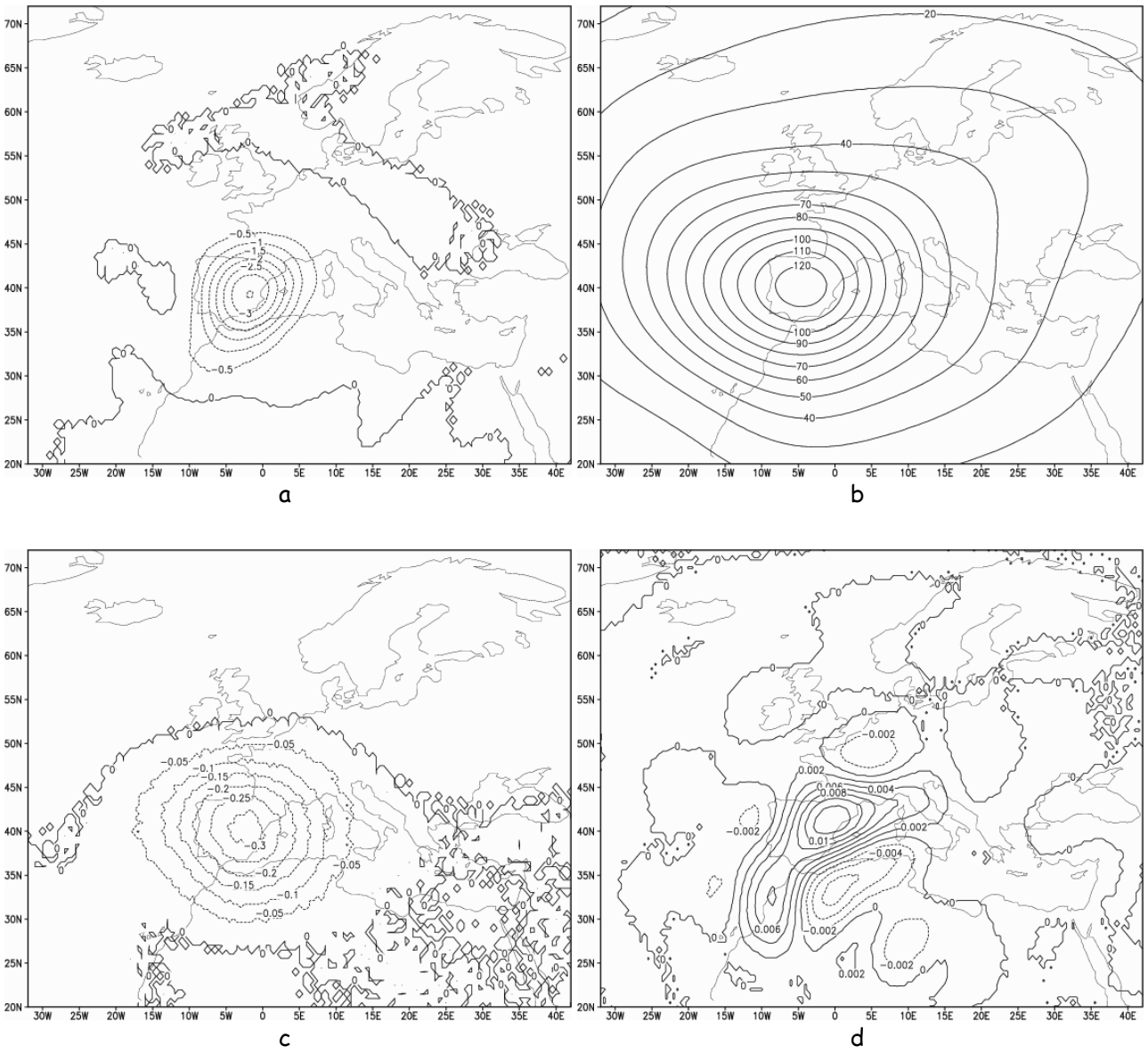

Figure 7 : Increments at 15:00 UTC caused by a single geopotential observation for : a) specific humidity, b) geopotential, c) temperature, d) vertical velocity, .

When looking at the vertical zonal and meridional slices of increments for the different prognostic variables, we realize that all the information comes from the surface (Fig. 8), indicating the vertical influence of a surface geopotential observation.

Figure 6a shows a temperature field with relatively large values in a thermal dorsal regime (values between 4°C and 14°C) over Spain, associated to large *"RT"* horizontal gradients (Fig. 9d), large geopotential gradients (Fig. 6d), relatively high vertical velocities (Fig. 6b) and low pressures (Fig. 6c).

As said in part 1.2, the trajectory quantity that contributes to the specific-humidity increments (when an observation informing on temperature is used) is mainly :

$$(R_v - R_d) / Cp_d \cdot T\omega / P = 0.17 \; T\omega / P$$

Figure 9c shows the corresponding field, demonstrating that when an atmospheric situation presents simultaneously the following 3 ingredients, specific humidity has a great probability to behave in an abnormal way over a region devoid of humidity observations :

1. High temperatures

2. Low pressures
3. Great vertical velocities

The representation of temperature, vertical velocity and pressure on Figs 6a-c show that these fields verify the above-mentioned conditions over Spain leading to a large difference in $C_{T(bef)} - X_{T(\alpha\phi\tau)} \approx 0.17 T\omega / P$. This term is represented in Fig. 9c and shows effectively absolute minima over the entire domain. The term $C_T \cdot Grad(T)$ gives a minimum over Spain corresponding very well to the anomaly area.

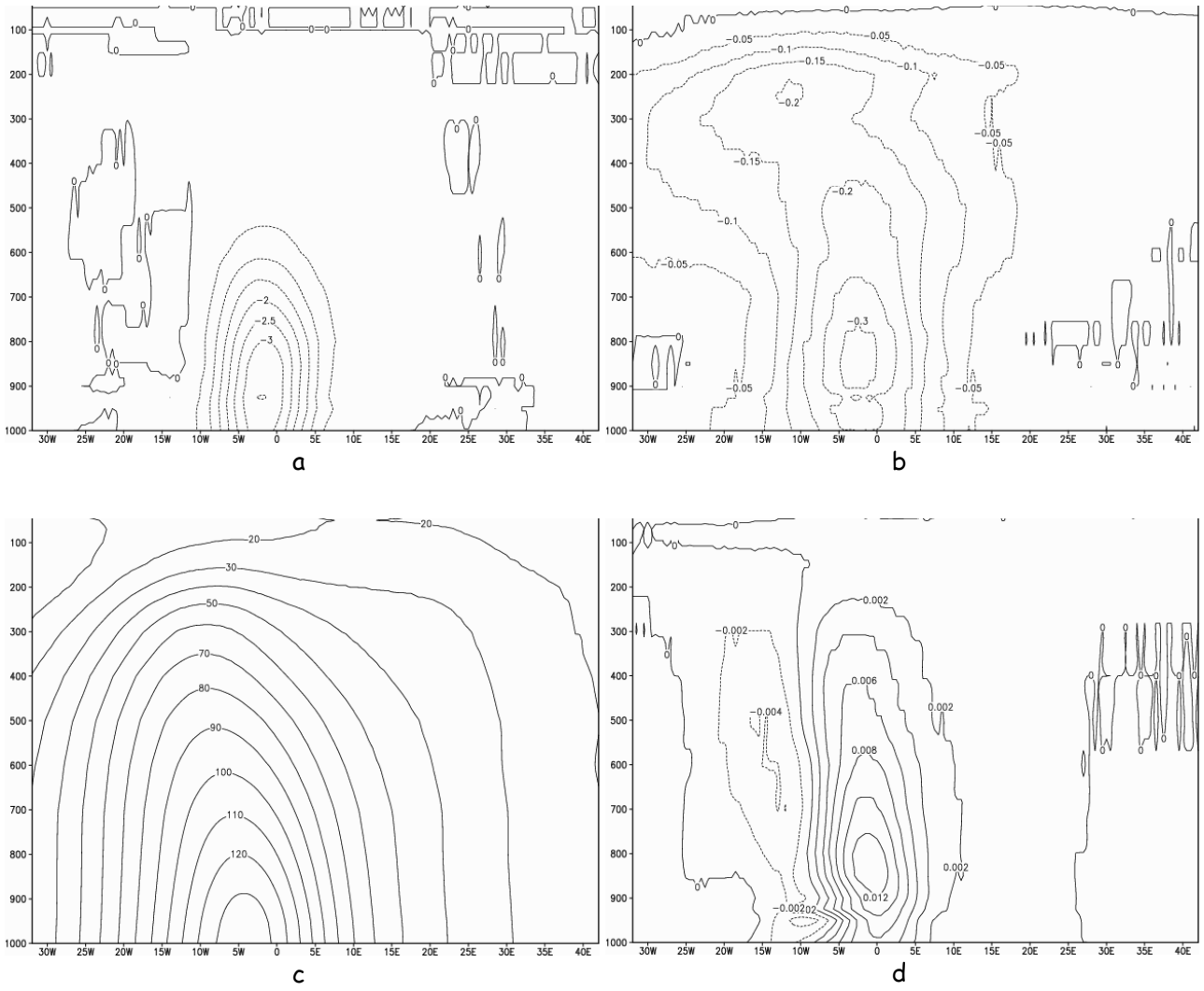

Figure 8 : Vertical slice on a zonal axis of increments at 15:00 UTC for : a) specific humidity, b) temperature, c) geopotential, d) vertical velocity .

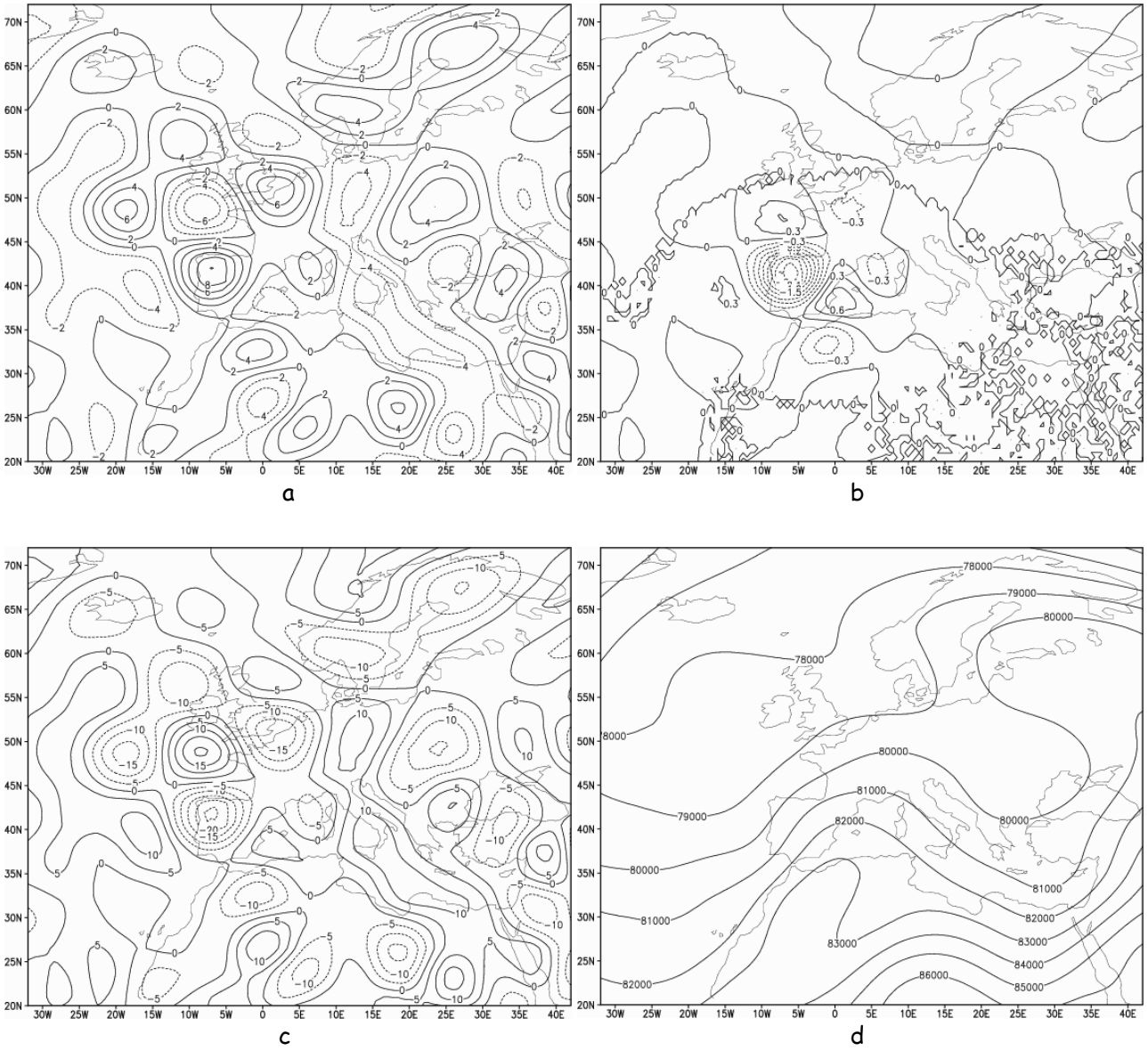

Figure 9 : Derived fields at 850 hPa and 15:00 UTC : a) C_T multiplied by 10^5 , b) $C_T \cdot Grad(T)$, c) $C_{T(bef)} - C_{T(aft)} \approx 0.17\ T\omega/P$, multiplied by 10^5, d) RT.

2.7 Impact of a single AIREP wind observation on specific-humidity increments.

The following table gives the characteristics of the concerned AIREP wind observation :

Identifier	Parameter	Latitude	Longitude	PPP	OMF	VAR
EU4593	U component	41.44	2.36	83369 Pa	0.09	8.64
	V component				-0.02	5.61

It is not possible to find one single AIREP wind contributing alone significantly to specific-humidity increments. All individual observations contribute in the same proportion. That is why the figures represented below (Fig. 10) show a little (but not negligible) effect of wind data from a single AIREP element. But if we use all the observations available in one AIREP report (as EU4593 or EU1456), the

effect is then visible and corresponds to the summation of all the individual effects of each elementary observation (Fig. 11). The term involved here is obviously :

$$(R_v - R_d)\left[-\int_{\eta}^{1}\left(\vec{\nabla}(\ln P)+\frac{\partial \ln P}{\partial \eta}\vec{\nabla}\right)(T\,\bullet)d\eta - T\vec{\nabla}(\ln P)\cdot\bullet\right]\cdot Grad(\vec{u})$$

The trajectory quantities governing its magnitude are the temperature and its horizontal gradient, the horizontal and vertical gradients of pressure. If we define the operator ν as :

$$\int_{\eta}^{1}\bullet\, d\eta = \nu\,.$$

then this term has the following form :

$$-(R_v - R_d)\left[(\nu+1)T\vec{\nabla}\ln P + \nu\frac{\partial \ln P}{\partial \eta}\vec{\nabla}T + \nu\frac{\partial \ln P}{\partial \eta}\vec{\nabla}\bullet\right]\cdot Grad(\vec{u})$$

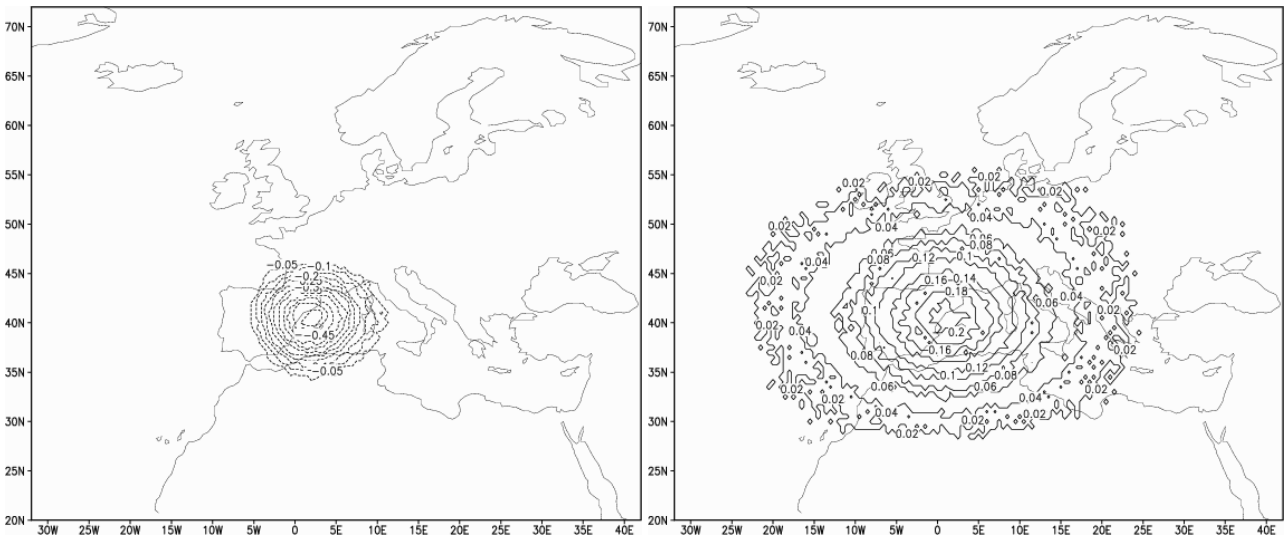

a b

d

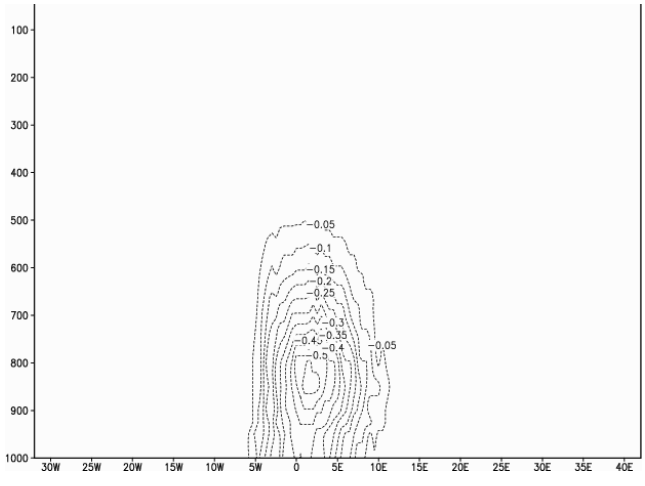

c

Figure 10 : (a) Specific-humidity increments at 850 hPa caused by one AIREP wind (the minimum is 6.10^{-5}), (b) corresponding temperature increments at 850 hPa, (c) vertical slice of specific-humidity

increments at latitude 37° N, (d) geopotential increments in the same environment.

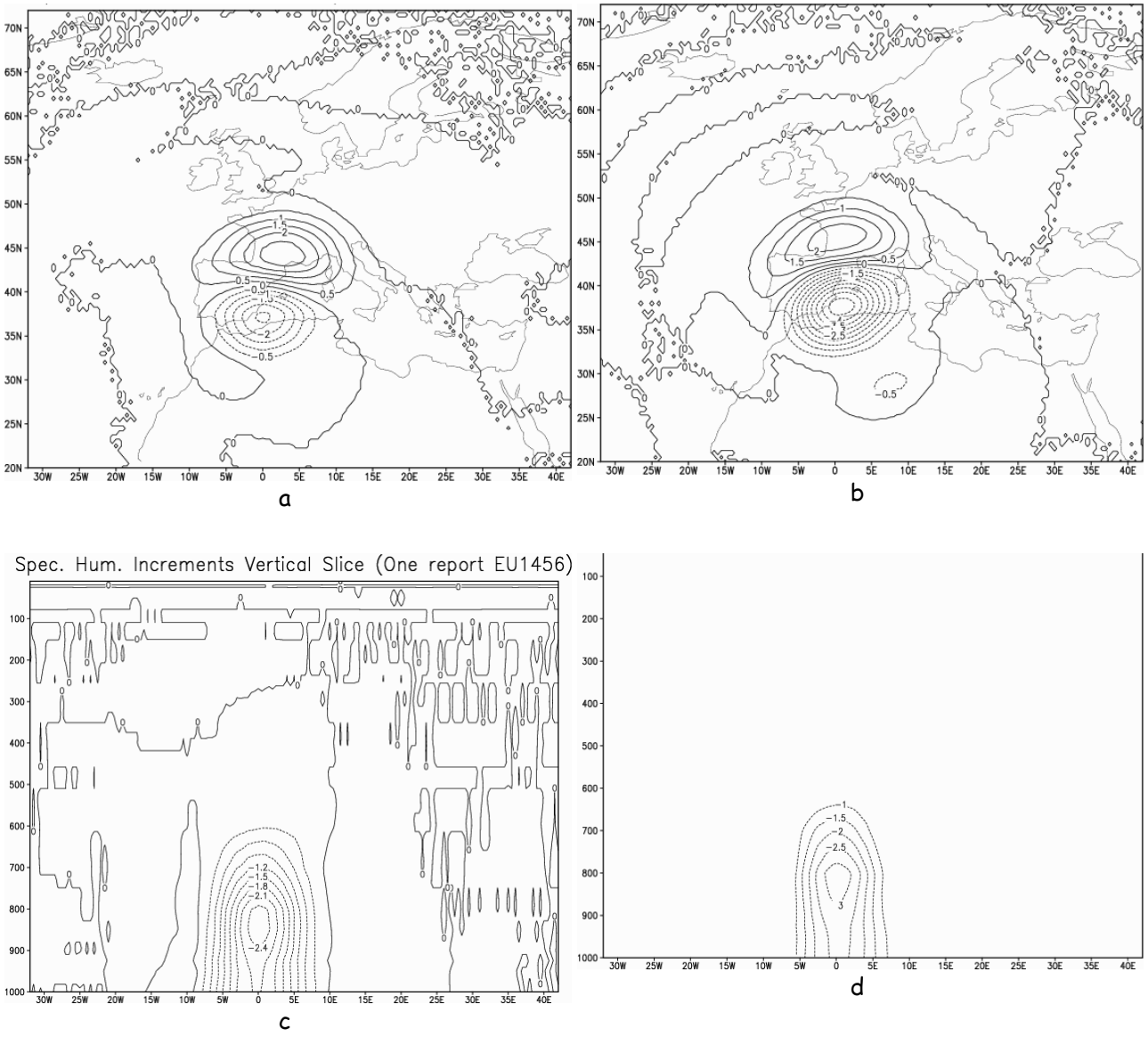

Figure 11 : Specific-humidity increments at 850 hPa caused by : a) EU1456 report and b) EU4593 report. (c) and (d) are the corresponding vertical slices.

3. Conclusion and discussion

One problem of the humidity analysis is the appearance, in a certain atmospheric context, of large analysis increments at the lowest model levels, over some subtropical land areas and also sometimes over temperate regions. These areas are characterized by high temperatures and dry conditions. Investigations done by Anderson et al., 1998, with ECMWF 3d-var, showed that these humidity increments were caused by geopotential observations rather than humidity data. Geopotential data can be fitted by changing both temperature and humidity. In the absence of any other data, the relative changes of humidity and temperature when fitting geopotential data are governed by the background-error standard deviations (of temperature and humidity). Anderson et al. concluded that there was a problem with the specification of humidity background-errors in hot and dry conditions. An easier but less correct solution would have been to disable the dependency on humidity of the geopotential observation operator.

This was a problem observed in 3d-var data assimilation. With 4d-var this problem is still present and

more complicated to diagnose, because in 4d-var the observation operators include in addition the forecast model. There can also be a great influence on the humidity analysis from surface pressure and upperair geopotential or temperature data, through at least the virtual-temperature effects of the pressure force (including its geopotential part and its pressure part), and the conversion term of the thermodynamic equation : in addition to the relations involved in observation operators.

Rabier et al., 1998, showed that 4d-var analyses are moister than 3d-var analyses, by up to 0.3 g/kg when zonally averaged along the equator. The interpretation given to this fact is that the effective background-error standard deviations are larger than for 3d-var, taking into account the fact that the implied background-error standard deviations are those which would be produced by a Kalman filter implemented over the assimilation window. Although this is one major advantage of 4d-var if the dynamics and simplified physics used in the tangent-linear and adjoint models are accurate, it could be a drawback if this simplified model is not a good approximation of the evolution of the atmosphere. Rabier et al. recommended then to work more and more on the physical parameterization part in the TL/AD, to avoid mismatches between the full nonlinear model and its tangent-linear and adjoint versions.

This recommendation is certainly very important, but efforts must also be done on the regularization of the adiabatic model because in some cases such as the one studied in this paper under some dynamical characteristics and over areas containing no humidity data, model nonlinearities lead to unrealistic increments.

In this study, investigations have been performed on a case of unrealistic specific-humidity analysis over Spain, which happened on April 24th, 2001. The experiments showed that the anomaly is due mainly to AIREP and SYNOP data. AIREPs act through their wind observations and SYNOPs act through their surface-geopotential (pressure) informations. The examination of the terms in the TL/AD formulations responsible for the contribution to these unrealistic increments revealed that AIREP and SYNOP data don't act in the same way, but through two different terms that could be zeroed by imposing dry adiabatic nonlinear and TL/AD models. These terms constitute a great strength of 4d-var allowing multi-variate effects and the use of dynamics as a new source of information to be combined to other ingredients in a data assimilation process. But, they could be very harmful if TL/AD assumption is not satisfie,d especially in presence of high nonlinearities which could be caused by a baroclinic atmosphere evolving rapidly during the assimilation window.

Single-observation experiments enforce this stipulation and indicate in a more comprehensible way the context favouring the occurrence of such phenomena.

The solution of such problem could be, besides the work on enriching data assimilation systems with informations on humidity, to regularize some terms in the nonlinear model in order to avoid the rapid development of nonlinearities, or to add some extra terms parameterizing the second order terms in the TL/AD formulations. This will be the next action to be achieved.

References.

Rabier, F., J.-N. Thépaut and P. Courtier, 1998a : Extended assimilation and forecast experiments with a four-dimensional variational assimilation system. *Q. J. R. Meteorol. Soc.*, **124** , 1861-1887.

Rabier, F., H. Jarvinen, E. Klinker, J.-F. Mahfouf and A. Simmons, 2000 : The ECMWF operational implementation of four-dimensional variational assimilation. I : Experimental results with simplified physics . *Q. J. R. Meterol. Soc.*, 1**26**, 1143-1170.

Rabier, F., and P. Courtier, 1992 : Four-dimensional assimilation in the presence of baroclinic instability. *Q. J. R. Meteorol. Soc.* , **118**, 649-672.

Rabier, F., E. Andersson, J. Haseler, P. Unden, P. Courtier, G. Kelly, D. Vasiljevic, C. Brankovic, C. Cardinali, C. Gaffard, A. Hollingsworth, C. Jakob, P. Janssen, E. Klinker, A. Lanzinger, M. Miller, A.

Simmons, B. Strauss, J.-N. Thépaut, P. Viterbo, 1998: The ECMWF implementation of three-dimensional variational assimilation (3D-Var). III: Experimental results. *Quart. J. Roy. Meteor. Soc.*, **124**, 1831-1860.

Joly. A., 1992 : ARPEGE/ALADIN : adiabatic model equations and algorithm. ARPEGE/ALADIN Formulation version 0.0.

Rabier, F. and J.-F. Mahfouf, 2000 : The ECMWF operational implementation of four-dimensional variational assimilation. II : Experimental results with improved physics. *Q. J. R. Meterol. Soc.*, **126**, 1171-1190.

Klinker, E., F. Rabier, G. Kelly and J.-F. Mahfouf, 2000 : The ECMWF operational implementation of four-dimensional variational assimilation. III : Experimental results and diagnostics with operational configuration. *Q. J. R. Meterol. Soc.*, **126**, 1191-1215.

PAPER III

Radi Ajjaji

Introduction

4d-var is able to extract information from the observations in a way consistent with the dynamics of the model. Assuming the latter is perfect, it is equivalent to a Kalman filter for the result at the final time; it uses flow-dependent structure functions, though it does not allow them evolve in time explicitly.

A practical way of exhibiting the implicit 4d-var structure functions is to perform a 4d-var assimilation experiment with a single observation : the analysis increments are proportional to the forecast error-covariances between the observed variable at the observation point and all other locations and variables.

Thépaut et al. (1996) have shown how complex forecast error covariances can be when they evolve according to primitive equation dynamics. The shape of the analysis increments provides a three-dimensional picture of the covariances of the background errors modified by the dynamics.

This paper presents a case study analysing the structure functions in 4d-var on a real meteorological situation characterized by a fictitious over-estimation of specific-humidity increments over Spain in the context of Météo-France ARPEGE 4d-var assimilation.

First, the tangent-linear hypothesis is examined in presence of this strange specific humidity feature. Then, a theoretical study, consisting in determining the vector of 4d-var increments when only one single observation is introduced in the cost function, is presented in order to show the different ingredients governing the increments magnitude.

Then, the randomisation technique, discussed by Fisher and Courtier (1995) and used by Anderson et al. (2000), giving global gridpoint values of background-error standard deviations in terms of observable quantities, is used to diagnose the specific-humidity background-error standard deviations involved implicitly in this case study.

1. Test of the tangent-linear hypothesis for the situation of April 24th, 2001

Comparisons were done between, on one hand the evolution over 6 hours of a perturbation (of the order of magnitude of analysis increments) with the simplified tangent-linear (TL) model $M(\delta x)$, and on the other hand the finite difference between two nonlinear forecasts, one from a basic state (x) and the other one from a perturbed state ($x+\delta x$). Theses runs are performed in adiabatic mode with simple linear vertical-diffusion and surface-drag schemes (Buizza, 1994). The perturbation used corresponds to the 4d-var increments resulting from an experiment with a single surface geopotential observation (40.93°N, 1.30°W, 902 m).

On Fig. 1, one can notice that there is no major difference between the adiabatic tangent-linear model and finite differences from the nonlinear model, for temperature and wind fields. Concerning specific humidity, finite differences show a region of large differences, over the Atlantic West of Spain. Intuitively, one can explain that by the lack of physics in the used TL model. But, as shown on Fig. 2, when switching on the entire simplified-physics package (vertical turbulence, gravity wave drag, stratiform precipitations, convection and radiation), the TL model still shows the same features around 20°W.

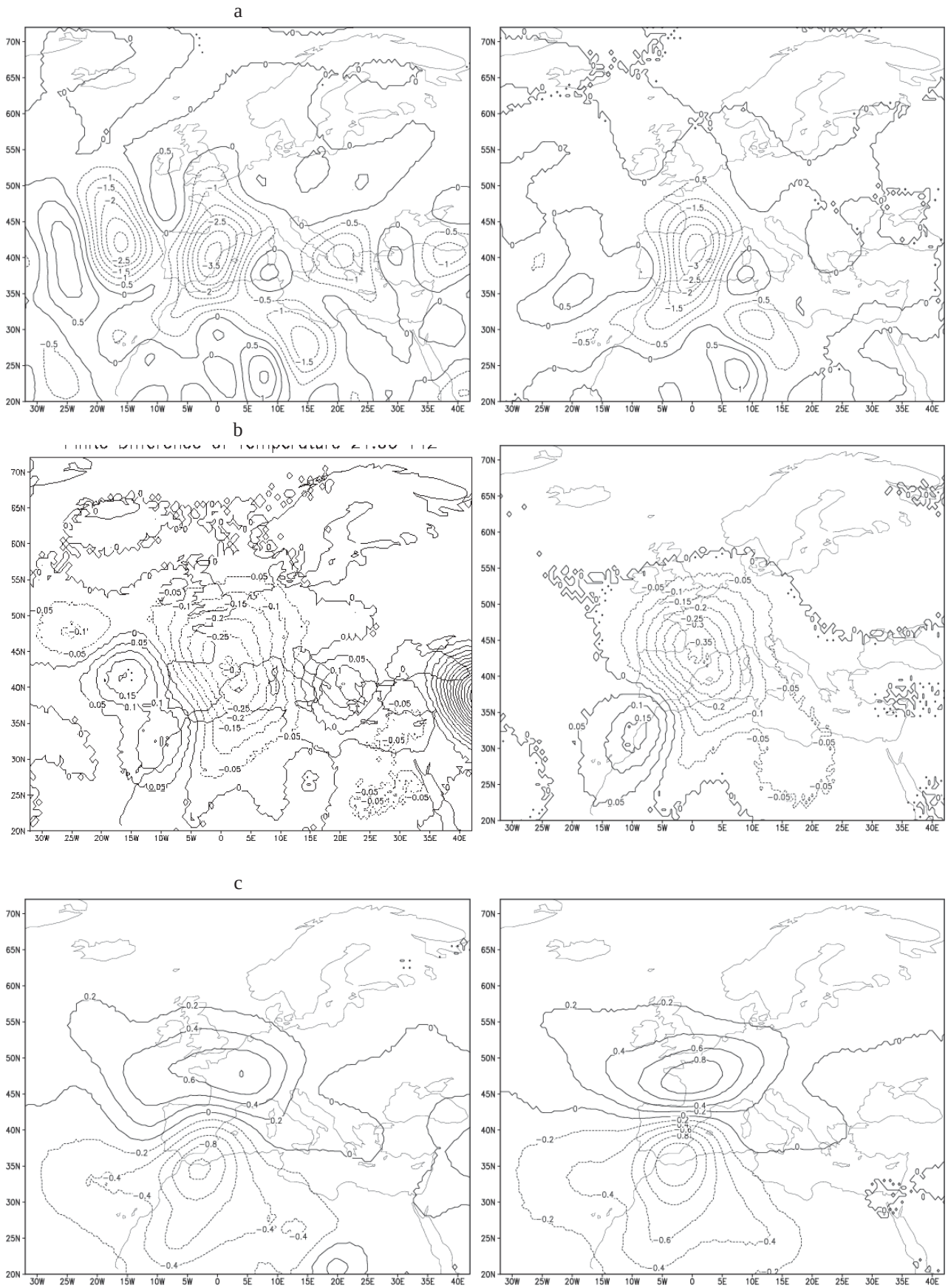

Figure 1: Finite differences (left) and tangent-linear integration (righ, at the end of the assimilation window (i.e. at 21:00 UTC on April 24th, 2001), for : a) specific humidity, b) temperature, c) zonal wind, at 850 hPa (when a single geopotential observation located at [40.93°N,1.30°W, 902 m].is introduced at 18:00 UTC)

a b

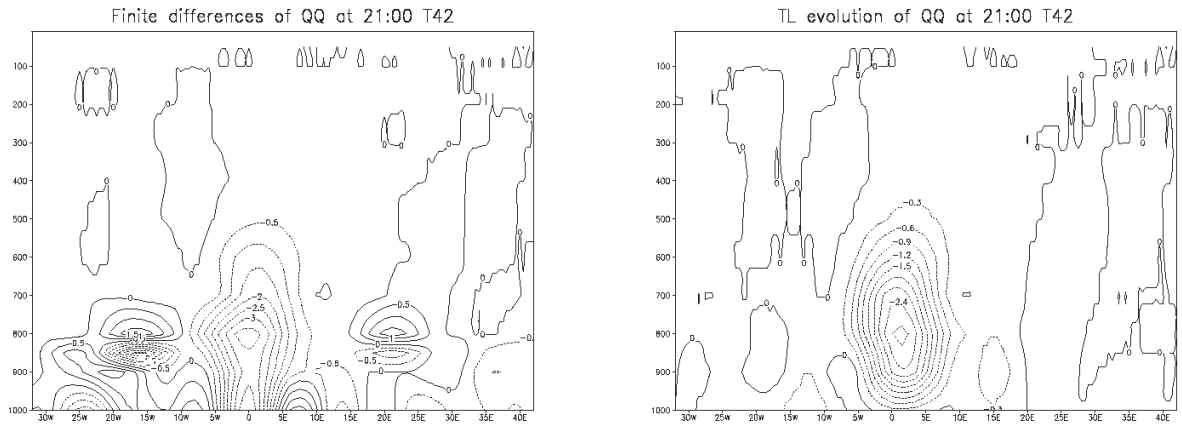

Figure 2: Vertical cross-sections of specific humidity at 42.5°N for : a) finite differences, b) tangent-linear evolution with full simplified physics. The values are multiplied by 10^4 and valid at the end of the assimilation window.

The pattern that appears on the Atlantic is however very local on the vertical : it concerns a small layer between 900 hPa and 800 hPa. Simplified physics is eventually not enough realistic to catch it efficiently. On the other hand, some other localized features appear near to the surface, along the cross-section axis, in the finite differences for specific humidity. They denote certainly, a weakness of the simplified vertical-turbulence scheme.

Concerning the pattern associated to the large increment given by 4d-var analysis over North-West Spain and visible on the cross-sections at the vertical of 0°W, finite differences from the nonlinear evolution of the associated perturbation remain very similar to the TL evolution, on the horizontal and the vertical, despite the existence of a slight difference near the surface. Thus, it appears that the tangent-linear hypothesis is likely not to affect viciously the specific-humidity increments.

The above-discussed results, relative to the context of a single geopotential observation, are also obtained when using a perturbation corresponding to the 4d-var increments implied by the full set of observations (Fig. 3).

2. Theoretical expression of 4d-var specific-humidity analysis increments induced by a single observation

In an analysis (3d-var or O.I. or each analysis step of a Kalman filter), the analysis increments, x^a-x^b, are a linear combination of the innovations, y-$H(x^b)$ (Lorenc, 1986) :

$$\delta x = x^a - x^b = BH'^{\mathrm{T}}(H'BH'^{\mathrm{T}}+R)^{-1}[y - H(x^b)]$$

where y stands for the vector of observations, x^b for the background, H for the operator which predicts the observations from the model initial state, R for the covariance matrix of observation errors and B for the covariance matrix of background errors; H' is the linearization of H in the vicinity of the background x^b, $^{\mathrm{T}}$ denotes the transpose of a matrix.

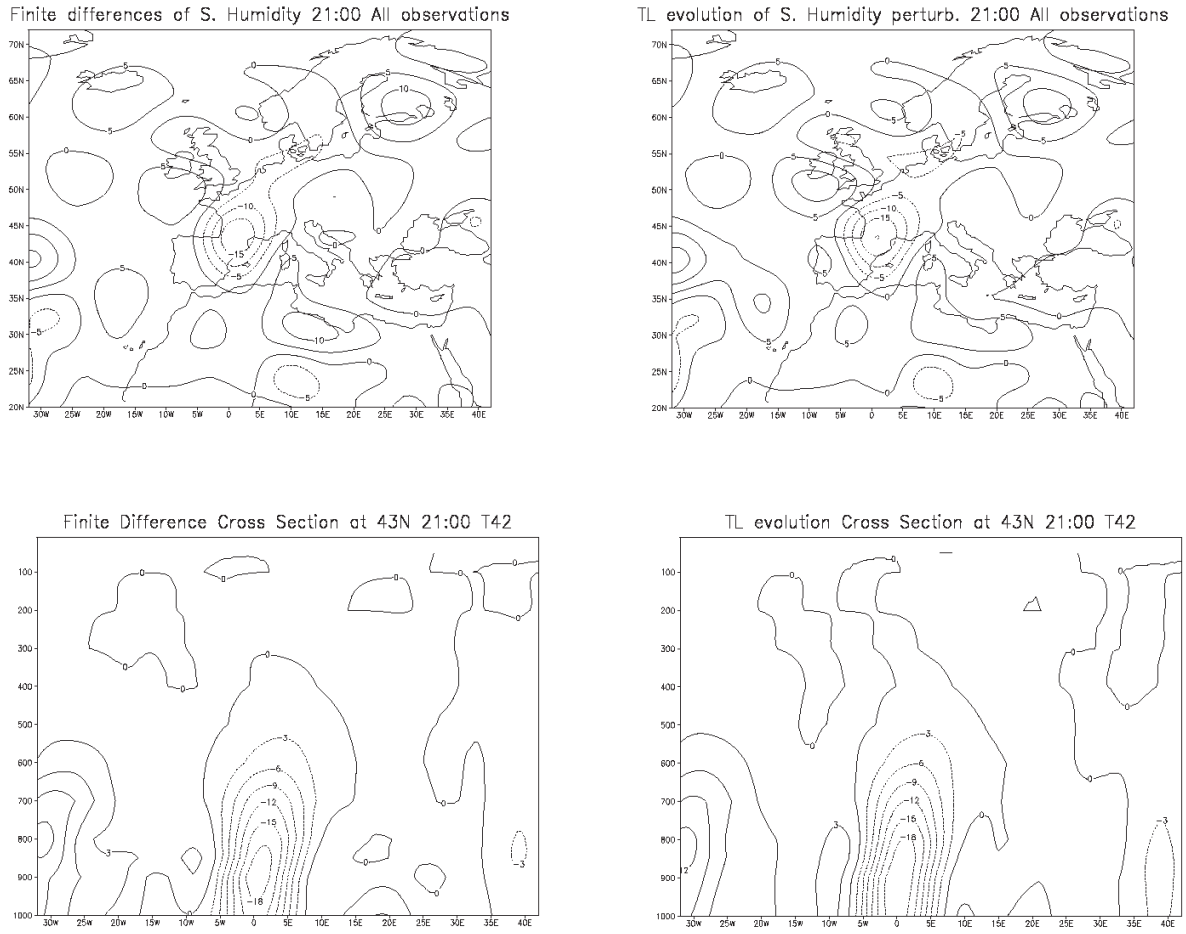

Figure 3: Finite differences (left) versus tangent-linear evolution (right) for specific humidity. The perturbation used corresponds to the 4d-var increments associated to a full set of observations (maps at 850 hPa and vertical cross-sections at 42.5°N).

To simplify the interpretation, we suppose that the state variable x is reduced to five variables : u, v, P, T and q. The temporal step is taken equal to 1 second (Δt =1).

On one tangent-linear timestep evolution, we can write :

$$\begin{bmatrix} \vec{u}'(t+1) \\ T'(t+1) \\ q'(t+1) \\ P'(t+1) \end{bmatrix} = M \begin{bmatrix} \vec{u}'(t) \\ T'(t) \\ q'(t) \\ P'(t) \end{bmatrix} \tag{1}$$

where the tangent-linear operator M is given by the following matrix (cf. paper II) :

$$\begin{pmatrix} A_u & \vec{B}_u & \vec{C}_u & \vec{D}_u \\ \vec{A}_T & B_T & C_T & D_T \\ \vec{A}_q & 0 & C_q & D_q \\ \vec{A}_P & 0 & 0 & D_P \end{pmatrix} \tag{2}$$

If we consider a B matrix in which cross-covariances between different variables are not taken into account, then we have :

$$\mathrm{B} = \begin{pmatrix} \mathrm{B}[\vec{u}'(t)] & 0 & 0 & 0 \\ 0 & \mathrm{B}[T'(t)] & 0 & 0 \\ 0 & 0 & \mathrm{B}[q'(t)] & 0 \\ 0 & 0 & 0 & \mathrm{B}[P'(t)] \end{pmatrix} \tag{3}$$

$$\mathrm{B}M^T = \begin{pmatrix} A_u \mathrm{B}[\vec{u}'(t)] & \vec{A}_T \mathrm{B}[\vec{u}'(t)] & \vec{A}_q \mathrm{B}[\vec{u}'(t)] & \vec{A}_p \mathrm{B}[\vec{u}'(t)] \\ \vec{B}_u \mathrm{B}[T'(t)] & B_T \mathrm{B}[T'(t)] & 0 & 0 \\ \vec{C}_u \mathrm{B}[q'(t)] & C_T \mathrm{B}[q'(t)] & C_q \mathrm{B}[q'(t)] & 0 \\ \vec{D}_u \mathrm{B}[P'(t)] & D_T \mathrm{B}[P'(t)] & D_q \mathrm{B}[P'(t)] & D_p \mathrm{B}[P'(t)] \end{pmatrix} \tag{4}$$

If we introduce a single wind-observation at time t +1 on one particular gridpoint, the observation-operator matrix is then reduced to a row vector containing the value 1 at the gridpoint corresponding to the observation and the value 0 elsewhere.

The matrix $BM^{\mathrm{T}}H^{\mathrm{T}}$ contains then the covariances between (u',v')(t +1) at the observation location and the errors on the five variables at time t. $BM^{\mathrm{T}}H^{\mathrm{T}}$ involves the auto-covariances between the observation point and all the gridpoints :

$$\mathrm{B}M^T H^T = \begin{pmatrix} A_u \hat{\mathrm{B}}[\vec{u}'(t)] \\ \vec{B}_u \hat{\mathrm{B}}[T'(t)] \\ \vec{C}_u \hat{\mathrm{B}}[q'(t)] \\ D_u \hat{\mathrm{B}}[P'(t)] \end{pmatrix} \tag{5}$$

In the case of a single observation, the matrix ($HMBM^{\mathrm{T}}H^{\mathrm{T}}$+$R$) is reduced to a scalar value :

$$HMBM^T H^T + R = \sigma_b^2[\vec{u}'(t+1)] + \sigma_o^2[\vec{u}'(t+1)] \tag{6}$$

On the other hand, if we calculate $HMBM^{\mathrm{T}}H^{\mathrm{T}}$, then we deduce :

$$\sigma_b^2[\vec{u}'(t+1)] = A_u^2 \cdot \sigma_b^2[\vec{u}'(t)] + \vec{B}_u \cdot \vec{B}_u \cdot \sigma_b^2[T'(t)] + \vec{C}_u \cdot \vec{C}_u \cdot \sigma_b^2[q'(t)] + \vec{D}_u \cdot \vec{D}_u \cdot \sigma_b^2[P'(t)] \tag{7}$$

Thus the operator that transforms the innovation at time t +1 to an increment at time t is :

$$\mathrm{B}M^T H^T (HMBM^T H^T + R)^{-1} = \begin{pmatrix} A_u \hat{\mathrm{B}}[\vec{u}'(t)] \\ \vec{B}_u \hat{\mathrm{B}}[T'(t)] \\ \vec{C}_u \hat{\mathrm{B}}[q'(t)] \\ D_u \hat{\mathrm{B}}[P'(t)] \end{pmatrix} / (\sigma_b^2[\vec{u}'(t+1)] + \sigma_o^2[\vec{u}'(t+1)]) \tag{8}$$

This equation is equivalent to the following one :

$$\mathrm{B}M^T H^T (HMBM^T H^T + R)^{-1} = \begin{pmatrix} A_u \hat{\mathrm{B}}[\vec{u}'(t)] / \sigma_b^2[\vec{u}'(t+1)] \\ \vec{B}_u \hat{\mathrm{B}}[T'(t)] / \sigma_b^2[\vec{u}'(t+1)] \\ \vec{C}_u \hat{\mathrm{B}}[q'(t)] / \sigma_b^2[\vec{u}'(t+1)] \\ D_u \hat{\mathrm{B}}[P'(t)] / \sigma_b^2[\vec{u}'(t+1)] \end{pmatrix} \cdot \frac{\sigma_b^2[\vec{u}'(t+1)]}{(\sigma_b^2[\vec{u}'(t+1)] + \sigma_o^2[\vec{u}'(t+1)])} \tag{9}$$

The second term in the right-hand-side of (9) corresponds to a stage in the analysis process during which the observed information is filtered; it gives the value of the wind analysis increment $d(u,v)(t+1)$ at the observation point knowing the wind innovation $[y - H(x^b)]_{wind} = \delta(u,v)(t+1)$:

$$d\vec{u}(t+1) = \frac{\sigma_b^2[\vec{u}'(t+1)]}{(\sigma_b^2[\vec{u}'(t+1)] + \sigma_o^2[\vec{u}'(t+1)])}\,\delta\vec{u}(t+1) \tag{10}$$

The first term in the right-hand-side of (9) corresponds to the spatio-temporal multi-multivariate propagation of the filtered information. It indicates how $d(u,v)(t+1)$ is transformed to the analysis increments $dx(t)$ of all state-vector variables (the five variables here) with the adjoint momentum equation.

In 4d-var, unlike 3d-var, there exist an impact (caused by the introduction of the model in the observation operator) of wind observations on the initial conditions for specific humidity, through the adjoint momentum equation. We have :

$$\begin{aligned}
d\vec{u}(t) &= A_u\hat{\mathrm{B}}\left[\vec{u}'(t)\right] / \sigma_b^2\left[\vec{u}'(t+1)\right] \cdot d\vec{u}(t+1) \\
dT(t) &= \vec{B}_u\hat{\mathrm{B}}\left[T'(t)\right] / \sigma_b^2\left[\vec{u}'(t+1)\right] \cdot d\vec{u}(t+1) \\
dq(t) &= \vec{C}_u\hat{\mathrm{B}}\left[q'(t)\right] / \sigma_b^2\left[\vec{u}'(t+1)\right] \cdot d\vec{u}(t+1) \\
dP(t) &= D_u\hat{\mathrm{B}}\left[P'(t)\right] / \sigma_b^2\left[\vec{u}'(t+1)\right] \cdot d\vec{u}(t+1)
\end{aligned} \tag{11}$$

The complete equation for specific-humidity increments is :

$$dq(t) = \frac{-\hat{\mathrm{B}}[q'(t)]}{\sigma_b^2[\vec{u}'(t+1)]}(R_v - R_d)\left[\int_\eta^1 \left(\vec{\nabla}(\ln P) + \frac{\partial \ln P}{\partial \eta}\vec{\nabla}\right)(T\,\bullet)\,d\eta + T\vec{\nabla}(\ln P)\cdot\bullet\right]\cdot d\vec{u}(t+1) \tag{12}$$

The same approach applied when using a single temperature-observation leads to the following equation :

$$dq(t) = \frac{-\hat{\mathrm{B}}[q'(t)]}{\sigma_b^2[T'(t+1)]}\frac{RT\omega}{PC_p}\left[\frac{R_v - R_d}{R} - \frac{C_{pv} - C_{pd}}{C_p}\right]\cdot dT(t+1) \tag{13}$$

From these equations, we can deduce the following suggestions :

- To reduce the multivariate effects (between specific humidity and other variables), we can try to adjust the background-error standard deviations of specific humidity (decrease them). But in the same time, we must also adjust the corresponding observation-error standard deviations in order to keep the information coming from observations.
- Use more and more observations informing on humidity to avoid a great impact of wind or mass observations on humidity. The anomaly of specific humidity increments shown in my previous papers happened in a region devoid of humidity observations. An experiment consisting in introducing an artificial TEMP observation (created from the guess field) in North-West Spain resolved completely the problem.

Specific humidity increments given by the above equations imply that if 4d-var tries to fit wind observations at time $t+1$ - for example to reduce $d(u,v)(t+1)$ -, it may create a large modification of the initial specific humidity. Thus, the unrealistic increments could appear when, for example, the remaining observations and dynamics (temperature observations and temperature evolution in particular) tend to lead to a modification of initial temperature that does not contribute to a reduction of wind increments (or in contrary tend to amplify them). In that case when adding temperature and pressure observations, specific humidity is excessively amplified.

3. Background specific-humidity error diagnosis (following Rabier et al., 1998)

When studying the background errors at radiance observation points, that appeared to be locally unrealistically large over the West coast of Africa, in an ECMWF 4d-var experiment, Anderson et al. (2000) noticed that this was associated to a maximum of background specific-humidity errors. A simple modification to limit these humidity background errors in very dry areas was developed and tested : arbitrarily limiting the standard deviation of background errors ($\sigma(q)$) to a maximum of 125% of the background field (q), above 800 hPa. In doing so the general features of the humidity background errors were unaltered, but the extremely high values were reduced.

In the ARPEGE/IFS assimilation system, the humidity background errors are not cycled ; the specification of the standard deviations is not derived from the NMC statistics but from statistics of radiosonde observations minus background fields, stratified according to observed temperature and relative humidity. They are modelled as a function of the background temperature T_b and relative humidity Hu_b :

$$\sigma_b(Hu) = -0.002T_b - 0.0033|T_b - 273.| + 0.25Hu_b - 0.35|Hu_b - 0.4| + 0.70,$$

$$\sigma_b(Hu) = \min[0.18, \max(0.06,\sigma_b(Hu))].$$

The standard deviation in terms of relative humidity is then converted to specific humidity, deriving the variations of q from the equation :

$$q = Hu\, e_{sat}(T)/[(R_v/R_d)\cdot P - (R_v - R_d)/R_d \cdot Hu\, e_{sat}(T)],$$

where e_{sat} is the saturation water-vapour pressure, depending on temperature (Tetens' formula) and P is pressure.

Humidity increments are forced to be negligibly small above the tropopause to avoid a systematic drift of stratospheric humidity over extended periods of data assimilation. Humidity in the stratosphere is then mainly driven by the model, and not controlled by observations. This is achieved by setting a very low value (10^{-8}) for $\sigma_b(Hu)$:

- wherever the pressure is lower than 70 hPa,
- at any other point with pressure in the range 70-500 hPa, if the background temperature and pressure fields are such that the square of the buoyancy frequency exceeds $2.10^{-4}\,s^{-2}$ everywhere above that point till 70 hPa.

In addition, any value of $\sigma_b(Hu)$ lower than 10^{-8} is reset to 10^{-8}.

For pressure less than 800 hPa, and over sea, the above model of background errors is modified as :

$$\sigma_{back}(Hu) = \sigma_b[1 - a + a\cdot \exp(-(\Delta P/\beta)^2)], \quad \Delta P = P_b - P_o, \quad a = 0.5(1-LSM),$$

where LSM is the land-sea mask and β=12500 Pa.

Fisher and Courtier (1995) suggested that a randomisation method can be used to diagnose the effective background-error variances and compute matrix B in 3d-var. The method allows the calculation of a low rank estimate of B in terms of model variables in gridpoint space, and is known as randomisation estimate. The method applies to 3d-var, since no account is taken of the evolution of background errors in time. In a 4d-var system, this provides a diagnosis of the effective background errors at the beginning of the assimilation period. This method could be extended to compute an approximation to the background error in terms of observable quantities (Anderson et al., 2000).

This method is applied for the situation of April 24th , 2001, (at 15:00 UTC), in order to diagnose the effective background standard deviations used by 4d-var.

On Fig. 4, one can notice the correspondence between large 4d-var increments and strong STD assigned to both specific and relative humidity (for this situation). This is more visible for low levels (between 500 hPa and the surface).

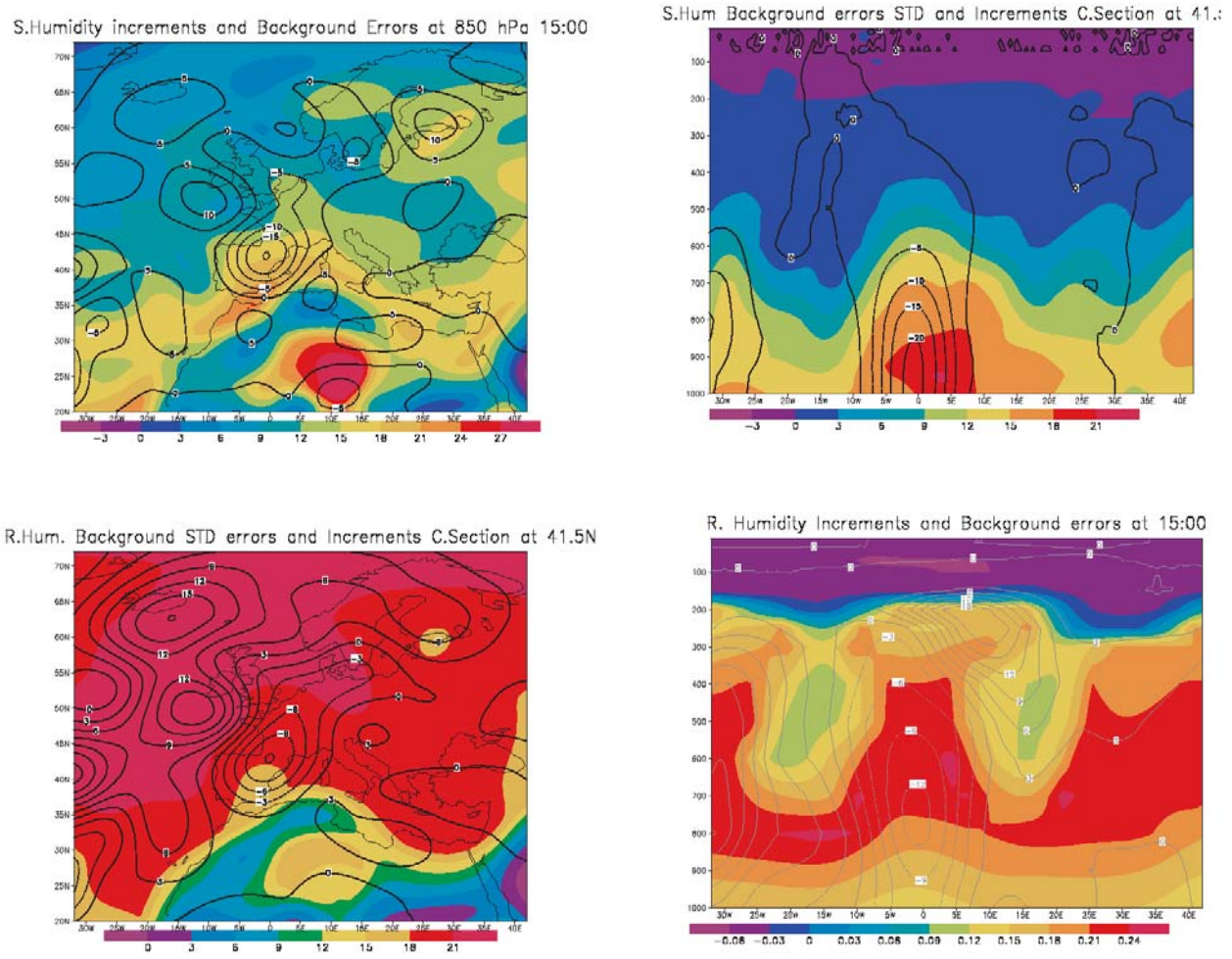

Figure 4: Superimposed standard deviations of background errors (STD, color scale) and 4d-var increments (isolines) at 15:00 UTC for relative humidity (bottom panel) and specific humidity (top panel). The cross-sections on the right are performed at latitude 41.5°N. Specific-humidity values multiplied by 10^4, both for STD and increments. For relative humidity, absolute STD values are mentioned, while increments are in %.

These large background error standard deviations are amplified during the tangent-linear integration along the assimilation window. And this forces 4d-var to remain far from the guess field (as far as specific humidity is concerned) at each time step, because the process of minimization has no other information on humidity except the multivariate information imposed by the remaining analysed fields and their dynamics and observations. In other words, when trying to analyse specific humidity, 4d-var relay on mainly three components :

- humidity observations,
- humidity background,
- multivariate effect.

For the case of April 24th, 2001, the first ingredient does not play any part because over Spain there was no TEMP along the assimilation window. The second ingredient is governed by the magnitude of the background errors assigned to the humidity variable at the beginning of the assimilation window and by the implicit evolution of these quantities during the minimization. The specific atmospheric dynamics (discussed and shown below) is in favour of an amplification of these

quantities along the assimilation window. As a consequence, background humidity information is only weakly taken into account. It is then clear that the multivariate effect will predominantly govern alone the behaviour of the analysis of specific humidity.

4. Experimental study of the multivariate terms affecting specific humidity

As shown in a previous paper, the adjoint terms governing the magnitude of the gradient (with respect to specific humidity) are:

$$- \ (R_v - R_d)\left[-\int_{\eta}^{1} \left(\frac{\partial \ln P}{\partial x} + \frac{\partial \ln P}{\partial \eta}\cdot\frac{\partial \bullet}{\partial x}\right)(T\bullet)\,d\eta - T\cdot\frac{\partial \ln P}{\partial x}\bullet \right] Grad(u)$$

$$- \ (R_v - R_d)\left[-\int_{\eta}^{1} \left(\frac{\partial \ln P}{\partial y} + \frac{\partial \ln P}{\partial \eta}\cdot\frac{\partial \bullet}{\partial y}\right)(T\bullet)\,d\eta - T\cdot\frac{\partial \ln P}{\partial y}\bullet \right] Grad(v)$$

$$- \ \frac{RT\omega}{PCp}\left[(R_v - R_d)/R - (Cp_v - Cp_d)/Cp\right] Grad(T)$$

$$- \ \left[\dot{\eta}\frac{\partial \bullet}{\partial n} + u\frac{\partial \bullet}{\partial x} + v\frac{\partial \bullet}{\partial y}\right] Grad(q)$$

The two first terms corresponds to the wind information that will act on humidity. For instance, *Grad(u)*, which contains mainly the contribution of wind observations, will affect humidity in a proportion depending on the tendency and magnitude of the term between brackets. If 4d-var tends to decrease wind gradient (wind increments) to fit wind observations, whereas the dynamics (of mainly temperature and pressure) does not allow that (i.e. terms between brackets remain large at each time step), then 4d-var has only one choice : to act on humidity.

When studying the above first three terms, it appears that their magnitude is governed by the following quantities :

$(R_v - R_d)\,T/P\,\partial_x P$, $(R_v - R_d)\,T/P\,\partial_y P$, and $RT/Cp\ \omega/P\left[(R_v - R_d)/R - (Cp_v - Cp_d)/Cp\right] \approx 2/49 R_v/R_d\ T\omega/P$

The common term contributing the most in these three expressions is T/P. This leads us to expect large magnitudes in regions characterized by :

- high temperatures (Sahara, continental regions during summer),
- low pressures (e.g. Saharan low pressures : "dépressions sahariennes"),
- high horizontal pressure gradients (mountainous areas),
- high vertical velocities (mountainous areas).

The term T/P is proportional to $1/\rho$ (ρ being the air density). That means that we could expect bad specific humidity analysis in regions devoid of humidity observations and characterized by small air density. A first try to solve the problem is to decrease specific humidity increments in areas with small ρ.

The following figures give the magnitude of some relevant above-mentioned terms.

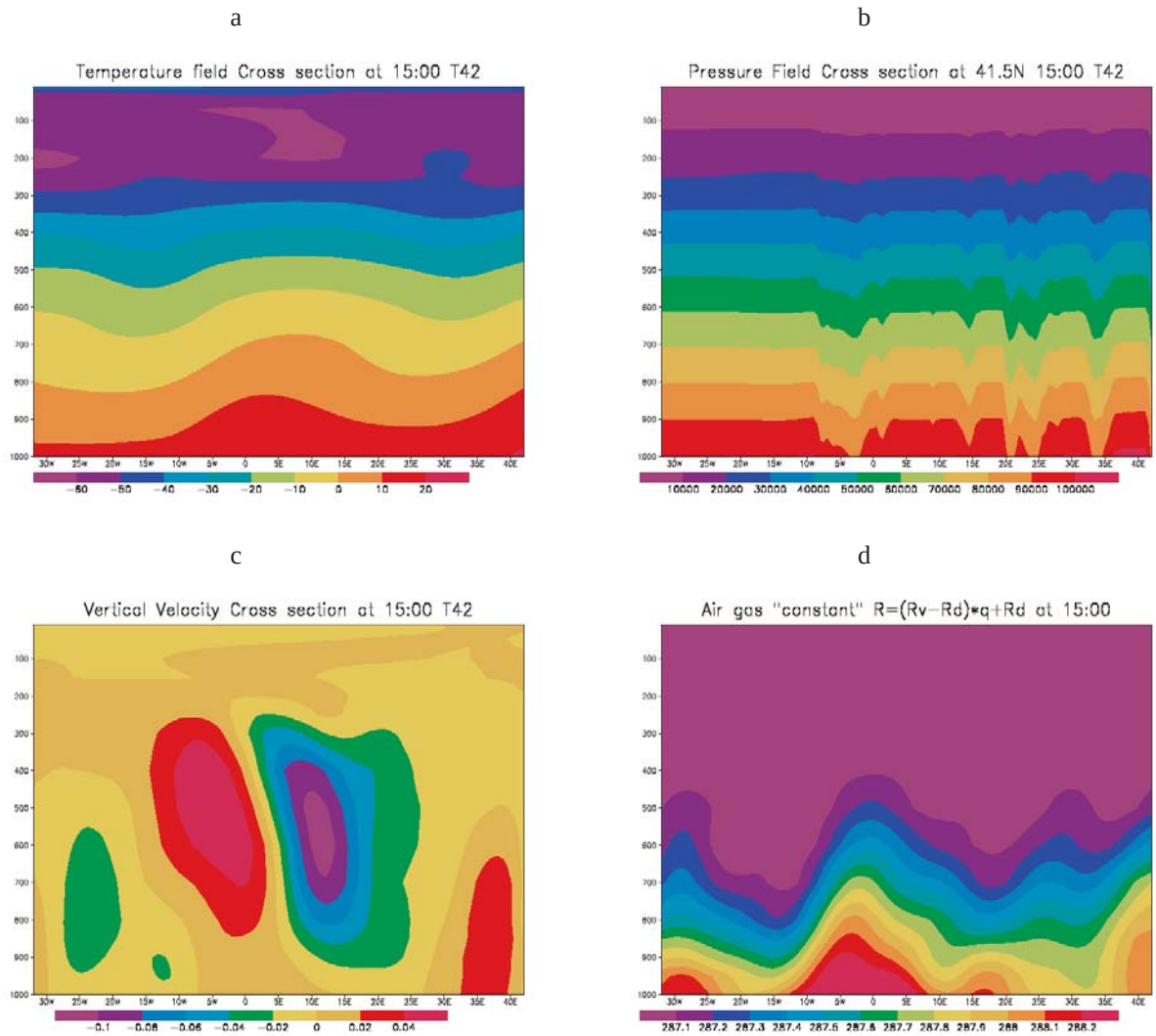

Figure 5: Vertical cross-sections at latitude 41.5°N for : a) temperature, b) pressure, c) vertical velocity, d) air gas constant. One can notice high temperatures, low pressures, high vertical velocities and high *R* values between longitudes -5° and +5°E.

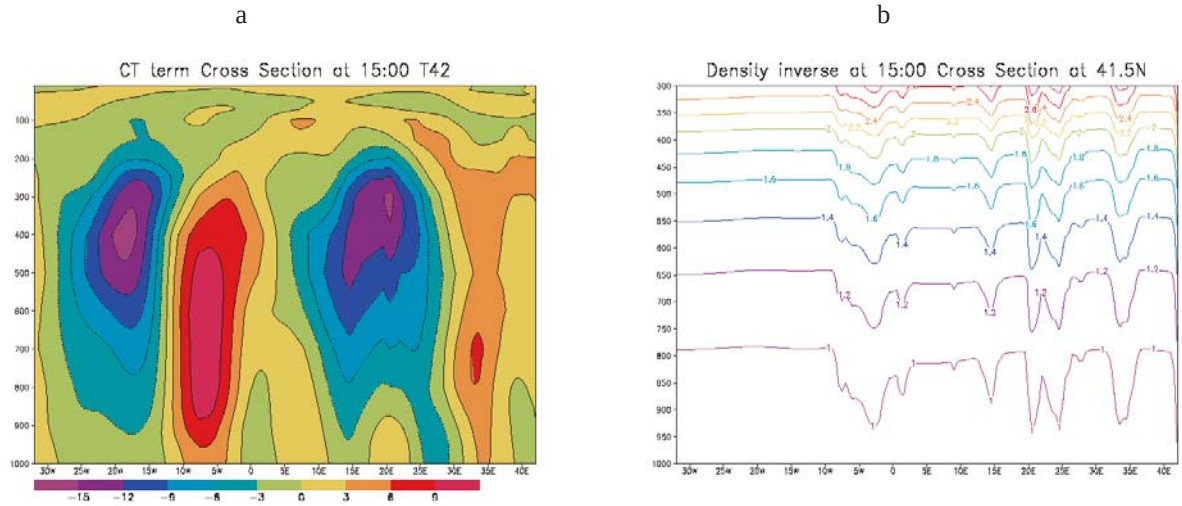

Figure 6 : *CT* term on (a) is the dynamics term coupling temperature observations and specific humidity increments (cf. 4.). This term presents a maximum on a vertical column between 900 hPa and 500 hPa slightly at the west of our area of interest. This corresponds on (b) to relatively high values of density inverse (the corresponding cross section is truncated at 300 hPa).

Figure7 hereafter, by comparison with Fig.5, informs on dynamics, showing the time-evolution of some characteristic fields between 15:00 and 18:00 UTC.

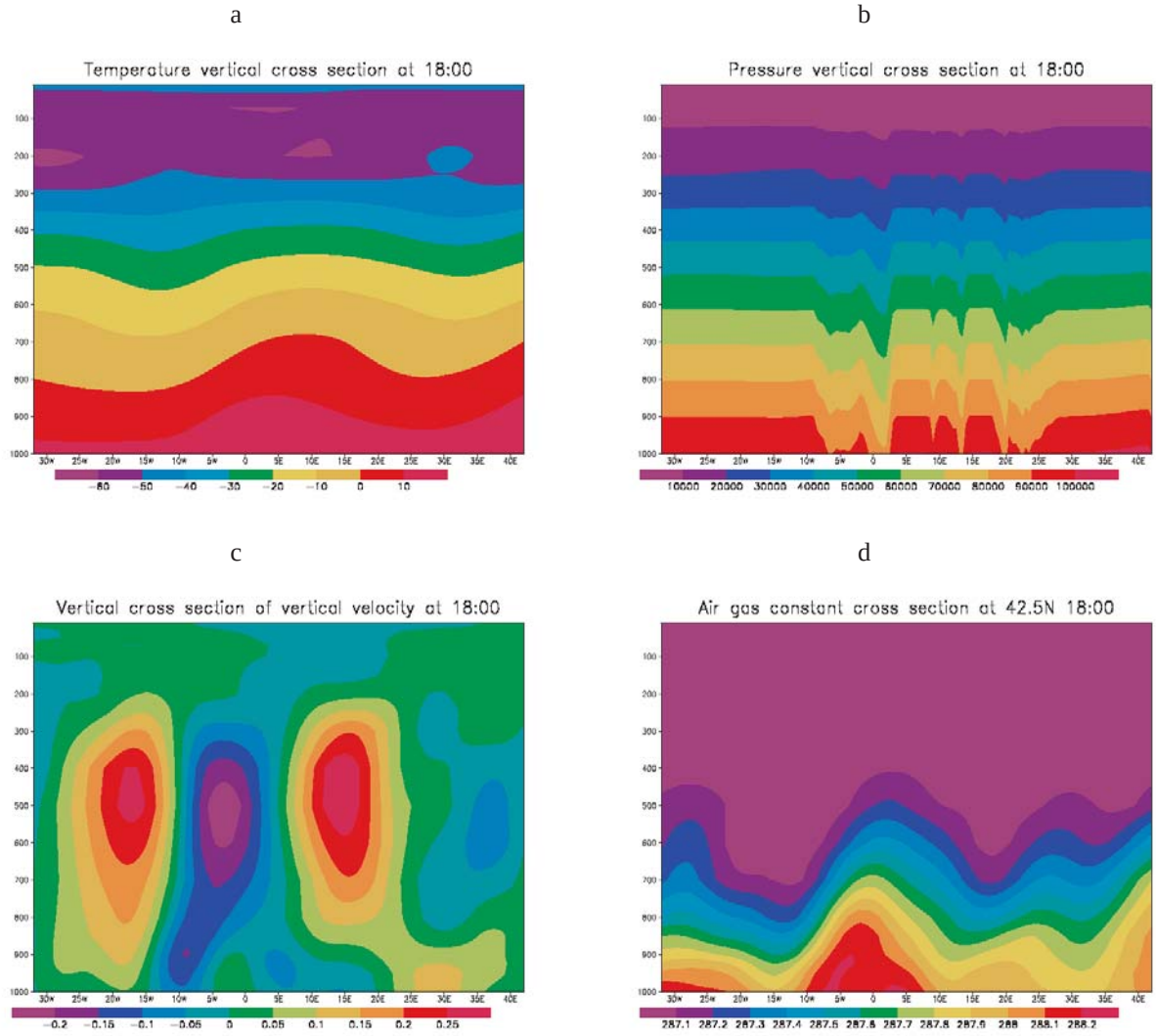

Figure 7: Same as figure 5 at 18:00 UTC.

5. References

Anderson, E., and M. Fisher, 1999 : Background errors for observed quantities and their propagation in time. pp. 81-90 in *Proceedings of the ECMWF workshop on diagnosis of data assimilation systems*, Reading, UK, 1-4 November 1998.

Anderson, E., M. Fisher, R. Munro and A. McNally, 2000 : Diagnosis of background errors for radiances and other observable quantities in a variational data assimilation scheme, and the explanation of a case of poor convergence. *Q. J. R. Meteorol., Soc.*, **126**, pp. 1455-14

Buizza, R., 1994: Sensitivity of optimal unstable structures. *Q. J. R. Meteorol. Soc.*, **120**, 429-451

Daley, R., 1991 : Atmospheric Data Analysis. Cambridge Atmospheric and Space Science Series, Cambridge University Press. ISBN 0-521-38215-7, 457 pages.

Fisher, M., and P. Courtier, 1995 : Estimating the covariance matrices of analysis and forecast error in variational data assimilation. *ECMWF Tech. Memo. 220*. Available from ECMWF, Reading, UK.

Janiskova, M., J.-N. Thépaut and J.-F. Geleyn, 1999 : Simplified and regular physical parameterisations for incremental four-dimensional variational assimilation. *Mon. Wea. Rev.*, **127**, 26-45.

Jazwinski, A.H., 1970 : Stochastic processes and filtering theory. Academic Press.

Lorenc, A., 1986 : Analysis methods for numerical weather prediction. *Quart. J. Roy. Meteor. Soc.*, **112**, 1177-1194.

Mahfouf, J.-F., R. Buizza and R.M. Errico, 1997 : Strategy for including physical processes in the ECMWF data assimilation system. In *Proceedings of the ECMWF Workshop on non-linear aspects of data assimilation*, Shinfield Park, Reading, RG2 9AX, 9-11 September 1996.

Rabier, F., A. McNally, E. Anderson, P. Courtier, P. Unden, J. Eyre, A. Hollingsworth and F. Bouttier, 1998a. The ECMWF implementation of three-dimensional variational assimilation (3D-Var). II: Structure functions. *Q.J.R.Meteorol. Soc.*, **124**, 1809-1829.

Thépaut, J-N., P. Courtier, G. Belaud and G. Lemaître, 1996 : Dynamical structure functions in a four-dimensional variational data assimilation: A case-study. *Q.J.R.Meteorol. Soc.*, **122**, 535-561.

7. Appendix : background standard deviations obtained by randomization vectors technique for surface pressure, temperature, specific humidity on low atmospheric model levels

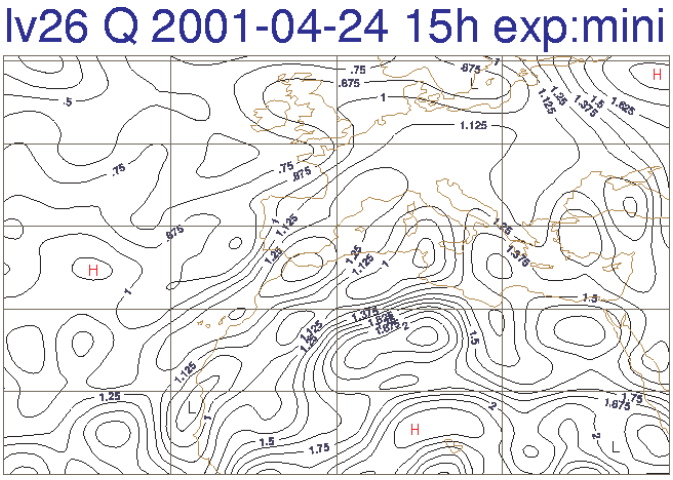

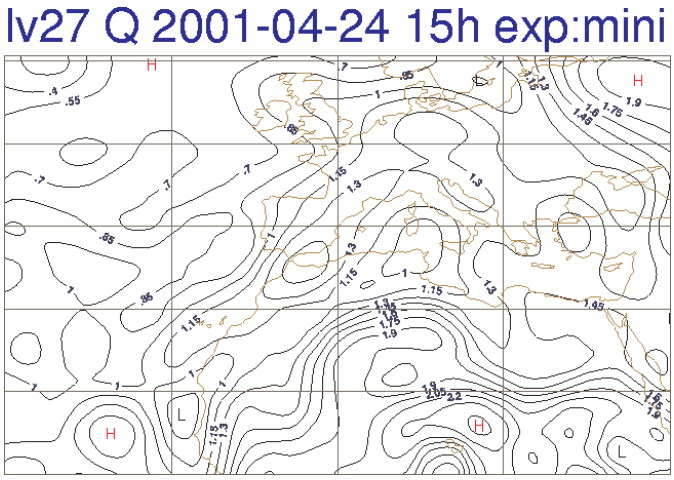

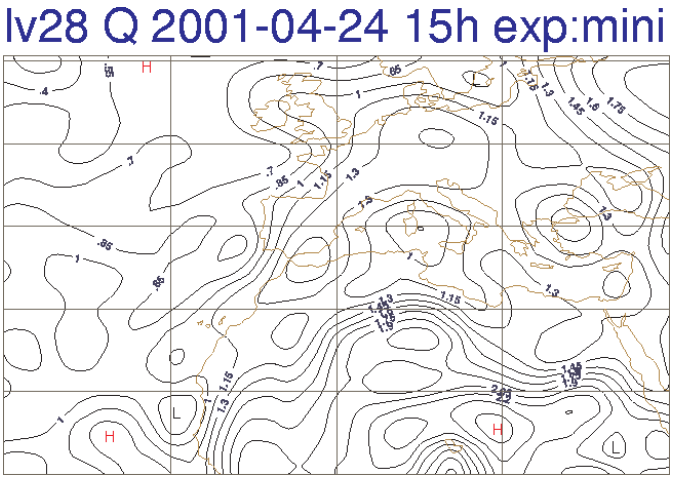

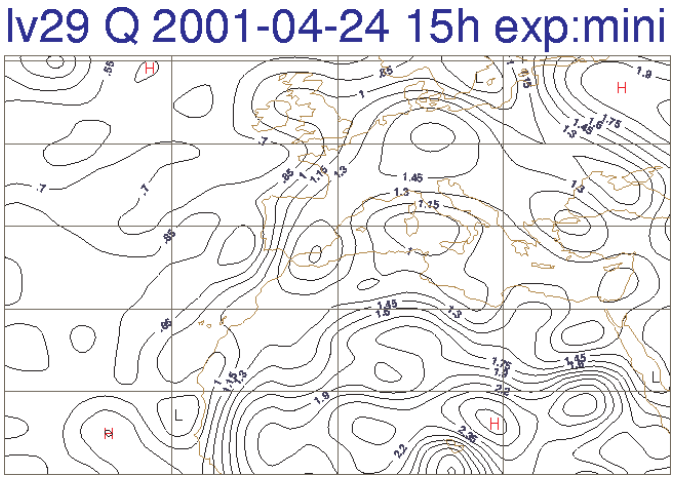

lv30 Q 2001-04-24 15h exp:mini

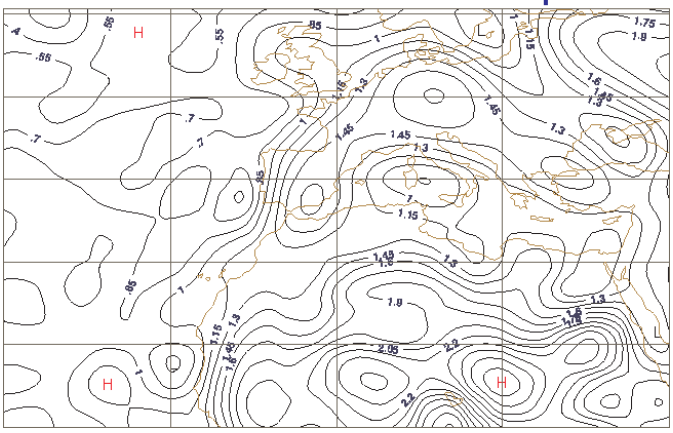

lv31 Q 2001-04-24 15h exp:mini

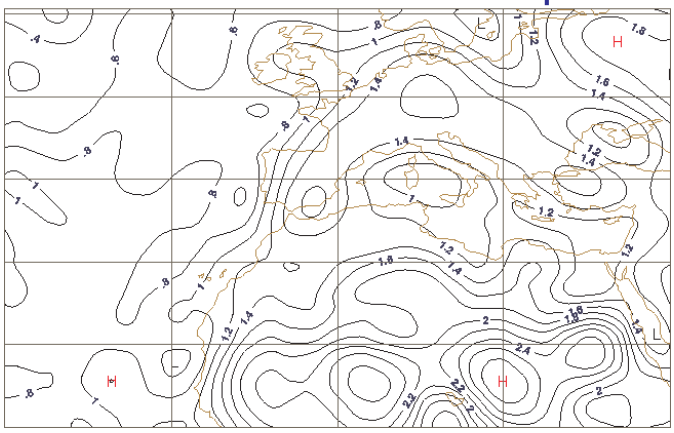

lv25 T 2001-04-24 15h exp:mini

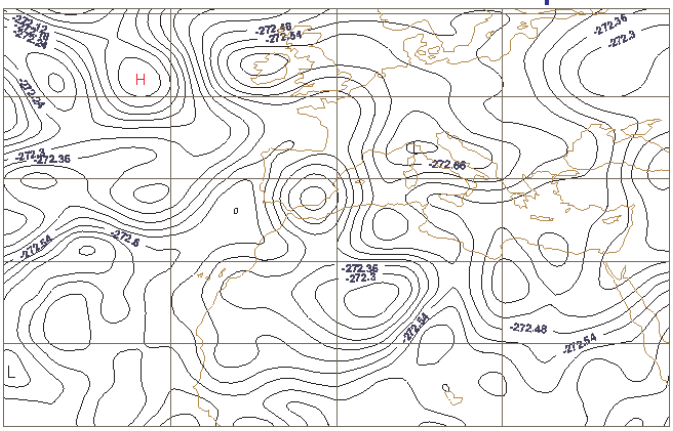

lv27 T 2001-04-24 15h exp:mini

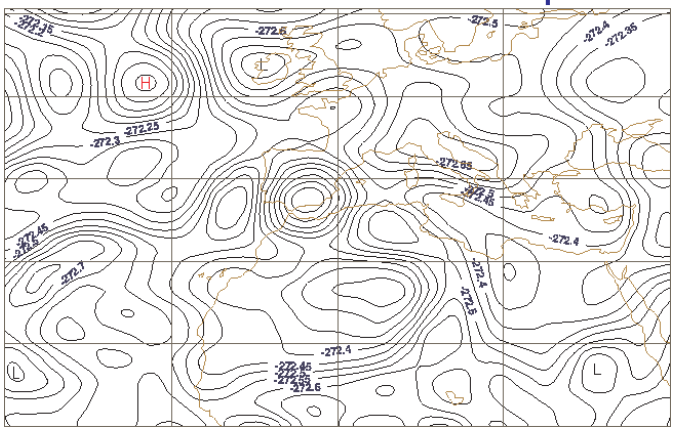

lv28 T 2001-04-24 15h exp:mini

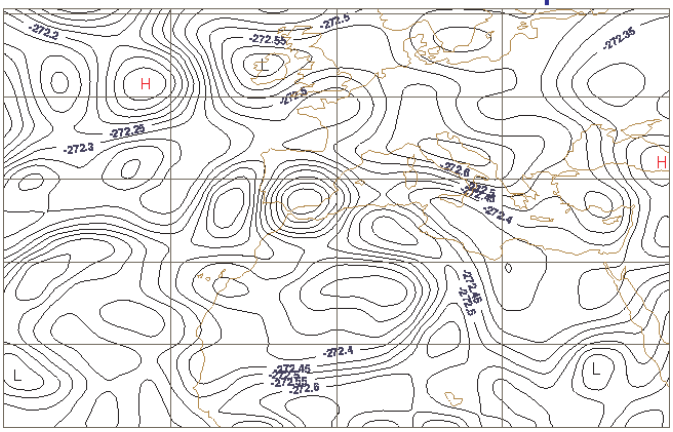

lv1 LNSP 2001-04-24 15h exp:mini

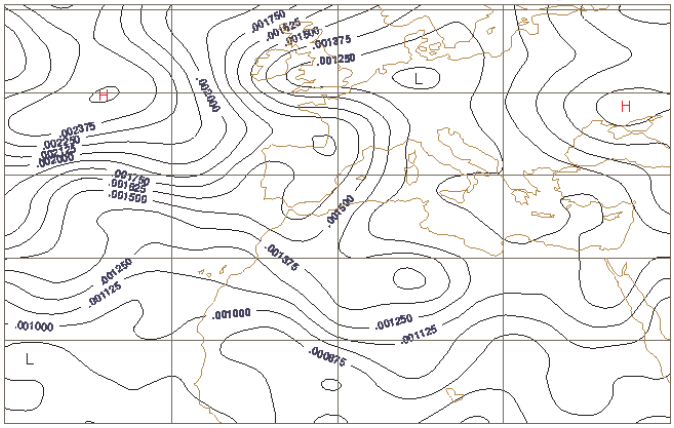

2. Karim BERGAOUI: "Investigation of the potential of a convection scheme using prognostic mass fluxes for NWP in the African-Mediterranean domain"

No research work along these months, devoted to the implementation of ALADIN at INM. However, this was not at all a waste of time, since first a local implementation of the model is of greatest help to work at home, and second the research topic had to be changed after the decisions of the ALADIN-AROME workshop in Prague. The provisional new PhD topic is : Improvement of the analysis of boundary-layer fields considering the anisotropy of surface**.**

First results on compactly-supported background error covariances in ALADIN

Vincent GUIDARD

1. Introduction

Due to biperiodisation and to the length-scales of the structure functions, some problems may occur when using observations near the border of the C+I domain (cf. previous Newsletter).

2. Principle of compactly-supported covariances

Let ENIL1 and ENIL2 be the distance for starting the modification of the covariances and the distance of effective zeroing, respectively. Let *mask* be the mask defined by :

$$mask(x) = \begin{cases} 1 & \text{if } x \leq \text{ENIL1} \\ \frac{1}{2}\left(1+\cos\left(\pi \frac{x - \text{ENIL1}}{\text{ENIL2} - \text{ENIL1}}\right)\right) & \text{if } \text{ENIL1} \leq x \leq \text{ENIL2} \\ 0 & \text{if } \text{ENIL2} \leq x \end{cases}$$

To obtain compactly-supported ("COSU") autocorrelations, one has to apply this mask in the gridpoint space :

$$q_{\text{cosu}}(x, y) = q(x, y) \times mask(\sqrt{(x^2+y^2)}),$$

which is the exact formula if the observation is located at (0, 0). This multiplication corresponds to a convolution in the spectral space :

$$\text{F}(q_{\text{cosu}})(m, n) = (\text{F}(q)*\text{F}(mask))(m, n)$$

According to Gaspari and Cohn (1999), this mask should be applied to the square root of the gridpoint correlations. Therefore, the autocorrelations won't be exactly zero from ENIL2, but from some distance between ENIL2 and 2×ENIL2. Here is the method used in this study, which has been proposed by Loïk Berre :

1. convert the power spectrum into modal variances
2. calculate the square roots
3. fill a 2D spectral array from the 1D square roots of the modal variances
4. convert into gridpoint structure (inverse bi-Fourier transform)
5. mask the gridpoint structure
6. convert back to spectral 2D array (direct bi-Fourier transform)
7. collect isotropically
8. square to obtain modified modal covariances
9. convert into power spectrum

3. 1D model

The 1D model used in this study is a gridpoint model, with 289 gridpoints in the C+I domain and a 11-gridpoints wide E-zone, only used to perform an analysis. It is a uni-variable (so univariate) model. Everything is done in gridpoint space. The formula used for the analysis is :

$$x_a = x_b + B H^{\text{T}} (H B H^{\text{T}} + R)^{-1} (y_0 - H x_b)$$

where x_a is the analysed state, x_b the initial state, H the observation operator, B and R the background and observation error covariances matrices. The observations are given in exact

gridpoint coordinates. *H* only contains 0 and 1 (to select the gridpoints to be compared). *B* is obtained from the actual ALADIN lagged J_b power spectrum of the variable to analyse.

3.1 Modification of the length of the E-zone

The 1D model provides an opportunity to evaluate the impact of an enhancement of the length of the extension zone. In order to mimic such a modification, with constant C+I zone, we have only to modify the horizontal autocorrelations. It has been decided to extrapolate the missing values from the original gridpoint variances. The extrapolated values are all equal to each other and are continuous with the original values.

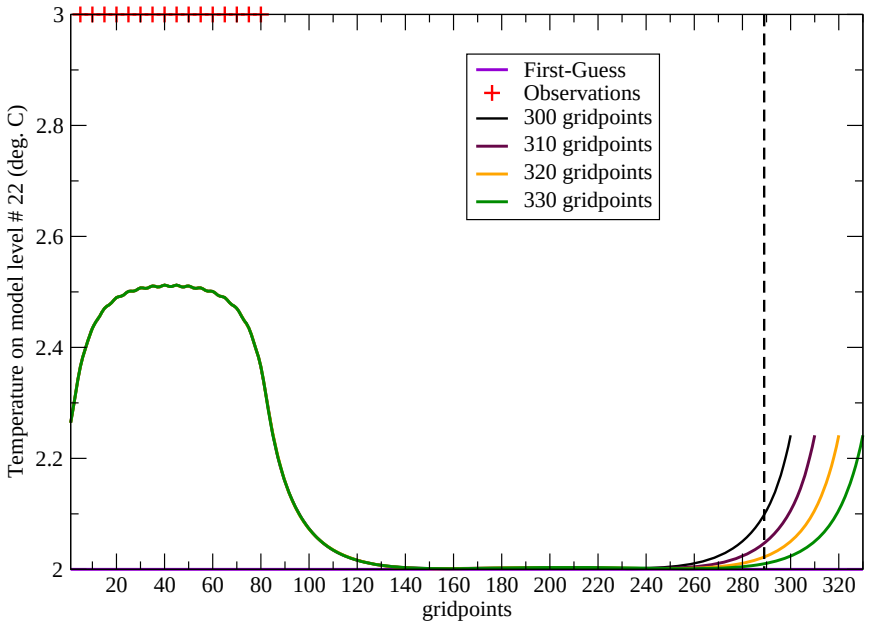

Figure 1 : Observations, first-guess and analysis for various lengths of the E-zone, for temperature on model level # 22.

Figure 1 shows that there is no modification in the neighbourhood of the observations. But the value of the analysis (and the value of the analysis increment) at the border of C+I and E-zones is not the same. The analysis increment at the border can be reduced to 22.5 % of its initial value when using a three times bigger E-zone. Even if it was quite obvious, this is a really positive cure to the "wrap-around" effect due to the biperiodisation.

3.2 Compact support

From now, "no COSU" refers to the original power spectrum, and "COSU xx-yy" refers to compactly-supported autocorrelations with ENIL1=xx and ENIL2=yy (xx and yy are gridpoint values; remember that ENIL2 is the distance of zeroing for the square root of the autocorrelations).

The modified power spectra are obtained following the above-mentioned method. The impact on the power spectrum, for various values of ENIL1 and ENIL2 (and various combinations), is shown on Fig. 2a. In a global overview, since the autocorrelations are compactly supported, the values of the power spectrum for the 3 first total wavenumbers are decreased. There is hardly no change of the power spectrum for total wavenumbers ranging from 40 to 140. Some oscillations appear when ENIL1 and ENIL2-ENIL1 are too small. The tuning "COSU 10-20" is to be rejected, for instance.

To observe the real impact on the autocorrelations in gridpoint space, the power spectra previously generated are converted into gridpoint structures. Figure 2b shows these gridpoint structures for the reference ("no COSU") and various tunings of compact support. First, with a zoom (not shown), one could notice that compactly-supported autocorrelations are not exactly zero. It is due to not totally symmetric steps (direct and inverse Fourier transforms, and fill-in of the ellipse and collect).

But the values for the COSU autocorrelations are quite satisfying : for a distance greater than 50 gridpoints, values are less than 2.10^{-4}, that is to say less than $1/5000^{th}$ of the maximum value. The general impact is as expected.

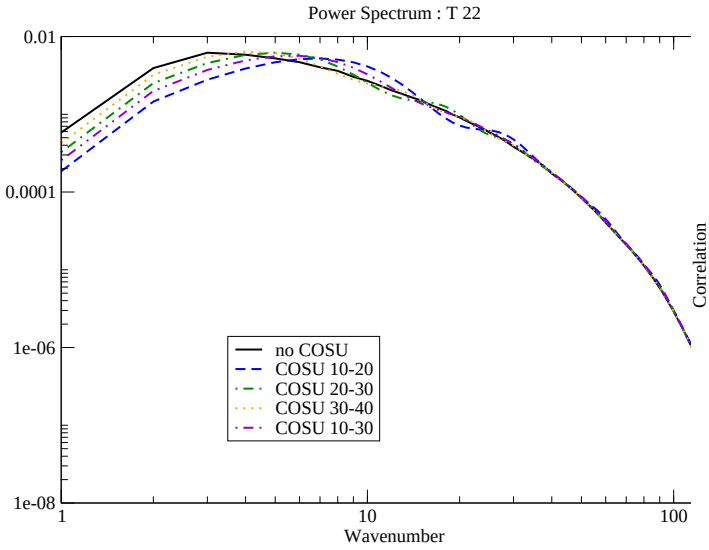

Figure 2a : COSU power spectra for temperature on model level # 22

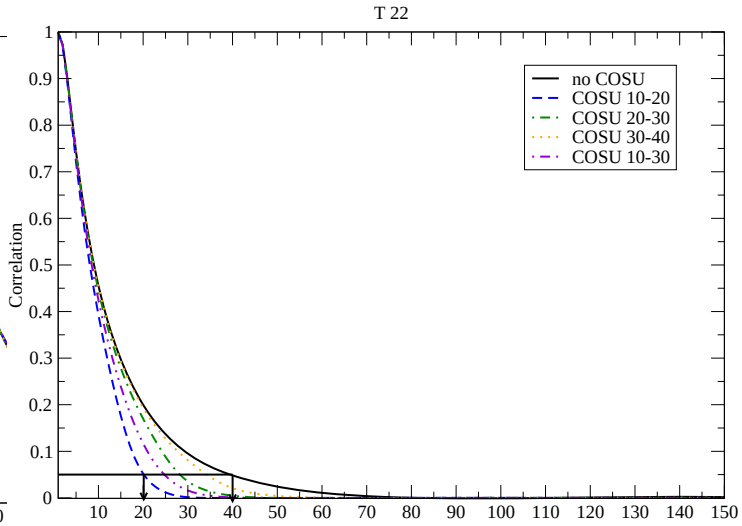

Figure 2b : COSU gridpoint autocorrelations for temperature on model level # 22.

The decrease of the length-scale obtained for the gridpoint autocorrelations is confirmed in the analysis of 15 observations (cf. Fig. 3). The shape of the analysis increment is slightly modified. The values of the analysis increment in the area containing no observations, and far enough from the observations, are efficiently reduced thanks to the compact support. This method also offers a cure to the "wrap-around" effect. The value of the analysis increment at the border between C+I and E zones is 4.5 times smaller in the COSU experiment than in the reference (which is equivalent to the results obtained with the modification of the E-zone length).

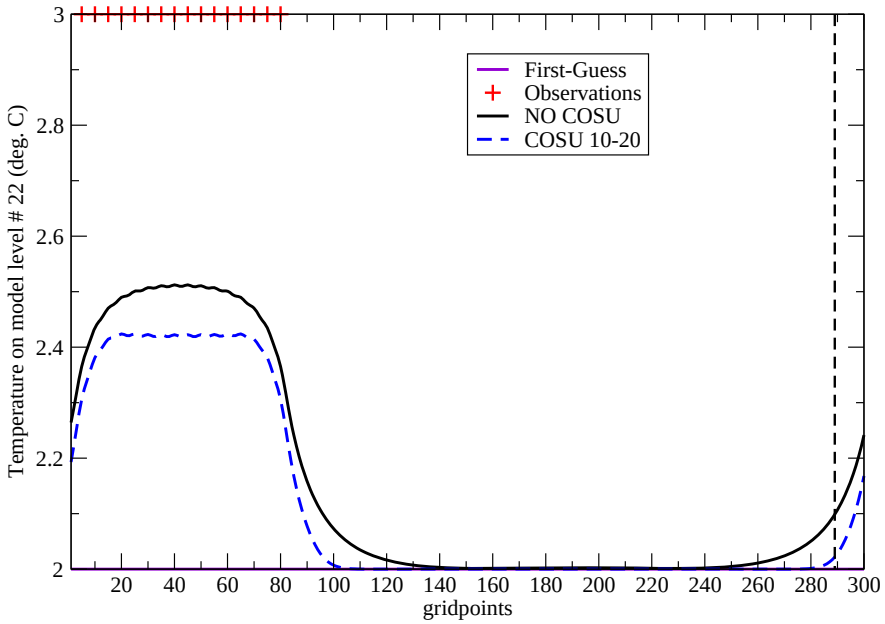

Figure 3 : Observations, first-guess and analysis for COSU and non COSU covariances, for temperature on model level # 22.

4. Implementation in ALADIN

Following both the implementation of compactly-supported horizontal correlations in ARPEGE (cf. routine SUJBCOSU written by François Bouttier) and the first results of COSU horizontal autocorrelations, the SUEJBCOSU routine has been implemented in ALADIN, with the great help of Claude Fischer. Its purpose is to compactly support the horizontal correlations and the vertical cross-correlations (and also the horizontal balance).

4.1 Univariate approach

The univariate case is the closest to what was done in the 1D model. The compact support has only to be applied to horizontal autocorrelations. COSU horizontal autocorrelations imply a damping of residual noise farther than a given distance (between ENIL2 and 2×ENIL2). Some geometric noise still remains (cross centred on the observation, plus a rhombus). But the results are quite the same as in the 1D model and encourage us to run a multivariate 3D-VAR with COSU horizontal autocorrelations.

4.2 Multivariate approach

The multivariate formulation used in this study is based on the work of Loïk Berre (2000). In this section, single observation (of temperature at 500 hPa) experiments are performed and compared through their temperature analysis increment on model level # 15.

Naive first experiments

In this paragraph, only the horizontal autocorrelations are compactly supported. Neither vertical cross-correlations nor balance operators are modified. Some astonishing results are obtained. Though quite few benefits (even neutral results) were expected, "worse" patterns are generated. These results remain unchanged whatever the values of ENIL1 and ENIL2. An explanation could be that the main part of the temperature increment is balanced, while only the vorticity (ζ) horizontal correlations are compactly supported, but not $H_b\zeta$, where H_b is the horizontal balance operator.

Digging a bit deeper

If we consider that the statistical inverse Laplacian H_b and the analytical inverse Laplacian Δ^{-1} are equivalent, $H_b\zeta$ is equivalent to $\Delta^{-1}\zeta$, that is to say the streamfunction. The power spectrum of the vorticity can be modified to obtain COSU horizontal correlations for the streamfunction. Compactly supporting the streamfunction gives neutral results, but it allows to eliminate the "worse and weird" increments. Moreover, using COSU vertical cross-correlations additionally leads to the same results (that is a mostly neutral impact).

Drastic measures

Another point of view, a bit more drastic, is to consider the horizontal balance as an operator which can be compactly supported. The compact support is first applied with "short" ENIL1 and ENIL2 (Fig. 4b, to be compared to the reference, Fig. 4a). This method is really efficient in controlling the length-scale of the increment. Note that COSU horizontal balance is an "antidote" to COSU vorticity horizontal correlations. Other values for ENIL1 and ENIL2 have been tested (not shown). It seems that the length-scale of the horizontal balance is the leading one, as the shape of the increment seems to depend only on what is applied to the horizontal balance. Some experiments using different distances of zeroing for correlations and horizontal balance have been performed. They reinforce the feeling that the horizontal balance is the most important element to be modified to obtain COSU analysis increments.

4.3 Towards operational applications

All these single observation experiments are only a step towards the use of the SUEJBCOSU routine with real observations on real cases. That is why preliminary tests of compactly-supported structure functions are performed (not shown). First, a band of observations (all observation types) over a

southern third of the domain is considered. There are only few changes in comparison to the reference, but the "wrap-around" effect is a bit reduced. As a second step, a 3D-VAR analysis is performed with all observations (i.e. as "usual"). There is *no* modification, despite very short distances of zeroing. This has to be further investigated.

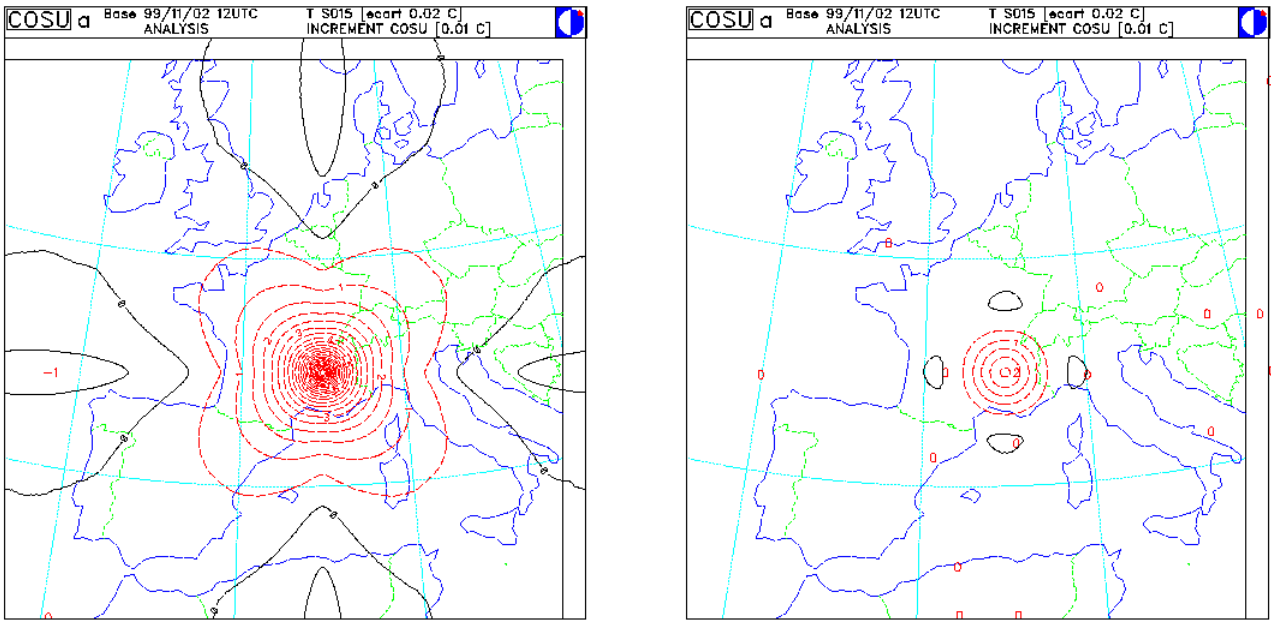

(a) (b)

Figure 4 : Temperature on model level # 15, analysis increment of a single temperature observation at 500 hPa (units : 0.01 K).
(a) reference, with original B; (b) all COSU 10-30 (horizontal correlations, horizontal balance operator).

5. Conclusion

Having a wide enough E-zone is important if all observations inside the C+I domain are used : it prevents the analysis increment from "wrapping around". But, one should be aware of the over-costs generated by a drastic enhancement of the E-zone. In the case of ALADIN with a 289-gridpoints wide square C+I domain, a 320-gridpoints (or more) wide square C+I+E domain is recommended.

To control the length-scale of the increment, compactly-supported horizontal correlations can be used (background statistics). In the univariate case, this is sufficient to have a real control. But in the multivariate case, it appears that, to obtain similar results, the horizontal balance operator has to be compactly supported too. As the distance of zeroing is tunable, one can experiment different values to reach a "realistic" limit. To keep in mind the theoretical benefit of COSU structure functions : for temperature on model level # 22, the distance from which the horizontal correlation is less than 0.05 is 400 km for the original B and *only* 250 km for the COSU 10-30 experiment.

References

Berre, L. (2000). Estimation of synoptic and mesoscale forecast error covariances in a limited-area model. *Mon. Wea. Rev.*, **128**, 644-667.

Gaspari, G. and S. Cohn (1999). Construction of correlation functions in two and three dimensions. *Quart. J. Roy. Meteor. Soc.*, **125**, 723-757.

4. Jean-Marcel PIRIOU: "Correction of compensating errors in physical packages; validation with special emphasis on cloudiness representation"

Precipitating convection:

The cloud ascent in the A*CCVIMP* scheme has been modified, in order to introduce a diagnostic vertical velocity and thus change entrainement / detrainement computations. The sensitivity to the environmental humidity is increased. This work is still under progress.

Diagnosing the tropical diurnal cycle of clouds in ARPEGE:

Hovmöller diagrams of outgoing longwave radiation and precipitation fluxes predicted by ARPEGE have been compared to observed ones.

Intercomparison cases from the EUROCS Research project:

Interaction with the leaders of these 3 cases, as co-author of 3 papers. These papers were submitted to QJRMS in July.

5. Wafaa SADIKI: "A posteriori verification of analysis and assimilation algorithms and study of the statistical properties of the adjoint solutions"

The PhD manuscript is progressing. The defence is scheduled for next year only, for a baby will come very soon.

SEMI-LAGRANGIAN ADVECTION SCHEME WITH CONTROLLED DAMPING - - AN ALTERNATIVE WAY TO NONLINEAR HORIZONTAL DIFFUSION IN A NUMERICAL WEATHER PREDICTION MODEL

Filip Váňa

ABSTRACT

Introduction

Horizontal diffusion schemes have been common features of numerical models since the beginning of NWP. The reason for keeping them in models is to maintain a balance of kinetic energy in the simulated atmosphere between its generation through conversion of available potential energy and its dissipative transformation into thermal energy, in order to be in agreement with so-called "turbulence theories".

The typical representation of the horizontal diffusion contribution is through the $K\nabla^r$ operator. In case the aim of the horizontal diffusion is to maintain suitable kinetic energy and enstrophy spectra, it is sufficient for the diffusion coefficient K to be a constant (Koshyk and Boer, 1995). The same condition for K was found when the horizontal diffusion is seen as a self-corrector of the model (Jakimow et al., 1992). In contrary to both above interpretations, when the horizontal diffusion scheme is seen as a kind of physical parameterisation for horizontal turbulence and molecular dissipation, the diffusion coefficient K should be made flow-dependent (Sadourny and Maynard, 1997).

The spectral representation of the linear horizontal diffusion operator is very efficient and allows infinite possibilities for its tuning (Sardeshmukh and Hoskins, 1984). Similarly, in grid-point models, the linear diffusion can also be treated in a very efficient way (Li et al., 1994, McDonald, 1994). Once a non-linear operator is required to represent the horizontal damping processes, its spectral or grid-point representation becomes relatively expensive. The problem is further complicated by the fact that such a diffusion scheme is generally only conditionally stable.

The aim of this work is to propose, introduce and validate a stable non-linear scheme for horizontal diffusion in any model with semi-Lagrangian advection. The method of this alternative technique is based upon the idea of controlling the degree of interpolation needed for this advection technique (thus the scheme will be hereafter referred as SLHD - semi-Lagrangian horizontal diffusion scheme). Most of the tuning and validation work has been done within the framework of the spectral limited area model ALADIN.

Formulation of the SLHD scheme

The general form of an adiabatic model equation for a prognostic variable Ψ discretised for example by a three-time-level semi-Lagrangian scheme and following the space averaging of the right hand side $\mathcal{R}$ proposed by Tanguay et al. (1992) can be written as:

$$\Psi(\vec{x}, t+\Delta t) = \left[\underbrace{\Psi(\vec{x}-2\vec{\alpha}, t-\Delta t) + \Delta t \mathcal{R}(\vec{x}-2\vec{\alpha}, t)}_{I} \right] + \Delta t \mathcal{R}(\vec{x}, t) \quad . \tag{1}$$

The terms in square bracket marked as I have to be evaluated at point $\vec{x}-2\vec{\alpha}$. This point, known as the origin point, denotes the point from which a particle starting at time $t-\Delta t$ arrives at time $t+\Delta t$ to the grid point $\vec{x}$. Since the origin point is generally off the model grid, some interpolation method has to be used for its evaluation. The interpolator used to be chosen in order not to be too expensive and still accurate enough with respect to the other model simplifications. The compromise is typically a cubic polynomial type interpolator (Staniforth and Côté, 1991).

The semi-Lagrangian diffusion scheme is then simply defined by evaluating the interpolator in equation (1) as a combination of two interpolators:

$$\begin{aligned} I &= (1-\kappa) I_A + \kappa I_D \\ &= I_A + \kappa (I_D - I_A) \quad . \end{aligned} \tag{2}$$

Here I_A is an interpolator of sufficient accuracy for use in the semi-Lagrangian scheme. The interpolator I_D is defined in such a way as to provide a larger degree of damping than I_A. Hence the difference $I_D - I_A$ can be interpreted as an additional damping to the original semi-Lagrangian scheme, introduced by the interpolator I_D. Following the same logic, the adimensional parameter κ can then be seen as the coefficient controlling the degree of this damping.

To be able to use the additional damping of the semi-Lagrangian interpolator I defined in equation (2) as horizontal diffusion scheme, the parameter κ has to be defined according the theory of the fluid dynamics. Sadourny and Maynard (1997) express the sub-grid scale contribution of the horizontal turbulence and molecular dissipation as function of the divergence and of the deformation of the flow. The latter is then fairly more important for the fluids being simulated by atmospheric models. Similarly to this, the parameter κ was defined as function of the scalar quantity representing the total deformation d, defined as:

$$d = \sqrt{\left(\frac{\partial u}{\partial x} - \frac{\partial v}{\partial y} \right)^2 + \left(\frac{\partial u}{\partial y} + \frac{\partial v}{\partial x} \right)^2}, \tag{3}$$

where u and v are the components of the horizontal flow. To avoid any dependency of such a diffusion to the integration timestep Δt, the parameter κ was defined in the following way:

$$\kappa = \frac{F(d)\Delta t}{1 + F(d)\Delta t} \quad , \tag{4}$$

where $F(d)$ stands for any monotonic function of d. In order to make the semi-Lagrangian diffusion scheme also independent of the model resolution, the function $F(d)$ was defined as:

$$F(d) = a \left(\frac{\Delta h_{ref}}{\Delta h} \right)^P \cdot d \left[\max(1, \frac{d}{d_0}) \right]^b \quad . \tag{5}$$

Here a, b and d_0 are tunable parameters for the proposed diffusion scheme while the $\left(\frac{\Delta h_{ref}}{\Delta h}\right)^P$ term ensures the quasi-independence with respect to the chosen model resolution. Δh is a general parameter representing the horizontal model resolution (which is proposed like $\Delta h \equiv \sqrt{\Delta x^2 + \Delta y^2}$ for grid-point models or $\Delta h \equiv \sqrt{k_x^{-2} + k_y^{-2}}$ for spectral models), Δh_{ref} its reference value and P a tunable parameter generally dependent on b. Equations (2) - (5) with the tunable parameters a, b, d_0 and P then fully define the proposed non-linear semi-Lagrangian diffusion scheme.

Idealised frontogenetic simulation by a NWP model

To test the skills and properties of the SLHD scheme the academic 3D Eady wave frontal development was introduced into the spectral limited area numerical weather prediction model ALADIN. Such a situation is very sensitive to the level of model dissipation (MacVean, 1983) and thus tends to be an ideal tool for testing any diffusion scheme in the model. Another advantage of this special situation is its capability to study clearly the impact of model diffusion without harmful feedbacks being generated during the moist diabatic simulation of a "full model".

Otherwise the model used for the simulations was kept as close to a typical NWP operational configuration as possible (resolution of current NWP applications, boundary conditions, coupling and so on...). The only differences occurred in the model geometry (ideal plane, constant Coriolis parameter) and in the definition of simulated atmosphere (dry, no diabatic forcing allowed).

The simulation was performed with the model periodic in the zonal (y) direction. The size of the model domain was defined as 3600 km along the y direction times 9000 km along the x direction with the horizontal resolutions $\Delta x = 20$ km and $\Delta y = 50$ km. Once the non-linear processes start to play a sufficiently important role in the formation of the front, the simulation is repeated on a nested domain with finer uniform horizontal mesh $\Delta x = \Delta y = 10$ km. The distribution of the 41 vertical levels is kept the same for both simulations with the intention to fulfil the theoretical ratio between the horizontal and vertical resolution in the bottom most frontogenetic part of the atmosphere in the nested run. Like that the frontogenetic process is prevented from the generation of spurious destroying gravity waves of numerical origin (Persson and Warner, 1991).

The upper boundary of the frontogenetic area was treated by introducing a slanted tropopause and activating enough horizontal diffusion (the spectral one) for the levels above it.

Even with the nested model, the frontal gradient was not strong enough to impose the model collapse. This is fully in agreement with Garner (1989) concluding that the model horizontal resolution must be at least of order of 1 km to be harmed by numerical instability generated from a simulated frontogenesis. Consequently, the simulated kinetic energy growth rate was at a certain time deviating from its asymptotical theoretical value and the further growth of frontogenetic gradients was stopped, which is also fully in agreement with observations of Gall et al. (1987).

Since the intention was to study the academic experiment with a model similar to any typical NWP application, there was no space to create the model numerical instability causing at a given time the collapse of the model. Thus, instead of measuring the time of the model collapse as a function of level of horizontal diffusion, a special statistical tool has been developed to diagnose the impact of any horizontal diffusion scheme acting in this model. The diagnostic simulation was then defined as the 12 hour simulation of the nested model before the maximum gradient was reached. This diagnostic was found sensitive enough to any horizontal diffusion scheme used in the model.

As diagnostic output, the kinetic energy spectrum of the lowest (most frontogenetic) model level has then been used.

Method for computing the parameters of an equivalent diffusion

As a measure to quantify the observed diffusivity of any diffusive feature within the academic diagnostic simulation, a statistical tool was introduced. Its aim is to fit the unknown diffusivity by a spectral linear diffusion with the closest possible properties. This simple approach allows to express any model damping scheme by the well-describing parameters of a linear diffusion scheme: the coefficient of diffusion K and the order of diffusion r. Since the non-linear effects of horizontal diffusion start to be important with high model resolution (around 1 km of horizontal mesh) it is believed that the performance of the proposed SLHD scheme can be fitted by the linear diffusion without any loss of relevance in the framework of the academic simulation running at 10 km of horizontal mesh.

The principle of the proposed method is to decompose the resulting kinetic energy spectra of the idealised simulation as sums of the kinetic energy spectra of simulations without any horizontal diffusion scheme and of a remaining part proportional to the used diffusion. It is known that the logarithm of kinetic energy spectra is close to a linear function of the logarithm of wave-number. Hence the statistical model has been built on logarithms of the kinetic energy spectra, rather than just on kinetic energy spectra themselves. Once the spectral coefficients of the kinetic energy have been recomputed from the kinetic energy values for the elliptic bands corresponding to the zonal wave-numbers of the model, the logarithm of such spectra can be expressed as: $(\log \psi^m = \log \psi_0^{(m)} - \Delta\psi^{(m)})|_{m=0}^{M}$. Here $\psi_0^{(m)}$ represents the resulting spectrum of the model without diffusion scheme, $\Delta\psi^{(m)}$ the influence on $\log \psi^{(m)}$ caused by the tested diffusion scheme and M is the total truncation of the model. The statistical model has

thus been built as the linear regression of all combinations of parameters of spectral linear diffusion r and $\mathcal{H}$ up to third order:

$$\log \psi^{(m)} = \log \psi_0^{(m)} - \sum_{i=0}^{3} \sum_{j=0}^{3} a_{ij}^{(m)} r^i \mathcal{H}^j \quad . \tag{6}$$

The parameter $\mathcal{H}$ is derived from the horizontal diffusion coefficient K which is, for the ALADIN model, with a given truncation and at any given model level fully determined by just r and $\mathcal{H}$.

The values of the parameters $a_{ij}^{(m)}$ were then set according to the spectrum of 150 experiments with spectral linear diffusion with known parameters r and $\mathcal{H}$. The statistical model correlation was for all wave-numbers at least 0.9, which allows to use this model in the following with confidence in its relevance.

Knowing the values of $a_{ij}^{(m)}$, the properties of an unknown diffusion can then be characterised by most closely fitting the parameters of spectral linear diffusion r^* and $\mathcal{H}^*$ by solving the following minimising formula:

$$\sum_{m=1}^{\mathcal{M}} \frac{\log\left(\psi^{*(m)}\right) - \log\left(\psi_0^{(m)}\right) + \sum_{i,j=0}^{3} a_{ij}^{(m)} r^{*i} \mathcal{H}^{*j}}{\log\left(\psi_0^{(m)}\right)} = \min \quad . \tag{7}$$

Behaviour of the SLHD scheme in the ALADIN model

The SLHD scheme defined by equations (2) - (5) is not fully specified unless the interpolators I_A and I_D are defined. When introducing this scheme into the model ALADIN, its standard semi-Lagrangian interpolator (Ritchie at al., 1995) was set as the accurate interpolator I_A. The linear interpolator was then used as the damping interpolator I_D.

To study the property of the SLHD scheme, 90 experiments with different sets of tunable constants a, b and d_0 were launched in the framework of the idealised 3D frontal development. The damping characteristics of this scheme then were estimated by the best fitting parameters of spectral diffusion r^* and $\mathcal{H}^*$. The results of 66 from all, with r^* and $\mathcal{H}^*$ falling inside the values of the statistical model were then plotted in the $\mathcal{H}$-r plane.

As expected the strongest diffusion obtained by the SLHD scheme corresponds to the damping characteristics of the interpolator I_D. Weakening the diffusion by allowing an increasing proportional participation of the interpolator I_A to the resulting semi-Lagrangian interpolator I, the characteristic points on the $\mathcal{H}$-r plane were distributed along a specific curve starting at the characteristic point of I_D. Further diagnostics showed that the main factor influencing the position of the characteristic points on the $\mathcal{H}$-r plane is the average value of the κ coefficient. This implies that there is just one degree of freedom between the characteristics r and $\mathcal{H}$ of the SLHD scheme. Thus, from

the damping point of view, just one tunable constant would be sufficient to control the properties of the SLHD scheme.

Another important outcome from the above is the fact, that the SLHD scheme is, within usable model damping rates, always less selective than the operational 4^{th} order diffusion.

When testing performances in the framework of real atmospheric simulations, the following two main differences were found with respect to the academic case behaviour.

First, in order to obtain the same amount of kinetic energy as with the spectral diffusion with the characteristics of the best fitting parameters r^* and $\mathcal{H}^*$ measured in the framework of the academic experiment, the SLHD scheme has to be tuned to much stronger values. The reason for this comes from the dependency of the properties of the SLHD scheme upon the average of the field of total deformation d of the simulated atmosphere. Due to the very specific case simulated by the academic test, the values of d were about one order of magnitude greater than the ones reached in the real atmospheric simulation. Consequently the SLHD diffusion tuned for the extreme values of d in the academic simulation would act in a much weaker way in the real atmosphere characterised by lower values of the d field.

Beside this first difference, which seems to be just a problem of tuning, the second factor responsible for a different behaviour of the SLHD scheme in real atmospheric conditions from that in the academic environment seems to be of a more systematic nature. As seen from the equation (1) the SLHD diffusion modifying the semi-Lagrangian interpolators affects just one part of the value for the prognostic field $\Psi(\vec{x}, t + \Delta t)$. The remaining part unaffected by this diffusion is represented by the last term $\Delta t \mathcal{R}(\vec{x}, t)$ on the right hand side. Analysing this residual for each model equation, one can find that the prognostic equation for the components of the horizontal wind contains the derivatives of the model orography. This field, obviously constant during the model integration, has been found as a source of noise that couldn't be treated by the SLHD scheme. To remove such a weakness of the proposed diffusion scheme two solutions have been proposed, from which none is ideal. First the model orography could be filtered in such a way to be in equivalent spectral slope to the expected kinetic energy spectral tail. The second solution is to keep in the model another (weak and selective) diffusion scheme controlling the tail of the kinetic energy spectra together with the SLHD one.

Since there are several numerical reasons to keep a spectral diffusion in the ALADIN model even if the physical contribution of the horizontal dissipation would be represented by another device on top of SLHD, the second solution to control the small-scale kinetic energy waves seems to be clearly preferable.

Aspects of the implementation of the SLHD scheme into the ALADIN model

On top of the described parameters controlling the performance of the SLHD diffusion scheme, some other technical parameters have been coded during the implementation

of the scheme into the ALADIN NWP model. One of them works as a limitation for the SLHD "coefficient of diffusion" κ prescribing a maximum value for this parameter. The reason for its implementation into the source code is the opportunity to guarantee a minimum amount of interpolation by the accurate interpolator I_A. Another technical parameter specifies the additional diffusion that can be used for the boundary points for which the semi-Lagrangian trajectory originates outside the model domain.

Since the SLHD scheme depends on the used interpolators I_A and I_D, the spectral sensitivity of the different interpolators available in the ALADIN code - the cubic Lagrangian, the four-point spline and the linear interpolator - has been investigated within a special 1D experiment. From there the specific sensitivity of the four-point natural cubic spline has been detected. This interpolator was found to behave similarly to the linear interpolator for the long waves, with one order higher accuracy. There the cubic Lagrangian interpolator sensitivity to the wave number is different and the accuracy is about two orders higher than for the four-point spline. Once the waves from the middle of the spherical expansion with the quadratic truncation (with wavelength about twice and less the minimal wavelength represented by the last term of the expansion) are interpolated, the four-points spline starts to perform interpolation with higher accuracy as compared to the other two tested interpolators. This trend is kept till the smallest scales represented by the model spectrum, but the differences in accuracy are decreasing there for all methods. Such a result seems to be promising for giving the possibility to impact the waves from the middle of the spectral expansion if introducing the four-point spline interpolator as the accurate interpolator I_A. Unfortunately there is not much space to impact the small-scale end of the model spectra by any of these interpolators.

Finally the coexistence of the spectral horizontal diffusion and of the SLHD scheme in the model is described. As already mentioned, when the SLHD scheme, acting like the model physical diffusion, is activated, there is still need to keep the spectral diffusion to remove the numerical noise. For such a case the spectral diffusion is kept untouched in the high atmosphere where it plays an important role as the damping mechanism for gravity waves of numerical origin. In the low atmosphere where the numerical reason for keeping it in the model is just its role to remove the small scale noise caused by orography in the fields of components of wind, this linear diffusion is weakened and made very selective, if not suppressed completely in the case of temperature and moisture fields for example.

Validation of the SLHD scheme

Once implemented in the ALADIN model, the new horizontal diffusion has been validated. Two kinds of validations have been proposed: the parallel run with the spectral horizontal diffusion for a random period and the verification of the scheme's ability to act in specific case studies sensitive to the level of horizontal diffusion in a model.

For the parallel test, the three configurations of horizontal diffusion have been used, running with the ALADIN/LACE operational domain (Janoušek, 1999). As reference

run, the spectral linear horizontal diffusion representing the current operational scheme was taken. The SLHD diffusion scheme with the additional weak and selective spectral diffusion controlling the tail of the model spectra was used as the second test. Finally the third test used just the SLHD diffusion scheme in the troposphere with the orography field filtered by a relatively strong 5^{th} order spectral diffusion (the last wave-number had been reduced to 40 % of its original value). As testing period, the 20 days between March 3^{rd} and March 22^{nd} 2000 were randomly chosen.

The evolution of scores (BIAS and RMSE) behaved for all three runs in very similar way during the testing period. The differences were very small if ever detectable. This is not surprising with the 12.18 km of horizontal resolution of the ALADIN/LACE model, which is far from the scales where the non-linear effects in horizontal dissipation are of theoretical importance. Anyway a few deviations have been detected between the SLHD and the spectral diffusion scheme. First the BIAS of the MSL pressure is systematically worsening during the model simulation for the SLHD scheme compared to the reference. This feature is a consequence of the local character of the grid-point diffusion that is not conserving the mean of the diffused fields contrary to the globally acting spectral diffusion. On the other hand the SLHD scheme is formulated in a more accurate way with respect to the orographic features than the spectral diffusion acting along the quasi-horizontal terrain-following model levels. Hence the RMSE of the MSL pressure is nearly the same for all three tests. The lower conservative properties of the grid-point SLHD are compensated by the more accurate formulation of horizontal dissipation over the orographic features. Second a slight tendency of cooling the atmosphere is detected in the areas where the SLHD scheme acts as the main damping scheme. This (positive) impact on the model scores is probably a consequence of the 3D formulation of the SLHD diffusion, which is smoothing as well along the vertical and thus completing the vertical diffusion as parameterised by the model physics. The role of controlling the temperature dissipation through the flow deformation when the SLHD scheme is acting might be important as well.

The above differences were highlighted by the test of the SLHD diffusion without spectral supplement in the low atmosphere. Surprisingly, this run was not resulting in bad scores for the upper atmosphere. The smoothing of the model orography affected just the near surface variable (mainly wind field) and the geopotential in the low troposphere (between surface and 700 hPa).

Contrary to the parallel tests meant to detect some systematic tendencies, case study simulations can show the ability of a studied scheme with respect to situations for which it is specially suited. As shown for example by MacVean (1983) and Hello et al. (1999), cyclogeneses simulated by a numerical model are sensitive to the model diffusion scheme. To test the benefits of the proposed SLHD scheme several cyclogenetic situations as well as events on very small scales have been studied. Most of them showed no impact with respect to the spectral diffusion scheme used as the reference. The reason was mainly due to the fact that cyclogenesis is a consequence of the large scale forcing, thus its simulation in the limited area model is extremely dependent upon the initial and lateral boundary conditions. However a few cases of very local character or from meso-cyclonic development and sensitive to the model horizontal diffusion scheme

could be found, even when using the simulation within a relatively small domain like for the operational ALADIN models.

The first presented case study concerns the storm from December 26^{th} 1999. This time the strong meso-cyclone was created just to the west of the French Atlantic coast. The cyclone was moving eastward with a speed of about 100 km/h. This event was very well forecast by the operational ALADIN applications covering the affected area, as well as by the coupling model of ALADIN - the French global model ARPEGE. The simulation was provided with the ALADIN/LACE operational domain. The cyclone enters this domain already developed but continuing its development. Both diffusion schemes (SLHD and spectral diffusion) produced very similar results. The maximum difference between the two simulations appeared 9 hours after the cyclone entered the model domain. The difference in the MSL pressure was less than 2 hPa. After another 12 hours of integration the minimum value of MSL pressure in the centre of the cyclone was about the same in both cases.

The case just mentioned exhibits that the two different diffusion schemes can act very similarly for an event that has been successfully forecast by the model in both cases.

The ensuing case was, contrary to the previous one, unrealistically exaggerated in the operational configuration of ALADIN/LACE. The small meso-cyclone appearing during July 20^{th} 2001 in the Adriatic sea approached the Dalmatian cost with a lowest value of MSL pressure of about 1006 hPa. The ALADIN/LACE forecast with the spectral diffusion simulates this event with a lowest MSL pressure value of 990 hPa. Of course, such a low was in the model simulation accompanied by extreme weather events, which didn't occur in reality. When applying the SLHD scheme to this forecast the depth of the low was reduced to 1004 hPa. Further analysis of the model simulation showed that this kind of locally acting diffusion prevents a strong and unrealistic stratiform precipitation generation in the model behind the moving cyclone. The analysis of the potential vorticity in the atmosphere clearly exhibited that for this case the SLHD scheme with an equivalent strength to the operational spectral diffusion significantly improved all the tropospheric part of the atmosphere in the vicinity of the simulated low.

The last presented situation concerns a small-scale event again not really well simulated by the ALADIN/FRANCE operational forecast. During the August 24^{th} 2001 12 UTC simulation, 3 hours after the model start an extreme and unrealistic downburst developed above the Atlantic ocean westwards from Gibraltar. This event was of very local character (horizontal scale of about 100 km). Even if the reason for this event can be traced to some other part of the model (mainly the stratiform precipitation), the (spectral) horizontal diffusion scheme was felt to act too weakly. When the SLHD scheme of similar impact on the model kinetic energy spectra was used to recompute this situation, the descending motions were reduced by 35 % . A similar impact could be reached with the spectral horizontal diffusion tuned to be eight times stronger than the operational one. But this re-tuning of course affected drastically the whole kinetic energy spectrum (and thus as well the quality of the model forecast), which was not the case for the locally acting SLHD diffusion.

Conclusion

A new alternative way to the horizontal diffusion treatment in numerical models using semi-Lagrangian advection has been proposed. The scheme was diagnosed in the framework of a specific academic testing tool specially developed for the purpose of this work. Then the behaviour of the scheme was studied in the real atmosphere. Finally the scheme was validated with respect to the spectral linear diffusion scheme in a parallel test as well as for several specific case studies.

The properties of the proposed diffusion scheme are of such nature that they make this scheme to be advantageous mainly for the numerical weather prediction applications. The new scheme offers the following pleasant technical aspects for horizontal diffusion in a model. First to incorporate such scheme into a semi-Lagrangian model is from the technical point of view very easy. Moreover, except the semi-Lagrangian model advection, the SLHD diffusion implies no other restriction for the model dynamics. Second the computational cost of the SLHD scheme is mainly limited by the time spent for additional interpolations of the semi-Lagrangian amounts by the diffusive interpolator I_D which is typically a cheap (tri-)linear interpolator. Similarly to the spectral diffusion scheme, the computational cost of the SLHD scheme is fixed with respect to its chosen selectivity. Third the proposed diffusion scheme is unconditionally stable in the sense of damping characteristics. Its stability restriction is given by the stability criteria for the semi-Lagrangian advection. Consequently the model timestep is generally not more restricted when the SLHD scheme is activated in a model than without it.

For spectral models the SLHD scheme offers other clear advantages compared with the spectral linear diffusion schemes typically used there. First the SLHD scheme proposes a stable and efficient way for a non-linear and thus more realistic description of the effects of horizontal dissipation processes. Although it is believed that non-linear effects don't play any important role on horizontal scales like 10 km and bigger, it has been demonstrated that for some extreme situations they can be of specific importance. However with the increasing model resolution, the importance of non-linear horizontal dissipation will be constantly growing. Second the grid point formulation of the SLHD scheme allows to use this scheme for representing the horizontal damping of those variables which are not passing through spectral space (i.e. atmospheric liquid water and ice, pollutants,...). Third the grid point character of the SLHD diffusion scheme enables efficiency and accuracy when forcing diffusion to be homogeneous over a variable mesh, by making it easily resolution dependent.

As usual, the proposed scheme brings also some disadvantages when comparing it to the separate sophisticated diffusion schemes. The main two of them are as follows. The way by which the proposed SLHD scheme makes the spectra of kinetic energy (or the horizontal components of the flow field) dependent on the small scale spectra of the model orography. To be able to control these model variables therefore requires either to significantly filter the model orography or to add another horizontal diffusion scheme removing the small-scale noise of the kinetic energy spectra. The second limitation of the proposed SLHD scheme is its limited tuning possibilities. In case the influence

of a diffusive scheme is characterised by the coefficient of diffusion and the order of diffusion, the SLHD scheme makes one of them to be fully expressed as a function of the other. To change the property of a given SLHD characteristic function is indeed possible just by changing the semi-Lagrangian interpolators. This is from a practical point of view rather uncomfortable.

The proposed SLHD scheme however seems to be a viable alternative to the currently used diffusion schemes in numerical models. Its benefit arises mainly from the fact that it reverts the known disadvantage of the semi-Lagrangian advection - the additional non-excessive damping - to an advantageous control of the complex separation between the model signal keeping predictive skills and the noise.

References

R. L. Gall, R. T. Williams, and T. L. Clark.
On the minimum scale of surface fronts.
J. Atmos. Sci., 44(18):2562–2574, September 1987.

S. T. Garner.
Fully Lagrangian numerical solutions of unbalanced frontogenesis and frontal collapse.
J. Atmos. Sci., 46(6):717–739, March 1989.

G. Hello, F. Lalaurette, and J.-N. Thépaut.
Combined use of sensitivity information and observations to improve meteorological forecast: A feasibility study applied to the "Christmas storm" case.
Quart. J. Roy. Meteor. Soc., 126:621–647, January 2000.

G. Jakimow, E. Yakimiw, and A. Robert.
An implicit formulation for horizontal diffusion in gridpoint models.
Mon. Wea. Rev., 120:124–130, January 1992.

M. Janoušek.
National status report of Czech Hydrometeorological Institute.
In *EWGLAM newsletter*, number 29, pages 55–56, 1999.

J. N. Koshyk and G. J. Boer.
Parameterization of dynamical subgrid-scale processes in a spectral GCM.
J. Atmos. Sci., 52(7):965–976, April 1995.

Yong Li, S. Moorthi, and J. R. Bates.
Direct solution of the implicit formulation of fourth order horizontal diffusion for gridpoint models on the sphere.
Tech. Memo 109466 Vol. 2, NASA, December 1994.

M. K. MacVean.
The effects of horizontal diffusion on baroclinic development in a spectral model.
Quart. J. Roy. Meteor. Soc., 109:771–783, 1983.

A. McDonald.
Using second, fourth and sixth order implicit horizontal diffusion to control noise in three dimensional semi-Lagrangian, semi-implicit, limited area, gridpoint models of the primitive equations.
Technical report, Irish Meteorological Service, 1994.
Unpublished note.

P. O. G. Persson and T. T. Warner.
Model generation of spurious gravity waves due to inconsistency of the vertical and horizontal resolution.
Mon. Wea. Rev., 119:917–935, April 1991.

H. Ritchie, C. Temperton, A. Simmons, M. Hortal, T. Davies, D. Dent, and M. Hamrud.
Implementation of the semi-Lagrangian method in a high-resolution version of the ECMWF forecast model.
Mon. Wea. Rev., 123:489–514, February 1995.

R. Sadourny and K. Maynard.
Formulations of lateral diffusion in geophysical fluid dynamics models.
In *Numerical methods in atmospheric and oceanic modelling - The André J. Robert memorial volume*, pages 547–556. NRC Research Press, 1997.

P. D. Sardeshmukh and B. J. Hoskins.
Spatial smoothing on the sphere.
Mon. Wea. Rev., 112:2524–2529, December 1984.

A. Staniforth and J. Côté.
Semi-Lagrangian integration schemes for atmospheric models - a review.
Mon. Wea. Rev., 119:2206–2223, September 1991.

M. Tanguay, E. Yakimiw, H. Ritchie, and A. Robert.
Advantages of spatial averaging in semi-implicit semi-Lagrangian schemes.
Mon. Wea. Rev., 120:113–123, 1992.

1. Steluta ALEXANDRU : "Scientific strategy for the implementation of a 3D-VAR data assimilation scheme for a double nested limited area model"

Forecast of the Czech floods from August 2002
using the 3D-Var scheme for the ALADIN model

Introduction

A data assimilation system based on a three-dimensional variational (3D-Var) scheme is being developed for the ALADIN mesoscale limited area model (LAM). The scheme was applied for ALADIN/Hungary, which is a double-nested mesoscale LAM. The aim of the new experiments was to compare the forecast of the model using the 3D-Var scheme, with the one in dynamical adaptation mode (which is the operational system of the ALADIN/Hungary model at the moment), for some interesting meteorological situations. The case studies have been chosen on the one hand, when the operational model failed to provide a good prediction and on the other hand, when the operational forecast was considered reasonably good.

In a previous ALATNET report (Alexandru, [2] 2003) a case study from the first category has been presented. For the second one, the Czech floods from the 11-13th of August 2002 have been chosen to be analysed using the 3D-Var scheme.

A short description of the synoptic situation of these floods is presented below. There were two events. The first one was on the 6-7th of August, when a high altitude low-pressure system from the Gulf of Genoa reached the area of Alps causing heavy rain and thunderstorms in Austria. The quantity of precipitation decreased temporarily between the 8-10th of August in the Alps. Then the second event was between 11-13th of August, when a new active cyclone reached the upper parts of the Danube. The motion of the cyclone slowed down and its occluded front spread over the central part of Austria and the Czech basin for almost three days. As an effect of this stationary front, the quantity of precipitation was significant in Austria, Bavaria and Bohemia, i.e. 100-150 mm in 24 h, and in some places more than 300 mm (Fig. 1). (IABM, 2002).

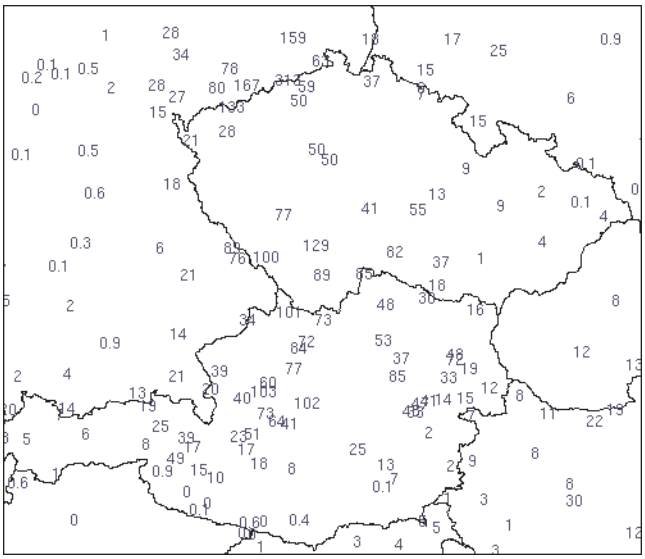

Figure 1 : The quantity of precipitation (mm/24h) measured over Austria and Czech Republic between 12.08 06 UTC - 13.08 06 UTC

3D-Var experiments

For this case study, two sets of experiments using 3D-Var were carried out. The first set was performed using the operational lateral boundary conditions (LBC) for ALADIN/Hungary (from the ALADIN/LACE model) and the SYNOP and TEMP data available at the Hungarian Meteorological Service (HMS). From SYNOP observations, temperature and relative humidity have been considered, and from TEMP ones, wind, geopotential, temperature and relative humidity. Hereafter the name of this set of experiments is "*3dvar(T,RH)*". As coupling strategy, time-consistency has been chosen both in cycling and in production (Alexandru, 2002).

The other set of experiments which has been carried out, was similar to the "*3dvar(T,RH)*" set, with LBC provided by the ALADIN/LACE model and data from HMS, keeping the same variables from TEMP, but using only geopotential from SYNOP observations. The notation is "*3dvar(Z)*".

Later we discovered that generally the temperature and relative humidity from the SYNOP observations is not analysed in the assimilation cycle for the ARPEGE model, because they can cause some spurious features in the upper troposphere. As the first set of experiments has been already performed at that time, we decided to present here these results also.

In both sets of experiments, the standard NMC statistics (Parrish and Derber, 1992) have been used. The reference of these experiments was the operational forecast of the model in dynamical adaptation ("*oper*"). The assimilation cycle was started from 07.08.2002 06 UTC, i.e. four days before the event. Further mainly the results from the "*3dvar(Z)*" set will be shown.

Results

For this case study, the forecasts for different fields from 11.08 - 12.08, 00 UTC and 12 UTC model runs, have been analysed. In order to point out the location of the event, the maps with the 24 h cumulated precipitation have a zoom between 45°-52° N in latitude and 10°-20° E in longitude.

11.08 00 UTC run

The forecast from this model run shows the beginning of the second flood, started over Austria, and moving to the Czech Republic. Both models, with and without data assimilation, predict a low-pressure system located in the southern part of the Czech Republic.

The area where the moisture is available, is very large, covering the western part of Austria, Bavaria, Saxony and the western part of Czech Republic. The air masses have here an intensive vertical motion (up to 6.5 Pa/s). So there is an increased likelihood that heavy precipitation will develop.

All three experiments overestimate in some places in Austria the quantity of precipitation, predicting more than 200 mm in 24 h (the real measurements being around 100 mm). But the location of the rainfall is well forecasted. Moreover this model run gives the first indication of the new location of the heavy rainfall over the border of Germany and Czech Republic.

One can say that the models, with and without data assimilation, succeeded to give a good forecast of the beginning of these floods.

11.08 12 UTC run

Both models show the air streaming from North-West, bringing cold air especially in the western part of Czech Republic. The low-pressure system has deepened in-between and moved more to the South, in the north-western part of Hungary.

The operational and 3D-Var forecasts of relative humidity at 700 hPa surface show the same pattern of high humidity (the northern and western parts of Austria, Bohemia and Saxony). The air masses have also an intensive vertical motion in those areas, reaching values as 5 hPa/s. These indicate that a heavy rainfall is likely to occur.

The quantity of precipitation, cumulated for 24 h, between 12.08 06 UTC and 13.08 06 UTC (Fig. 2), reaches values bigger than 100 mm in Austria, which is very close to reality. All experiments predict a significant quantity of precipitation in some places over the border of Germany and Czech Republic (more than 100 mm in 24 h). Indeed in that region the real maximum was 313 mm, so the forecast underestimate it, but still the models give an indication of the intensive rainfall. More to the East, one can see an area of heavy precipitation, forecasted by all experiments, probably, as the maximum of the event. Unfortunately the location is too far. In the central part of Czech Republic, a significant quantity of precipitation has been forecasted.

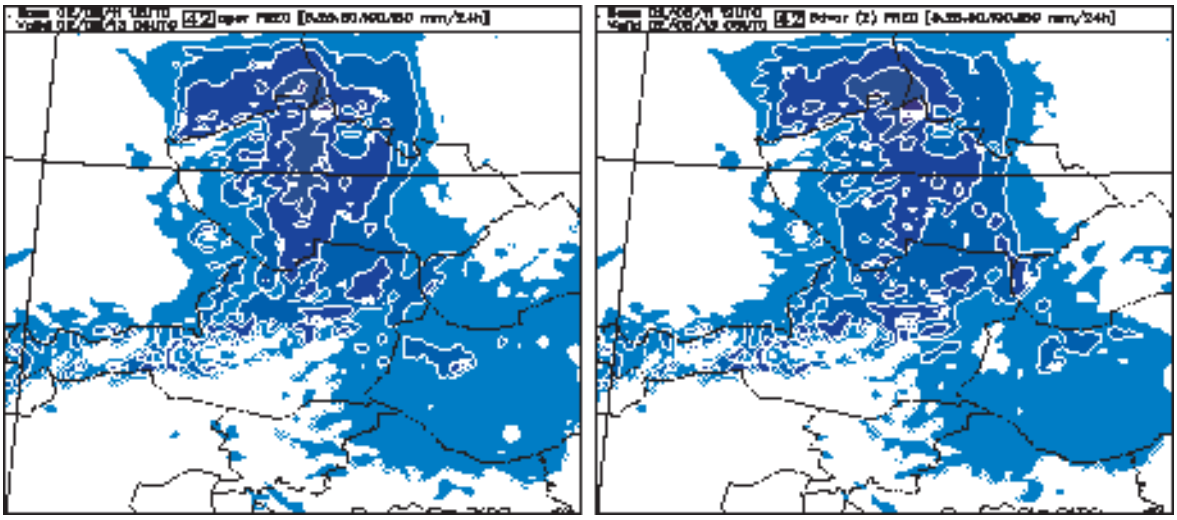

Figure 2 : The quantity of precipitation (mm/24h) forecasted by the operational model (*oper*) and using 3D-Var scheme (*3dvar(Z)*) between 12.08 06 UTC - 13.08 06 UTC, from 11.08 12 UTC model runs.

It can be concluded that the forecasts of the two models, with and without 3D-Var scheme, are comparable. They did not succeed to predict the real quantity of precipitation over the border of Germany and Czech Republic, but still this was more than 100 mm in 24 h. The location of the maximum of the event was forecasted more to the East.

12.08 00 UTC run

The direction of the cold air remains north-westerly. The low-pressure system begins to fill in, progressing on a north-eastward track. The differences between the operational forecast and those using the 3D-Var scheme for geopotential are less than 2 damgpm.

The area of high humidity starts to decrease comparing to the forecast from the previous run. But still in the northern and western parts of Austria, Saxony and Bohemia, the sky is mostly cloudy. Strong ascending motion has been forecasted in these regions.

Figure 3 shows the precipitation cumulated in 24 h between 12.08 06 UTC and 13.08 06 UTC. In some places in Austria, the quantity of precipitation is more than 100 mm in 24 h, which is a slight overestimation, compared to real measurements. Unlike the previous run, all the models predict the right place of the rainfall in Saxony, where values like 296 mm in 24 h are shown. The operational forecast has the closest value to reality. But also the 3D-Var experiments predict an important quantity in that area. A good prediction of the rainfall over Bohemia has been performed by the "*3dvar(Z)*" experiment. The other sets overestimate the quantity of precipitation, predicting more than 150 mm, comparing with real measurements like 50 mm.

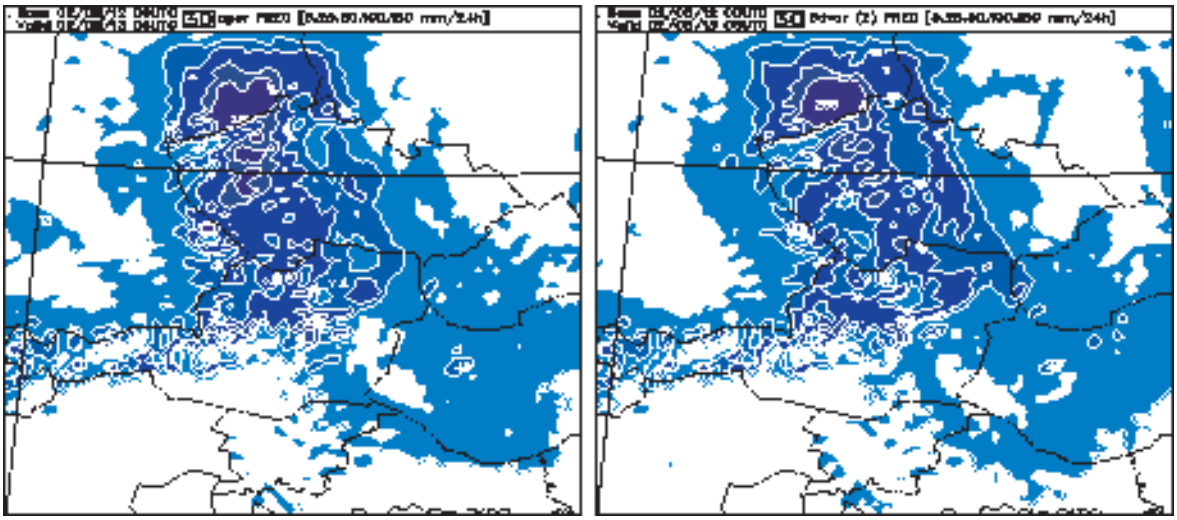

Figure 3 : The quantity of precipitation (mm/24h) forecasted by the operational model (*oper*) and using 3D-Var (*3dvar(Z)*) between 12.08 06 UTC - 13.08 06 UTC, from 12.08 00 UTC model runs.

One can see over the border of Poland and Czech Republic, an area with 100 mm precipitation forecast. The quantity is overestimated, in reality it hasn't been more than 37 mm. But it is an indication of the new place where significant rainfall is expected.

In conclusion one can say that all three sets of experiments had shown a good forecast of the event. The great quantity of precipitation has not been predicted exactly, but it was significant, giving warning to the forecasters about the future flood.

12.08 12 UTC run

The last model run showed that the low-pressure system continued to move in a north-eastward direction. The pressure gradients weakened and the winds subsided, so the cyclone begins to fill in. The differences between the operational forecast for geopotential and those using 3D-Var are very small, less than 1 damgpm.

The models predicted almost the same quantity of precipitation, and the location is also similar. Comparing to reality, the models in dynamical adaptation and using the 3D-Var scheme, showed an underestimation of the quantity of precipitation in some places and an overestimation in others. However the locations of the maximum values at the border of Czech Republic and Poland, and in Moravia were well predicted. So the forecast still can be considered good in reasonably limits.

So it can be concluded that the models succeeded to give a good forecast for the end of these floods. The quantity of precipitation started to decrease, and the location to move to the eastern part of Czech Republic.

Conclusions

In this paper, the Czech floods from the 11-13th of August 2002 have been analysed using the 3D-Var scheme for the ALADIN/Hungary model. The aim of these experiments was to show if the 3D-Var scheme is able or not to keep the good performance of the operational model (in dynamical adaptation). For this case, the forecasters considered that the operational model succeeded to predict correctly the event.

Two sets of experiments using 3D-Var scheme were carried out. For both of them, the operational lateral boundary conditions for ALADIN/Hungary and the SYNOP and TEMP data available at the Hungarian Meteorological Service have been used. The difference between them is that one

analysed temperature and relative humidity from the SYNOP observations, and the other one, only geopotential. The reference of these experiments was the forecast of the operational model.

The forecasts from the 11.08 00 UTC model run show the beginning of the event, with an intensive rainfall started over Austria (more than 200 mm), and moving to the Czech Republic. This run gave the first indication of the new location of the heavy rainfall over the border of Germany and Czech Republic. There is no significant difference between experiments in the forecast of the rainfall.

All three experiments from the 11.08 12 UTC model run, predicted a significant quantity of precipitation (more than 100 mm in 24 h) over the border of Germany and Czech Republic. But comparing to real measurements (maximum as 313 mm), the forecast was underestimated. Despite this, the models gave an indication of the intensive rainfall. Both models predicted heavy precipitation more to the east, which has not happened in reality.

The forecast from the 12.08 00 UTC model run was the closest one to the maximum of the event, both as moment of time, and as significant rainfall. Large quantities of precipitation have been measured and predicted also. The operational forecast had the closest value to reality. But also the 3D-Var experiments predicted a significant rainfall in that area, giving warning about the future flood.

The last model run, from 12.08 12 UTC, did not show differences between the forecasts of the models in dynamical adaptation and using 3D-Var scheme. Similar locations and quantity of precipitation have been predicted. In some places the precipitation forecast of the models has been overestimated, and in others, it has been underestimated, comparing to real measurements. But the location of the most intensive rainfalls was well predicted.

The good forecast of the operational ALADIN/Hungary model is partly due to the good information provided through the lateral boundary conditions. Being a double-nested limited area model, it means that both ALADIN/LACE and mainly ARPEGE models had a good forecast for the floods. In the 4D-Var scheme for the global model ARPEGE more other observations have been assimilated, comparing to the 3D-Var scheme for ALADIN/Hungary model. So this fact explains the good performance of the global model.

The accurate information from the lateral boundary conditions, together with the assimilation of more SYNOP observations, helped the model with 3D-Var scheme to obtain a good prediction of the event. The influence of the new information coming from the SYNOP data was rather small, the first guess being close enough to the observations. Probably, that is why, there are not big differences between the two sets of experiments using the 3D-Var scheme.

Being a large scale phenomenon, the models with and without data assimilation predicted a similar evolution of the forecast. So it has been shown that the 3D-Var scheme do not deteriorate the good performance of the reference model. (Alexandru [1], 2003).

References

Alexandru, S., [1] 2003 : Forecast of the Czech floods from August 2002 using the 3D-Var scheme for the ALADIN mesoscale limited area model. *ALATNET Internal Note.*

Alexandru, S., [2] 2003 : 3D-Var experiments for the ALADIN/Hungary model: a case study (I). *ALATNET Newsletter 6.*

Alexandru, S., 2002 : 3D-VAR data assimilation experiments for the double-nested limited area model ALADIN/Hungary. *ALATNET Internal Note*.

IABM, 2002 : Up Front. *Newsletter of the International Association of Broadcast Meteorology* (IABM), 14, 2--4.

Parrish, D., and Derber, J., 1992 : The National Meteorological Center's spectral statistical interpolation analysis system. *Mon. Weather Rev.*, **120**, 1747--1763.

3D-Var experiments for the ALADIN/HUNGARY model: a case study (II)

Introduction

The research on the 3D-Var data assimilation scheme for a double-nested limited area model has been continued with another case study, from the 4th of August 2002, when the operational model (in dynamical adaptation) has not been able to predict an important quantity of precipitation over Hungary.

The synoptic situation of this event is presented briefly. On the 4th of August 2002, a lower pressure field dominated over the central-eastern part of Europe. In altitude, the ridge of the anticyclone from North Africa was extended over the central-southern part of Europe, and a low cut-off was located more to the West. The temperatures in the western part of Hungary were in the morning around 23°C, increasing till 30°C at noon. The air in this area was very humid, which determined an unstable atmosphere.

A cold front was moving to the north-eastern part of Europe, through Austria and Hungary. So cold and dry air was streaming south-westerly. Advancing, the cold air moved the humid air upward, determining a convective instability. The non-frontal surface line, along which convective instability occurs, is called an instability line. Here the turbulence is severe, because of the violent updrafts and downdrafts. Thus rain showers and thunderstorms occur, with significant quantities of precipitation. Such an instability line developed in the north-western part of Hungary, causing an intensive rainfall. Thus, in less than six hours, the quantity of precipitation reached a maximum of 65 mm. (Fig. 1).

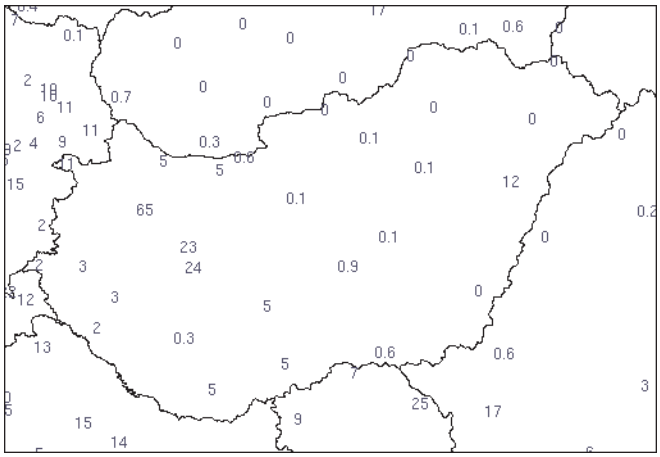

Figure 1 : The quantity of precipitation (mm/6h) measured over Hungary on 04.08, between 06 UTC - 12 UTC

3D-Var experiments

The ALADIN/Hungary model is using for the background term the standard NMC statistics, and for the observation term, only SYNOP and TEMP data are considered in the assimilation cycle. As coupling technique, the time-consistency has been chosen both in cycling and in production. Digital

filter initialization (DFI) has been applied at the beginning of the integration, both in cycling and in production (Alexandru, 2002).

The 3D-Var experiments were carried out using the operational lateral boundary conditions (LBC) for ALADIN/Hungary (from ALADIN/LACE model). From SYNOP observations, temperature and relative humidity information have been considered, and from TEMP data, wind, geopotential, temperature and relative humidity. Hereafter the name of this set of experiments is "*3dvar*". The reference of these experiments was the operational forecast of the model in dynamical adaptation ("*oper*"). The assimilation cycle was started from 01.08.2002 06 UTC, i.e. three days before the event.

Results

In this chapter the forecasts of different fields from the model runs are described, then the impact of observations over forecast has been analysed. The maps with the cumulated precipitation have a zoom between 44°-50° N in latitude and 14°-25° E in longitude, in order to point out the location of the rainfall.

For the 04.08 00 UTC model run, both models, with and without data assimilation, did not predict the significant rainfall, either at the right moment, nor later. The quantity of precipitation do not exceed 6 mm, which is a strong underestimation, the real maximum being 65 mm. So the operational model, in dynamical adaptation, failed to predict the rainfall. The 3D-Var experiment did not have a better forecast, which means that the information coming from the observations did not give any indication about the future development of an instability line.

Also the results of the *3dvar* set were checked from the 04.08 06 UTC run, but still no indication about heavy precipitation. One reason of this misforecast could be the lack of any TEMP observation near to this region, so only information from SYNOP data were taken into account. Probably because the event has happened between 06 UTC and 12 UTC, especially to the end of the period, the surface observation at 06 UTC did not have information about the event.

04.08 12 UTC run

The main difference in the forecasts of the two models, with and without 3D-Var scheme, appeared in this run. The operational analysis shows the air streaming south-westerly. The pressure gradients are rather small, the wind is not too strong, over Hungary. The difference between the models, in the forecast of the geopotential, appeared since the beginning of the integration. The *3dvar* set predicted a lowest pressure over the western part of Hungary. After 6 h integration, the difference between the models for the forecast of the geopotential is almost 3 damgpm.

The operational model predicted the sky partly cloudy over Hungary and no vertical motion of the air masses. So, no precipitation is expected to develop. The model using 3D-Var scheme (*3dvar*), forecasted an area in the western part of Hungary with high humidity. Also the air masses have an ascending vertical velocity, reaching values as 5 hPa/s.

In the north-western part of Hungary a significant rainfall has been forecasted by the experiments using 3D-Var scheme, the quantity reaching 173 mm in 6 h. However the operational model did not predict any precipitation. One can see in Fig. 2 the great difference between the operational forecast and that when data assimilation has been used.

Seeing the difference between the two models, another set of experiments has been proposed. It is similar to the *3dvar* set, but the lateral boundary conditions were provided by the ARPEGE model. The forecasts of same fields have been analysed, but they are rather similar. Only the quantity of precipitation is smaller than in the *3dvar* experiments, the maximum being around 126 mm in 6 h.

So the experiments using 3D-Var scheme succeeded to forecast a huge quantity of precipitation, but with six hours delay. On the one hand, this represents a failure of the model, but on the other hand, the rainfall was still predicted. We tried to see how it was possible.

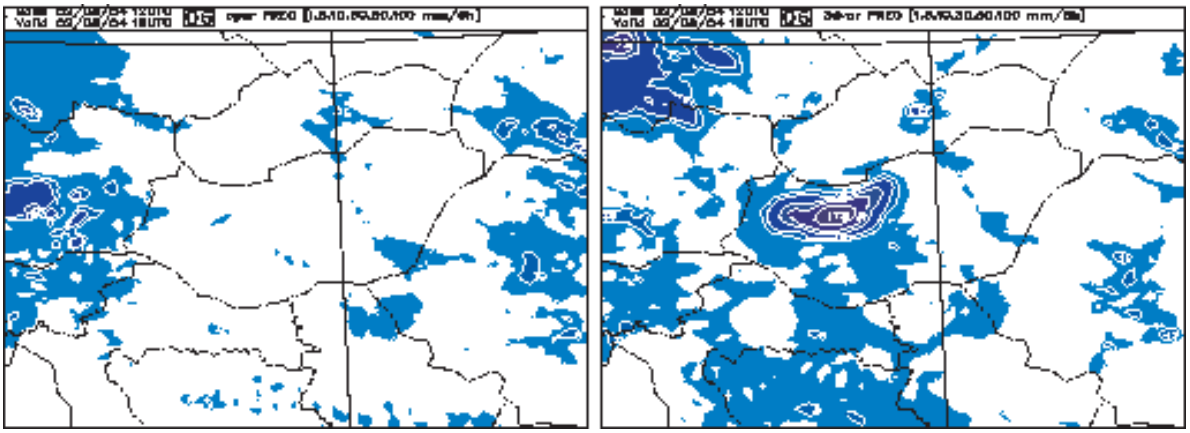

Figure 2 : The quantity of precipitation (mm/6h) forecasted by the operational model (*oper*) and using 3D-Var scheme (*3dvar*) between 04.08 12 UTC - 18 UTC, from 04.08 12 UTC model run

It was investigated if there are some imbalances between the models, with and without data assimilation. But the time evolution of the mean-sea-level pressure checked during 6 h integration in production, for the model in dynamical adaptation, and using 3D-Var, showed that the fields are in balance.

The impact of observations on forecast

Trying to understand how the models using data assimilation forecasted the important quantity of precipitation, some experiments were carried out, similar to the *3dvar* set, except that different combinations of variables and data have been used, all along the assimilation cycle. In the first two sets of experiments only TEMP, respectively only SYNOP, observations have been taken into account. The names are 3*dvar TEMP* and *3dvar SYNOP(T,RH)*. In the last one, only the relative humidity and temperature variables have been assimilated.

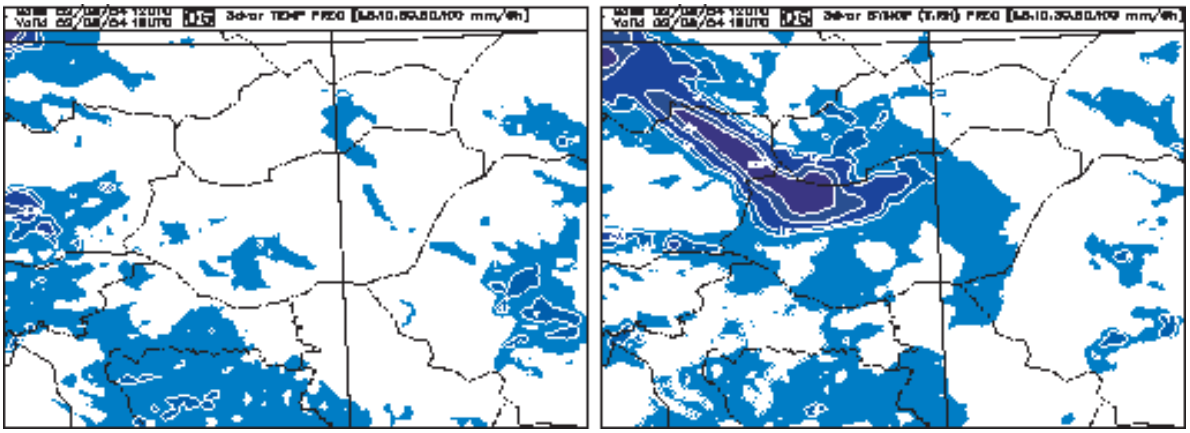

Figure 3 : The quantity of precipitation (mm/6h) forecasted by the model using 3D-Var with TEMP (*3dvar TEMP*) and SYNOP data (*3dvar SYNOP(T,RH)*) between 04.08 12 UTC - 18 UTC, from 04.08 12 UTC model runs

For all experiments, only the precipitation cumulated in 6 h, from the 04.08 12 UTC run, between 12 UTC and 18 UTC, has been plotted. As can be seen in Fig. 3, the *3dvar TEMP* set did not predict any rainfall, which means that all the information about it came from the surface observations.

Indeed, using only SYNOP data, the quantity of precipitation is significant. The shape of the area of rainfall differs as it was predicted by the *3dvar* set, but still in the north-western part of Hungary more than 50 mm precipitation has been forecasted.

The next experiments have been performed using different observed variables only from SYNOP data. So in turn, relative humidity ("*SYNOP(RH)*") has been assimilated from the surface observations, then geopotential, then geopotential and temperature, and finally geopotential, temperature and relative humidity. Other experiments were carried out, being similar with the previous one's, only that TEMP observations have been added also in the assimilation cycle. The observed variables from TEMP data are wind, geopotential, temperature and relative humidity. The conclusions from these experiments were that the geopotential and temperature measurements did not influence the rainfall forecast (not shown). The main information is coming from the relative humidity. As one can see in Fig. 4, when only relative humidity from surface observations has been assimilated, the quantity of precipitation is more than 260 mm in 6 h.

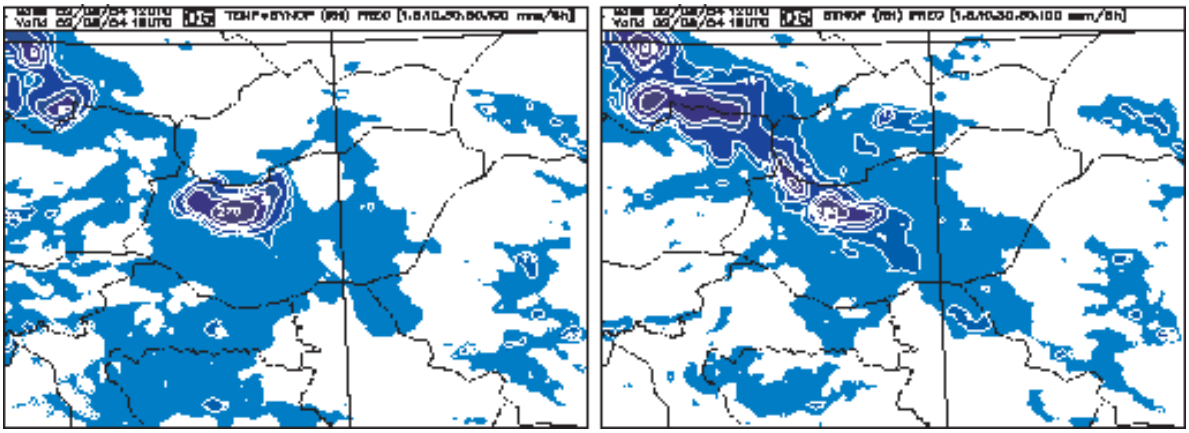

Figure 4 : The quantity of precipitation (mm/6h) forecasted by the model using 3D-Var with TEMP and SYNOP data (*3dvar TEMP+SYNOP(RH)*) and only SYNOP data (S*YNOP(RH)*) between 04.08 12 UTC - 18 UTC, from 04.08 12 UTC model runs

Few precipitation (around 29 mm) has been predicted also by the 3D-Var experiments when TEMP data together with the temperature and geopotential from the surface observations were assimilated. This can be an effect of the inefficient coupling between the planetary boundary layer and the troposphere, made by the observation operator. Thus the 2m temperature observation increment can influence the temperature increments from the high troposphere.

In conclusion, the measurements of the 2 meter relative humidity have been responsible for the information introduced in the model, which caused the forecast of this significant rainfall. Also the temperature measurements, from the surface and upperair observations, determined the prediction for some precipitation.

Conclusions

A case from the 4th of August 2002 has been presented in this paper. An instability line has been developed very fast in the morning, causing an intensive rainstorm. The operational model (in dynamical adaptation) was not able to predict this phenomenon. So new experiments have been performed in order to see whether the model using the 3D-Var scheme can have a better forecast.

For these experiments, different lateral boundary conditions (from the ARPEGE or ALADIN/LACE model) and SYNOP and TEMP observations available at the Hungarian Meteorological Service have been used. The reference of these experiments was the operational forecast of the model in dynamical adaptation.

The forecasts from the 04.08 00 UTC and 06 UTC runs showed that both models, with and without data assimilation, did not predict the intensive rainfall, neither at the right moment, nor later. It means that the information coming from the observations did not bring any indication about the future development of this instability line.

The 04.08 12 UTC run brought the main difference in the forecasts of the two models, in dynamical adaptation and with 3D-Var scheme. The operational model predicted fair weather, without any sign of rainfall. Comparing to reality, one can say that for this particular period of time, the operational model has a good forecast, the rainfall happening earlier than this model run. But in the same time, it is also a failure of the operational model, which did not predict the precipitation at the right moment, but neither later. Being a local phenomenon which has developed very fast, it was not forecasted by the coupling model. So no information about it came through the lateral boundary conditions from the ALADIN/LACE to ALADIN/Hungary model.

Instead, the experiments using 3D-Var scheme forecasted a huge quantity of precipitation (more than 100 mm), but with six hours delay. On the one hand, this represents a failure of the model, but on the other hand, the rainfall was still predicted.

Other experiments were carried out using only SYNOP or TEMP data, in order to find out what observations could have influenced so much the precipitation forecast. Thus it was shown that the model using the 3D-Var scheme and only TEMP data, did not predict any rainfall, which means that all the information about it came from the surface observations. Indeed, assimilating only SYNOP data, the quantity of precipitation is significant.

The last experiments have been performed using different combinations of the observed variables from the SYNOP observations, with and without TEMP data in the assimilation cycle. The observed variables from SYNOP are the relative humidity, geopotential and temperature. From the TEMP data, the wind, temperature, relative humidity and geopotential have been assimilated. The precipitation forecasts from these experiments showed that the measurements of the 2 meter relative humidity have been responsible for the information introduced in the model, which caused the forecast of this significant rainfall. Also the temperature measurements, from the surface and upperair observations, determined the prediction for some precipitation, but not so important.

So the information from the observations (from 04.08 at 12 UTC) reproduced the state of the atmosphere, with high humidity. Thus the analysis of the model caught the end of the storm. Because any other information from the lateral boundary conditions or from the first-guess did not give any indication about an existing storm, the model "said" that it is the beginning. So, one can say that the model using 3D-Var scheme had good initial conditions, but it was beyond its capacity to predict such a rainstorm. (Alexandru, 2003).

References

Alexandru, S., 2003: 3D-Var experiments for the ALADIN/Hungary model: a case study (II). *ALATNET Internal Note*.

Alexandru, S., 2002: 3D-VAR data assimilation experiments for the double-nested limited area model ALADIN/Hungary. *ALATNET Internal Note*.

Note : All the internal notes (5 up to now) written by Steluta Alexandru are available in its personal pages, on the ALATNET web site.

2. Margarida BELO PEREIRA : "Estimation and study of forecast error covariances using an ensemble method in a global NWP model"

Introduction

The background error covariance matrix is one very important element in a data assimilation system, since it determines the filtering and propagation of observations. In operational ARPEGE assimilation system the covariance coefficients of this matrix are estimated using the NMC method (Parrish and Derber, 1992). In this method the background errors are given by the differences between 12 h and 36 h forecasts valid at the same time. In 2001, another method, known as Analysis Ensemble Method, hereafter referred as Ensemble method, which was tried before in Canada (Houtekamer et al., 1996) and at ECMWF (Fisher, 1999) was implemented and tested in ARPEGE 3d-var (Belo Pereira, 2002). Presently, the Ensemble method was implemented in ARPEGE 4d-var.

The results presented in the current document are derived from an ensemble which contains five 4d-var cycles of the non-stretched version of ARPEGE model with T299 and 41 levels, for the period from 1st of February to 24th of March of 2002. The members of this ensemble were arbitrarily numbered from 33 to 37. The differences between the 6-hours forecasts for consecutively numbered members were computed for each 12 UTC cycle between 04/02/2002 and 24/03/2002. This provides $4 \times 49 = 196$ differences between background fields, from which the global standard deviation, the vertical and horizontal correlations of the background error are diagnosed.

Ensemble Method versus NMC method

Several statistics of the background errors were analysed, in order to study the differences between the two methods, both in spectral and in gridpoint space. This document will make reference only to the spectral space results.

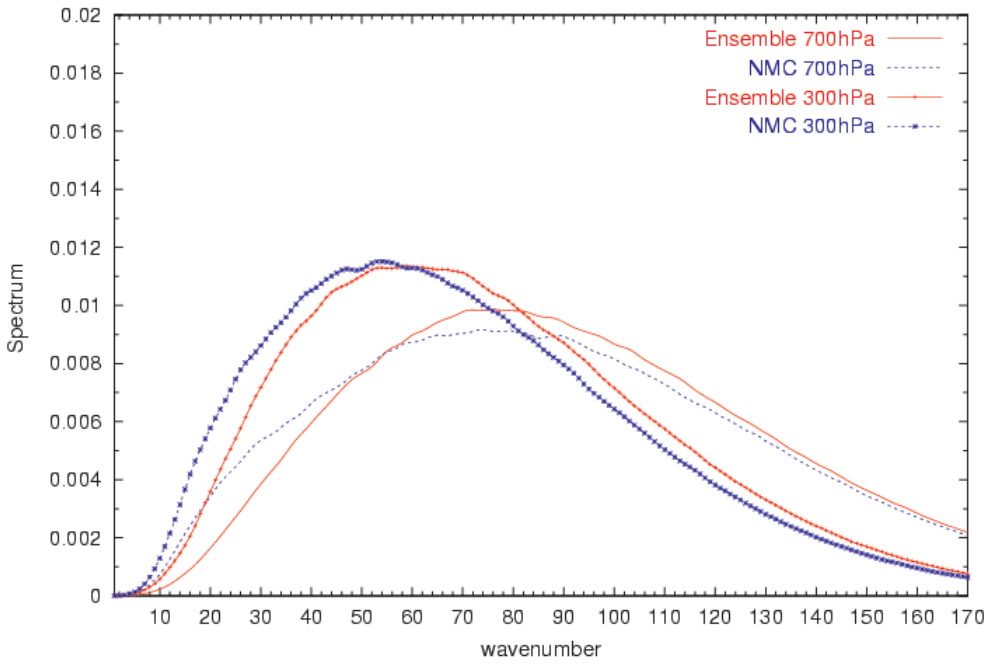

Figure 1. Auto-correlation spectra of vorticity at levels 27 (near 700 hPa) and 16 (near 300 hPa) for NMC and Ensemble methods.

Figure 1 shows the auto-correlation spectra of vorticity estimated by the two methods. It can be seen that both at 700 hPa as near the jet level, the auto-correlation spectra show that the variance maximum is shifted towards the smaller scales in the Ensemble method. This means that the variance of vorticity background error has a larger contribution from mesoscale phenomena, when estimated by the Ensemble method than by the NMC method. This occurs also for the other atmospheric variables.

It is also interesting to mention that according to the NMC method the larger contribution for the background error of surface pressure comes from the synoptic scales, while in the Ensemble method the contribution from the planetary scales seems to be so important as the one from synoptic scales.

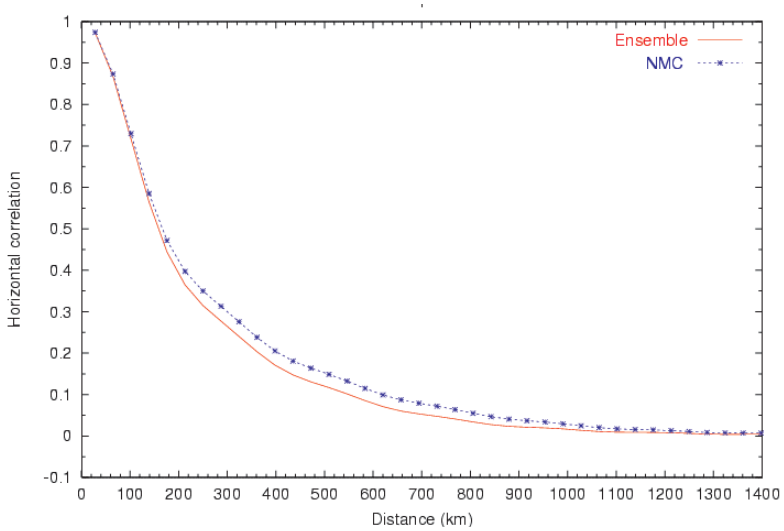

Figure 2. Horizontal auto-correlation of surface pressure background error estimated by Ensemble and NMC methods.

Figure 2 shows the mean horizontal correlations for surface pressure for the two methods. When the Ensemble method is used the correlation is sharper than in the NMC method. This result is valid also for the other variables, except for divergence.

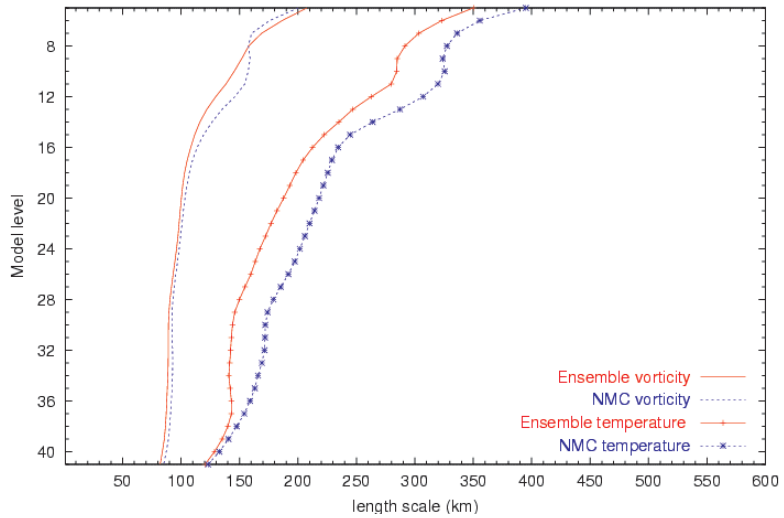

Figure 3. Horizontal length scale of auto-correlation function of temperature and vorticity estimated by NMC and Ensemble methods.

Figure 3 shows the horizontal length-scale of auto-correlation function of temperature and vorticity estimated by the two methods. The results show that for both methods the length-scale of vorticity is smaller than the one of temperature, as it would be expected. Moreover, it can be seen that

according to the Ensemble method the horizontal length-scale is smaller than when estimated by the NMC method. This difference is more notorious for temperature. On the contrary, the horizontal length-scale of divergence is very similar in the two methods.

The mean vertical correlations and the North-South variation of the vertical correlations were both analysed. The results show that the Ensemble method produces much sharper vertical correlations than the NMC method, mainly for middle and high latitudes (see figure 4).

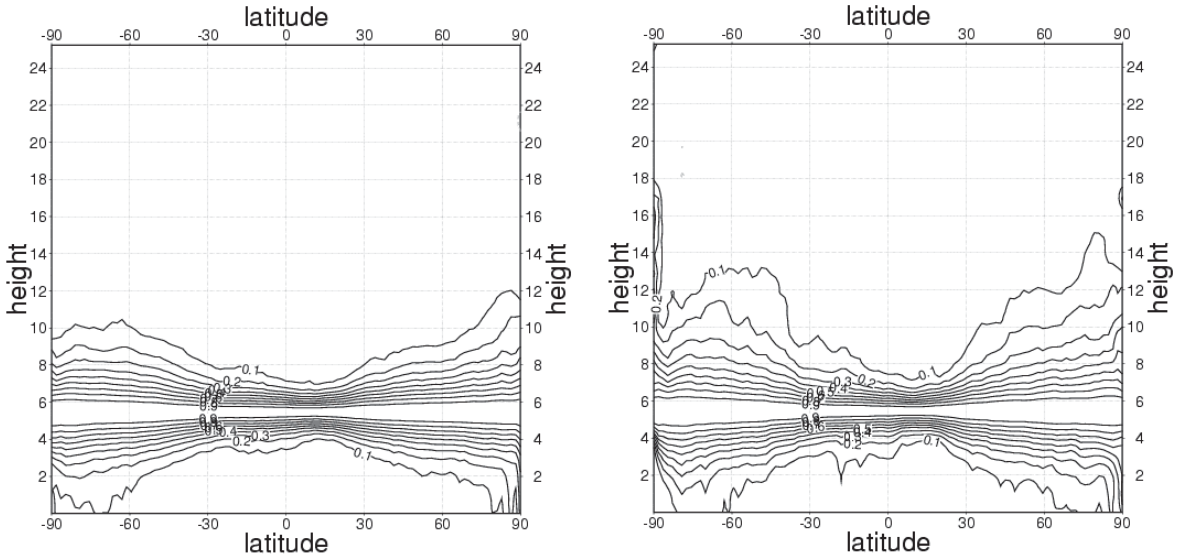

Figure 4 - North-South variation of vertical correlation (at level 21) of vorticity background error estimated by the Ensemble method (left side) and by the NMC method (right side).

Impact on forecasts

On operational 4d-var assimilation system, the vertical profiles of total standard deviation of the background errors are rescaled by a factor of 0.9 in order to account for mismatch between the magnitudes of the 12 / 36-hours forecast differences and the 6-hour forecast errors. In order to study the impact of the statistics from the Ensemble Method against the ones from NMC method (operational), some tests were performed to find out the optimal factor to rescale the vertical profile of the standard deviation of the background errors. Figure 5 shows the vertical profile of the standard deviation of vorticity and temperature for the NMC method and for the Ensemble method, multiplied by different factors.

For both methods the largest errors of vorticity are located at the jet level. However, if the factor of 1.3 is used, the Ensemble method gives larger errors in the middle troposphere, but smaller error in the low troposphere than the NMC method. On the other hand, if the factor of 1.5 is used, the background errors of vorticity given by the Ensemble method are larger in all troposphere than the ones given by the NMC method.

Both methods agree that the largest errors of temperature are located in the top level. Nevertheless, the Ensemble method produces larger errors at this level than the NMC method. Moreover, according to the NMC method the second maximum of the temperature background error is located at tropopause, while according to the Ensemble method the second maximum error occurs in middle troposphere.

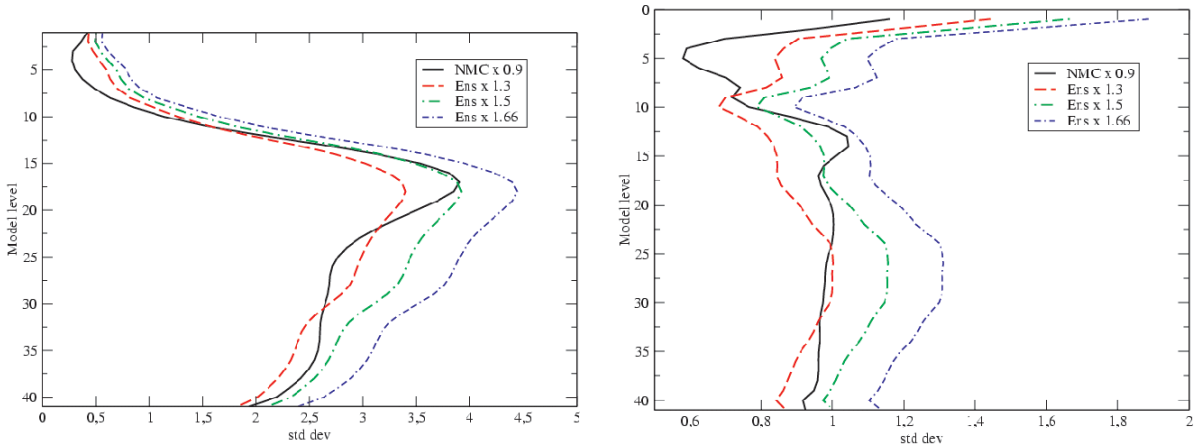

Figure 5 : Vertical profile of rescaled standard deviation of vorticity (left side) and temperature (right side) background error estimated by NMC and Ensemble methods.

The impact of the statistics derived from the Ensemble method against the ones from NMC method were tested for two different periods; from 5 of February to 4 of March of 2002 (here referred as first period, which includes the period from which the statistics were computed) and from 24th of October to 20th of November of 2002 (referred as second period). The results of the impact experiences revealed that the factor of 1.5 is the optimal value, since the scores were clearly better than when using factor of 1.3 and the differences between using factor of 1.5 or 1.66 were neutral.

The wind scores against ECMWF analysis are clearly positive over the regions of North America, Europe and North Atlantic, for forecast ranges larger than 24 hours. This positive impact is larger in the middle and upper troposphere and increases with the forecast range. In the tropics, the scores for wind are positive on stratosphere and on middle and upper troposphere, for all forecast ranges. On the other regions, the scores for wind are slightly positive or neutral. The positive impact is less impressive for the second period.

For both periods, the scores for geopotential are clearly positive on the stratosphere over the first day of forecast and on the troposphere for forecast ranges larger than 36 hours. For the first period, the scores of geopotential are strongly positive in the stratosphere in the North Hemisphere, for all forecast ranges. In the South Hemisphere and in the tropics the scores are positive on the high troposphere. However, for the second period, the scores for geopotential are negative in the South Hemisphere for all forecast ranges.

The temperature scores are slightly positive (for instance near the 10 hPa) or neutral.

References

Belo Pereira, M., 2002 : Improving the assimilation of water in a NWP model. Report for *ALADIN Newsletter 21 - ALATNET Newsletter 4*, April 2002, pp 37-41.

Fisher, M., 1999 : Background Error Statistics derived from an Ensemble of Analyses. *ECMWF Research Department Technical Memorandum*, **79**, 12 pp.

Houtekamer et. al., 1996 : A system Simulation Approach to Ensemble Prediction. *Mon. Wea. Rev.*, **124**, 1225-1242.

Parrish, D. and J. Derber, 1992 : The National Meteorological Center's spectral statistical interpolation analysis system. *Mon. Wea. Rev.*, **120**, 1747-1763.

3. Martin GERA : "Improved representation of boundary layer"

Summary of Activities

During the last period of my stay at the Royal Meteorological Institute of Belgium, supported by ALATNET Training Network, I concentrated my work on the following scientific topics:

- Investigation of a numerical scheme for solving the TKE (Turbulent Kinetic Energy) equation
  - ♦ Stability
  - ♦ Positive roots of TKE equation
- Testing some derived and suggested methods
  - ♦ Linearized version of TKE equation
  - ♦ Nonlinear approach for solving TKE equation
  - ♦ Predictor-corrector method
  - ♦ Split-implicit method for the diffusion term (as in the Meso-NH model)
- Comparison of chosen methods
- Results analysis
- Writing a final scientific report

Summary of findings

One needs to solve a second order nonlinear partial differential TKE equation. It is not possible to find an analytical solution. We have to find an appropriate numerical scheme, which converges to the "true" result. Considering the vertical mesh of ALADIN one must use the finite element method for numerically solving TKE equation.

- For the linearized version of the TKE equation we found that in some cases there can exist levels where total reflection of TKE occurs.

When we analyse the energy-density function of the TKE, the reflection properties of linearized TKE depend on the wavenumbers (for long waves it can be a total barrier, but for short waves it can be a transparent level). For these reasons, the linearized version cannot be used. In some meteorological conditions the solution is in resonant mode, which abnormally increases the amplitude of the solution. However, from the linearized version of the equation we get some knowledge about the equation properties.

- In the next step we try to solve directly the TKE equation in nonlinear mode.

The purpose of solving the TKE equation, after rewriting to discrete form is to find a zero of a system of `KLEV` nonlinear functions in `KLEV` variables by a variant of the Powell hybrid method, where `KLEV` is the number of vertical levels in the numerical model. The main principle of this method is to find an approximate solution by iteration. The Jacobian, which is necessary for finding the gradient is calculated by a forward-difference approximation.

- Next we try to take advantage from previous methods and avoid known problems. We try to apply a Predictor-corrector method.

Here we performed a deep analysis for the choice of the linear operator. For this operator we use information form stationary TKE. Using the average values of stationary TKE as a background term, the reference state diverges from the real profile, but it is one possible choice for the linear operator. Alternatively the linearization can be done with help of a simplified TKE equation. For

zero tendencies, TKE equation can be reduced to the stationary TKE equation. This equation can be linearized around the stationary TKE. Now there is no average profile of stationary TKE. But this form is more "pure" for other terms.

A next possibility is to combine the previous linear operators by averaging the dissipation term.

The solved problems are more complicated than to find stable scheme. The roots of our system should be positive, because they represent TKE or square of TKE. For this reason we expect a "balance" behaviour. Mathematically we can formulate the definition of our problem in the following way. The inverse equation operator should have positive matrix elements and the right-hand side must be positive. In this case we have positive real roots with positive right (forcing) side (this definition may be incomplete).

To have positive forcing we need to analyse the buoyant and shear terms together with the dissipation term. For the instable case there is no problem, the forcing term is always positive.

For the stable case the situation is more complicated. In the neutral case momentum and heat flux are differed by inverse Prandtl number. It means that the drag coefficient for heat flux is larger than the drag coefficient for momentum flux for neutral air stratification. The dominant contribution to the final forcing term is from the buoyant part at this moment. It means that $F(z,t)<0$, where $F(z,t)$ is the forcing term which contains shear and buoyant production or consumption terms in the TKE equation.

At this moment dissipation term and source terms have an important role. The sign of $F(z,t)$ should be changed by these terms. For these properties it is important to have restriction of the critical Richardson number. It should not have large values, so as not to have a big negative value for $F(z,t)$. These features are significant in upper (model levels) atmosphere, where stable stratification of atmosphere is observed frequently.

In the PBL layer or in the border troposphere and tropopause other problems create obstructions. In these layers we frequently observe strong turbulent mixing. It has an influence on the mixing length. When the turbulence occurs in a thick layer we also have a sharp fluctuation of the mixing length. Increasing the mixing length increases the exchange coefficient dramatically. This feature has a close connection with the numerical stability of the scheme and with properties of positive inverse matrix operators.

This is the main problem for all methods. From results which are not completely presented, one can say that the best and most robust method is direct use of the nonlinear equation. This method still has limitations, but it can be improved.

The negative fluctuations effect of mixing length is increased by shallow convection. For this reason there is no possibility to solve the prognostic TKE equation with these methods when using the current shallow-convection scheme. One way to implement air saturation caused by turbulence is by adding the liquid water in the dependency in potential temperature. Without the shallow-convection scheme one can compute the tendency of TKE. This method does not use the complete TKE equation as a prognostic equation. This method is comparable to the current scheme for computation of fluxes, since it does not contain direct knowledge of "history" from the previous time-step. The difference is in the nonlinear approach of the computation.

For these properties we can solve at this moment TKE equation in "prognostic-diagnostic" regime with a very short integration step (around 10 s). To keep stability in appropriate range in all time-steps we initialize the TKE profile with the stationary TKE and then we compute the tendency of TKE with the described method. Some results are presented in the figures hereafter.

This method is good for scientific investigation, but not good for operational weather forecast. For longer time-step in case of rapid changes of the mean variables in the vertical direction, which can be caused by the discrete mesh (the density of mesh is insufficient), we obtain negative values for

TKE below or above this region : which is not allowed. Without initialization with stationary TKE the model blows up after a few minutes.

To compare these methods for solving the nonlinear equation we did some experiments. These negative features can be suppressed by term-by-term splitting of the equation, by finding a better approximation for the derivatives or by changing the stability of the integration scheme. Other possibilities are to increase the number of vertical levels by additional interpolation. Interpolation can be done only for solving TKE. We have plan to investigate these ideas in the near future.

Implementation to ALADIN model

From analyses is apparent that the method for computation of fluxes depends on the distance to the surface. Kinematic turbulent fluxes are expressed close to the surface by TKE dependence. The computation assumes small change (10%) of fluxes in the ground layer. Therefore we apply constant statistical moments for this case. This approach is applied on the surface layer, which coincides with the last full level. In the free atmosphere we use a modified expression.

One can remark now, that spectral characteristics are used for the computation of some coefficients (c_m, c_e, ...), although the vertical grid is irregular. From linear spectral analysis, it is apparent that the integral value of total TKE is unaltered by a change of density of the grid. This method serves an estimation of the coefficients' magnitude. Their value, as was shown, must be tuned.

Every derivation is derived from the fact that TKE is computed on "half" levels. For the Lagrangian computation of horizontal advection it is more convenient to have TKE on "full" levels. For this reason we plan to compute the difference of TKE between two "half" levels.

For initialization the stationary (balanced) TKE is used.

Dry static energy for Richardson number expression is used in the ALADIN model. The moisture is included in the gas constant. The virtual potential temperature (there is a connection with dry static energy) is used for computation of the heat flux. Correction for shallow convection is not applicable at this moment.

For initialization of TKE we use a derived relation.

After taking into account our expressions and computing tendencies for TKE the exchange coefficients K_h, K_m can be expressed. The computation of tendency for TKE is done in a diagnostic-prognostic regime at this moment. For the computation of the exchange coefficients we have to specify the parameterization coefficients c, c_0 and c_e. We suppose that c_m is set from the spectral approach. Limitation of the Richardson number is garbled from current ALADIN scheme. The new form of the exchange coefficients, calculated at the time "+", repress the need for an anti-fibrillation scheme for the computation of mean variable tendencies.

Conclusion

During my 19 months stay in Bruxelles I improved my knowledge about Planetary-Boundary physics parameterization. I have a better overview of model ALADIN structure. I took part in the seminar and workshops. The complete scientific documentation of my 19 months stay in Brussels was created and distributed.

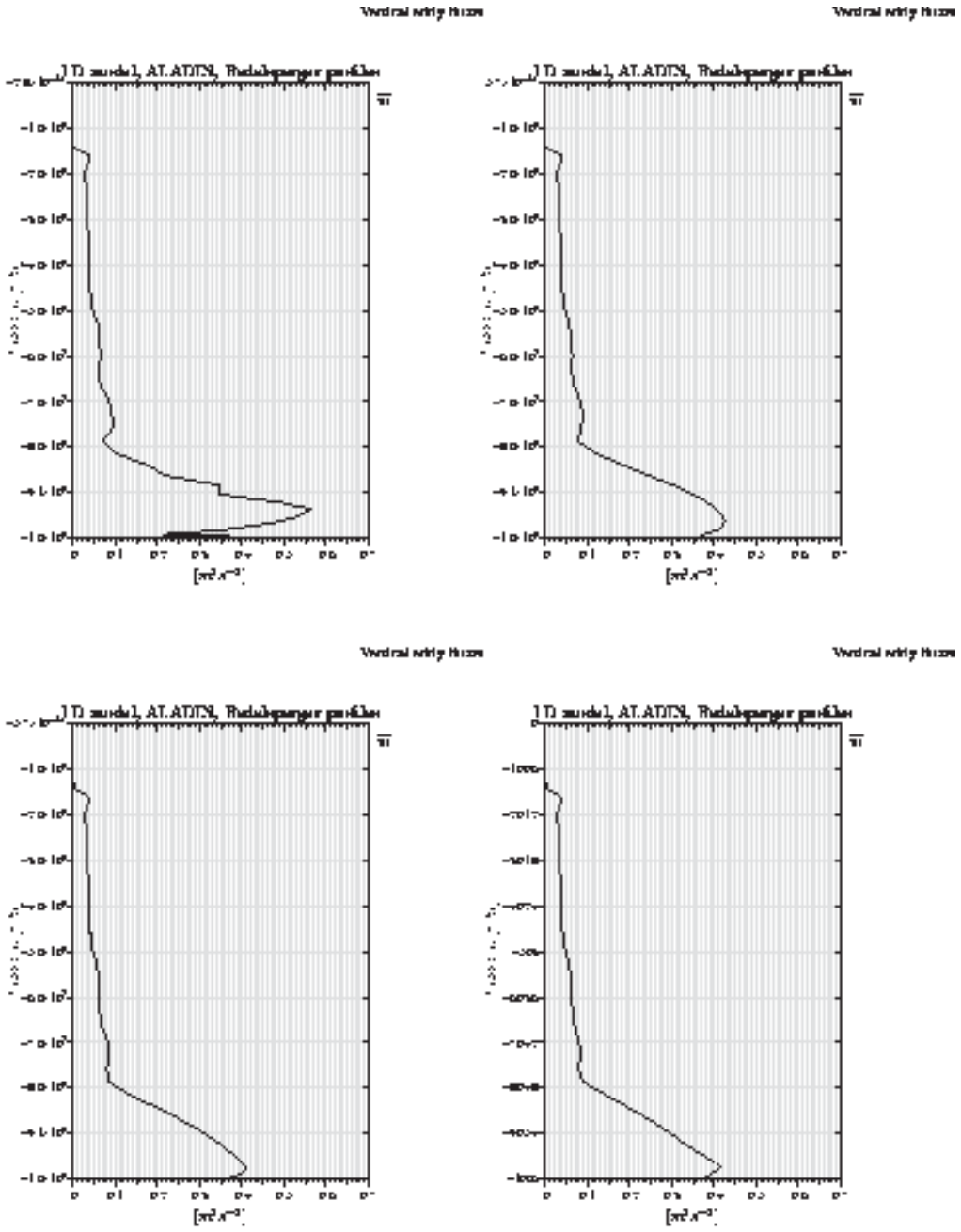

Figure 1: (a,b,c,d) The turbulent kinetic energy $[m^2 s^{-2}]$, for parameterized constants setting $c = 5.639$, $c_0 = 1.2$, $c_\varepsilon = 0.831$, $c_m = 3.115$, $c_{2m} = 0.2$. For time step $\Delta t = 10s$, $USURICE = 0.5$. The left upper corner represents picture (a) for $t = 0h$, the right upper corner represents picture (b) for $t = 1h$, the lower left corner represents picture (c) for $t = 2h$ and the lower right corner represents picture (d) for $t = 3h$ of model integration.

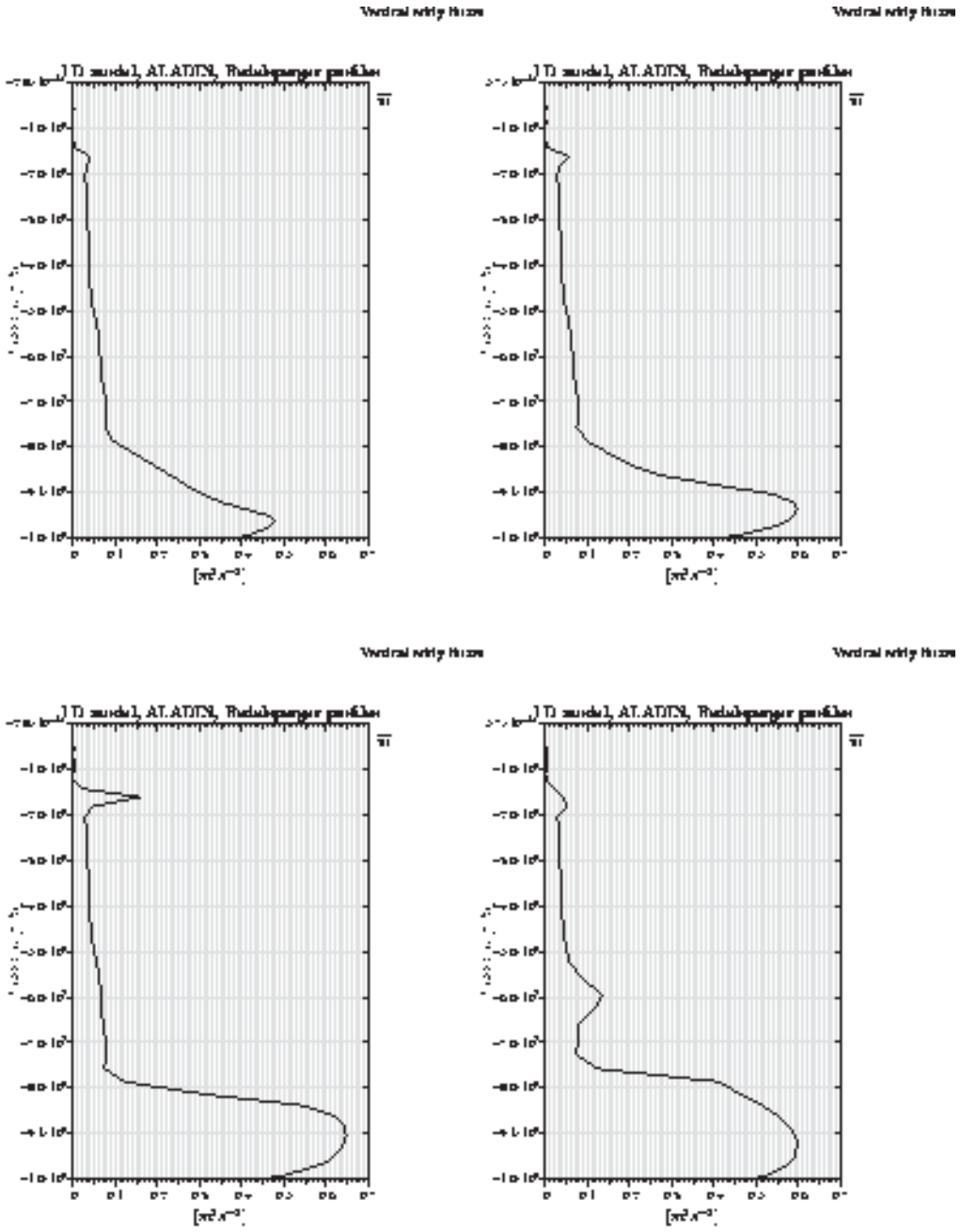

Figure 2: (a,b,c,d) The turbulent kinetic energy $[m^2 s^{-2}]$, for parameterized constants setting $c = 5.639$, $c_0 = 1.2$, $c_\varepsilon = 0.831$, $c_m = 3.115$, $c_{2m} = 0.2$. For time step $\Delta t = 10s$, $USURICE = 0.5$. The left upper corner represents picture (a) for $t = 4h$, the right upper corner represents picture (b) for $t = 5h$, the lower left corner represents picture (c) for $t = 6h$ and the lower right corner represents picture (d) for $t = 7h$ of model integration.

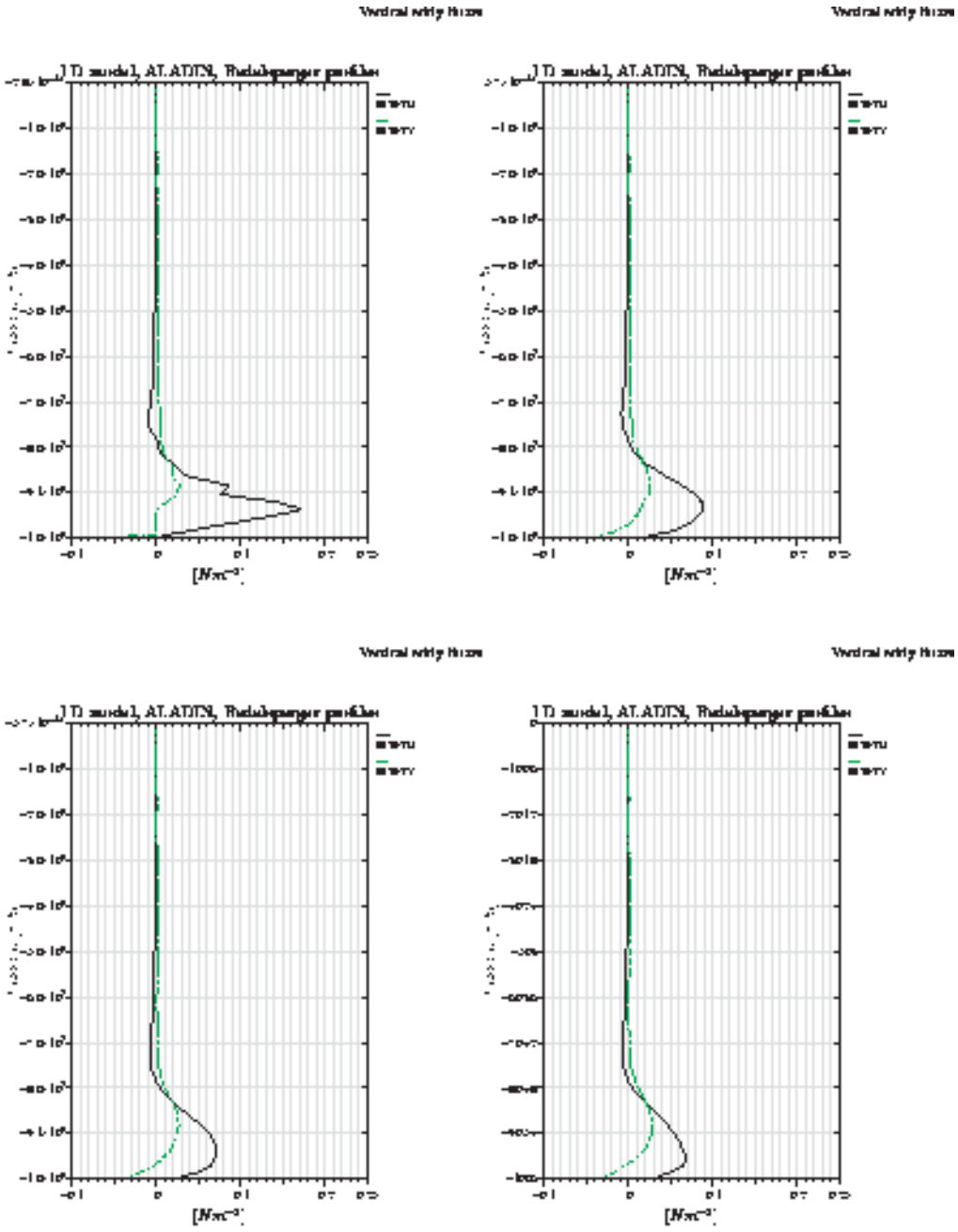

Figure 3: (a,b,c,d) The turbulent momentum flux for "U" and "V" wind components $[Nm^{-2}]$, for parameterized constants setting $c = 5.639$, $c_0 = 1.2$, $c_\varepsilon = 0.831$, $c_m = 3.115$, $c_{2m} = 0.2$. For time step $\Delta t = 10s$, $USURICE = 0.5$. The left upper corner represents picture (a) for $t = 0h$, the right upper corner represents picture (b) for $t = 1h$, the lower left corner represents picture (c) for $t = 2h$ and the lower right corner represents picture (d) for $t = 3h$ of model integration.

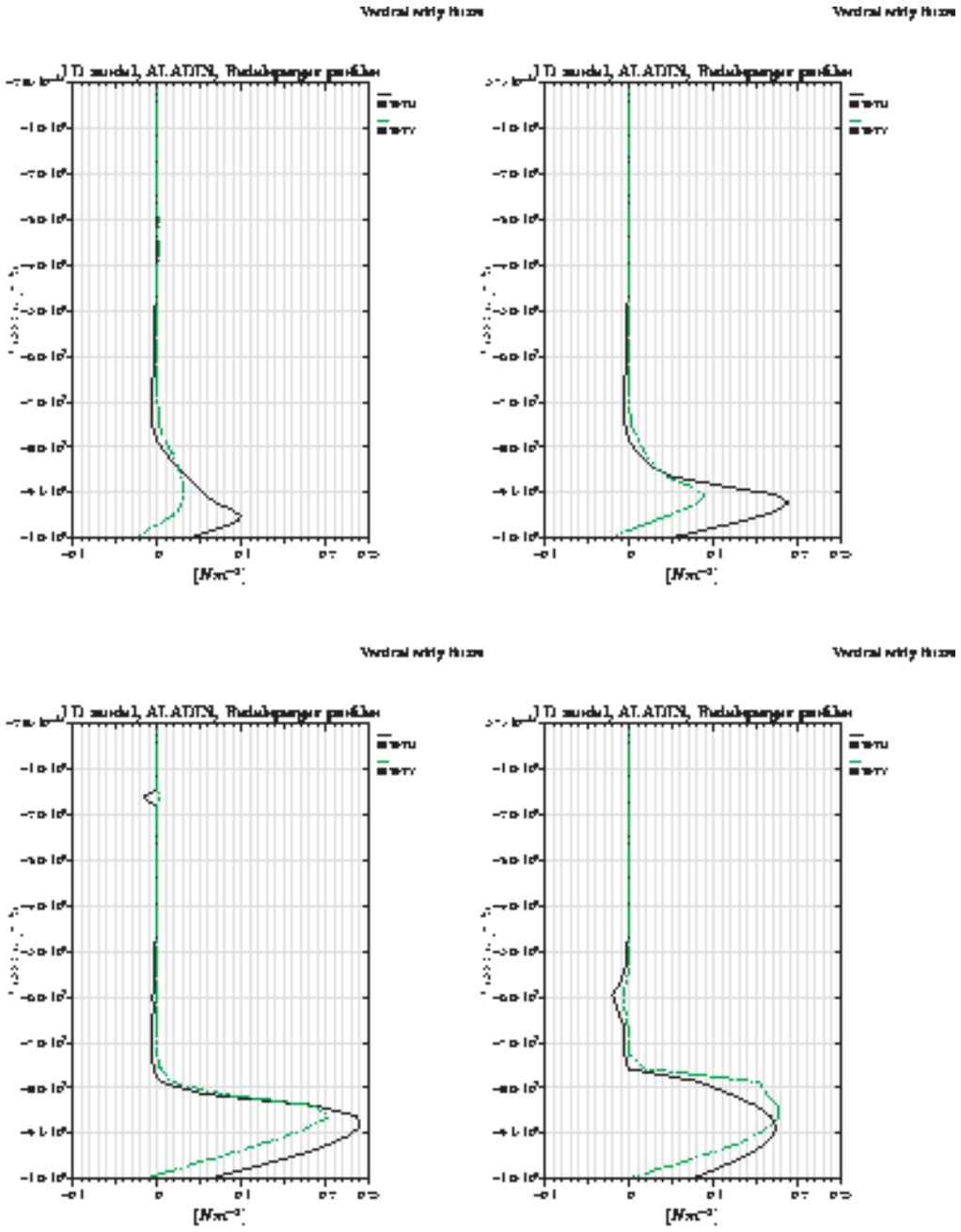

Figure 4: (a,b,c,d) The turbulent momentum flux for "U" and "V" wind components $[Nm^{-2}]$, for parameterized constants setting $c = 5.639$, $c_0 = 1.2$, $c_\varepsilon = 0.831$, $c_m = 3.115$, $c_{2m} = 0.2$. For time step $\Delta t = 10s$, $USURICE = 0.5$. The left upper corner represents picture (a) for $t = 4h$, the right upper corner represents picture (b) for $t = 5h$, the lower left corner represents picture (c) for $t = 6h$ and the lower right corner represents picture (d) for $t = 7h$ of model integration.

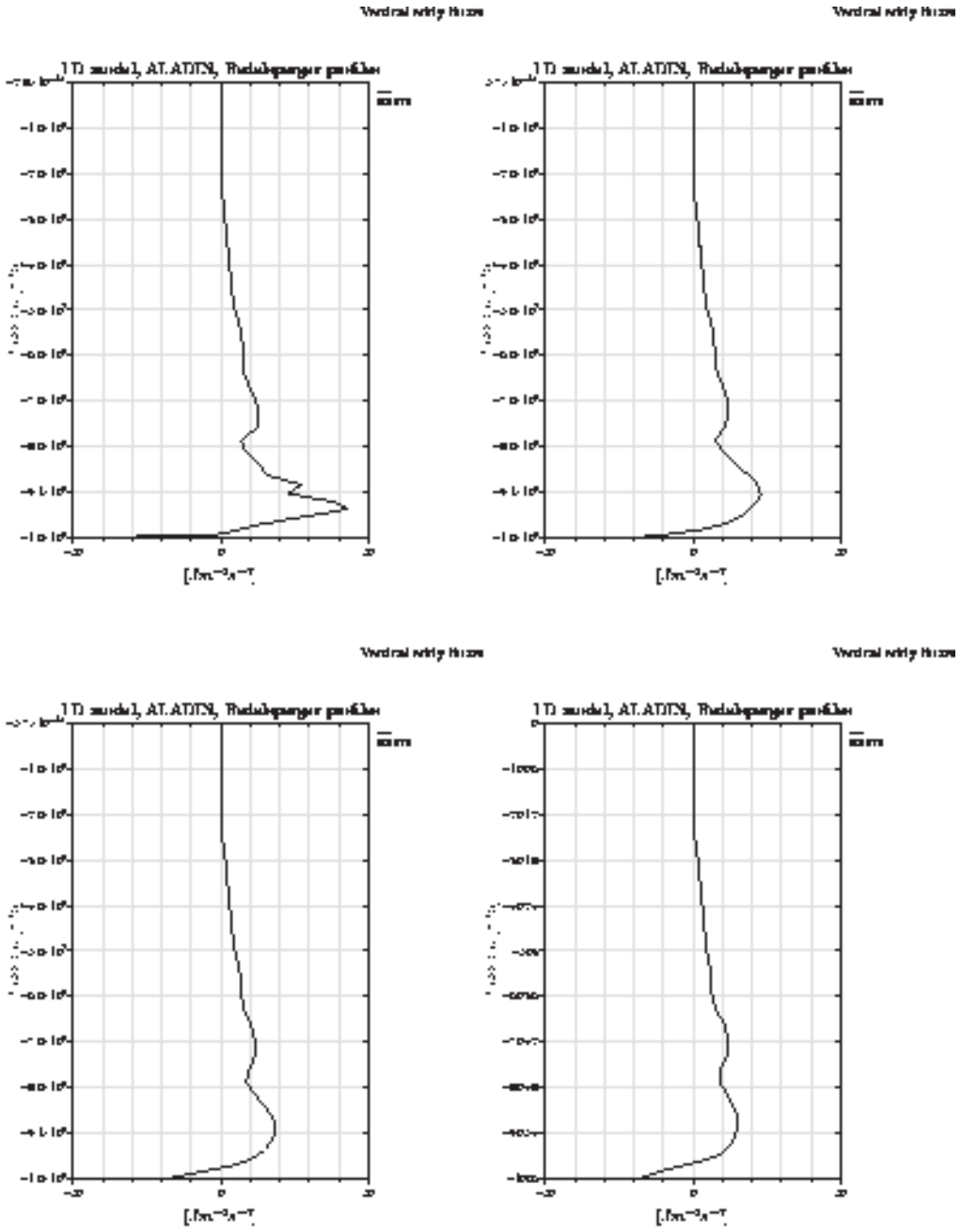

Figure 5: (a,b,c,d) The turbulent heat (dry static energy) flux $[Jm^{-2}s^{-1}]$, for parameterized constants setting $c = 5.639$, $c_0 = 1.2$, $c_\varepsilon = 0.831$, $c_m = 3.115$, $c_{2m} = 0.2$. For time step $\Delta t = 10s$, $USURICE = 0.5$. The left upper corner represents picture (a) for $t = 0h$, the right upper corner represents picture (b) for $t = 1h$, the lower left corner represents picture (c) for $t = 2h$ and the lower right corner represents picture (d) for $t = 3h$ of model integration.

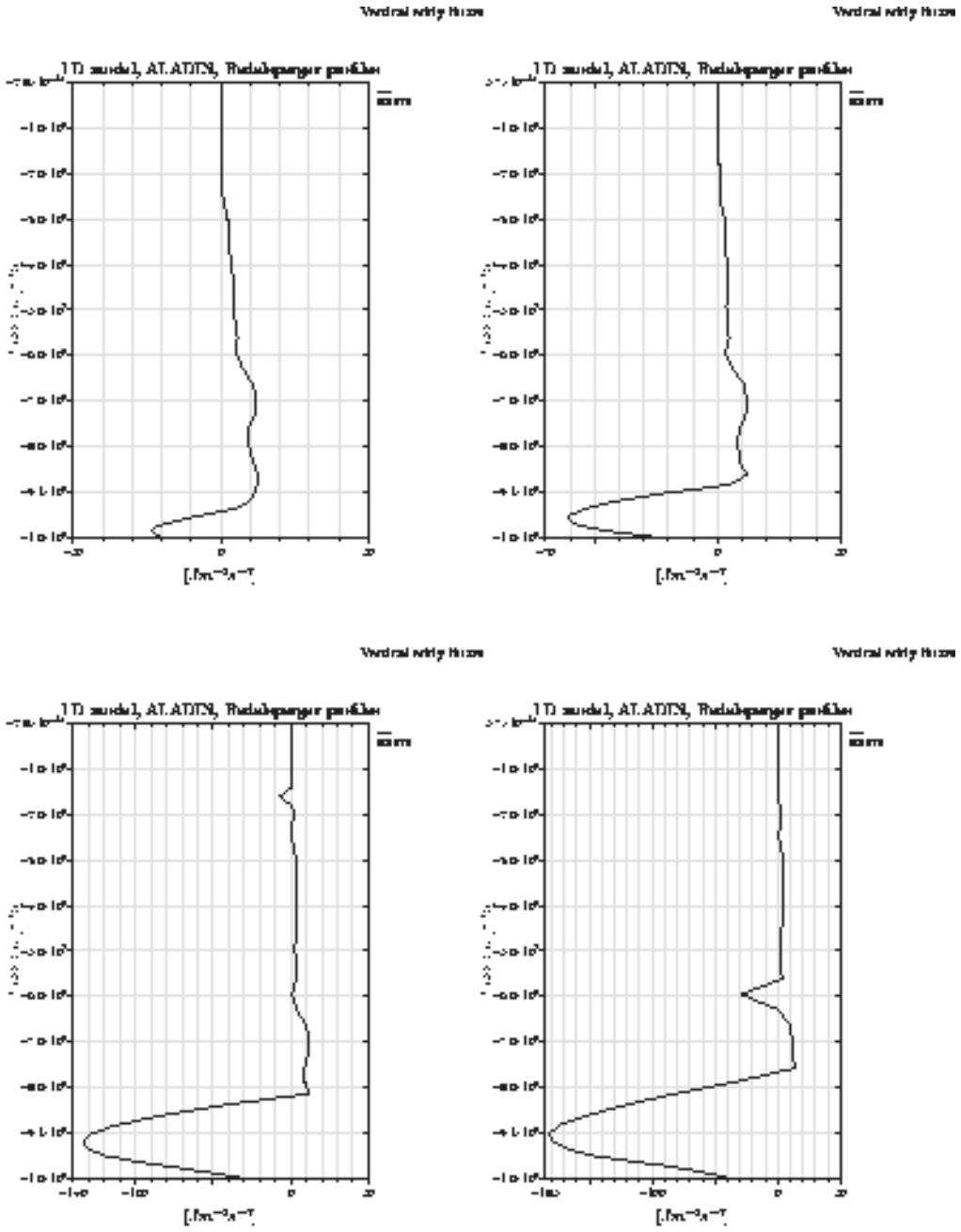

Figure 6: (a,b,c,d) The turbulent heat (dry static energy) flux $[Jm^{-2}s^{-1}]$, for parameterized constants setting $c = 5.639$, $c_0 = 1.2$, $c_\varepsilon = 0.831$, $c_m = 3.115$, $c_{2m} = 0.2$. For time step $\Delta t = 10s$, $USURICE = 0.5$. The left upper corner represents picture (a) for $t = 4h$, the right upper corner represents picture (b) for $t = 5h$, the lower left corner represents picture (c) for $t = 6h$ and the lower right corner represents picture (d) for $t = 7h$ of model integration.

4. Raluca RADU: "Extensive study of the coupling problem for a high resolution limited area model"

A large part of these six months was spent at INMH (Romania). The PhD work either was already reported in the last Newsletter, or will be described in the next one.

5. Andre Simon : "Study of the relationship between turbulent fluxes in deeply stable PBL situations and cyclogenetic activity"

(results related to ALATNET topic achieved during the period between 01.02.2003 and 31.08.2003)

Description of experiments with dry and conditional symmetric instability in the ARPEGE / ALADIN model

Introduction

The experiences with simulation of the 20 December 1998 storm, as well as the outputs of diagnostics and adjoint sensitivity tests considerably modified the original concept of the study. It was written in the previous issues of the ALATNET newsletters [7] and [8], that the success of the current vertical diffusion scheme in forecasting deep cyclogenesis in Northern Atlantic was build upon unrealistic reduction of static stability in the upper PBL levels. This kind of parameterisation had apparently drawbacks in enhancement of false cyclogenesis and destruction of inversion without possibility of a reasonable compromise based on simple retuning of the scheme. Experiments with different physical parameterisations, including Mellor-Yamada second-order closure scheme for turbulent fluxes and Smith scheme for precipitation (described in [9]), proved that the matter of forecasting deep cyclogenesis can be related to different parts of model physics (e.g. to the parameterisation of stratiform precipitation). However, the evaluated physical parameterisations didn't give realistic results on the 20 December 1998 storm evolution. Although these experiments were necessary to understand the behaviour of the simulated storm, the relationship between stratiform precipitation or cloudiness parameterisation and cyclogenesis is already beyond the scope of the originally proposed topic.

Hence it was decided to find further ways how to develop the operational vertical diffusion scheme, that could be useful for more realistic forecasts of cyclogenesis.

Theoretical background

One of the possibilities, how to adjust the current scheme of the vertical diffusion, was to find an analogue to the parameterisation of slantwise (shear-linked) convective processes. It was shown that this kind of parameterisation, described in [2], has a strong impact on model cyclogenesis (both for the false and the realistic cases). Hence it was supposed that a counterpart in the scheme of turbulent transport is necessary to reach a physical equilibrium (strong slantwise motions should be accompanied by increased turbulence and exchange of physical properties on a slope). Further motivation to continue in this direction was the problem of the shear-linked convection scheme in destroying the forecast of the 20 December 1998 cyclone and some unwanted effects in tropical convection (exaggerated height of the tops of the clouds).

The idea, how to introduce the effects of slantwise motions into the currently pure vertical physical parameterisations of ARPEGE/ALADIN, followed the work of Bennets and Hoskins (see article [1]) about symmetric instability.

For a dry atmosphere, the satisfactory criterion for symmetric instability is to reach negative values of potential vorticity. One can easily express this condition in a 2d system, using the formula :

$$P = S^4 (F^2 N^2 / S^4 - 1) = S^4 (Ri' - 1) < 0 \qquad (1)$$

where : $F^2 = f(f + \partial v/\partial x)$, $N^2 = g/\theta_0 (\partial\theta/\partial z)$, $S^2 = f(\partial v/\partial z) = g/\theta_0 (\partial\theta/\partial x)$

Hence F^2 represents the absolute vorticity of a 2d system, N^2 is the square of the Brunt-Väisälä frequency and the term S^2 contains the vertical wind-shear linked to the horizontal gradient of temperature through the "thermal wind" equation.

Consequently, the modified Richardson number *Ri'* represents the ratio between the slopes of "absolute momentum" and "potential temperature" surfaces [4]. Hence the dry-symmetric instability appears when the slope of the "potential temperature" surfaces exceeds the slope of the "absolute momentum" surfaces.

In the parameterisation we expect that similar relationships as in the 2d case can be used also for the 3d model. This is done in a simplified way by replacing the absolute vorticity and the wind-shear of the 2d systems by anological fields in 3 dimensions. Further we invert the relationship (1), saying that if dry-symmetric instability appears, the modified Richardson number will reach the neutrality in the turbulent scheme. Thus we come from the originally used Richardson number *Ri* to the modified one, named Ri_p, following the relationship :

$$Ri_p = Ri' - 1 = (\zeta / f)\, Ri - 1 \qquad (2)$$

For the surface fluxes, the way of introducing the symmetric instability is more difficult, because we don't know and we basically cannot neglect the surface values of vorticity. Hence we estimate them by a very simple power-extension formula :

$$\xi_s = \xi_{ref}\, (z_s / z_{ref})^{\alpha}, \qquad \xi = \zeta - f \qquad (3)$$

where the power is dependent on the stability between the surface and the reference lowest model level.

We can get a similar relationship as (1) for the conditional symmetric instability in a moist atmosphere. The satisfactory condition for the instability is the negative value of the moist potential vorticity, where the square of the Brunt-Väisälä frequency (N^2) in (1) is replaced by the square of the "moist" Brunt-Väisälä frequency (N_w^2). The computation of the moist Brunt-Väisälä frequency follows the expression proposed by Durran and Klemp in [3], that is already used for the parameterisation of the shear-linked convection.

The formula used for the parameterisation of the Richardson number modified by conditional symmetric instability after some approximations yields :

$$Ri_p = (N_w^2 / N^2)\, (\zeta / f)\, Ri - 1 \qquad (4)$$

The surface fluxes are treated in a similar way as in the case of the dry-symmetric instability. However, realistic diagnostics of conditional symmetric instability is a much more difficult task, as it was shown in the experiments of Bennets and Hoskins in [1]. The intensity of the slanted ascent (descent) should be dependent on such parameters as the depth of the atmosphere or the width of the updraught.

First tests with the parameterisation of the dry symmetric instability showed difficulties, when the equation (2) was applied for negative Richardson numbers. Hence the further tasks split in two parts:

a) application of the Richardson number modification only by stable stratification, where dry (conditional) symmetric instability appears,

b) different modification of the Richardson number, with indirect dependency on dry (conditional) symmetric instability represented by the Ri_p number. This dependency is separated in two formulas, with respect to the type of stratification (stable, unstable) and curvature of the flow (cyclonic, anticyclonic). The scheme gives a linear dependency of the

modified Richardson number Ri^* on the original one, with the possibility of tuning the slope of the $Ri^*(Ri)$ function.

Hence for the cyclonic case and for $Ri_p < 0$ the formula for Ri^* leads to :

$$Ri^* = \left[\left(1 + 1/a\,(1+ |\zeta / f|)^{-a}\right) / (1 + 1/a)\right] Ri \qquad (5)$$

and for the anticyclonic case (and $Ri_p > 0$) we have :

$$Ri^* = \left[(1 + 1/a) / \left(1 + 1/a\,(1+ |\zeta / f|)^{-a}\right)\right] Ri \qquad (6)$$

where "a" is a tunable parameter.

Thus we support turbulent transport in regions with dry or conditional symmetric instability in both cyclonic and anticyclonic environment and we suppress it for the anticyclonic case without presence of any instability.

Evaluation of the modified vertical diffusion

Parameterisation of the dry symmetric instability, conditional symmetric instability and conditional symmetric instability together with shear-linked convection was tested on several case studies. These included the cases with rapid cyclogenesis such as the cyclone of 20 December 1998 or the famous Christmas storms from 25 and 26 December of 1999. Besides, several cases of false mesoscale cyclogenesis in the ALADIN-France or ALADIN-LACE were evaluated.

A particular case was the simulation of the so-called "Balearic super-storm" event from November 2001, described in [6] on ALADIN-France. Forecasts of this situation by ARPEGE and ALADIN represented an intermediate between the false mesoscale cyclogenesis and the storms from December 1998 and 1999. A common characteristics for all situations is a strong baroclinic environment, where the cyclones develop very rapidly.

a

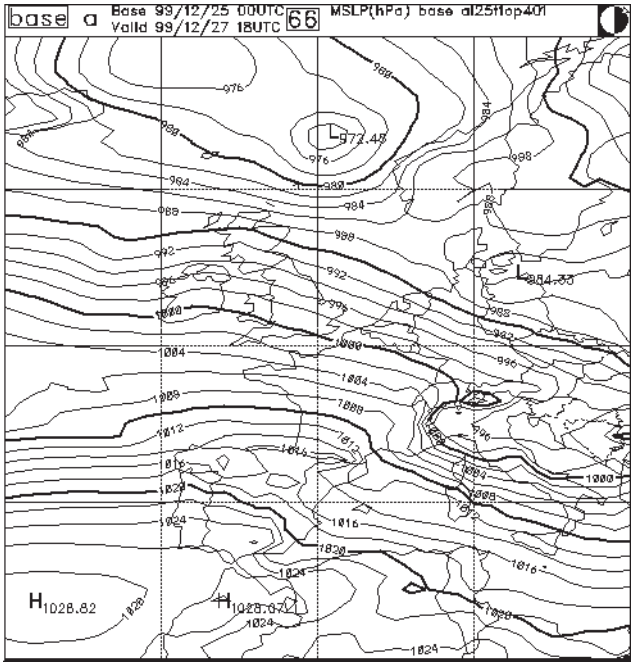

Figure 1a : 66-hour forecast of mean-sea-level pressure, based on 25.12.1999 00 UTC, in the reference ARPEGE run with the operational package of physical parameterisation (cycle 25T1_op4). Note the pattern of shallow trough towards West from the French coast.

b

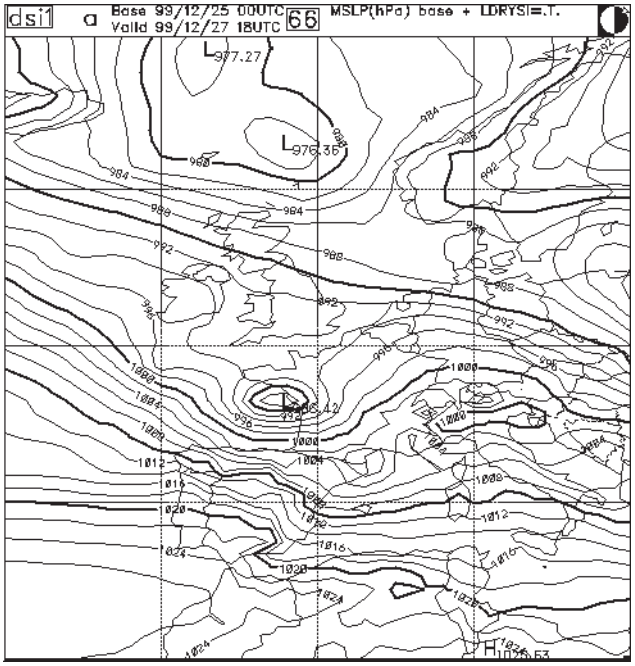

Figure 1b : The same as in Fig.1a but with activation of the parameterisation of dry symmetric instability inside the vertical diffusion scheme.

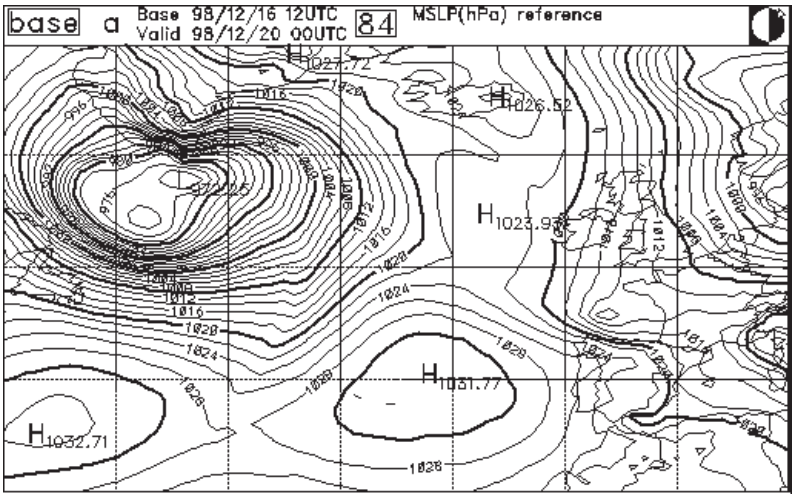

Figure 2a : 84-hour forecast of mean-sea-level pressure, based on 16.12.1998 12 UTC, in the reference ARPEGE run with the operational package of physical parameterisation (cycle 25T1_op4).

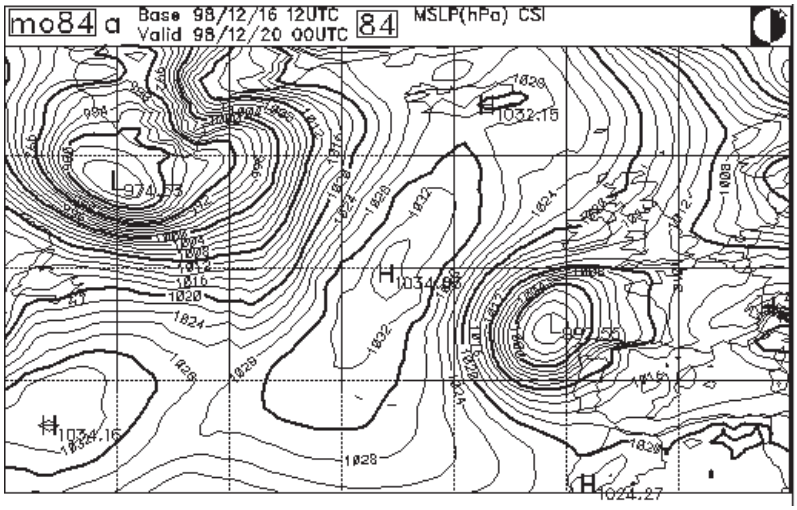

Figure 2b : The same as in Fig. 2a, but with activation of the Richardson number directly modified with respect to conditional symmetric instability.

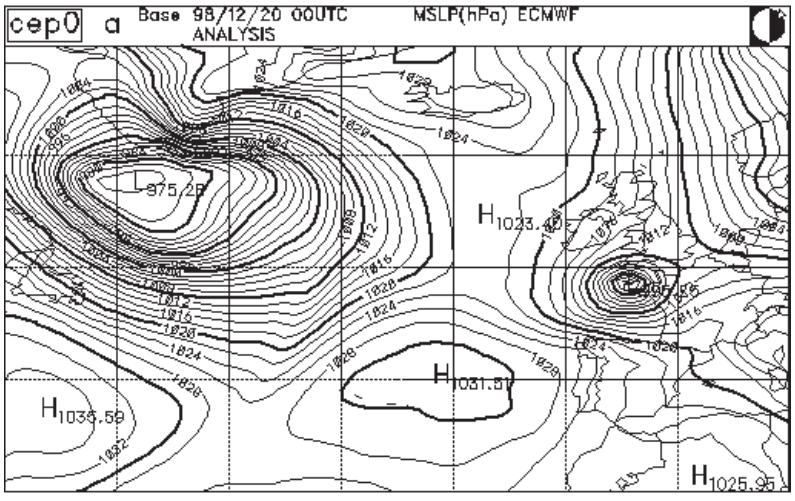

Figure 2c : Verifying model analysis valid at 20.12.1998 00 UTC

The direct application of the dry symmetric instability scheme after (2) had a very small impact on both 84- and 96-hour forecasts of the "20 December 1998" storm. On the other hand, one can see a strongly positive impact in the case of the second Christmas storm in the run from 25.12.1999 00 UTC (Fig. 1b). However, case studies on false cyclogenesis showed worse results for runs with this kind of parameterisation than for the reference model runs. The scheme was even able to trigger mesoscale cyclogenesis (e.g. in the case of false cyclogenesis from 2 May 2002).

The scheme of the conditional symmetric instability (after formula 4) had a surprisingly big effect, above all in the case of the "20 December 1998" cyclogenesis (Fig. 2). In both 84- and 96-hour runs the storm was forecasted with the scheme, whereas the reference run predicted only a shallow low or trough. On the other hand, the position of the cyclone and the shape of the mean-sea-level pressure field are not corresponding to the model analysis valid at 20 December 1998 00 UTC. Looking at the development of the storm for the period 16 December 1998 - 20 December 1998, the forecasted cyclone was never in the dissipative stage in the first 66 hours of this period. Hence the development doesn't fit with the evolution based on the model analysis [8].

Experiments on further case studies showed mostly positive impact, in contrary to the scheme of dry symmetric instability. Moreover, the parameterisation of conditional symmetric instability keeps still better performances against the reference run in the case study of the second Christmas storm. In situations with false mesoscale cyclogenesis the modified vertical diffusion was able to cancel it (runs from 02.05.2002 00 UTC and 23.08.2002) or at least to be neutral (for the case of the so-called Adriatic storm of 20.07.2001).

The worst results of the evaluated turbulent diffusion scheme were obtained for the case study of the so-called "Balearic super-storm", above all in the run from 10.11.2001 12 UTC (Fig. 3). The scheme was not able to correct the extreme gradient of pressure near the centre of the cyclone, and the depth of the cyclone was even amplified.

Additional activation of the shear-linked convection improved most of the results obtained by experiments with dry or conditional symmetric instability. This positive impact is visible on the forecasts of the "20 December 1998" cyclone, where both the position and the shape of the mean-sea-level pressure field look more realistic.

a

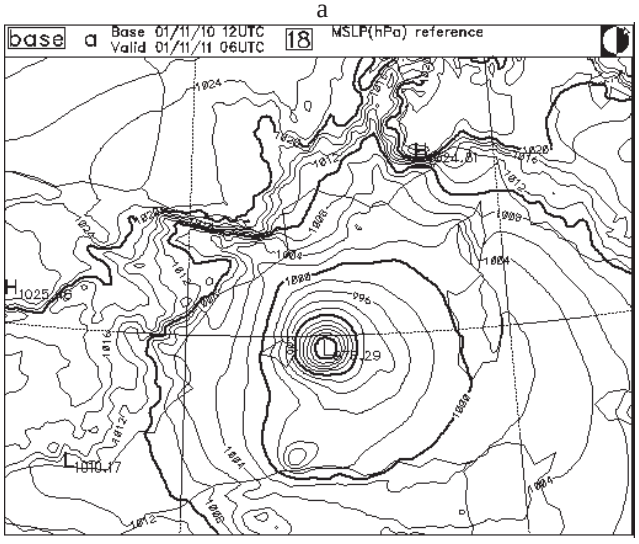

Figure 3a : 18-hour reference forecast of mean-sea-level pressure in the case study of the so-called Balearic "superstorm", based on 10.11.2001 12 UTC.

b

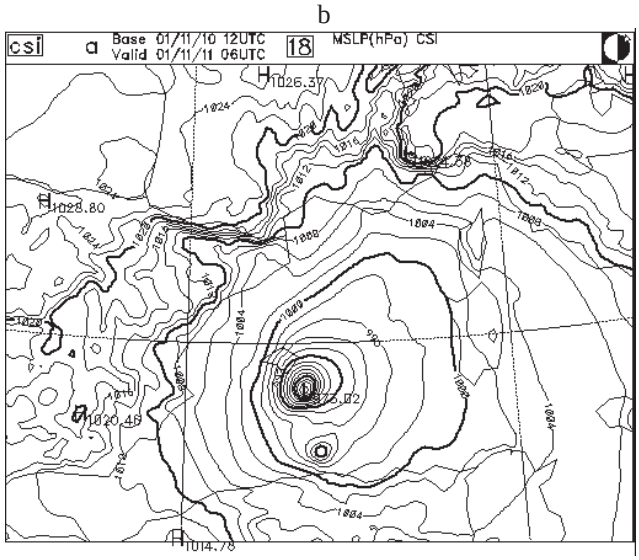

Figure 3b : The same, with activation of the conditional symmetric instability parameterisation inside the vertical diffusion scheme.

The introduction of the indirect representation of conditional symmetric instability (based on formulas 5 and 6) was tested mostly on the cases with rapid cyclogenesis (as the case of the "20 December 1998" cyclone). It seems that a linear dependency of the modified Richardson number on the original one is too weak to simulate turbulent processes connected to symmetric instability, that develop perhaps in a strongly nonlinear way.

To evaluate the global impact of the modifications based on the equations (2) and (4) budget calculations were provided on 96-hour runs of the ARPEGE model. For the scheme of the dry symmetric instability one can already see a not negligible change, mainly in the budget for temperature (Fig.4).

Apparently, the static stability at the top of the PBL is decreased mainly as a direct consequence of the changes in the vertical diffusion scheme.

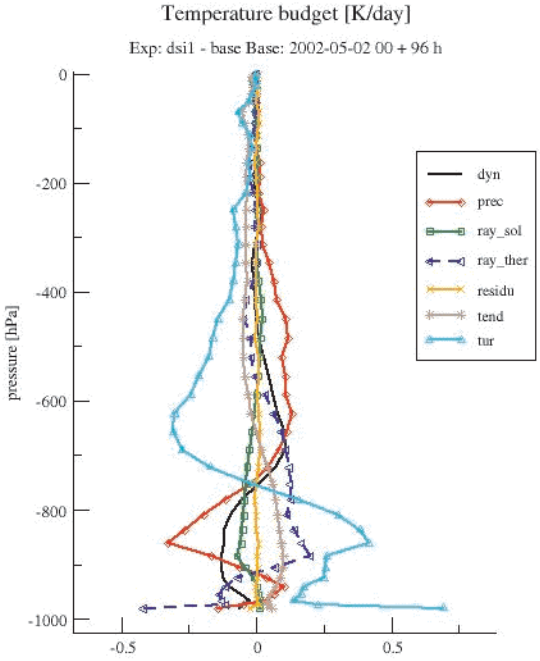

Fig.4 : Comparison of the global temperature budgets between the run with the parameterisation of dry symmetric instability and the run using the operational package of physical parameterisation (cycle 25T1_op4). Note the contribution of the turbulent fluxes (light blue line), the precipitation fluxes (prec) and the overall tendency (tend).

If we speak about considerable impact in the case of the dry symmetric instability, the parameterisation of conditional symmetric instability has already a global impact of unwanted dimensions (Fig.5). The tendency of warming the PBL and cooling the layers of mid- and upper troposphere by vertical diffusion is much bigger than in the previous case. For water-vapour budget there is a tendency to increase the transport of moisture from lower PBL levels upwards and to compensate it partially with the precipitation fluxes.

The activation of the shear-linked convection scheme has only a small influence on global temperature and water-vapour budgets, hence it is insufficient to compensate the large effect of a modified vertical diffusion scheme.

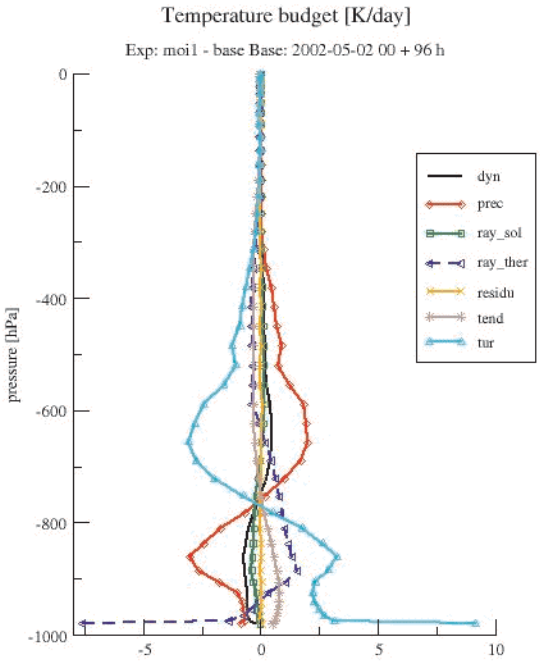

Fig.5 : Comparison of the global temperature budgets between the run with the parameterisation of conditional symmetric instability and the run using the operational package of physical parameterisation.

Conclusion

Results of the above-mentioned experiments tell us, that a decrease of stability in an environment with dry or conditional symmetric instability can be very important in the development of polar cyclones. However, the link between the conditional (dry) symmetric instability and cyclogenesis is most probably the same as it was discovered in the case of the "20 December 1998" cyclone, forecasted with the operational model scheme. Thus, cyclogenesis is generally enhanced due to large destruction of areas with high static stability in the planetary boundary layer. In contrary to the operational versions of ARPEGE/ALADIN, the vertical diffusion modified with respect to symmetric instability is more selective and dependent on the characteristics of the flow.

Nevertheless, it seems that the application of the scheme, as it was proposed using the equations (2) and (4), will not keep the desired equilibrium in the atmosphere. Adjustments of the Richardson number after equations (5) and (6) are not capable to haa ve significant impact on the selected cases because of their linear character.

Correct solution of the problem would require three conditions:

a) better diagnostics of the areas with conditional symmetric instability. The large global effect of modified vertical diffusion is most probably a consequence of overestimation of the conditions for symmetric instability by the model scheme.

b) understandings of the behaviour of turbulent processes in environment with slantwise ascent (descent). The turbulent transport in the case of symmetric instability reacts probably on the slantwise distribution of static stability and momentum. Hence it is not clear, if the turbulence propagating on a slope should be always treated in the same way as

by neutral or unstable conditions. However, there is a lack of observations, that would confirm or refuse the hypothesis applied in (2) and (4).

c) redistribution of the fluxes on a slope, where the symmetric instability in the reality acts. It is possible that a slantwise turbulent transport doesn't lead to destruction of vertically stable layers, or at least not in such amount as by the pure vertical diffusion. A similar scheme of heat distribution resulting from slantwise convection was introduced by Nordeng (1987) and published in [5]. Nevertheless, in the current 1d physical parameterisation of the ARPEGE/ALADIN model it would be very difficult (if not impossible) to compute physical tendencies in a three dimensional frame.

All of these three tasks are not trivial and not promising automatically an improvement of forecasted cyclogenesis in the case of finding the proper solution. Hence the study will in the future evaluate also different possibilities how to support cyclogenesis and anticyclogenesis through the vertical diffusion scheme. A flow-dependent representation of mixing length could be an alternative topic for the research of the relationship between turbulent fluxes and cyclogenesis.

Bibliography

[1] Bennets, D.A., Hoskins B.J.., 1979 : Conditional symmetric instability - a possible explanation for frontal rainbands, *Quart. J. R. Met. Soc.*, **105**, 945-962

[2] Bouyssel, F., Geleyn, J.-F., 2002 : Description of the so called "shear-linked convection" parameterisation, *ALADIN Newsletter*, **22**, 128-130

[3] Durran, D. R., Klemp, J. B., 1982 : On the effects of Moisture on the Brunt-Vaisala Frequency,, *Journal of Atmospheric Sciences*, **39**, 2152-2158

[4] Holton, J. R., 1992 : An Introduction to Dynamic Meteorology, ACADEMIC PRESS, third edition, 277-281

[5] Nordeng, T. E., 1987 : The effect of vertical and slantwise convection on the simulation of polar lows, *Tellus*, **39A**, 354-375

[6] Romero, R., et al., 2002 : Baroclinic and Diabatic Regulation of the 10-12 November 2001 Superstorm in the Balearics, *European Conference on Severe Storms 2002* (Prague, Czech Republic, 26-30 August 2002), powerpoint presentation and collection of abstracts

[7] Simon, A., 2002 : Relationships between turbulent fluxes and cyclogenesis, *ALATNET Newsletter*, **5**, 83-86

[8] Simon, A., 2003 : New investigations in the study of rapid cyclogenesis in Northern Atlantic, *ALATNET Newsletter*, **6**, 98-107

[9] Documentation (cycle 24T1) ARPEGE/CLIMAT, 2002, Météo-France

6. Cornel SOCI: "Sensitivity study at high resolution using a limited-area model and its adjoint for the mesoscale range"

The last months were devoted to the redaction of the PhD thesis and another paper, beside operational duties at INMH. The defence is still scheduled for 2003.

7. Klaus STADLBACHER: "Systematic qualitative evaluation of high-resolution non-hydrostatic model"

Generalities

During the last months experiments with ALADIN Cycle 25 on different domains at high resolution were performed. On the one hand it has been tried to have a look at the influence of the use of a smoothed orography on the forecasted fields (for details see the last Newsletter), while on the other hand the focus has been put on identifying the advantages of the non-hydrostatic (NH) dynamics compared to the hydrostatic (HYD) one.

Details 1

Based on the previous promising results concerning the use of a smoother orography for improving the forecasted precipitation fields at high resolution domains, one question should be answered : How much relevant meteorological information is destroyed when the original orography (which has the same spectral truncation as the meteorological fields) is replaced by a smoother one, that represents a worse description of the shape of the real surface ? A general answer won't be given here, cause this would probably require the calculation of standard verification scores, but nevertheless some hint can be found in the pictures 0 to 3. The domain is located in mountainous central Austria, the resolution is 2.5 km, the model was run with hydrostatic dynamics and coupled to the LACE model, and the shown case is taken from MAP-IOP 5. Figures 0a shows the "normal" orography (applying the Jerczinsky cost function), while in figure 0b the orography after smoothing with the additional spectral cost function is displayed. Figures 1a and 1b show the 24-hour forecast of the precipitation field using the orographies from Figs 0a and 0b, respectively. 6-hours accumulated precipitation amounts are displayed. It is evident, that the precipitation field in Fig. 1b (smoother orography) does not include that many and that extreme peaks like in Fig. 1a and using the smoothed orography generally gives a much more realistic precipitation field, that doesn't include that "chaotic" orographically caused patterns, although the significant high amounts are not totally lost. In comparison to the mentioned positive impact on the precipitation field, Figs 2a-b as well as 3a-b show the 10m wind forecast and the 2m temperature forecast respectively, for the same time. Besides other parameters these two should be considered as very sensitive to the orography description in the model. The shape of the orography influences the wind field, while the height of the mountain itself has an additional impact on the 2m temperature. For the wind just very slight differences can be seen, but in general both fields look nearly identical. For the temperatures all basic structures, like e.g. the warmer Inn, Saalach and Salzach valley are kept (Fig. 3b), but smoothing the orography logically causes a smoother 2m temperature field, which doesn't show that much small-scale variances as the original one (Fig. 3a).

The use of a smoother orography seems to make a lot of sense with high-resolution model runs, because of the remarkable positive impact on the strongly orographically affected forecasted precipitation fields and the fact that other near surface fields are not that much influenced to spoil the forecasts in a dramatic way. For this reason all further experiments on domains with high mountains are performed with a smoothed orography to make results more comparable to observations.

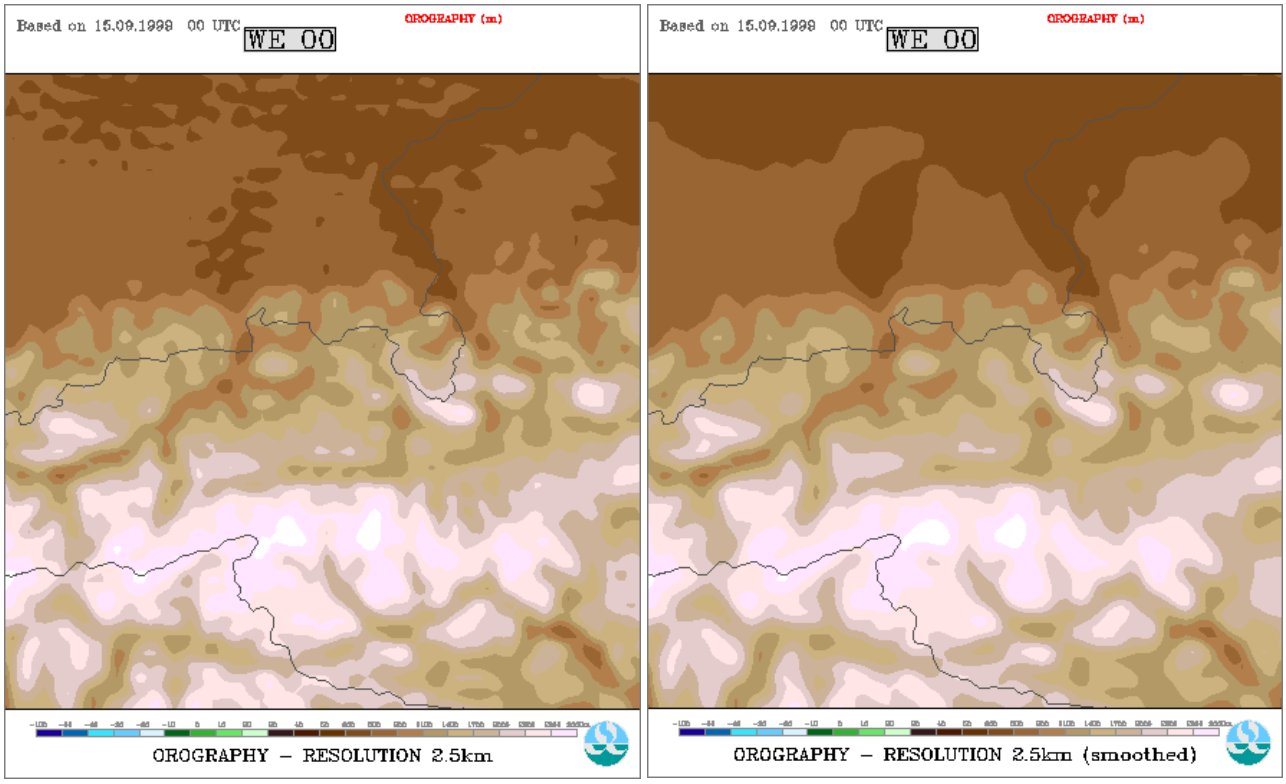

a b

Figure 1 : Model orography : a) "standard", b) "smoothed"

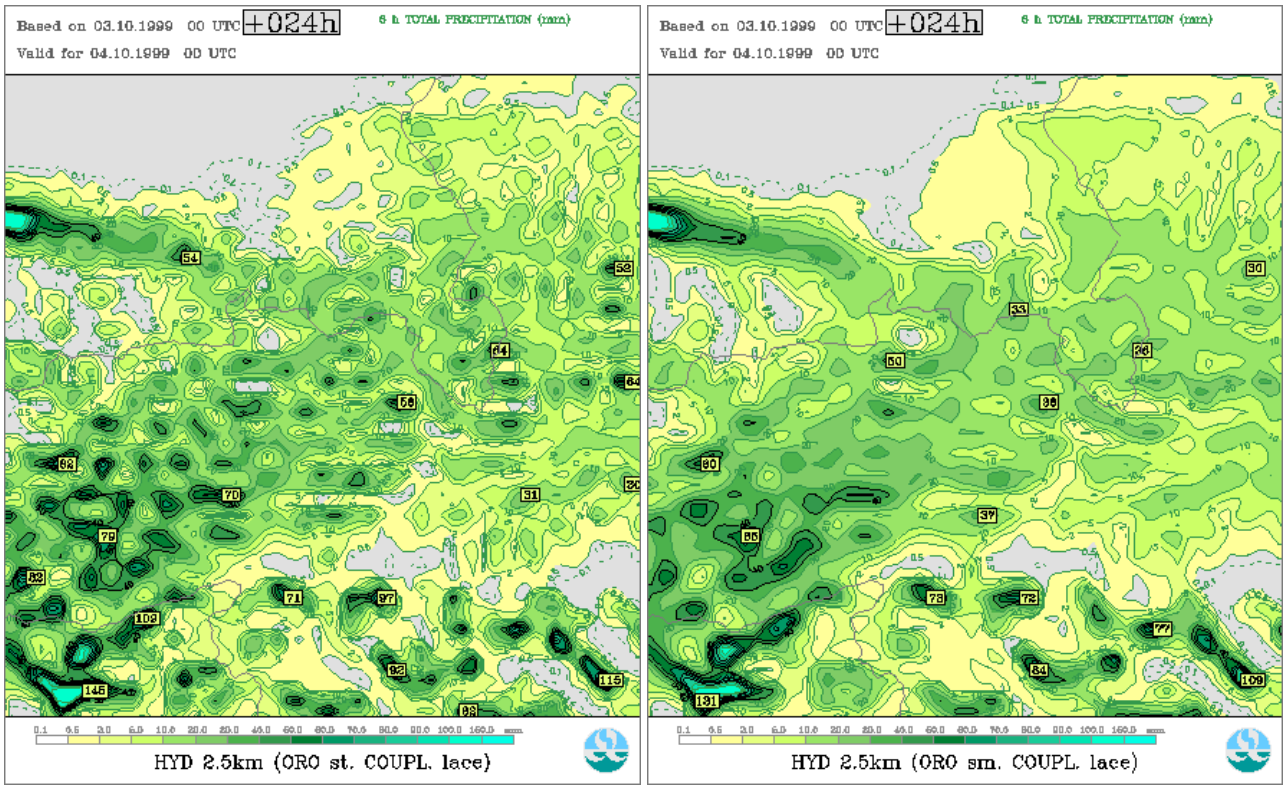

a b

Figure 2 : 24h forecast of precipitation (6h accumulated) : a) "standard" orography, b) "smoothed" orography

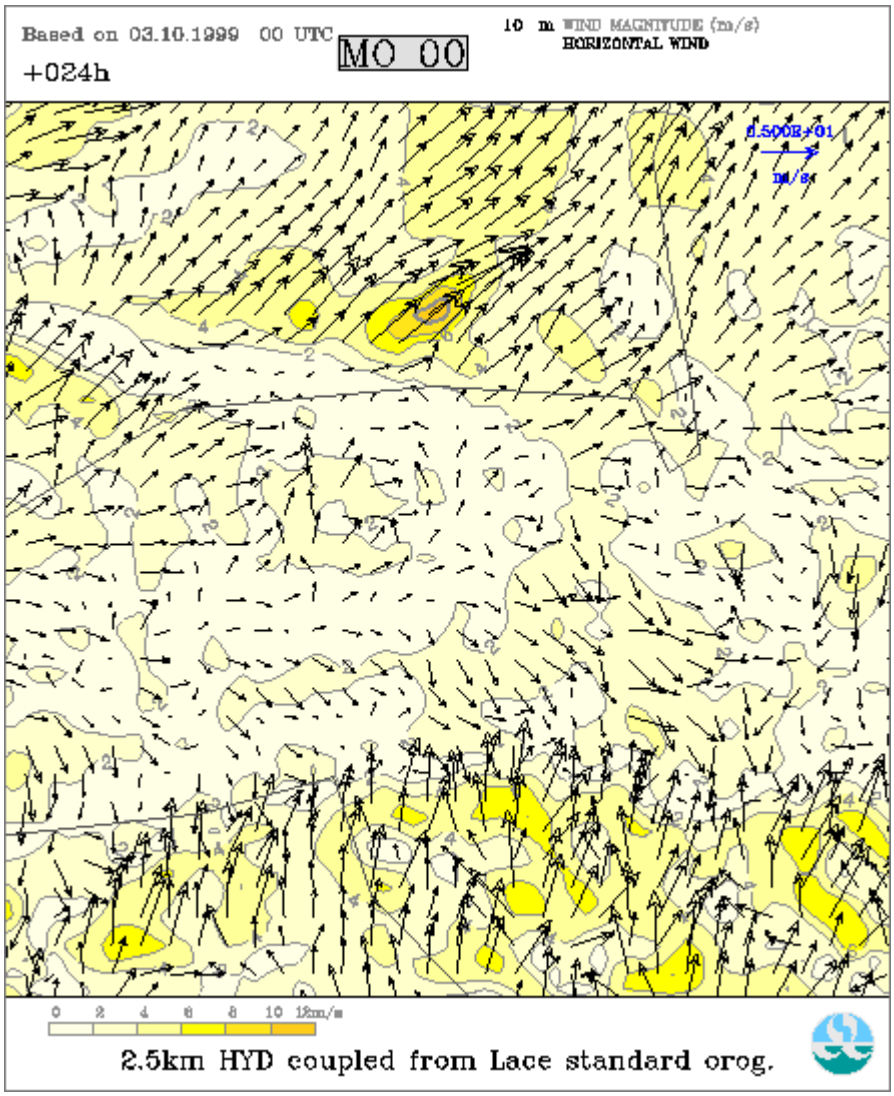

Figure 3 : 24h forecast of 10m horizontal wind : a) "standard" orography, b) "smoothed" orography

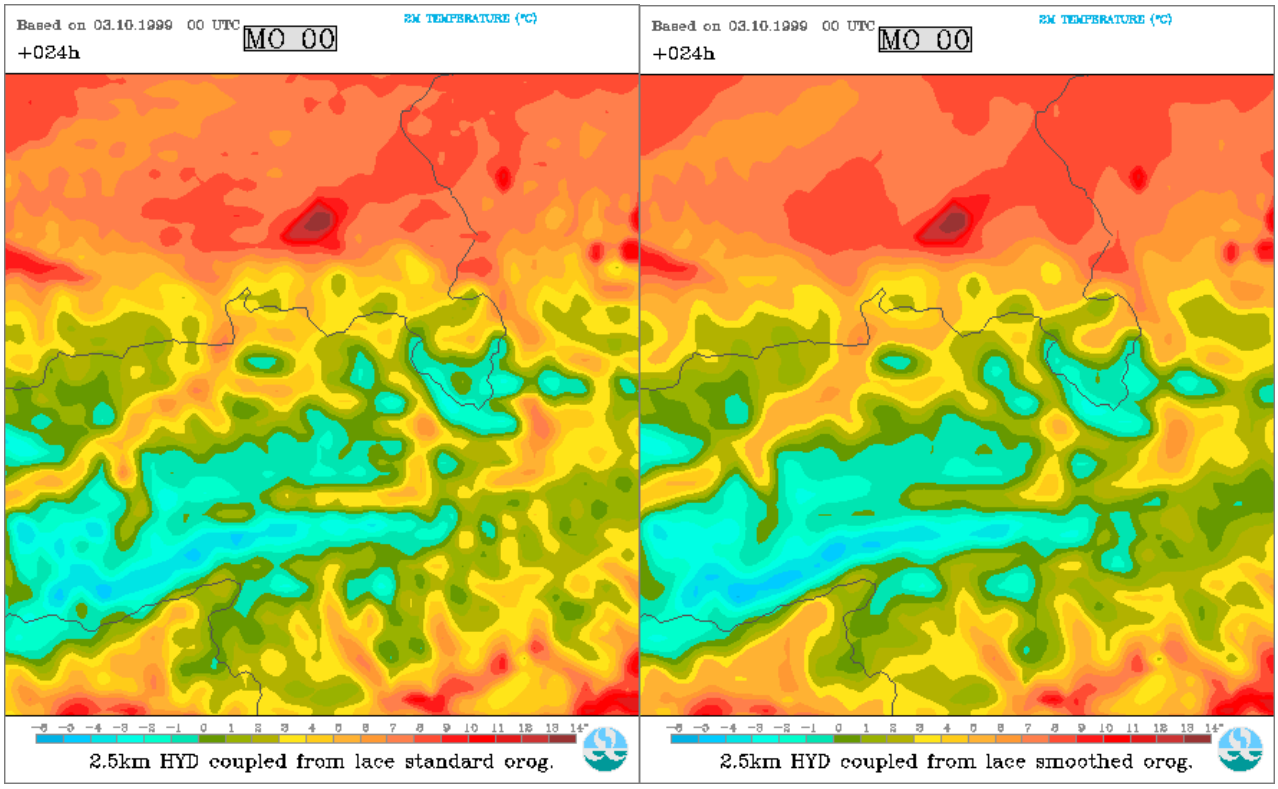

a b

Figure 4 : 24h forecast of 2m temperature : a) "standard" orography, b) "smoothed" orography

Details 2

The most recent NH developments, that were introduced into Cycle 25, led to some reconsiderations about the impact of the non-hydrostatic dynamics at different resolutions. In the previous cycles the forecasted fields at 5 km resolution seemed to be nearly independent on the dynamics used, which could be seen in very similar forecasted fields (e.g. vertical velocity and precipitation, which should clearly reveal the differences, if they are present). In Figs 4a-b, precipitation forecasts at 5 km resolution are shown. Figure 4a shows the field for the hydrostatic run, while in Fig. 4b the non-hydrostatic dynamics is used. The most evident difference can be found in the maximum peak in the South-West of the displayed domain. While the hydrostatic run produces a huge maximum (above 80mm/6h) this peak is missing in the non-hydrostatic forecast, which is much closer to the observations, that did not measure such high amounts in this region (see Fig. 4c). The other parts don't show those big differences. So in this case the impact of the non-hydrostatic dynamics can even be seen at 5 km resolution and additionally it pushes the model in the right direction in damping the unrealistic high peaks of precipitation.

Additionally the above-mentioned fact leads directly to the conclusion, that the results at a higher resolution, which are obtained with coupling to the 5 km model, are much more influenced by the dynamics used in the coupling model than seemed to be the case before.

Figures 5a and 5b show a comparison of precipitation forecasts at 2.5 km with non-hydrostatic dynamics. In Fig. 5a the model was coupled with the 5 km hydrostatic run, while in Fig. 5b the non-hydrostatic 5 km run was used for coupling. In both cases the maximum peak appears, but in the pure non-hydrostatic chain most of the peak amounts are significantly less than in the other case. Here the non-hydrostatism allows to reduce the vertical velocities to more realistic values, than is the case for the hydrostatic one.

The facts mentioned before might also be considered as important to answer the question about the nesting chain, namely to find the right resolution to go from hydrostatic to non-hydrostatic dynamics. It might give a strong hint that the resolution jump should not be too big, in order not to

loose possible advantages that might be gained in using an intermediate resolution with non-hydrostatic dynamics. Figure 6 shows the NH run at 2.5 km, when the model is directly coupled to the LACE model. This last figure should also be compared with Fig. 1b which shows the hydrostatic run for the same coupling files. Differences can be seen in the number and magnitude of the peaks (higher in the NH case !) as well as in the general shape of the field, which shows a precipitation free area in the east of the domain, that is missing in the hydrostatic case.

Try of a summary

Since cycle 25 the differences in the forecasted fields between NH and HYD dynamics have become more evident than before. This is not just true for the 2.5 km runs, but also at 5 km significant differences occur. The usage of a smoothed orography seems a proper way to get (partly) rid of strange-looking precipitation fields without doing big harm to the other meteorological quantities. It is very likely that the non-hydrostatic dynamics at high resolution do the required job, although a pure systematic evaluation should be used additionally to prove it. The fact, that the non-hydrostatism may start to act noticeable already at 5 km and therefore indirectly influences the answer to the question of the coupling model for the 2.5 km runs, might lead to the conclusion, that a pure non-hydrostatic nesting chain below resolutions of 10 km would really be the best way.

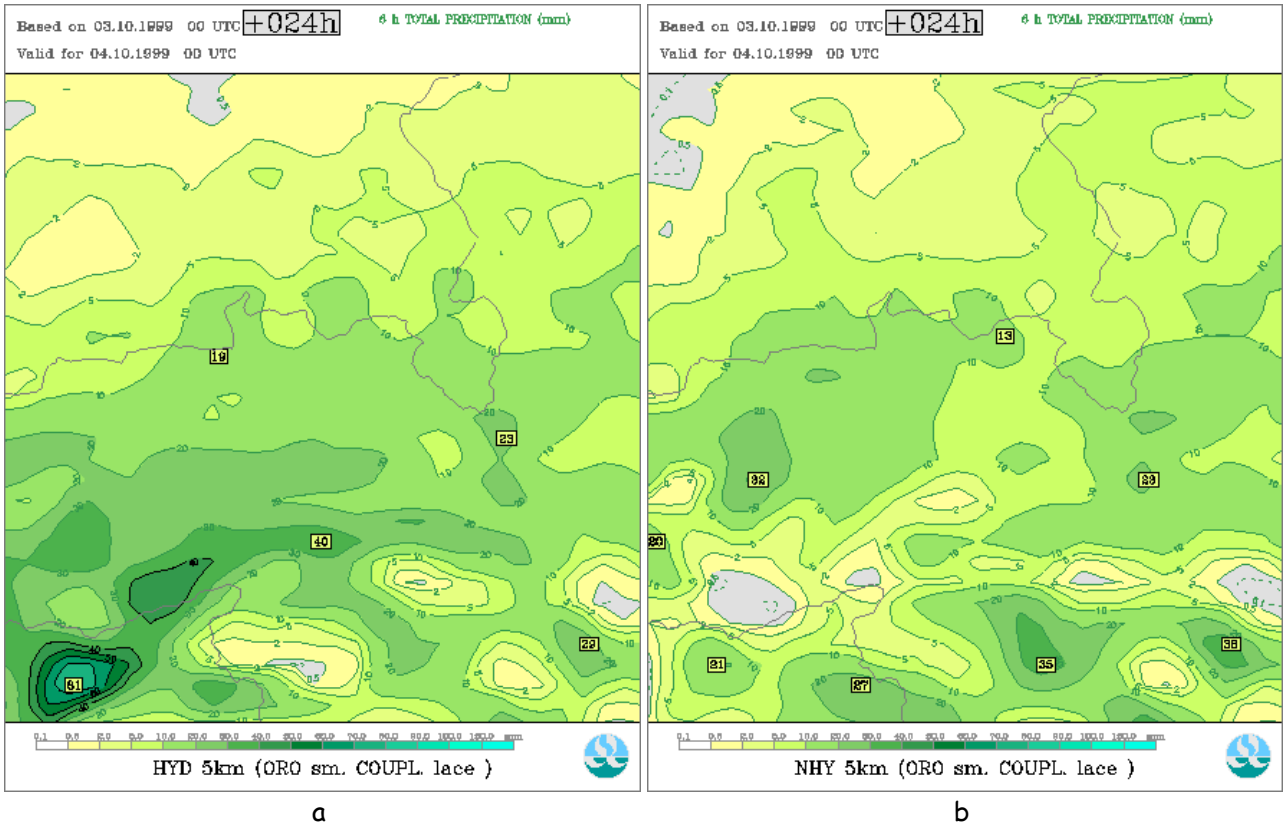

a b

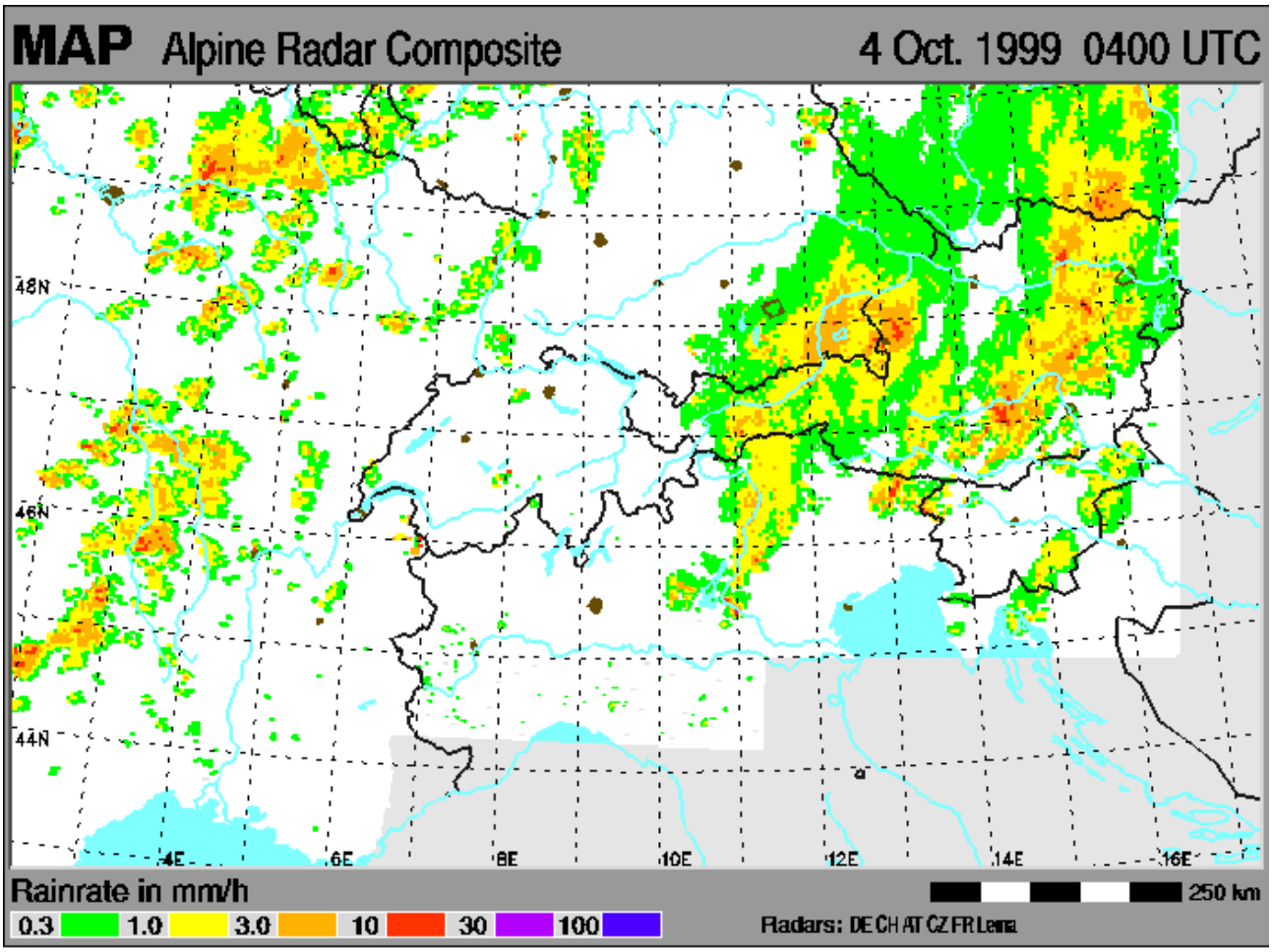

c

Figure 5: a) 24h-precipitation forecast (6h accumulated), resolution 5 km, HYD, b) 24h-precipitation forecast (6h accumulated), resolution 5 km, NH, c) precipitation measured by radar in the middle of the 6hour interval.

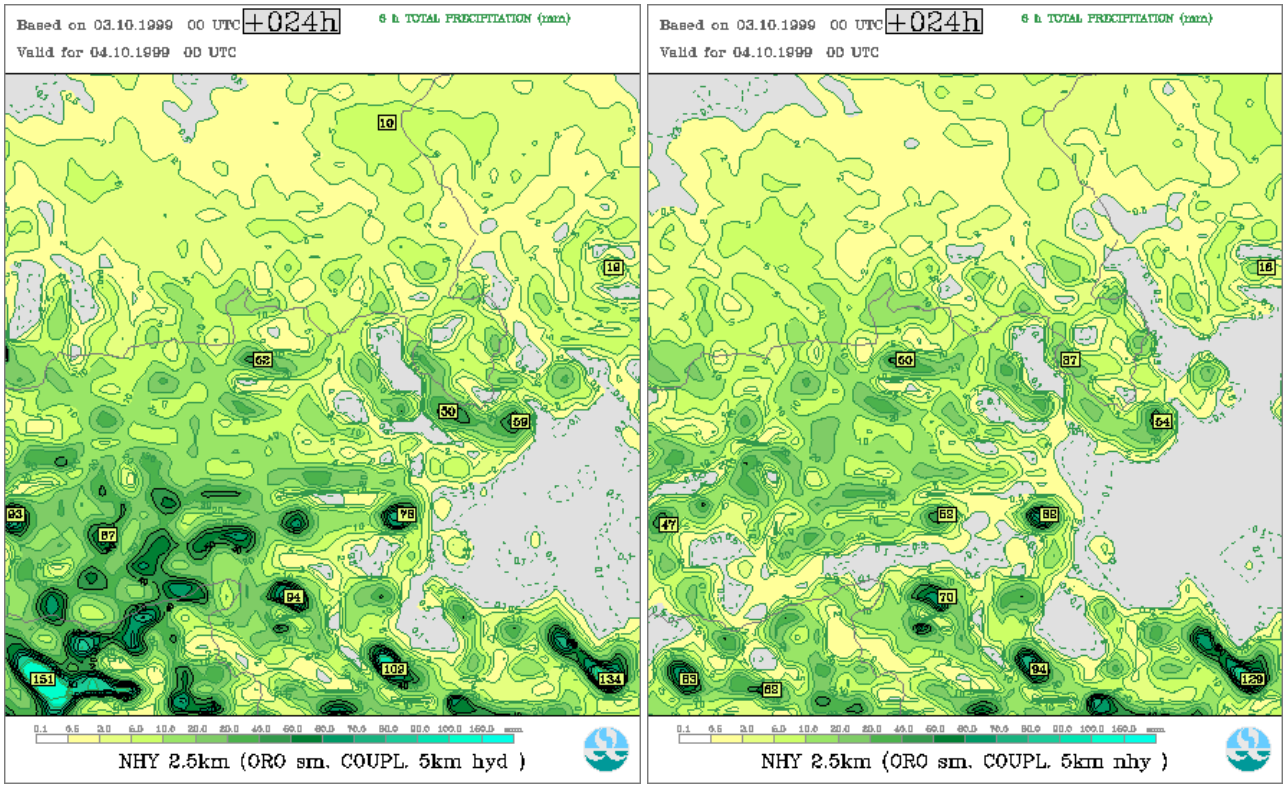

a b

Figure 6 : 24h precipitation forecast (6h accumulated), resolution 2.5 km, NH, coupled to a) HYD, b) NH

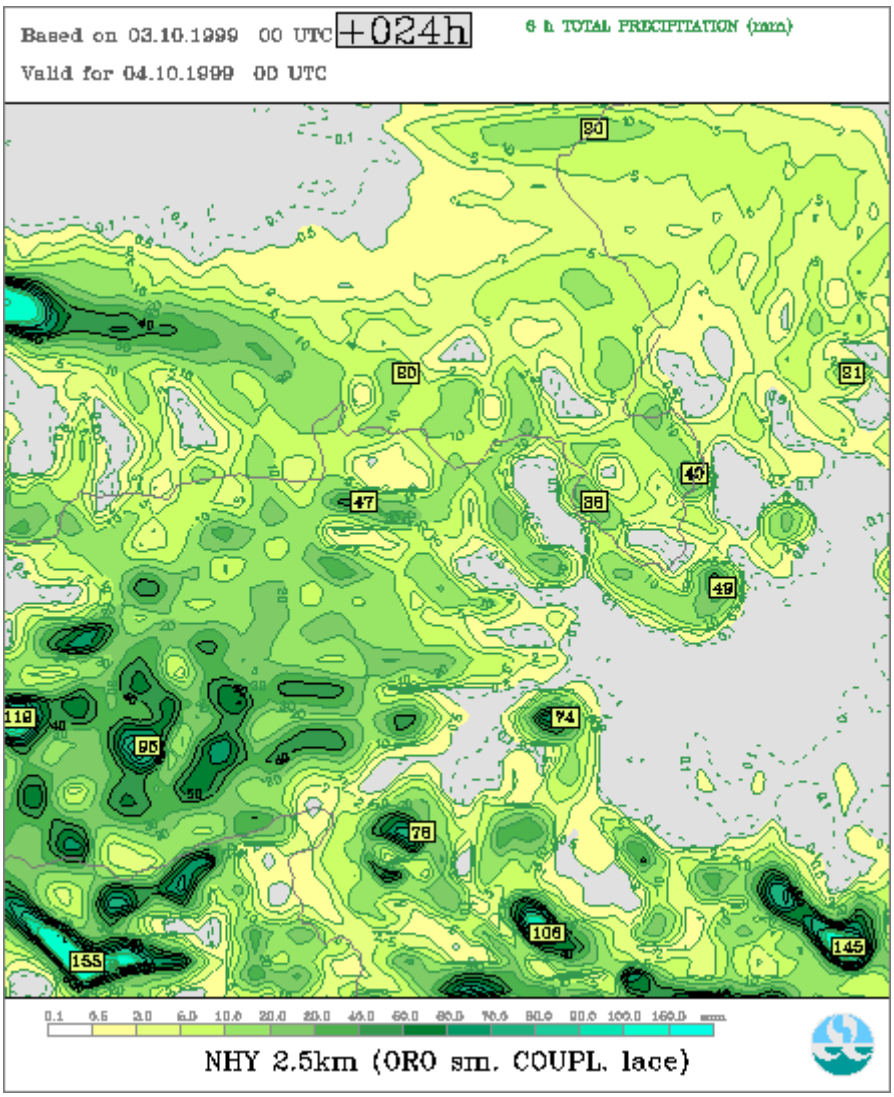

Figure 7 : 24h-precipitation forecast (6h accumulated), resolution 2.5 km, NH, coupled to LACE

8. Malgorzata SZCZECH-GAJEWSKA : "Use of IASI / AIRS observations over land"

Spectral surface emissivity for use in assimilation of IR radiance data over land

I. Introduction

The use of very high spectral resolution satellite measurements over land, as given by AIRS or IASI instruments, will certainly increase in the next few years. Preparatory studies have begun with the creation of appropriate "climatological" maps for surface spectral emissivity (SSE). In this report I will present maps of these quantities. Emissivity maps were prepared on the base of the new ECOCLIMAP (Masson et al., 2002) vegetation and land cover types and the infrared SSE values from spectral libraries (MODIS, ASTER and JPL) compiled with the ones modelled by Snyder et al. (1998). New emissivity maps were produced separately for 18 wavebands in the infrared spectral range and for each month. The final maps were validated with MODIS channel 31 and 32 land surface emissivity products based on the "split-window" method. Further validation of this new SSE was performed by quantifying the impact brought by this new emissivity when computing simulated radiances for IR sounder. It was carried out first in the radiative-transfer model RTTOV-7 and High-resolution Infra-Red Sounder (HIRS) channel 8 data. A successive step has consisted in the validation of the emissivity with Atmospheric Infrared Sounder (AIRS) measurements. Extensive tests of the SSE with the AIRS data are currently performed. Additionally, preliminary experiments with emissivity as a control variable in a 1-dimensional variational assimilation model (1D-Var) have been run.

II. Land surface types and emissivity climatological maps

The new classification of surface types was based on ECOCLIMAP, a complete surface parameter global dataset (Masson, 2003). In general, areas of homogenous vegetation were represented by 215 ecosystems. They were derived by combining existing land cover maps, climate maps, normalised difference vegetation index (NDVI) inferred from observations of the Advanced Very High Resolution Radiometer (AVHRR) instrument and The Food and Agriculture Organisation (FAO) database of soil texture.

Most of these ecosystems were a combination of only one of the following 12 vegetation types (so-called pure ecosystems) : bare soil, rocks, permanent snow and ice, crops type C3 (omnipresent except tropical and equatorial belts, and where the corn is intensively cultivated), crops type C4 (applied for crops C3 exceptions), irrigated crops, natural herbaceous (temperate), natural herbaceous (tropics), wetland herbaceous or irrigated grass, needle-leaf trees, evergreen broad-leaf trees, and deciduous broad-leaf trees. Those pure ecosystems with addition to urban areas and water gave us full description of 14 simplified global land cover types, for further emissivity assignments. Currently in the climatological files for the ARPEGE model, 5 land-cover types exist : high vegetation, low vegetation, bare soil, permanent ice and water. The estimation of the emissivity covariance matrices was based on these 5 ARPEGE types, as there was not enough emissivity spectra samples to built separate background error covariance (B) matrices for each type. ARPEGE land-cover types were believed to be representative enough to use them for the characterization of the emissivity background errors.

The Infrared Atmospheric Sounding Interferometer (IASI) range (645-2760 cm^{-1}, 8461 channels) has been divided into 18 wavebands with respect to their usefulness for the channel selection (informative bands). The wavebands have been chosen more narrow and dense in areas with high (> 0.5) transmittance running average over 40 channels. This was done in order to follow the variability of the land cover types spectra and to validate the emissivity climatology created from MODIS emissivity maps (channels 31 and 32). The resulting wavebands are: 645-760, 760-805, 805-885, 885-950, 950-1000, 1000-1068, 1068-1135, 1135-1210, 1210-1240, 1240-1968, 1968-2020, 2020-2064, 2064-2120, 2120-2180, 2180-2450, 2450-2575, 2575-2720, 2720-2760 cm^{-1}. Climatological fields of surface spectral emissivity were created respectively to these wavebands. The creation was based on the global new land cover types and vegetation maps with resolution of 0.5 all over the globe (Masson, 2003) and SSE calculated for each of 14 simplified types from separate emissivity spectra of different natural and man-made materials. Then, the SSE maps were taken as an input for the modified climatological configuration of the ARPEGE model in which emissivity was interpolated to the final model grid.

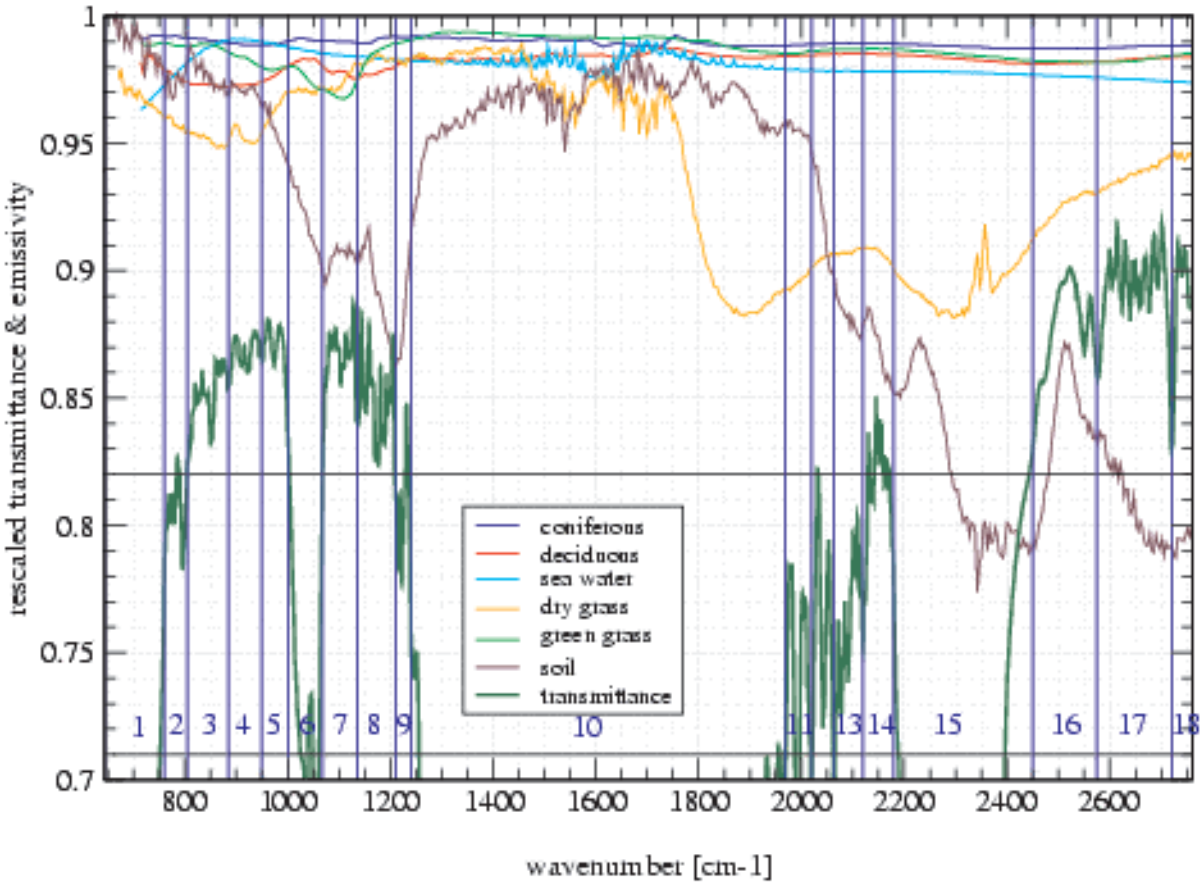

Figure 1 : IASI transmittance and emissivity spectra of different land cover types. Transmittance (thick green) is a running average over 40 channels (scaled by 1/3 then shifted by +0.6).

III. Validation of the SSE maps

The validation of the spectral emissivity climatological maps has been done in a few steps. Firstly we have compared (subjective) SSE maps for wavebands 805-885 cm^{-1} and 885-950 cm^{-1} with the MODIS emissivity maps for channels 32 and 31 respectively. The next step consisted in testing the new SSE in the radiative-transfer model RTTOV-7 with use of observations of HIRS instrument channel 8, which points to the surface. Finally, tests were performed with real AIRS data in pre-selected 324 channels (also using RTTOV-7).

MODIS

The Moderate Resolution Imaging Spectro-radiometer (MODIS) instrument on board NASA's Terra satellite routinely retrieves land surface products, and SSE among them. The method used for retrieval of emissivity maps which were used for our initial comparison was the "split-window" technique, using MODIS bands 31 (centred at 900 cm^{-1}) and 32 (833 cm^{-1}). These data are available at 1 km spatial resolution, and temporally divided into groups: individual swath data, 1-day average and 8-day average. Figure 2 presents an example of comparison of the surface spectral emissivity climatological map for the month of August against the MODIS SSE composite of individual swaths for the 20 of August 2000. One can note a good correspondence between the emissivity fields.

MODIS data are free of charge and can be accessed from the webpage referenced in bibliography.

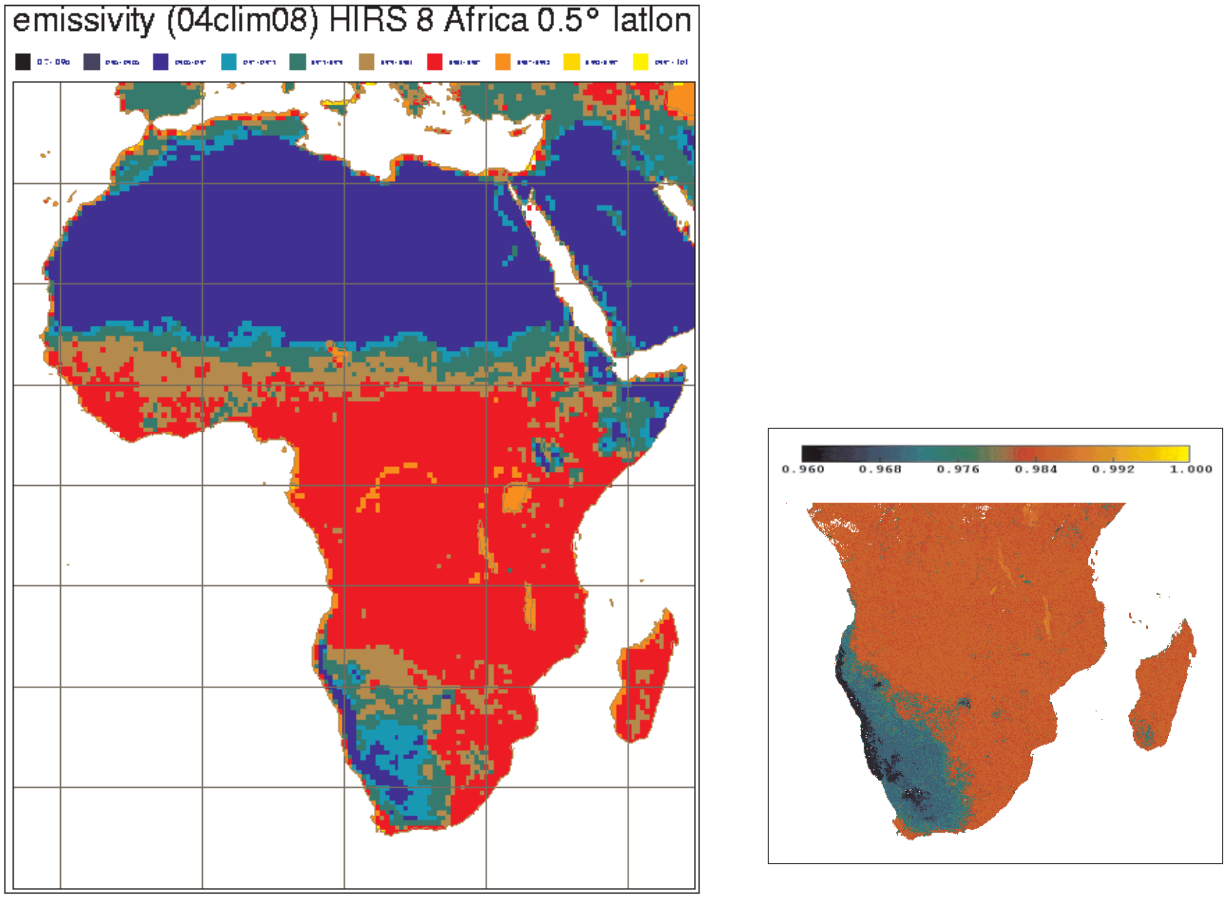

Figure 2 : On the left side - climatological map of the SSE for the month of August, and on the right one the SSE composite map retrieved from MODIS band 31 measurements. Both figures have the same colour scale.

HIRS-8

As already mentioned, this new SSE was also tested against observations of the HIRS instrument, for channel 8. This channel is centred at 900 cm^{-1} with half-power bandwidth equal to 35 cm^{-1}. It corresponds very well to MODIS band 31, is very sensitive to surface parameters and it can be used to detect cloud contamination. As we work with surface data, so there is a strong requirement that the radiances we use were measured in clear-sky conditions. Tests have been done on the differences between measured and the forecasted brightness temperatures (obs-guess) in this channel window. As a forecasted brightness temperature (Tb) we use the brightness temperatures

calculated in RTTOV-7 from atmospheric state vector taken from the 6-hour ARPEGE model forecast. This state vector is a vertical atmospheric profile containing the temperature and humidity at 43 pressure levels, surface air and skin temperature, surface pressure and surface spectral emissivity. A cloud test to eliminate the cloudy points we applied on channel 8, assuming that for clear-sky conditions the difference between measured and the forecasted Tb lies in between -1 and 2 K and is not latitude dependent .

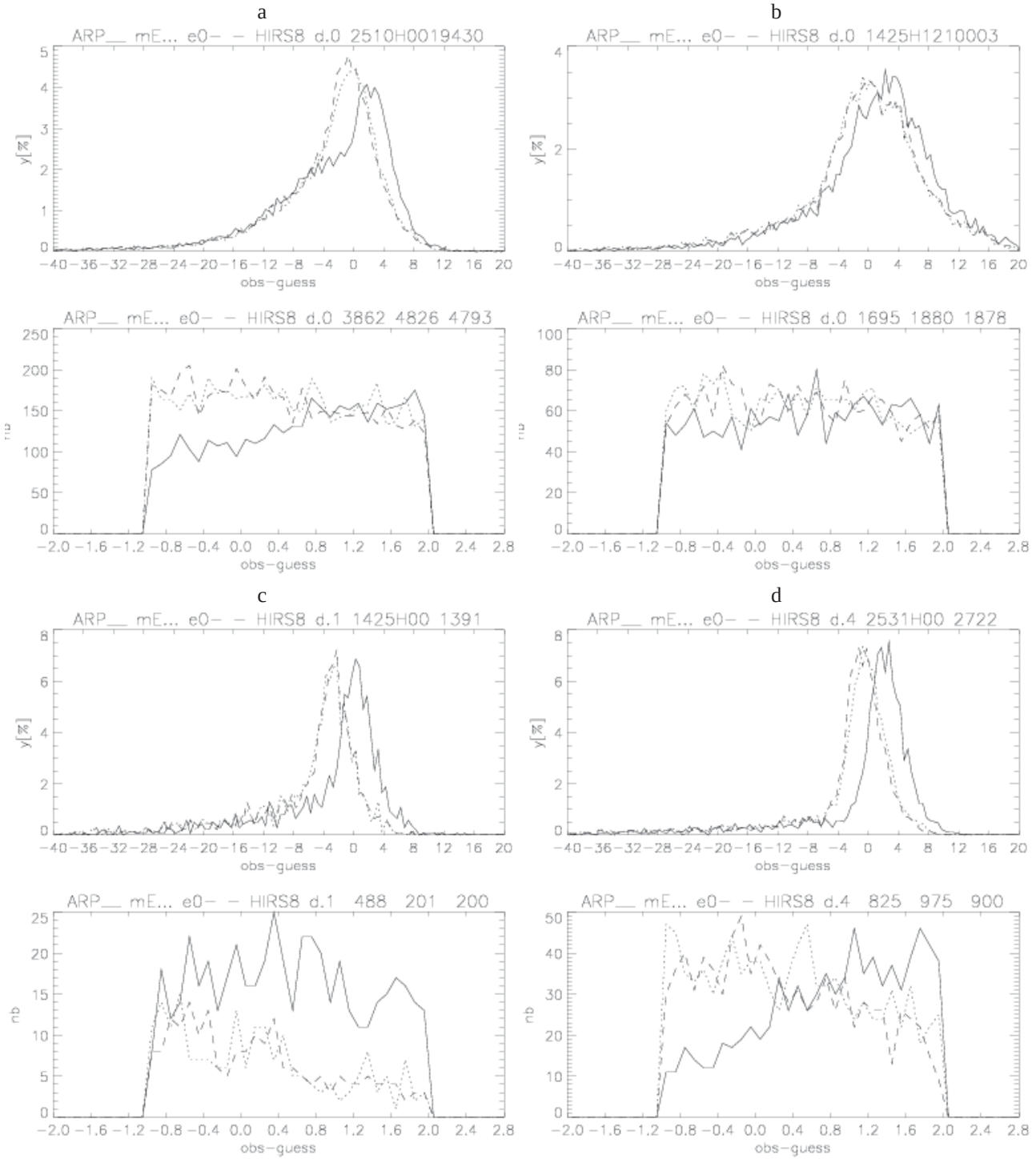

Figure 3 : Histograms of obs-guess values for different days and domains. a) and b) are cumulated over the whole globe, c) over Europe and d) over Africa. Temporal ranges are: a) 25-31.12.2002 cycle 00z, b) 14-25.06.3002 cycle 12z, c) as"b" but cycle 00z, d) as "a". Upper graphs : whole sample, lower ones : just "not cloudy" points considered. Solid lines : used ARPEGE emissivity, dotted lines : new SSE, dashed lines : RTTOV-7 emissivity.

To evaluate the quality and usefulness of the new climatology for emissivity, we compared the values of obs-guess with the RTTOV-7 run for different values of surface emissivity for the same state vector. As a first reference run the emissivity from ARPEGE was used, i.e. SSE=0.93 for dry land, 0.99 for moist land and partial snow-cover and 1.00 for ice-caps and full snow-cover.

The second one was RTTOV-7 run with its own emissivity value, i.e. SSE=0.98 everywhere over land. All the tests were performed on the same sample of initial profiles. On Fig. 3 the top graphs represent histograms of the full range of obs-guess values, and the bottom ones - the number of cloud free or small obs-guess points in each sample. The solid line is the ARPEGE reference, the dotted one corresponds to the new SSE, and the dashed one to the RTTOV reference. Note the values written in the titles of bottom graphs, they are the number of profiles for which obs-guess values pass the "cloud test".

The results are not obvious to interpret, they do not show clearly and unambiguously the general improvement of the estimated Tb converted by the radiative-transfer model with the use of the new surface emissivity. We compared the number of profiles for which the difference: observed Tb and estimated one in RTTOV, had stayed in the range -1 to 2 K ("cloud test"). What we can observe is that for the period 25.12.2002-10.01.2003 use of new SSE considerably improves the values of simulated brightness temperature in comparison with the ones obtained with the use of the SSE from the ARPEGE model (Fig. 3a). On the contrary for the period of 14-25.06.2003, especially in Europe, use of surface emissivity from global model gave the best results (Fig. 3c). One explanation of that could be the unusually hot and dry summer in that region this year. The state of vegetation was not similar to the "climatological" one. It means that instead of green grass and crops there were dry ones. As one can see on Fig. 1 the difference between dry and green grass emissivity spectra in band n° 4 (corresponding to HIRS channel 8) was significant. So, as the result SSE=0.93 (as it is in ARPEGE) appeared to be better for that unusual period than the new SSE with values between 0.973 and 0.987. Considering Tb calculated with use of SSE=0.98 (RTTOV default value for land) as a reference, it seems that the new SSE did not improve very much the estimation of brightness temperature. In some cases the difference in the number of "good" points was negligible (Fig. 3abc), in the others it could reach up to 8 percent (Fig. 3d).

In general one can say that the use of new SSE decreased the difference between measured and the simulated brightness temperatures, or stayed neutral. But there could exist exceptions while some extreme, long-term atmospherical conditions appeared. Moreover some additional tests on just clear sky profiles could give more detailed ideas about new SSE behaviour.

AIRS

For the validation of the new SSE with usage of AIRS measurements, the same strategy was applied, with a different cloud detection and channel selection. The AIRS cloud detection scheme was based on multi-channel data, and it was found to be quite sensitive to small clouds only partially filling the field of view, optically thin cloud and stratiform cloud with a top temperature near identical to the surface (Smith, 2003). So, it was more accurate with comparison to the "cloud test" we have applied to HIRS 8 data. Additionally the AIRS imager was also used to detect clouds. As a result the validation of new surface emissivity have started on profiles for purely clear sky conditions.

As the Atmospheric Infrared Sounder is an instrument with very high spectral resolution the use of all 2378 channels is not practical and efficient. So thinning of the data was advised and the subset of 324 channels was prepared by the NOAA AIRS Science Team. These channels were grouped into the 18 earlier mentioned bands, but because of some differences in spectral coverage of IASI and AIRS instruments, the wavebands number 11, 12, 13, 14 and 18 were out of AIRS range. Additionally in ARPEGE 1D-Var satellite radiances assimilation there was no ozone analysis included, so channels from bands 5, 6, 7 and partially 9 were blacklisted from the assimilation

process (i.e. they do not enter the analysis). The other problem was caused by "solar contamination" in the short-wavelength part of the spectrum. Channels touched by this problem could be used by night, but then the AIRS imager could not be used to detect clouds. As a consequence we rejected also the wavebands 16, 17 and partially 15. From the remaining bands we also excluded the ones with low transmittance values (these channels were not seeing the surface), namely number 1, 10 and also 2. Finally only two full bands remained : 3 (four channels) and 4 (four channels), and partially band 9 (one channel) and 15 in long-wave part. Considering the usefulness of the bands we neglected band 9 because of a lack of channels to compare with and to analyse impact of the SSE. From waveband 15 we kept four long-wave channels pointing to the levels closest to the surface. Summarizing, for SSE validation with the AIRS data and subsequently in 1D-Var we could use three bands 3, 4 and 15, with 12 channels.

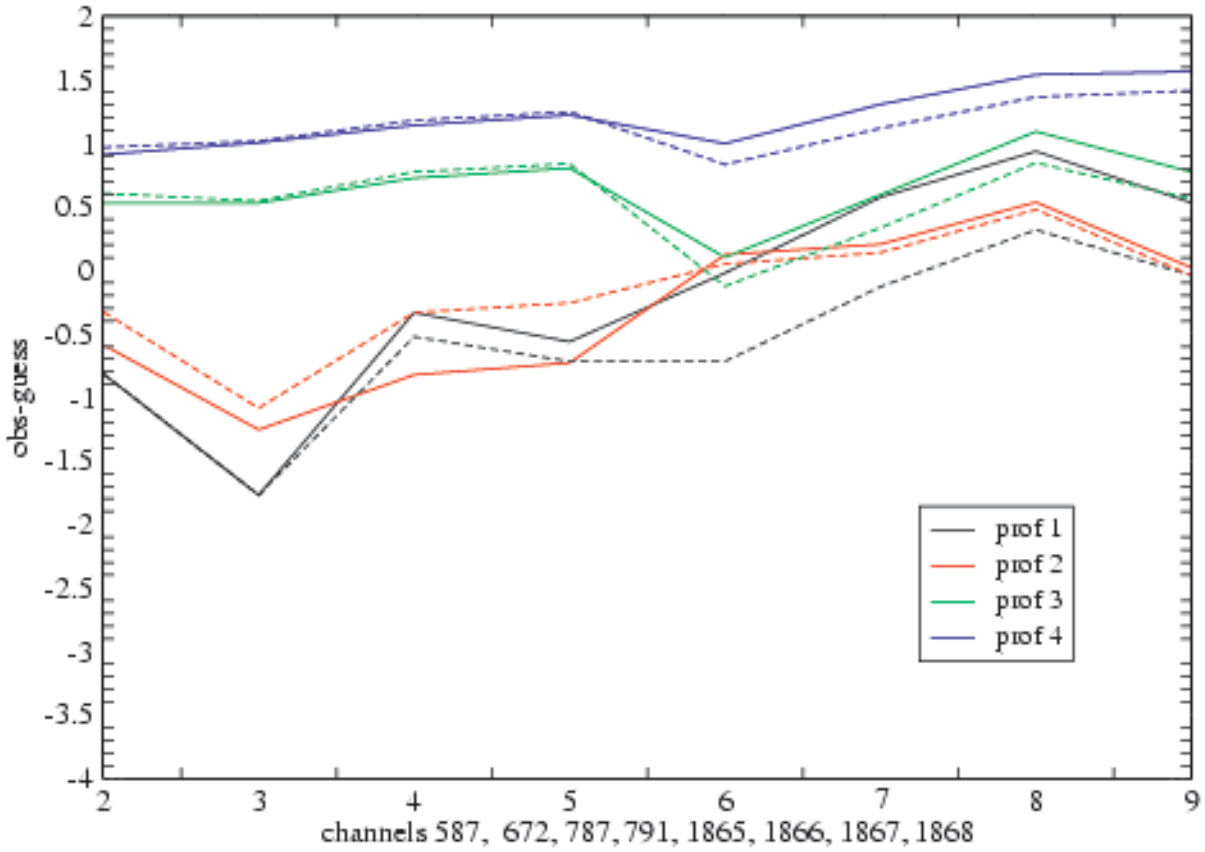

Figure 4 : Obs-guess values of Tb for 8 selected channels in 2 bands. Continuous line refers to SSE=0.98 (RTTOV, reference), the same colour but dashed line corresponds to new SSE.

As we intend to use the same wavebands for 1D-Var, the new B matrix has been calculated just for these bands, and very high correlation was found between adjacent bands 3 and 4, and almost zero correlation of these two bands with band number 15. For simplicity reason (diagonal B) we merged wavebands number 3 and 4 as the average emissivity values in those were relatively close. And the result was, that finally we would use 8 channels: four from merged bands 3 and 4, and four from band 15.

First validation tests were performed for 4 randomly chosen profiles over land. As can be seen on Fig. 4, introducing the new SSE values for separated channels in wavebands improved the estimation of the brightness temperature from the atmosphere state-vector especially for band 15. The integer values of x axis from 2 to 9 correspond respectively to AIRS channels : 587, 672, 787, 791 (merged bands 3 and 4) and 1865, 1866, 1867, 1868 (band 15). Further tests will be performed on a larger sample of profiles.

IV. 1D-Var

A scheme of "one-dimensional variational analysis" (1D-Var) is a method for extracting information from satellite-measured radiances for use in the data assimilation system. It is based on the same principles as 3D-Var, just applied to the analysis of atmospheric profile in single location, using a forecast profile and its error covariance as a constraint. Brightness temperatures corresponding to the state vector x are computed using radiative-transfer model RTTOV-7. The used background covariance matrices B for temperature, humidity and emissivity are those shortly described above, and in details in Szczech-Gajewska (2002).

Work on nonlinear 1D-Var has started, but still there no results to present. Up to that moment the introduction of emissivity as a control variable have been applied, but not yet tested.

V. Conclusions

In conclusion, new emissivity maps based on ECOCLIMAP are consistent with MODIS SSE maps retrieved with the "split-window" method for bands 31 and 32. Usage of the local surface spectral emissivity (at the closest point to the position of profile) in radiative-transfer model RTTOV-7 with HIRS 8 data have not clearly shown that the estimation of the brightness temperature from atmospheric profiles was really improved with comparison to default SSE value for RTTOV-7, but it was usually better than with the emissivity currently used in ARPEGE. In the case of Tb simulated with ARPEGE SSE as reference, the increase of the number of "good" points while using the new surface emissivity reaches up to 25 % globally (with some exceptions). Preliminary results for AIRS data showed that we could expect Tb values simulated in RTTOV with new SEE closer to the measured ones. But the validation on more numerous samples of profiles is still required. Finally the work on 1D-Var must be continued on the inversion of radiances and emissivity retrieval. Tests with background error covariances matrices, especially one for T, with explicit correlations between Ts and atmospherical T, should be performed.

Bibliography

V. Masson, 2003 : A Global Database of Land Surface Parameters at 1-km Resolution in Meteorological and Climate Models, accepted to *Journal of Climate*, **16**.

J. Smith, A. McNally, P. Watts, 2003 : Performance of a high spectral resolution cloud detection scheme for AIRS data used at ECMWF, P*roceedings of Symposium on Earth Observation and Satellite Meteorology*.

R. Snyder, 1998 : Classification-based Emissivity for Land Surface Temperature Measurement from Space, *Int. J. Remote Sensing*, **19**, n°.14, 2753-2774.

M. Szczech-Gajewska, 2002 : Parameterisation of background error statistics for surface parameters (LST, SSE), to be used for future assimilation of advanced IR sounders over land, *ALATNET Newsletter*, **5**.

Laboratory emissivity data were taken (autumn 2001) from : *http://speclib.jpl.nasa.gov/ , http://asterweb.jpl.nasa.gov/ , http://www.icess.ucsb.edu/modis/EMIS/html/em.html*

MODIS hdf files were ordered from : *http://edcimswww.cr.usgs.gov/pub/imswelcome/*

9. Jozef VIVODA: "Application of the predictor-corrector method to non-hydrostatic dynamics"

Application of the Predictor-Corrector method to non-hydrostatic dynamics stability of Rossby-Haurwitz modes. Theoretical and practical aspects.

1. Introduction

The class of schemes that are iterative approximations to fully implicit schemes applied on the Euler-equations (EE) system was studied in Bénard (2003). Any scheme of that kind is referred to as Iterative Centred Implicit (ICI) scheme in further text. The Semi-implicit (SI) scheme and Predictor/Corrector (PC) scheme are special cases of ICI scheme, with one respectively two solutions of the semi-implicit solver.

The EE system permits the gravity, acoustic and Rossby-Haurwitz (RH) modes. The stability analysis of the gravity and acoustic modes has been performed in Bénard, (2003) with EE system cast in hydrostatic pressure based σ vertical coordinate of Laprise, (1992). The stability of small amplitude oscillations was studied in an isothermal atmosphere with temperature T_0 over flat terrain. It was found that the gravity and acoustic modes are conditionally stable even in the limit of infinite time step, when an appropriate set of prognostic variables is used. The two-time-level predictor/corrector scheme is stable, if T_0 and the SI reference temperature T^* satisfy condition : $1/2\ T^* < T_0 < 2T^*$. Nevertheless, the classical two-time-level (2TL) SI scheme is stable only if the background and the SI reference temperatures are equal, and the PC scheme becomes compulsory for realistic simulations which are naturally non-isothermal.

The Rossby-Haurwitz (RH) modes are usually treated explicitly in the models with the SI time stepping. With introduction of the two-time-level schemes with semi-Lagrangian (SL) advection treatment, the Coriolis force terms are treated semi-implicitly in some models (Temperton, 1997). The RH modes are partially implicit in a PC scheme as well. It is known that the implicit treatment of a mode slows it down. This is an acceptable behaviour for the modes that are not of meteorological interest (gravity modes in large scale hydrostatic models, or acoustic modes in non-hydrostatic models). However, RH modes are the main synoptic scale signals and their accurate representation is a necessary condition to consider the scheme to be applicable in a local area model.

Here, we analyse the free RH modes on a middle latitude β plane in the framework described previously. We are interested in the stability and accuracy properties of the RH modes in the limit of long time steps under the conditions for which the gravity and acoustic modes are stable.

2. The linear system with RH modes

The analysed linearized system of prognostic equation around isothermal, resting and isothermally balanced state yields :

$$\frac{\partial D}{\partial t} = -R\mathbf{G}\Delta T + RT_0(\mathbf{G}-1)\Delta P - RT_0\Delta q + f_0\xi - \beta U$$

$$\frac{\partial d}{\partial t} = -\frac{g^2}{RT_0}\cdot \mathbf{L}P$$

$$\frac{\partial T}{\partial t} = -\frac{RT_0}{Cv}\cdot (D+d) \qquad (1)$$

$$\frac{\partial P}{\partial t} = \mathbf{S}D - \frac{Cp}{Cv}\cdot (D+d)$$

$$\frac{\partial q}{\partial t} = -\mathbf{N}D$$

$$\frac{\partial \xi}{\partial t} = -f_0 D - \beta V$$

We have used the formulation with prognostic variables q=ln(π_s), d=$-gp/\pi RT\cdot\sigma\cdot\partial w/\partial\sigma$, and P=(p-π)/π . f_0 is the Coriolis parameter on a reference latitude and β is the South-North horizontal derivative of the Coriolis parameter on that reference latitude. This approximation is sufficient to describe the behaviour of RH modes on a limited size middle-latitude domain (Lindzen, 1967). The system is further referred to as *A* and is formulated using divergence and vorticity as prognostic variables (D resp. ξ). We consider the tangent plane, therefore a local Cartesian horizontal coordinate system (x,y) can be introduced and the arrays can be decomposed horizontally into bi-Fourier series. In such a framework, the horizontal wind components can be expressed in the terms of divergence and vorticity as :

$$U = \frac{ikD - is\xi}{-k^2 - s^2} \qquad , \quad V = \frac{ikD + is\xi}{-k^2 - s^2} \qquad (2)$$

(k, s) are the horizontal wavenumbers defined along axes on horizontal plane.

To obtain, the SI linear system *B*, used in this study, we set f_0=0 and β=0, and substitute T_0 by the SI reference temperature T* in the system [1].

3. The two-time-level non-extrapolating ICI scheme

We analyse the stability and accuracy properties of the two-time-level non-extrapolating ICI scheme. The general ICI scheme written in vector formalism is :

$$\frac{X[t+\Delta t(n)] - X[t]}{\Delta t} = A\cdot\frac{X[t+\Delta t(n-1)] + X[t]}{2} + B\cdot\frac{X[t+\Delta t(n)] - X[t+\Delta t(n-1)]}{2} \qquad (3)$$

with state vector X =(D, d, P, q, T, ξ). The n index denotes the order of iteration ($n\in(1,...,NSITER$; n=0 SI scheme, n=1 PC scheme). When the process converges the last term on the rhs will converge to zero. The state at the beginning X[t+Δt(0)] is unknown and [3] cannot be used to figure it out. The non-extrapolating two-time-level SI scheme is used to calculate it :

$$\frac{X[t+\Delta t(0)] - X[t]}{\Delta t} = A\cdot X[t] + B\cdot\frac{X[t+\Delta t(0)] - X[t]}{2} \qquad (4)$$

and therefore the particular ICI scheme is referred to as non-extrapolating ICI scheme.

4. The stability and phase speed error of RH modes in the two-time-level non-extrapolating ICI scheme

Eigenfunctions of the system on the tangent plane are expressed in the form :

$$X(x,\sigma) = \hat{X} e^{i(kx+sy)} \sigma^{i\nu - \frac{1}{2}} \tag{5}$$

with ν being the dimensionless vertical wavenumber. The associated vertical wavelength for a given ν in an isothermal atmosphere is $l_z = 2\pi/\nu\, H$.

Assuming that the amplitude of the mode is time dependent and :

$$\hat{X}[t+\Delta t) = \lambda \cdot \hat{X}[t]$$

we can apply the classical Von-Neumann analysis of stability and look for complex amplification factors λ. The stability is defined by the magnitude of λ and the relative phase speed error r_p can be computed as $r_p = \arg(\lambda) / \omega_a \Delta t$. The analytical frequency ω_a is computed from the dispersion relation of the system [1].

The stability was computed for the horizontal spectrum of continental size domain (the zonal horizontal wavelength varies from 36 km to 3600 km). The meridional wavelength was fixed to 3600 km. The time step length used in analysis was 600 s. It is the settings of the case study in the following section.

The temperature of the isothermal atmosphere is T_0 = 300 K (vertical height scale H = 8.8 km). The SI scheme is determined by the reference temperature T^*= 300 K and the acoustic reference temperature T_a^* = 50 K (for detailed explanation see Bénard, 2004).

We analyse three vertical modes to assess the behaviour of the RH modes in the whole spectrum. The mode with ν=0, that represents the external mode of the model with top in infinity. To sample whole spectra we further choose the modes with the vertical wavelengths 10 km and 2 km (ν=5.5 and ν=27.5) . They are referred to as "slightly internal" and "internal" mode in further text.

The stability of predictor and corrector of the two-time-level PC scheme is shown in Figure 1. The dependence of stability on the horizontal wavelength (given in km) is shown. The modes are stable for all horizontal scales (from 36 km to 3600 km).

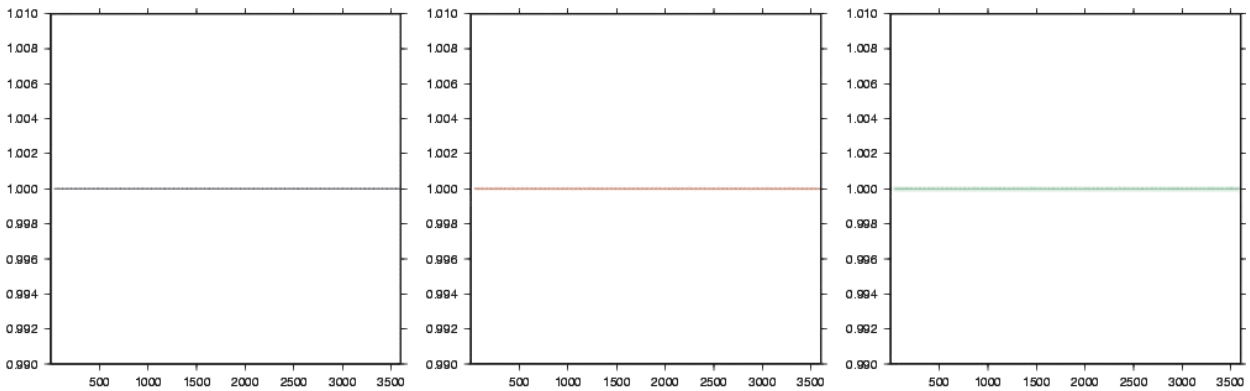

Figure 1 : The stability of external, slightly internal and internal RH modes as a function of zonal horizontal wavelength given in km. Meridional horizontal wavelength was fixed to 3600 km. The modes are stable for the whole horizontal spectrum.

The relative phase-speed error is shown in Figure 2. Solid curve represents the predictor and dashed curve the corrector. The external, slightly internal and internal modes are plotted as the left, middle and the right plot. The result is opposite to what could have been naively expected. The PC scheme accelerates the RH modes. However, the acceleration is very small about 0.1 %. The horizontal wavelength of accelerated modes depends on the vertical mode. The magnitude of acceleration is negligible comparing to the effects caused by other, mainly physical processes.

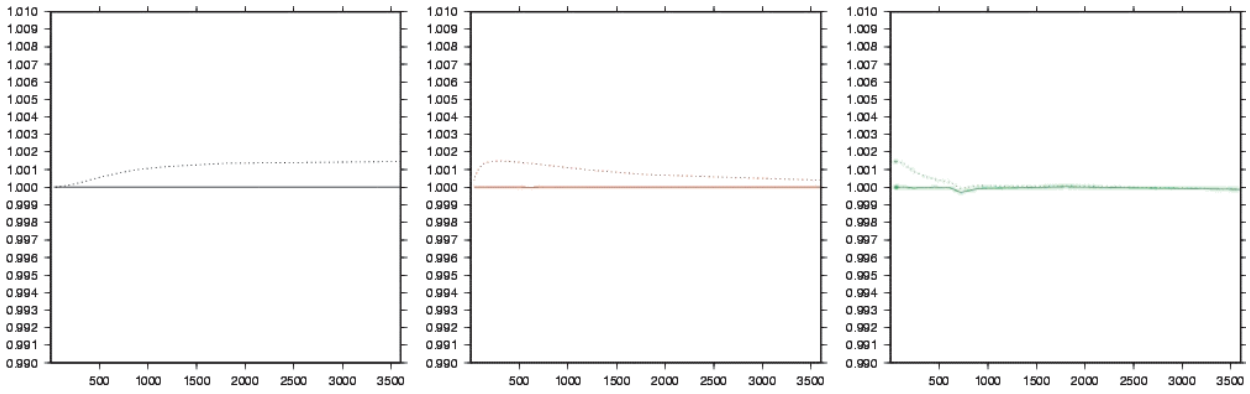

Figure 2 : The relative phase speed error of external, slightly internal and internal RH modes as a function of zonal horizontal wavelength given in km. Meridional horizontal wavelength was fixed to 3600 km. The PC scheme slightly accelerates the modes. The magnitude of acceleration is about 0.1 % and it is too small to have any practical impact on mesoscale model simulations.

5. Lothar storm case study

To test the accuracy of the model for synoptic scales the Lothar storm case was chosen. It is the first of the two storms from December 1999 that passed over Europe during Christmas. The meso-cyclone formed over Atlantic Ocean and it moved rapidly towards Europe. During the 26th of December 1999 the storm hit France, Germany, Switzerland and Italy and caused severe damages. Operational forecast of the global model ARPEGE provided reasonable guidance for Lothar storm. When ALADIN is coupled with ARPEGE prediction using quadratic coupling or 3 hour frequency coupling, the prediction of Lothar storm is sufficiently accurate to be considered successful in the view of current LAM performance. In Figure 3, we can see the 26th December 1999 analysis of ARPEGE at 12, 18 and 24 UTC.

The Lothar storm is possible to predict using the dry adiabatic model version. However, such prediction is not possible to verify against the model analysis. Therefore we used the diabatic version of model ALADIN. We run the prediction using initial condition from 12 UTC on the 25th of December 1999. The reference run was obtained with hydrostatic model version using the two-time-level SI SL scheme with `LSETTLS` extrapolation (Figure 4). The integration domain was the ALADIN/LACE domain, the horizontal mesh size is 12.2 km and Δt =600 s. The position of the cyclone is shifted slightly to the east and is 1 hPa shallower (972 hPa in the centre) than in the analysis (left plot in Figure 3).

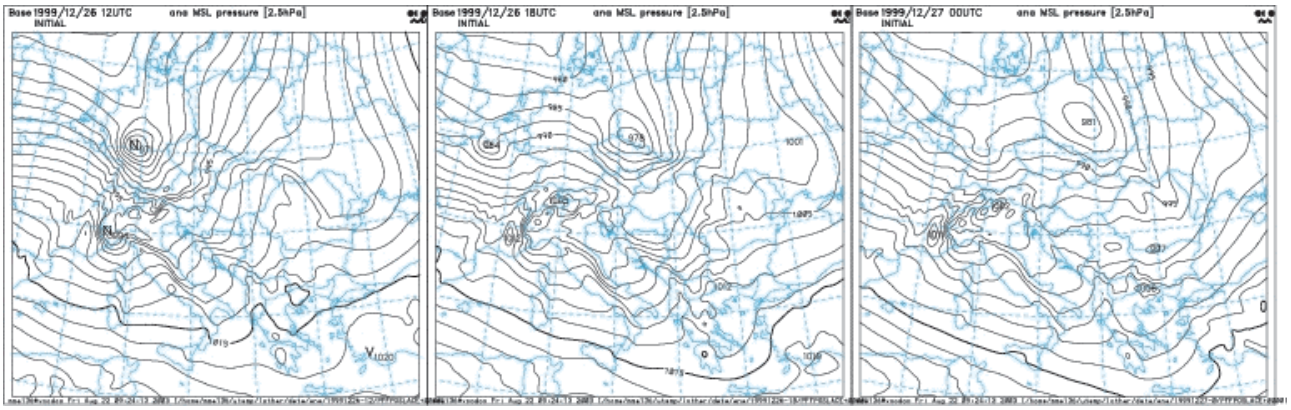

Figure 3 : The 3d-var analysis of model ARPEGE, of the Lothar storm case from the 26th of December 1999. The mean-sea-level pressure is plotted with contour interval 2.5 hPa. The storm moved eastward over France, Germany and finally during the 27th of December 1999 it weakened over southwest Poland.

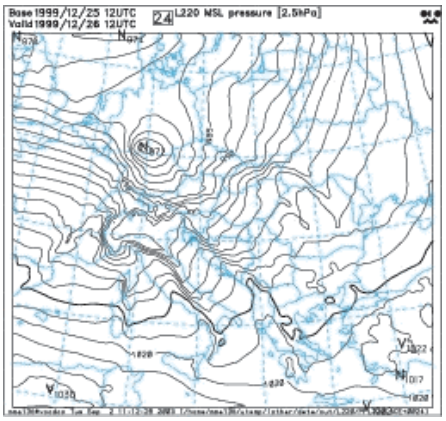

Figure 4 : The 24 h reference prediction of Lothar storm from 25th of December 1999 12 UTC. The prediction obtained with hydrostatic model version with 2TL SI SL LSETTLS scheme. The results obtained with the 2TL SI SL non-extrapolating scheme

To assess the impact of ICI scheme itself, we integrated the Lothar case using the two time-level non-extrapolating ICI scheme with hydrostatic model version. The method of extrapolation used to compute nonlinear residuals and the wind for trajectories was changed. The first order accuracy algorithm in time was used during predictor, while LSETTLS approach is second order accuracy. The second order accuracy is restored during subsequent iterations.

The physics was called once per time step, during predictor. The physical tendencies were considered to be valid in departure point of SL trajectories at time instant *t*.

In the left column of Figure 5, the 24 h prediction is showed computed with ICI scheme using different number of iterations (equivalent to n=0 and 1 as defined in [3]). The top left plot is calculated using two-time-level SI non-extrapolating scheme described by [4]. As it was mentioned already, it is a first order accuracy scheme, but the obtained results are reasonable in the case of Lothar storm. The cyclone is well positioned and the minimum mean-sea-level pressure (MSLP) is underestimated by 1 hPa comparing to analysis. Further iterations of the SI solver using ICI scheme did not bring any significant change in storm prediction. The differences between the SI non-extrapolating scheme and the PC scheme predictions are showed on top right plot of Figure 5 The maximum difference is 2.1 hPa. The PC scheme prediction itself is displayed in the bottom left plot and the differences gained by further iteration of ICI scheme are showed on the bottom right plot. It

is apparent that the scheme is converging since the differences between successive iterations of the ICI scheme converge towards zero.

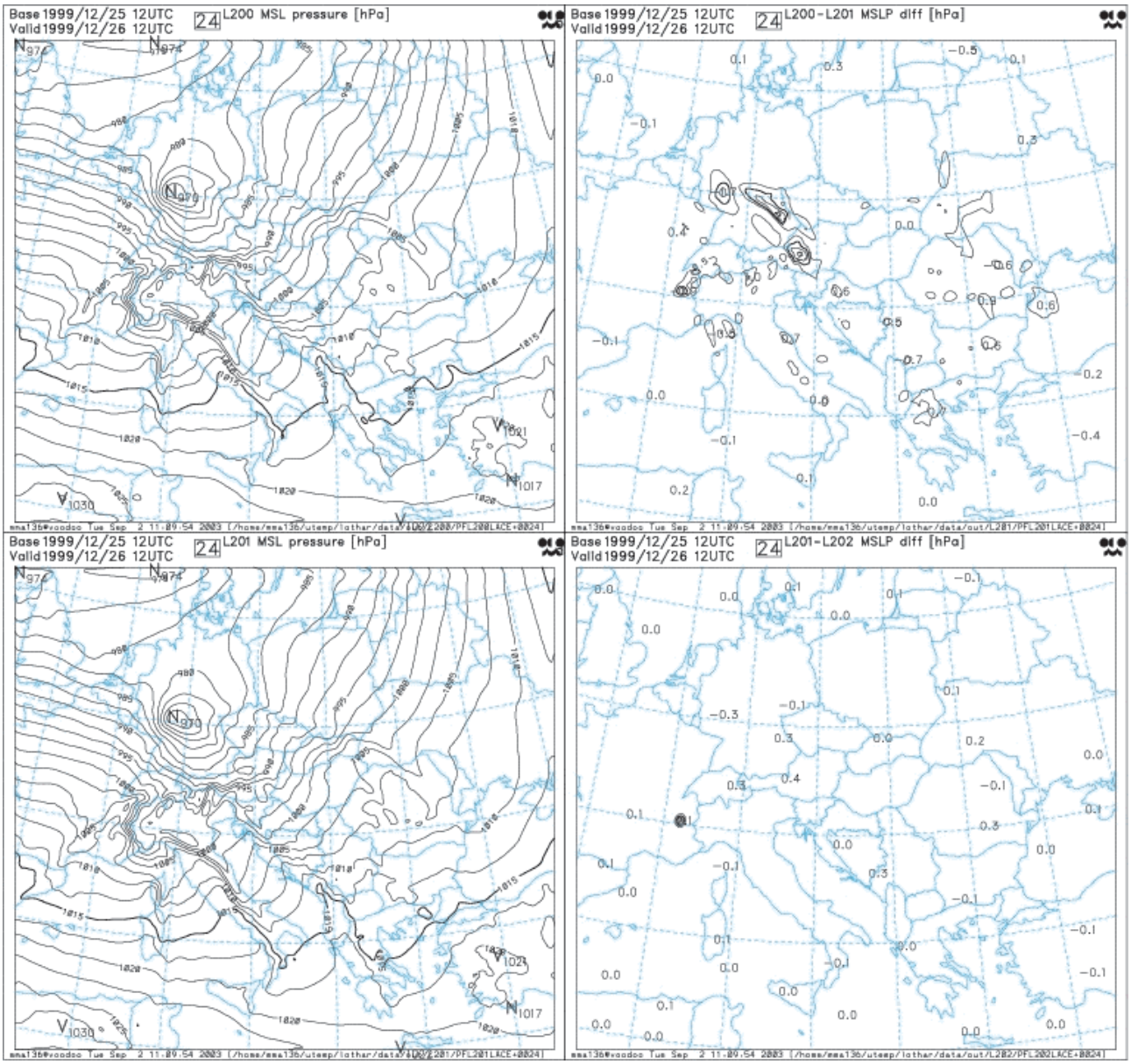

Figure 5 : The 24 h prediction from 25th of December 1999 12 UTC obtained with the 2TL ICI SL non-extrapolating scheme with *n*=0 (top left plot) and *n*=1 (bottom left plot). The differences between the runs with different number of iterations of ICI scheme are plotted in the right column. The differences between the SI scheme and the PC scheme runs are on top right plot, and the differences between the PC scheme and ICI scheme with *n*=2 are on the bottom right plot.

We have integrated the Lothar case using the non-hydrostatic model version as well. We used the prognostic variable *d*4 (namelist variable `NVDVAR`=4) and we set the SI acoustic temperature to 50K and keep the value of SI gravity temperature 350 K (namelist variables `SITRA`=50 K and `SITR`=350 K, for detailed explanation see Bénard, 2004). We used the 2TL ICI non-extrapolating scheme with SL advection. The results are showed on Figure 6. Comparing to the equivalent hydrostatic run, there is a further underestimation of the minimum MSLP by 1 hPa, but this difference disappears after the first iteration of ICI scheme. The results obtained with the non-hydrostatic model version are almost identical to the hydrostatic results. This proves that the tested scheme applied on ALADIN's non-hydrostatic dynamics efficiently stabilises all the possible sources of instabilities for the "hydrostatic" time step length (orographically induced waves, SHB

temperature and pressure instabilities), while keeping the quality of the simulation of the large scales as in the hydrostatic model. We can deduce from Figure 6, that the PC scheme is fully sufficient to integrate the model for resolution around 10 km, because there is no significant change in the results when using two or more iterations of the SI solver.

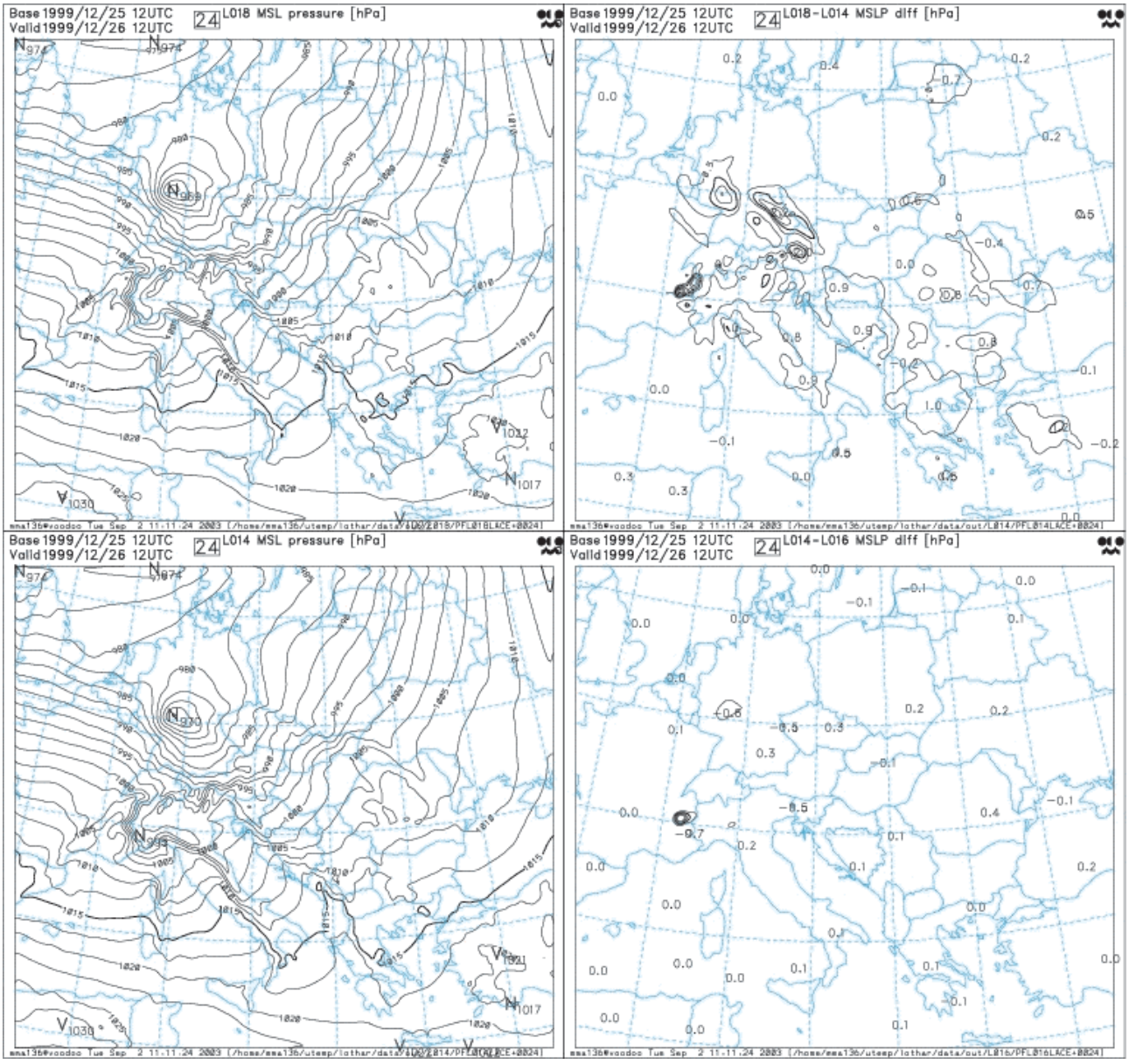

Figure 6 : The same as on Figure 5, but obtained with the non-hydrostatic version of ALADIN.

The aim of this study was to show that the 2TL ICI scheme doesn't deteriorate results obtained with the standard SI scheme when applied to a synoptic scale case. The linear analysis indicated that the RH modes are slightly accelerated by two-time-level PC scheme. The frequencies of the RH modes are 0.1 % greater than their analytical value. However, there are still nonlinear residuals not included in the analysis and a case study with the full nonlinear model has to be carried out to draw a final conclusions. We showed that the acceleration and remaining nonlinear residuals had no impact on accuracy of short-range diabatic model integration.

The results obtained with 2TL ICI SL non-extrapolating scheme with either hydrostatic or non-hydrostatic version are almost equivalent to the reference results from the hydrostatic model

integrated using the 2TL SI SL LSETTLS scheme at the 10 km scale. This confirmed that the partially implicit treatment of slow modes in ICI scheme doesn't deteriorate them.

The simulations using the non-hydrostatic model version further proved that the methods used to stabilise acoustic modes and the orographically induced instabilities are neutral to slow modes. The Lothar case study proved that for resolutions around 10 km the 2TL SL PC non-extrapolating scheme without additional filtering is sufficient to integrate NH model ALADIN formulated with the prognostic variables $d4$, P and q. No significant improvement can be gained by additional iterations of the SI solver.

Bibliography

[1] Bénard, P., 2003 : Stability of semi-implicit and iterative centred-implicit time discretization for various equations systems used in NWP, to be published in *MWR.*

[2] Bénard, P., 2004 : On the use of a wider class of linear systems for the design of constant-coefficients semi-implicit time-schemes in NWP, to be published in *MWR.*

[3] Laprise, R., 1992: The Euler equations of motions with hydrostatic pressure as an independent variable. *Mon. Wea. Rev*., **99**, 32-36.

[4] Lindzen, R.D., 1967 : Planetary waves on beta-planes. *Mon. Wea. Rev.*, **95**, 441-451.

[5] Temperton, C., 1997: Treatment of the Coriolis terms in semi-Lagrangian spectral models, In: Numerical methods in atmospheric and oceanic modeling. *The André J. Robert Memorial Volume*. NRC Research Press.